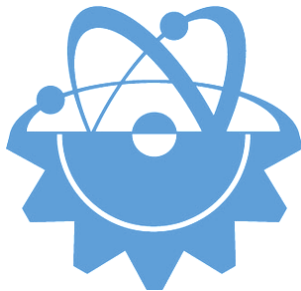


ISSN-Printed: 2536-5010
ISSN-Online: 2536-5134

Volume 15, No 1, 2025

EJT

EUROPEAN JOURNAL OF TECHNIC



Copyright © 2017

International Engineering, Science & Education Group

Email (for orders and customer services enquiries): info@ineseg.org, ejt@ineseg.org

Visit our home page on www.ineseg.org

All Rights Reserved. No part of this publication may be reproduced, stored in a retrieval system or transmitted in any form or by any means, electronic, mechanical, photocopying, recording, scanning or otherwise, except under the terms of the Copyright, under the terms of a license issued by the Copyright International Engineering, Science & Education Group (INESEG), without the permission in writing of the Publisher. Requests to the Publisher should be addressed to the Permissions Department, International Engineering, Science & Education Group (INESEG), or emailed to info@ineseg.org

Designations used by companies to distinguish their products are often claimed as trademarks. All brand names and product names used in this journal are trade names, service marks, trademarks or registered trademarks of their respective owners. The Publisher is not associated with any product or vendor mentioned in this journal.

This publication is designed to provide accurate and authoritative information in regard to the subject matter covered. It is sold on the understanding that the Publisher is not engaged in rendering professional services. If professional advice or other expert assistance is required, the services of a competent professional should be sought.



EUROPEAN JOURNAL OF TECHNIQUE (EJT)

ISSN-Printed: 2536-5010

ISSN-Online: 2536-5134

Scope: European Journal of Technique (EJT) established in 2010. It is a peer –reviewed international journal to be of interest and use to all those concerned with research in various fields of, or closely related to, Engineering disciplines. European Journal of Technique (EJT) aims to provide a highly readable and valuable addition to the literature which will serve as an indispensable reference tool for years to come. The coverage of the journal includes all new theoretical and experimental findings in the fields of Engineering or any closely related fields. The journal also encourages the submission of critical review articles covering advances in recent research of such fields as well as technical notes.

The scopes include:

- Mechanical Engineering
- Textile Engineering
- Electrical-Electronics Engineering
- Computer and Informatics Engineering
- Civil and Architecture Engineering
- Mining Engineering
- Chemical Engineering
- Metallurgical and Materials Engineering
- Environmental Engineering
- Food Engineering
- Geological Engineering
- Industrial Engineering
- Renewable Energy

EDITORIAL BOARD MEMBERS

Editor-in-Chief

- Musa YILMAZ

Publisher Of Journal

- Heybet KILIÇ

ETHICS and POLICIES

European Journal of Technique (EJT) is committed to following the [Code of Conduct](#) and [Best Practice Guidelines](#) of [COPE \(Committee on Publication Ethics\)](#). It is a duty of our editors to follow [Cope Guidance for Editors](#) and our peer-reviewers must follow [COPE Ethical Guidelines for Peer Reviewers](#). We expect all prospective authors to read and understand our Ethics Policy before submitting any manuscripts to our journals.

Please note that submitted manuscripts may be subject to checks using the iThenticate service, in conjunction with CrossCheck, in order to detect instances of overlapping and similar text.

The [iThenticate](#) software checks submissions against millions of published research papers, documents on the web, and other relevant sources. If plagiarism or misconduct is found, consequences are detailed in the policy.

The chief goal of our policy is threefold: to provide advice for our authors, to maintain the scholarly integrity of our journals and their content, and to detail the ethical responsibilities of EJT, our editors and authors.

We expect all authors to read and understand our ethics policy before submitting to any of our journals. This is in accordance with our commitment to the prevention of ethical misconduct, which we recognise to be a growing problem in academic and professional publications. It is important to note that most incidents of plagiarism, redundant publication, copyright infringement or similar occur because of a lack of understanding, and not through fraudulent intent. Our policy is one of prevention and not persecution.

If you have any questions, please contact the relevant editorial office, or European Journal of Technique (EJT)' ethics representative: ejtineseg@gmail.com

Download a PDF version of the Ethics and Policies [[PDF,392KB](#)].

Authors' Responsibilities

Authors should:

- Ensure that all researched work submitted is original, fully referenced and that all authors are represented accurately. The submission must be exclusive and not under consideration elsewhere.
- Provide accurate contact details for a designated corresponding author, who shall be deemed by the publisher and editor as fully responsible for the authorship of the paper and all communications concerning the ethical status and originality of the paper. This includes any queries or investigations that may arise, pre- or post publication.
- Openly disclose the source of all data and third party material, including previously unpublished work by the authors themselves. Anything that could compromise the originality of the submission should be expressly avoided and/or discussed with the editorial office in the first instance.
- Identify any third party material that they intend to include in their article, and obtain written permission for re-use in each instance from the relevant copyright holders. Such permissions should be submitted once the manuscript is accepted, or requires small changes to be accepted. For further guidance on seeking permission to use 3rd party material please see the Rights and Permissions section.
- Openly disclose any conflict of interest - for example, if publication were to benefit a company or services in which the author(s) has a vested interest.

- Expect to formally agree publication terms which defines the author and the publishers rights for the work. Visit our website for further information.
- Expect the editor to scan submissions using plagiarism detection software at [iThenticate](#) to check a paper's originality before sending out for review.
- Fully correspond and comply with the editor and publisher in any requests for source data, proof of authorship or originality in a timely manner, providing reasonable explanation for discrepancies or failures to disclose vital information.
- Fully co-operate with any consequent investigations if the editor and/or publisher are dissatisfied with the evidence available or the explanations provided.
- Expect transparency, efficiency and respect from the publisher and the editor during the submissions process.
- Remain in good communication with both the publisher and the editor.
- When necessary, submit corrigenda in a timely and responsible fashion.
- Co-operate fully with the publication of errata and with the retraction of articles found to be unethical, misleading or damaging.
- Remain in good communication with the editor(s), the publisher and any co-authors.

Editors' Responsibilities

Editors should:

- Read and understand COPE guidelines as well as EJT's ethics policy, and follow them during all editorial processes.
- Protect the reputation of their journal(s) and published work by only publishing content of the highest quality and relevance in a timely and responsible manner.
- Carry out thorough, objective and confidential peer review for original article submissions that pass the initial quality check and editorial assessment, in adherence with COPE guidelines and EJT' ethics policy.
- Detail and justify any article types which will not be peer reviewed (e.g. editorials, opinion pieces etc.).
- Provide a transparent review and publication process as far as is possible, with full respect and care paid to the author(s).
- Provide advice and give reasonable explanation and updates to authors during the submissions process and once a decision has been made.
- Allow authors the right to appeal any editorial decision.
- Only accept papers based on the original merit, quality and relevance of their content.
- Support authors in queries concerning the originality of their submissions and request the support of EJT if necessary.
- Advise the publisher of any third party material which has been included for which they do not believe sufficient permission has been cleared.

- Be ready and prepared to publish corrections, corrigenda, errata when necessary, as well as retract articles that (the editor and EJT) deem unethical, misleading or damaging.
- Remain in good communication with both the publisher and the author(s).

Reviewers' Responsibilities

Reviewers should:

- Adhere to EJT's policy of confidential peer review of their journals. This includes, but is not restricted to, keeping their identity hidden from authors and not externally distributing any work that is passed to them for their eyes only.
- Only accept invitations to review work that is relevant to their own expertise and speciality.
- Review submitted work in a responsible, impartial and timely manner.
- Report any suspected ethical misconduct as part of a thorough and honest review of the work.
- Avoid the use of unnecessarily inflammatory or offensive language in their appraisal of the work.
- Accept the commitment to review future versions of the work and provide 'follow up' advice to the editor(s), if requested.
- Seek advice from the editor if anything is unclear at the time of invitation.
- Remain in good communication with both the publisher and the editor.

EJT's Responsibilities

EJT will:

- Protect the reputation of our journals and published work by only publishing content of the highest quality and relevance in a timely and responsible manner.
- Provide detailed information concerning both our understanding of publication ethics and our implementation of the same. Emphasise a desire for prevention, not eventual detection, of ethical misconduct.
- Uphold our COPE membership (or of such similar organisations) and keep our editorial offices, publishing staff and society partners up-to-date with their guidelines and policies, adapting our own where appropriate (and publicising any update).
- When necessary, request proof of originality/accuracy from the corresponding author of any work submitted to any of our journals.
- Use plagiarism detection software when necessary for any submission to any journal at any stage of the submissions and publication process.
- Provide a transparent submissions and publication process, with full respect and care paid to the author. This includes detailed and dedicated instructions to authors for each journal, outlining referencing style, accepted article types and submission processes.
- Investigate thoroughly any suggestion of ethical misconduct detected during any stage of the submissions process. This can include, but is not restricted to, the following: plagiarism, redundant publication, fabrication or misuse of data and authorial disputes.

- When necessary, retract articles that we deem to be unethical, misleading or damaging.
- When necessary, publish errata, corrigenda and retractions in a timely and responsible fashion, detailing the decision online in an open access format and publishing in print as soon as possible.
- Remain in good communication with editors, authors, reviewers and society partners (where applicable).

Further reading

- Authorship of the paper: Authorship should be limited to those who have made a significant contribution to the conception, design, execution, or interpretation of the reported study.
- Originality and plagiarism: The authors should ensure that they have written entirely original works, and if the authors have used the work and/or words of others that this has been appropriately cited or quoted.
- Data access and retention: Authors may be asked to provide the raw data in connection with a paper for editorial review, and should be prepared to provide public access to such data.
- Multiple, redundant or concurrent publication: An author should not in general publish manuscripts describing essentially the same research in more than one journal or primary publication. EJT do not view the following uses of a work as prior publication: publication in the form of an abstract; publication as an academic thesis; publication as an electronic preprint. Information on prior publication is included within each EJT and its journal Guideline for Authors.
- Acknowledgement of sources: Proper acknowledgment.
- Disclosure and conflicts of interest: All submissions must include disclosure of all relationships that could be viewed as presenting a potential conflict of interest.
- Fundamental errors in published works: When an author discovers a significant error or inaccuracy in his/her own published work, it is the author's obligation to promptly notify the journal editor or publisher and cooperate with the editor to retract or correct the paper.
- Reporting standards: Authors of reports of original research should present an accurate account of the work performed as well as an objective discussion of its significance.
- Hazards and human or animal subjects: Statements of compliance are required if the work involves chemicals, procedures or equipment that have any unusual hazards inherent in their use, or if it involves the use of animal or human subjects.
- Use of patient images or case details: Studies on patients or volunteers require ethics committee approval and informed consent, which should be documented in the paper.

EJT has also accessed and learned from the existing policies of other publishers and leading experts as well as open access articles that detail and define ethical misconduct.

- 'Plagiarism and the law', Joss Saunders, Learned Publishing, 23:279-202: <http://www.ingentaconnect.com/content/alpsp/lp/2010/00000023/00000004/art00002>
- iThenticate Plagiarism Resources: <http://www.ithenticate.com/resources/6-consequences-of-plagiarism>

EDITORIAL BOARD MEMBERS

Editor-in-Chief : Musa Yilmaz

International Editorial Board

Aayush Shrivastava University of Petroleum and Energy Studies, Dehradun, India
Abdulkerim Oztekin Batman University, Batman, Turkey
Adelino Pereira Engineering Institute of Coimbra, Portugal
Ahmad Fakharian Islamic Azad University, Qazvin, Iran
Ahmed Saber Cairo University, Egypt
Arvind Kumar Jain Rustam Ji Institute of Technology, India
Aydogan Ozdemir Istanbul Technical University, Turkey
Baseem Khan Hawassa University, Hawassa, Ethiopia
Behnam Khakhi University of California Los Angeles, US
Behnam Mohammadi-ivatloo University of Tabriz, Tabriz, Iran
Bharti Dwivedi Institute of Engineering & Technology, Lucknow, UP, India
Carlos A. Castro University of Campinas – UNICAMP, Brasil
Cafer Budak Dicle University, Turkey
Deepak Kumar University of Petroleum & Energy Studies (UPES), India
Ernesto Vazquez University of Nuevo Leon, Mexico
Faisal Khan COMSATS Institute of Information Technology, Pakistan
Farhad Shahnia Murdoch University, Perth, Australia
Farrokh Aminifar University of Tehran, Iran
Fatih Kocyigit Dicle University, Turkey
Fiaz Ahmad National University of Computer and Emerging Sciences, Pakistan
Gouthamkumar Nadakuditi V R Siddhartha Engineering College, India
Hafiz Ahmed School of Mechanical, Coventry University, UK
Hamed Pourgharibshahi Lamar University, US
Hassan Bevrani University of Kurdistan, Iran
Hayri Yildirim Dicle University, Turkey
Hemant Kumar Gianey Thapar University, Patiala, Punjab, India
Hessam Golmohamadi Semnan University, Semnan, Iran
Heybet Kilic Dicle University, Turkey
Hilmy Awad Helwan University, Cairo, Egypt
Hüseyin Acar Dicle University, Turkey
Idris Candan Kocaeli University, Turkey
Jamshed Ahmed Ansari Sukkur IBA University, Pakistan
José A. Domínguez-Navarro University of Zaragoza, Spain
Kalpana Chauhan Galgotias College of Engineering and Technology, India
Khaled Ellithy Qatar University, Doha, Qatar
Kim-Doang Nguyen South Dakota State University, US
Kundan Kumar KIIT University, India
Lalit Kumar GBPIET Pauri, India
Leila Mokhnache University of Batna 2, Algeria
Linqun Bai ABB Inc., US
Mehmet Emin Asker Dicle University, Turkey
Md Shafiqullah King Fahd University of Petroleum & Minerals, Saudi Arabia
Mohamed Shaaban Universiti Malaysia Sarawak, Malaysia
Mohammed Albadi Sultan Qaboos University, Oman
Mohd Tariq Aligarh Muslim University, India
Mousa Marzband Northumbria University, Newcastle upon Tyne, United Kingdom
Necmettin Sezgin Batman University, Batman, Turkey
Neeraj Kanwar Manipal University Jaipur, India
Nishant Kumar Indian Institute of Technology Delhi, India
Nitin Kumar Saxena Wolaita Sodo University, Ethiopia
Nouar Tabet University of Sharjah, UAE
Omar Hafez Umm Al-Qura University, Makkah, Saudi Arabia
Omveer Singh Gautam Buddha University, India
Payam Teimourzadeh Baboli University of Mazandaran (UMZ), Iran
Payman Dehghanian George Washington University, US
Ragab A. El Sehiemy Faculty of Engineering, Kafrelsheikh University, Egypt
Rajeev Kumar Chauhan Galgotias College of Engineering and Technology, India
Rajiv Singh G.B. Pant University of Agriculture & Technology, India
Reza Sharifi Amir Kabir university Tehran, Iran
Rudranarayan Senapati Kalinga Institute of Industrial Technology, India
Saleh Y. Abujarad Universiti Teknologi Malaysia, Malaysia
Sanjay Dambhare College of Engineering, Pune, India
Saptarshi Roy NIT Warangal, India
Shailendra Kumar Indian Institute of Technology Delhi, India
Shariq Riaz The University of Sydney, Australia
Shengen Chen University of Maine, US
Syafaruddin Universitas Hasanuddin, Indonesia
T. Sudhakar Babu VIT University, Vellore, India
Thamer Alquthami King Abdulaziz University, Saudi Arabia
Theofilos Papadopoulos Democritus University of Thrace, Greece
Uday P. Mhaskar CSA Group, US
Vedat Veli Cay Dicle University, Turkey
Yogesh Rohilla K Lakshmi Pat University, Jaipur, India
Yunfeng Wen School of Electrical Engineering, Chongqing University, China
Zbigniew M. Leonowicz Wroclaw University of Science and Technology, Poland

Publisher of Journal

Heybey Kilic Dicle University, Turkey / TU Delft, Netherland



CONTENTS

Comparative Analysis of Voltage Segmentation (0.8Voc) and Sensorless MPPT Algorithms in PV Pump Systems Operating Under Partial Shading Conditions	1 - 7
Case Study on Energy Reliability Applications and Mathematical Models in The Distribution Network	8 - 14
Design of A Novel IoT Based Mobile ECG Data Transmission System using ESP8266	15 - 20
Some Numerical Techniques for Solution of Nonlinear Regularized Long Wave Equation	21 - 28
Eye State Classification from Electroencephalography (EEG) Signals Using the Extra Trees Classifier Algorithm	29 - 36
An Investigation into The Utilization of a Biodiesel Fuel Blend Supplemented with Mn(NO ₃) ₂ Additives in a CI Engine	37 - 43
The Potential of Transformer-Based Models for Automated Lung Cancer Detection from CT Scans	44 - 50
Prediction and Optimization of Tensile Strength Values of 3D Printed PLA Components with RSM, ANOVA and ANN Analysis	51 - 60
The Investigation of the Weldability of Ti6Al4V Alloy with Different Stainless Steel Series Using Copper Interlayer via Friction Welding	61 - 67
Sentiment Analysis in Turkish Using Language Models: A Comparative Study	68 - 74
Design and Implementation of an Individual Shooting Simulation System and Software	75 - 80
A Perspective View on Data Visualization Libraries Used in Data Analytics	81 - 96
Energy Geopolitics and Policies: The Case of Türkiye	97 - 108
Slope Stability Analysis in Road Cuts	109 - 115
Instagram Use in Education: Trends, Themes and Bibliometric Findings	116 - 126

Research Article

Comparative Analysis of Voltage Segmentation ($0.8V_{oc}$) and Sensorless MPPT Algorithms in PV Pump Systems Operating Under Partial Shading Conditions

Yunus Atagun^{1*} , Resat Celikel² ¹Firat University, Mechatronics Engineering Department, Elazig, Turkey. (e-mail: yunusatgn23@gmail.com).²Firat University, Mechatronics Engineering Department, Elazig, Turkey. (e-mail: rcelikel@firat.edu.tr).

ARTICLE INFO

Received: Jan., 13. 2025

Revised: Feb., 07. 2025

Accepted: April, 18. 2025

Keywords:

PV pump
 Partial shading
 Sensorless MPPT
 BLDC
 $0.8V_{oc}$

Corresponding author: Yunus Atagun

ISSN: 2536-5010 / e-ISSN: 2536-5134

DOI: <https://doi.org/10.36222/ejt.1616842>

ABSTRACT

When photovoltaic (PV) irrigation systems operate under partial shading conditions (PSC), traditional methods are insufficient. In addition to modified traditional methods, artificial intelligence and optimization-based smart methods are used to obtain maximum power from PV systems operating under PSC. These methods use one or more of the PV system's current, voltage, and atmospheric environment variables. In this study, a sensorless Maximum Power Point Tracking (MPPT) algorithm was developed. The proposed algorithm uses the values of the current and speed of the Brushless Direct Current Motor (BLDC) which used in the PV irrigation system. The current, voltage and other parameters of the PV system was not used. The proposed algorithm was compared the $0.8V_{oc}$ method that used panel data. The proposed MPPT algorithm was tested with a simulation study created in the MATLAB/Simulink environment. In the simulation study, four different PSCs were created and the $0.8V_{oc}$ method was compared with the proposed method. The obtained results are shown graphically. Accordingly, the superiority of the proposed method was observed in all cases except for the PSC2 case. On the other hand, there is a clear superiority in the speed of the $0.8V_{oc}$ method. The proposed sensorless MPPT technique operated the PV pump system with high efficiency as 99.9% in the case of PSC1, 95% in the case of PSC2, 99.9% in the case of PSC3 and 99.7% in the case of PSC4.

1. INTRODUCTION

With the developing technology, the need for energy sources is increasing day by day. Due to the rapid depletion of traditional fossil fuel energy sources and their harmful effects on the environment, interest in renewable energy sources is increasing. Solar energy is one of the most important of these sources. Photovoltaic panels (PV) are used to obtain electrical energy from solar energy. However, the efficiency of these panels is quite low. For this reason, various maximum power point tracking (MPPT) algorithms have been developed to extract maximum power from the panels [1]. The Perturb&Observe (P&O) and Incremental Conductance (InC) algorithms emerged as the oldest MPPT algorithms. These algorithms are still preferred today due to their ease of application and simple structure [2]. These algorithms work by observing the changes in voltage and current obtained as a result of changing the duty cycle of the DC-DC converter. Thus, increasing or decreasing the duty cycle according to the status of the PV system power provides maximum power from the PV system. However, modified versions of these methods have also been used and are still being developed in order to

respond faster to rapid atmospheric changes and to reduce fluctuations in the steady state [3,5].

The $0.8V_{oc}$ technique is derived from the Constant Voltage technique, one of the oldest well-known algorithms. This method is performed by determining the PV system voltage at which maximum power occurs. Then, the system is operated at this voltage point with a controller. In recent years, high-performance methods that can operate under challenging atmospheric conditions have been developed. The simplicity of the method has emerged as the most important advantage [6,7]. There are more than one MPP in PV systems operating under partial shading conditions (PSC). However, only one of them is the Global Maximum Power Point (GMPP). The $0.8V_{oc}$ technique has been reinterpreted by calculating the voltage inflection points and controlling these points. Thus, a high-efficiency method operating in the PSC has been developed [8]. A high-efficiency MPP algorithm derived from the $0.8V_{oc}$ algorithm has been developed. The voltage region can be selected by using voltage reference. This algorithm detects GMPP by monitoring power changes [9]. Similarly, the performance of a simple, high-efficiency voltage scanning algorithm that observes power changes and finds the GMPP

by performing a voltage scanning process has been investigated [10]. An algorithm that finds GMPP by obtaining I-V and P-V curves of PV arrays is actually a developed version of the 0.8Voc technique [11]. In another technique where the artificial intelligence algorithm is used, the current of the panels in the PV array is measured and entered into the artificial intelligence algorithm. The data obtained as output is the voltage value at which GMPP is formed. High efficiency has been obtained from this algorithm that works quite fast [12]. A two-stage algorithm has been proposed in a very recent study. In the first stage, the voltage regions are scanned and the MPP is detected, and in the second stage, the P&O algorithm is run at this point. Thus, the high performance of a new very efficient MPPT algorithm has been proven by simulation and experiment [13]. When the literature is examined, many studies based on the basic principles of the 0.8Voc algorithm are seen. The most important disadvantage of this method is the need to know the panel data with high accuracy. For this reason, different methods such as voltage scanning have also been developed.

Optimization based MPPT algorithms work with high performance in both normal solar irradiation and PSC. Although it has been the subject of much work in recent years, PSO (Particle Swarm Optimization) [14], CSA (Cuckoo Search Algorithm) [15], GWO (Gray Wolf Optimization) [16] and WOA (Whale Optimization Algorithm) [17] seem to be the most widely used optimization algorithms. However, the complex and demanding processing load of these algorithms is a significant disadvantage.

PV systems are used intensively in providing energy for irrigation systems. It is mandatory to use MPPT algorithms in these systems. Motors and pumps used in PV systems exhibit a non-linear load characteristic. Therefore, traditional methods respond late to rapid changes in atmospheric conditions and under PSC or are inadequate. A study has been conducted for a water pumping system with a PV-fed BLDC motor operating without a position sensor. The need for current sensors to measure motor phase currents in the system has been eliminated. The speed is automatically adjusted using an MPPT according to the highest power produced by the PV panel [18]. DC-DC converters are generally used to adjust the MPPT point in PV systems. DC-DC converters increase the system installation cost. Therefore, a PV pump system that feeds the BLDC pump without using a DC-DC converter has been developed [19]. Partial shading conditions are an important problem for PV irrigation systems. A study was presented that demonstrated the effect of PSC on the PV irrigation system through simulation and was verified experimentally [20]. In another study, BLDC was used to utilize the maximum power provided by the PV array and to increase the efficiency of the water pumping system. The proposed system used the CSA algorithm to obtain the MPP under partial shading conditions [21]. Synchronous reluctance motors are used in the industry with low cost and high efficiency. The MPP algorithm was developed without using a current sensor in a solar pump system using a synchronous reluctance motor. The PV system current was estimated using the system identification method and motor control data. This method, which operates with very high efficiency, showed very high performance under PSC [22]. In another study, the PSO method was used to operate the water pumping system using the PV-fed BLDC motor at maximum power point. In the study, it was proven that the PSO technique performed better than the traditional P&O technique [23]. A smart

method using radiation and temperature values as input was used for the MPP algorithm. BLDC connected to a PV system was operated at maximum power point using this method [24]. Optimization of the MPPT algorithm has been performed for a grid-connected PV-fed pump system. To demonstrate the effectiveness of the proposed method, the algorithm has been tested for three different DC-DC converters [25].

In this study, a two-stage MPPT algorithm is proposed for a PV system using BLDC operating under PSC. In the first stage, the PV system voltage is estimated using motor information and the MPP is found by looking at the motor power while the voltage changes. In the second stage, a P&O using motor information is used to find the real MPP around the estimated value. A sensorless MPPT algorithm is developed without using panel data, PV system and current information. Thus, unlike traditional algorithms, the system installation cost has been reduced. In addition, the problems that may arise from sensor errors have been reduced. Because the number of sensors used in the system has been reduced. In the proposed algorithm, motor current, speed and k coefficient, which is the parameter of the motor, are used. Simulation studies are performed using the MATLAB/Simulink program. The proposed algorithm is tested under four different PSCs.

2. PV IRRIGATION SYSTEMS

In this study, the PV irrigation system consists of PV panels, Zeta type DC-DC converter, three-phase inverter, BLDC and pump load. Here, the ZETA DC-DC converter is used for the operation of the MPPT algorithm.

2.1. PV System Model

A single diode model was used as the PV cell model. The equations of this model are seen between Equation 1 and Equation 3.

$$I = I_{PV} - I_D - I_{Rp} \quad (1)$$

$$I = I_{PV} - I_0 \left[\exp\left(\frac{V + R_s I}{a}\right) - 1 \right] - \frac{V + R_s I}{R_p} \quad (2)$$

$$a = \frac{N_s n k T}{q} \quad (3)$$

Here I_0 represents the reverse saturation current and leakage current. a is the ideality factor, N_s is the number of series-connected cells, n is the ideal diode constant, k is the Boltzmann constant ($1.3806503 \times 10^{-23}$ J/K), T is the cell temperature (Kelvin), q is the electron charge ($1.60217646 \times 10^{-19}$ C). The current produced by the PV panel under the influence of light is shown in Equation 4.

$$I_{PV} = \left(I_{pv,n} + K_1(T - T_n) \right) \frac{G}{G_n} \quad (4)$$

Here $I_{PV,n}$ represents the current generated at 25 °C and 1000 W/m² radiation value. T_n represents the nominal temperature (Kelvin), G represents the radiation value on the panel surface (W/m²), and G_n represents the nominal radiation value (W/m²). The saturation current of the diode, I_0 , is given in Equation 5.

$$I_0 = \frac{I_{SC,n} + K_I(T - T_n)}{\exp\left(\frac{V_{OC,n} + K_V(T - T_n)}{a}\right) - 1} \quad (5)$$

Here $I_{SC,n}$ is the nominal short circuit current, $V_{OC,n}$ is the open circuit voltage, K_I is the current coefficient and K_V is the voltage coefficient. In this study, the PV system consists of 6 series-connected panels. The model of the panel used in the simulation study is TPB125x125-72-P. The voltage produced by a panel at the maximum power point is given as 35.3V and its power as 154.967W. Accordingly, the maximum power that the PV system can produce is calculated as 929.8W at 211.8V.

2.2. BLDC and Pump Model

BLDC has a 3-phase stator winding. There are permanent magnets in its rotor. The position of the rotor is detected by field effect sensors placed inside the stator. The mathematical model of BLDC is shown in Equation 6.

$$\begin{bmatrix} V_A \\ V_B \\ V_C \end{bmatrix} = \begin{bmatrix} R & 0 & 0 \\ 0 & R & 0 \\ 0 & 0 & R \end{bmatrix} \begin{bmatrix} i_a \\ i_b \\ i_c \end{bmatrix} + \frac{d}{dt} \begin{bmatrix} L - M & 0 & 0 \\ M & L - M & M \\ 0 & 0 & L - M \end{bmatrix} \begin{bmatrix} i_a \\ i_b \\ i_c \end{bmatrix} + \begin{bmatrix} e_a \\ e_b \\ e_c \end{bmatrix} \quad (6)$$

Here V_A, V_B, V_C are phase voltages, i_a, i_b, i_c are phase currents, R is winding resistance, L is winding self-inductance and M is mutual inductance. The motor is switched with a six-step switching technique using the logic information coming from the field effect sensors. The simplicity of the switching technique is the most important advantage of this motor. The pump load connected to the motor is modeled to increase depending on the square of the speed. The expression of the load torque is seen in Equation 7. The parameters of BLDC used in the simulation study are given in [18].

$$T_L = k * \omega^2 \quad (7)$$

2.3. Zeta DC-DC Converter

Zeta converter is structurally composed of two coils, two capacitances and one diode. The basic circuit diagram of ZETA converter is shown in Figure 1. Here, the zeta converter, which includes components such as L_1 input inductor, L_2 output inductor and C_1 intermediate capacitor, is designed to always operate in continuous conduction mode.

The zeta converter is a fourth-order DC-DC converter that can operate in either boost or buck mode. This feature provides an unlimited area for maximum power point tracking. Unlike a conventional step-down converter, the zeta converter has a continuous output current. The output inductor makes the current continuous and ripple-free.

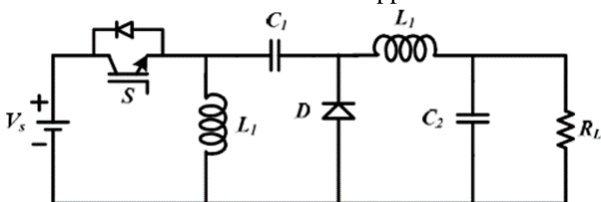


Figure 1. Zeta DC-DC Converter

The mathematical model used in the ZETA converter design is given between Equation 8 and Equation 12.

$$D = \frac{V_{dc}}{V_{dc} + V_{mpp}} \quad (8)$$

$$I_{dc} = \frac{P_{mpp}}{V_{dc}} \quad (9)$$

$$L_1 = \frac{D \cdot V_{mpp}}{f_{sw} \cdot \Delta I_{L1}} \quad (10)$$

$$L_2 = \frac{(1-D) \cdot V_{mpp}}{f_{sw} \cdot \Delta V_{C1}} \quad (11)$$

$$C_1 = \frac{D \cdot I_{dc}}{f_{sw} \cdot \Delta V_{C1}} \quad (12)$$

Here D is the duty cycle and its estimate is given in Equation 8. V_{dc} is the average output voltage of the zeta converter. The average current flowing through the inverter is given in Equation 9. After D and I_{dc} are calculated approximately, L_1 , L_2 and C_1 can be calculated as seen in Equations from 10 to 12.

3. 0.8V_{OC} and PROPOSED MPPT ALGORITHM

In PV systems, there may be uniform (homogeneous) radiation on the panels, as well as PSC where the radiation values on the panels are different. In this case, maximum power can be drawn by finding the highest MPP among the different MPPs. An example of the power changes obtained as a result of working under uniform radiation and PSC is given in Figure 2.

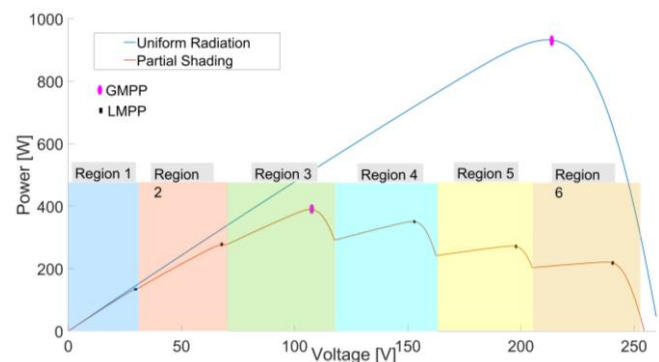


Figure 2. P-V graph resulting from uniform radiation and PSC in the PV system.

3.1. 0.8V_{oc} MPPT Method

While many traditional methods can be effective in the case of uniform sunlight, different MPPT algorithms need to be developed in PV systems operating under PSC. The 0.8V_{oc} value is used to obtain the MPP using the open circuit voltage of the PV array when the panels operate under uniform radiation. When the PSC is examined, it is noted in Figure 2 that MPP has formed in 6 different regions in the system where 6 panels are connected in series. In this technique, the coefficient of 0.8 is not definite in every application. However, it is seen that a value close to this is used in applications. Knowing the maximum power in each system is related to both the accuracy of the panel data and whether the coefficient used finds the definite value of the MPP. In PV systems operating under PSC, as the number of serial panels increases, the voltage of each panel is added and MPP is found in each region. For example, while the panel open circuit voltage in Region 1 is 43.5V, the voltage value at which the maximum power occurs is determined as 35.3V. In the 2nd region, while the open circuit voltage is 87V, the voltage value at which the maximum power is generated is found to be 69.6.

These voltage values are calculated for all regions and operation is provided at these voltages for each region respectively. The maximum power value obtained in each region is calculated. Finally, the voltage of the region where the largest maximum power is generated constitutes the reference voltage. The system continues to operate at this voltage with the help of a controller.

3.2. Proposed MPPT Algorithm

First, the reference voltage (V_{ref}) signal is generated between 1 and 220V to increase linearly for 1.5s. The DC line input at the inverter input is approximately determined using the speed and current information of the motor. The PI controller output generates the duty cycle for switching the ZETA converter. Since the inverter DC line voltage and duty cycle are sampled and known at the same time, the converter input voltage and therefore the PV system output voltage are estimated from the ZETA DC-DC converter output voltage

equation. As the reference voltage increases, the amount of change in the motor voltage and the amount of change in the mechanical power of the motor (ΔV_m and ΔP_{mech}) are calculated.

When $|\Delta V_m| < 0.001$ & $|\Delta P_{mech}| < 0.001$ & $V_m > 50$ condition is met, mechanical power and duty periods are sampled. When the $V_{ref} > V_{m,nom} * 0.85$ condition is met, Dint>0 becomes and the second stage is passed. In the second stage, the motor's back emf and current are checked to ensure that the motor's speed reaches its maximum.

The proposed algorithm consists of two stages. In the first stage, the PV system voltage at the MPP is estimated and this is an approximate value. Because the motor, inverter and DC-DC converter efficiencies are not taken into account. In the second stage, an improved form of the P&O algorithm that uses motor current and speed values is used to find the exact MPP point in the estimated voltage region. The flow chart of the proposed algorithm is given in Figure 3.

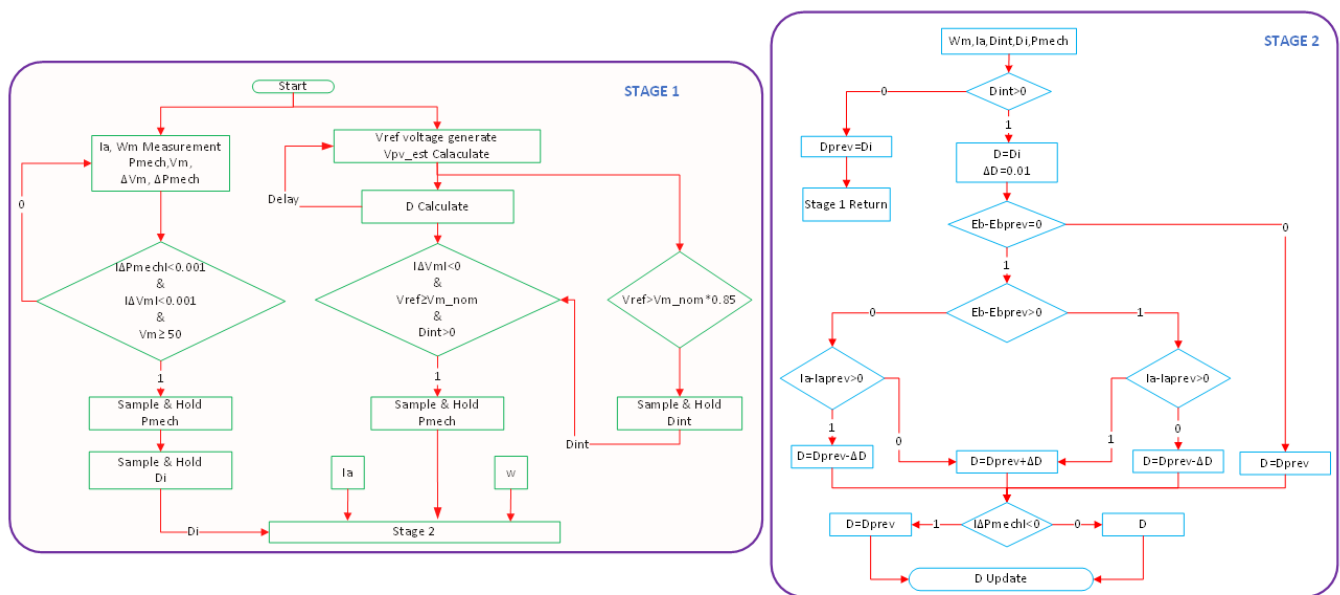


Figure 3. Flow chart of the proposed MPPT algorithm.

4. SIMULATION OF THE PROPOSED ALGORITHM

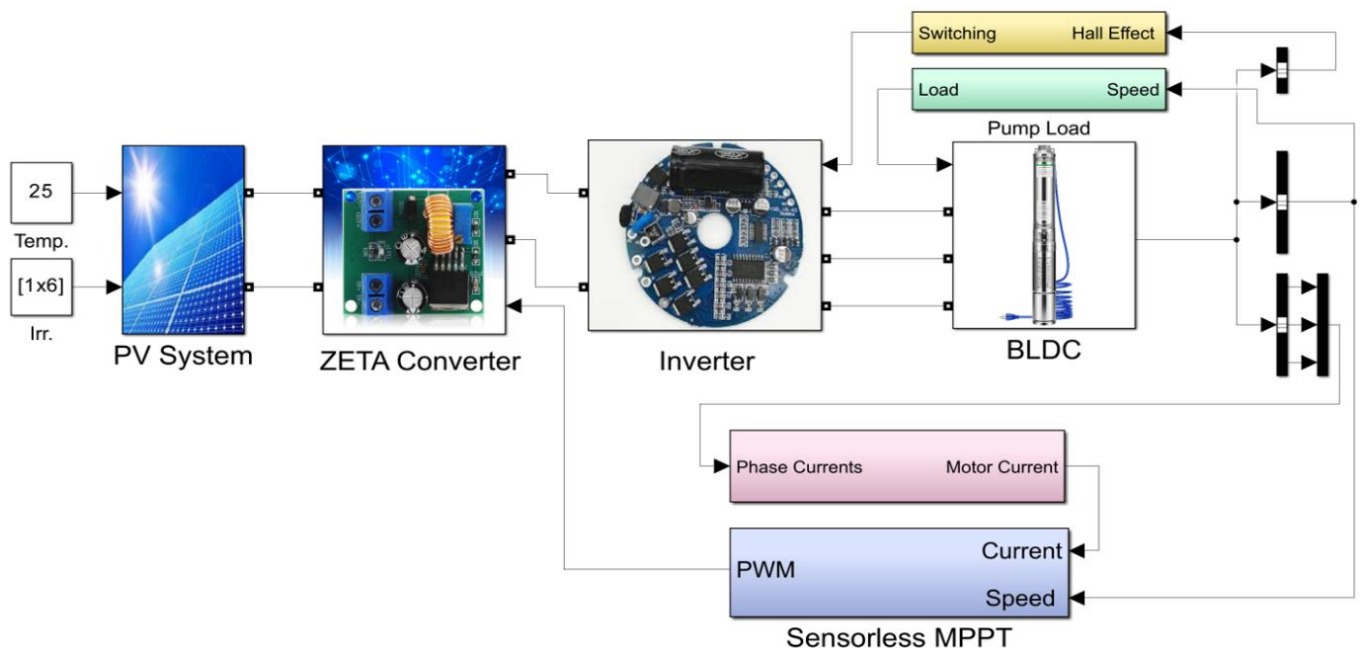


Figure 4. MATLAB/Simulink simulation of the PV pump system

In this study, 6 series-connected panels, each of which can produce 155W power at 35.3V, were used. While the total output power of the PV system is 930W, this power is produced at approximately 212V voltage. Here, the nominal power of the motor selected for the load is 746W and its nominal speed is 2000 rpm. ZETA DC-DC converter was used to run the MPPT algorithm. Figure 4 shows the PV pump system created in the MATLAB/Simulink environment.

The proposed algorithm and 0.8Voc technique were tested for four different atmospheric conditions where the PSCs were formed. The P-V graphs of the PSCs used for testing are shown in Figure 5.

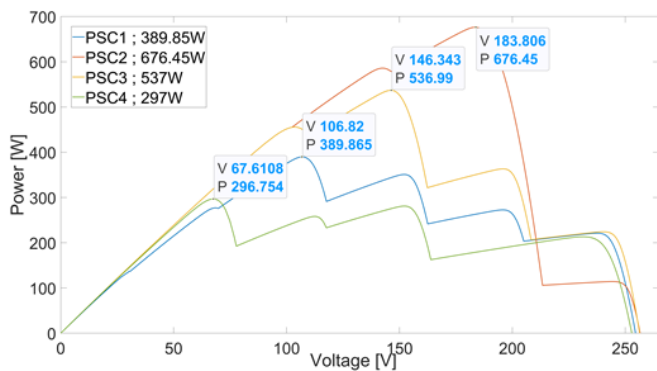


Figure 5. Maximum powers obtained from PV systems operating under four different PSCs

Figure 6 shows the power graphs obtained using 0.8Voc and the proposed MPPT techniques for four different PSCs. When Figure 6 is examined in detail, a much faster MPPT capture time is seen for all atmospheric conditions in the 0.8Voc method.

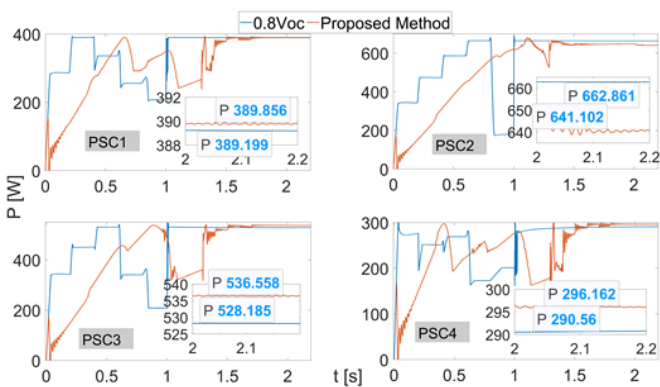


Figure 6. Power obtained using 0.8Voc and proposed MPPT methods in four different PSC

In the case of PSC1, there is a very small power difference between the proposed algorithm and the 0.8Voc method, but the proposed method was able to produce more power. The efficiency of the proposed method is greater than 99.9% and almost completely captures the maximum power. In the case of PSC2, the proposed algorithm was able to produce less power than the 0.8Voc method. The efficiency of the proposed method is approximately 95%. Although this efficiency value seems low, it is sufficient for many applications. The power value obtained from the PV pump system operating under PSC3 conditions is seen as 536.514W. In this case, the power value that can be obtained from the PV system is known as

537W. The efficiency of the MPPT algorithm in the steady state is calculated as 99.9%. The obtained value is higher than the 0.8Voc value. When the PSC4 case is examined, the power value obtained from the PV system is 296.16W. The maximum power value that can be obtained from the PV system is known as 297W. The steady state efficiency of the MPPT algorithm was determined as 99.7%.

Figure 7 shows the PV system voltage and current values obtained using 0.8Voc and the proposed method for four different atmospheric conditions.

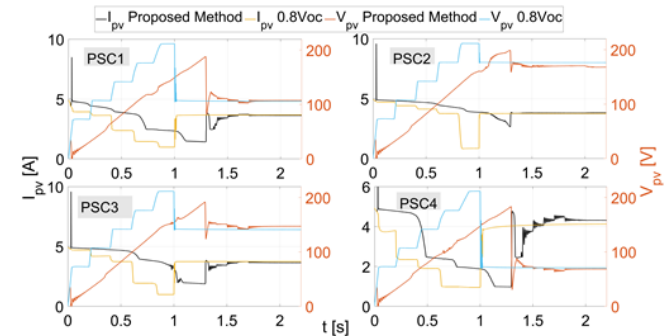


Figure 7. Power values obtained with 0.8Voc and proposed MPPT methods

Figure 8 shows the motor speeds obtained for both methods under all atmospheric conditions.

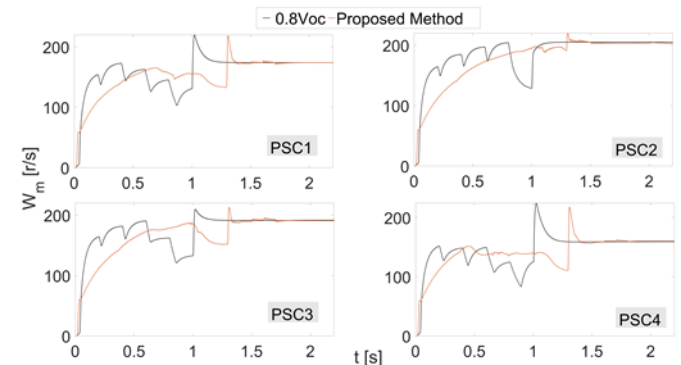


Figure 8. Speed of the BLDC motor obtained with 0.8Voc and proposed MPPT methods

Figure 9 shows the duty periods obtained using 0.8Voc and proposed method in all atmospheric conditions.

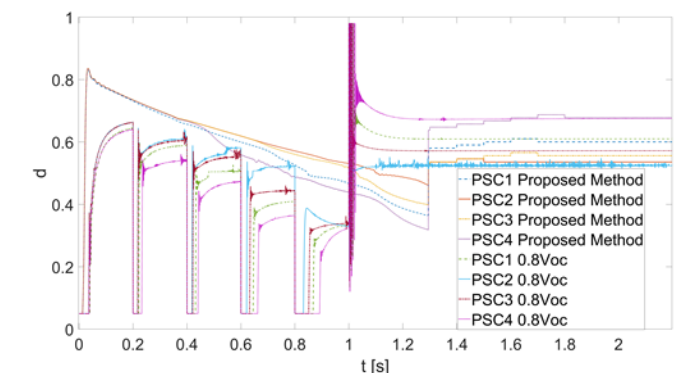


Figure 9. Duty periods obtained with 0.8Voc and proposed MPPT methods

When the proposed method is used, there is a very small decrease in motor speed in PSC2. Because the power transferred to the motor is approximately 20W less than the 0.8Voc method. The low maximum power value in PSC2 may

be due to the synchronization disorder between the measurement value and the processing time. In order to both increase the speed of the proposed method and to prevent the negative situation that occurs in PSC2, the P&O algorithm in the second stage can be modified to approach the maximum power with smaller changes. In addition, a direct duty cycle scanning algorithm can be developed instead of the voltage scanning algorithm seen in the first stage. In future studies, research will be continued for all scenarios.

In the 0.8Voc technique, if the coefficient of 0.8, which is the coefficient to be multiplied by the open circuit voltage, can be precisely determined to obtain the maximum power, faster results can be obtained. However, this requires excessive dependence on panel data. The data of the panels must be known perfectly. However, there is no dependence on panel data in the two-stage proposed algorithm. In addition, it does not require the measurement of current-voltage data of the PV system and environmental variables. The success of the proposed algorithm has been superior except for the PSC2 case. The most important advantage of the proposed algorithm is that it is both a sensorless method and superior to the traditional 0.8Voc method in many different cases. On the other hand, the operating speed of the algorithm is slower than the 0.8Voc method.

The proposed algorithm can be easily implemented with cheap microcontrollers due to its simple structure. Since it does not use the current and voltage values of the PV system, sensor costs are reduced. Thus, the initial installation cost of the system is reduced. In addition, since it does not need panel data, it can be easily integrated into different PV systems.

5. CONCLUSION

In this study, a simulation study of a PV pump system using BLDC motor and ZETA DC-DC converters was carried out. When operating under PSC in PV pump systems, conventional MPPT techniques are insufficient. At the same time, conventional methods measure one or more of the environment variables along with the current and voltage information of the PV system in addition to the motor current and speed information. Some methods such as 0.8Voc can only achieve superior success when they know the panel data perfectly. On the other hand, panel data may change over time depending on the operation and environment variables.

In this study, a two-stage MPPT technique is proposed. In this technique, k coefficient, current and speed information of the motor are used. No data such as current and voltage of the PV system is used in the proposed algorithm. In the first stage, the region where maximum power occurs is estimated approximately. In the second stage, the MPP point is found exactly. The proposed algorithm is tested under four different PSCs in MATLAB/Simulink environment. The proposed algorithm is compared with the 0.8Voc method under these different conditions. Except for the atmospheric condition of PSC2, the proposed algorithm is superior. However, it is seen that the speed of the proposed 0.8Voc method is higher than the proposed algorithm. The proposed sensorless MPPT technique operated the PV pump system with high efficiency as 99.9% in the case of PSC1, 95% in the case of PSC2, 99.9% in the case of PSC3 and 99.7% in the case of PSC4.

In future studies, the scanning speed of the algorithm will be increased by choosing smart methods in the first or second stage. In addition, different situations such as PSC2 will be

examined and the algorithm will be made to work with higher efficiency. On the other hand, studies will continue to operate the system with high efficiency by measuring the speed of the motor without a sensor.

ACKNOWLEDGEMENT

This article was written using the data obtained from the master's thesis titled "Development of sensorless maximum power point tracking algorithm for solar pump systems" prepared at Firat University, Institute of Science. (Supervisor: Assoc. Prof. Resat CELIKEL)

REFERENCES

- [1] Gündođdu, A. (2022). System identification based ARV-MPPT technique for PV systems under variable atmospheric conditions. *IEEE Access*, 10, 51325-51342. W.-K. Chen, Linear Networks and Systems. Belmont, CA, USA: Wadsworth, 1993, pp. 123-135.
- [2] Liu, L., Meng, X., & Liu, C. (2016). A review of maximum power point tracking methods of PV power system at uniform and partial shading. *Renewable and Sustainable Energy Reviews*, 53, 1500-1507.
- [3] Ahmed, J., & Salam, Z. (2015). An improved perturb and observe (P&O) maximum power point tracking (MPPT) algorithm for higher efficiency. *Applied Energy*, 150, 97-108.
- [4] J. Ahmed and Z. Salam, "A modified P&O maximum power point tracking method with reduced steady-state oscillation and improved tracking efficiency," *IEEE Trans. Sustain. Energy*, vol. 7, no. 4, pp. 1506-1515, Oct. 2016.
- [5] A. Loukrez, M. Haddadi, and S. Messalti, "Simulation and experimental design of a new advanced variable step size incremental conductance MPPT algorithm for PV systems," *ISA Trans.*, vol. 62, pp. 30-38, May 2016.
- [6] Bařođlu, M. E. (2018). An improved 0.8 Voc model based GMPPT technique for module level photovoltaic power optimizers. *IEEE Transactions on Industry Applications*, 55(2), 1913-1921.
- [7] Bi, Z., Ma, J., Man, K. L., Smith, J. S., Yue, Y., & Wen, H. (2020). An Enhanced 0.8Voc-Model-Based Global Maximum Power Point Tracking Method for Photovoltaic Systems. *IEEE Transactions on Industry Applications*, 56(6), 6825-6834.
- [8] Kesilmiř, Z., Karabacak, M. A., & Aksoy, M. (2020). A novel MPPT method based on inflection voltages. *Journal of Cleaner Production*, 266, 121473.
- [9] Li, X., Zhu, Y., Wen, H., Du, Y., & Xiao, W. (2022). Reference-voltage-line-aided power incremental algorithm for photovoltaic GMPPT and partial shading detection. *IEEE Transactions on Sustainable Energy*, 13(3), 1756-1770.
- [10] Celikel, R., Yilmaz, M., & Gundogdu, A. (2022). A voltage scanning-based MPPT method for PV power systems under complex partial shading conditions. *Renewable Energy*, 184, 361-373.
- [11] Aquib, M., Jain, S., & Ghosh, S. (2022). A technique for tracking the global peak of PV arrays during partially shaded conditions using the detection of current source and voltage source regions of I-V curves. *IEEE Journal of Emerging and Selected Topics in Industrial Electronics*, 3(4), 1096-1105.
- [12] Ye, S. P., Liu, Y. H., Pai, H. Y., Sangwongwanich, A., & Blaabjerg, F. (2023). A novel ANN-based GMPPT method for PV systems under complex partial shading conditions. *IEEE Transactions on Sustainable Energy*, 15(1), 328-338.
- [13] Anh, T. V., Trieu, T. N., Nghi, P. V. H., & Van Hien, B. (2024). Fast and accurate GMPPT based on modified P&O algorithm. *IEEE Access*.
- [14] Renaudineau, H., Donatantonio, F., Fontchastagner, J., Petrone, G., Spagnuolo, G., Martin, J. P., & Pierfederici, S. (2014). A PSO-based global MPPT technique for distributed PV power generation. *IEEE Transactions on Industrial Electronics*, 62(2), 1047-1058.
- [15] Hussaian Basha, C. H., Bansal, V., Rani, C., Brisilla, R. M., & Odofin, S. (2020). Development of cuckoo search MPPT algorithm for partially shaded solar PV SEPIC converter. In *Soft Computing for Problem Solving: SocProS 2018, Volume 1* (pp. 727-736). Springer Singapore.
- [16] Mohanty, S., Subudhi, B., & Ray, P. K. (2015). A new MPPT design using grey wolf optimization technique for photovoltaic system under partial shading conditions. *IEEE Transactions on Sustainable Energy*, 7(1), 181-188.

- [17] Kumar, C. S., & Rao, R. S. (2016). A novel global MPP tracking of photovoltaic system based on whale optimization algorithm. *International Journal of Renewable Energy Development*, 5(3), 225-232.
- [18] Kumar, R., & Singh, B. (2019). Solar PV powered-sensorless BLDC motor driven water pump. *IET Renewable Power Generation*, 13(3), 389-398.
- [19] Kumar, R., & Singh, B. (2016). BLDC motor-driven solar PV array-fed water pumping system employing zeta converter. *IEEE Transactions on Industry Applications*, 52(3), 2315-2322.
- [20] Mudlapur, A., Ramana, V. V., Damodaran, R. V., Balasubramanian, V., & Mishra, S. (2018). Effect of partial shading on PV fed induction motor water pumping systems. *IEEE Transactions on Energy Conversion*, 34(1), 530-539.
- [21] Ammar, A., Hamraoui, K., Belguellaoui, M., & Kheldoun, A. (2022). Performance enhancement of photovoltaic water pumping system based on BLDC Motor under partial shading condition. *Engineering Proceedings*, 14(1), 22.
- [22] Celikel, R., Boztas, G., & Aydogmus, O. (2022). A system identification-based MPPT algorithm for solar photovoltaic pumping system under partial shading conditions. *Energy Sources, Part A: Recovery, Utilization, and Environmental Effects*, 44(2), 5199-5214.
- [23] Jha, K. K., & Anwar, M. N. (2019, September). Solar photovoltaic based brushless DC motor driven water pumping system using PSO-MPPT algorithm. In *2019 54th International Universities Power Engineering Conference (UPEC)* (pp. 1-6). IEEE.
- [24] Akkaya, R., Kulaksız, A. A., & Aydoğdu, Ö. (2007). DSP implementation of a PV system with GA-MLP-NN based MPPT controller supplying BLDC motor drive. *Energy Conversion and Management*, 48(1), 210-218.
- [25] Oliver, J. S., David, P. W., Balachandran, P. K., & Mihet-Popa, L. (2022). Analysis of grid-interactive PV-fed BLDC pump using optimized MPPT in DC-DC converters. *Sustainability*, 14(12), 7205.

BIOGRAPHIES

Yunus ATAGÜN was born in 1993. He received the B.S. degrees in mechatronic engineering from the University of Firat, Elazig, Turkey. He is studying for his master's degree in mechatronic engineering at Firat University. His research interests include renewable energy and MPPT.

Reşat ÇELİKEL was born in 1980. He received the B.S., M.S., and Ph.D. degrees from Firat University, Elazig, Turkey. He has been an Associate Professor with Firat University. His current research interests include BLDC motors, flywheel energy storage, FPGA, renewable energy, and MPPT.



Research Article

Case Study on Energy Reliability Applications and Mathematical Models in The Distribution Network

Mehmet Rida Tur^{1*}

^{1*} Department of Electrical and Electronics Engineering, Faculty of Engineering, Batman University, Turkey, (mrida.tur@batman.edu.tr)

ARTICLE INFO

Received: Dec., 25. 2023

Revised: Jun., 24. 2024

Accepted: Dec, 11. 2024

Keywords:

Power Systems

Distribution Network

Reliability

Mathematical Models

Corresponding author: *M. Rida Tur*

ISSN: 2536-5010 / e-ISSN: 2536-5134

DOI: <https://doi.org/10.36222/ejt.1409607>

ABSTRACT

This study focuses on the reliability of power systems, examining it from technical, economic, and decision-making perspectives. Reliability is a crucial concept in assessing the ability of an energy system to operate smoothly and provide uninterrupted energy supply. First and foremost, it is pointed out that the majority of failures in power systems occur in distribution systems. This involves examining how customers might react to energy interruptions and the economic consequences of those reactions. At the component level, degradation models have been introduced to scrutinize reliability in greater detail. These models elucidate how components may degrade during system operation and how this degradation affects reliability. In conclusion, this study underscores the significance of integrating new technologies and renewable energy sources into energy systems. Additionally, it asserts that reliability and energy sustainability are two fundamental pillars for societal progress. As a result, the reliability and sustainability of energy systems hold critical importance in meeting the energy needs of societies and shaping the future of the energy sector.

1. INTRODUCTION

Energy planning is the process of developing long-term policies with the aim of guiding the future of the local, regional, or even global energy system. Globalization, rapid population growth, and the industrialization efforts of countries have led to a significant increase in the demand for energy and natural resources. The International Energy Agency predicts that the world's primary energy demand will increase by 40% between 2020 and 2030. This translates to an annual average demand growth rate of approximately 1.5%. Research indicates that this trend will take the world's primary energy demand from 12 billion Tons of Equivalent Petroleum in 2020 to 16.8 billion TEP by 2030.

Energy production sources are classified into primary energy sources and renewable energy sources. In primary energy sources, hydropower is related to water energy, thermal energy is associated with coal, oil, and gas, and nuclear energy refers to nuclear power. Renewable energy sources can also be considered as alternative energy sources and are exemplified as follows: wind, solar, geothermal, hydroelectric, biomass, wave power, and solar panels. It's important to note that alternative energy sources cannot fully replace primary energy sources. This is because alternative energy sources may fail to fulfill one of the most critical criteria of primary energy sources, which is "continuity."

Power system reliability primarily focuses on addressing issues related to service interruptions and energy loss. It is often defined as a target, particularly considering indicators that are directly relevant to customers. Typical reliability indicators for energy service providers include SAIFI, SAIDI, and CAIDI. Over time, these indicators have become standardized measures for assessing the reliability of electrical systems and are widely used in many publications. Recent studies conducted by [1] have identified reliability sub-criteria within decision-making features and presented an optimal model for a smart grid. These studies have gained popularity through applications in the field of power system reliability [2, 3]. One commonly used technique to optimize and manage power system reliability is reliability-centered maintenance (RCM). In many publications, it has been emphasized that in many cases involving multi-component systems, maintenance operations can either occur too early and have no impact on the system or occur too late and require corrective maintenance. This also addresses the provision of differentiated reliability services to customers with different reliability requirements. Recent publications have highlighted the importance of integrating reliability characteristics for maintenance operations, especially in scenarios involving deteriorating systems and components [4].

In addition, there is a need to improve the existing grid infrastructure and establish new transmission line facilities to reliably meet the increasing demand for electrical energy.

Electricity transmission systems typically form the backbone of interconnected power systems and operate at high voltage levels [5, 6]. The planning of electricity transmission systems aims to ensure grid security at the minimum cost. This planning includes long-term, medium-term, and short-term technical and economic grid analyses based on the growing demand [7]. Commonly, analysis tools such as load flow analysis, short circuit analysis, harmonic and flicker analysis, dynamic analysis, grounding, and protection coordination analysis are used to determine the operating conditions of transmission facilities [8]. Simulation studies have been employed in the literature to examine the impact of power electronics-based Flexible AC Transmission System (FACTS) devices such as STATCOM and SVC on voltage stability [9]. The effect of phase-shifting transformers on static voltage stability and the usability of On-Load Tap Changers (OLTC) transformers for voltage control have been evaluated [10, 11]. Voltage variations at busbars before and after the commissioning of series capacitors on a transmission line have been analyzed [12].

Voltage collapse issues in power systems have been analyzed using multi-layer sensor-based artificial neural networks [13]. Methods used to compensate for voltage disturbances in power systems have been explained. The effects of wind and solar power plants on voltage stability in the power system have been studied [14, 15]. Voltage collapse problems have been compared under different scenarios using Matlab and DigSilent programs [16].

In this study, the impact of changes in active power and reactive power, transmission line lengths, and series capacitor applications on voltage stability in the power system have been examined. Effective comparisons have been made based on the modeling of actual grid parameters in the DigSilent program.

2. ELECTRICAL POWER SYSTEM RELIABILITY ASSESSMENT AND INDICES

The reliability of electrical power systems is of vital importance in ensuring uninterrupted electricity supply to end-users. Reliability assessment helps identify potential risks and failures that can affect the overall performance of the system. It involves evaluating various components of the power system, including generators, transmission lines, transformers, and distribution networks. One of the primary reasons for conducting reliability assessment is to ensure that the system can withstand unexpected events such as natural disasters, equipment failures, or human errors. Engineers can identify weak points by assessing the system's reliability and develop strategies to mitigate them before they lead to significant disruptions. Various methods, including probabilistic and deterministic approaches, can be used to assess the reliability of electrical power systems. Probability-based methods take into account various factors, including weather models, human behavior, and equipment failures, while deterministic methods rely on specific rules and regulations. In conclusion, reliability assessment is critical to ensuring the smooth operation of electrical power systems. By identifying potential risks and developing measures to mitigate them, it helps provide continuous and reliable power supply to end-users [17].

Reliability in power systems is a crucial aspect, particularly concerning the uninterrupted supply of electricity to end consumers. Reliability indices are used to evaluate the performance and effectiveness of power systems in achieving

this goal. In this article, we will explore the world of reliability indices in power systems. One of the most important reliability indices is the System Average Interruption Duration Index (SAIDI). This index measures the average duration of electricity interruptions per customer in a year. Another significant index is the System Average Interruption Frequency Index (SAIFI), which determines the frequency of electricity interruptions per customer in a year. Other noteworthy indices include the Momentary Average Interruption Frequency Index (MAIFI), which measures the number of momentary interruptions in power supply per customer, and the Customer Average Interruption Duration Index (CAIDI), which determines the average time for electricity to be restored after an interruption.

Reliability indices are critical for power services because they help identify problematic areas and work towards improving their performance. By monitoring and enhancing these indices, electricity distribution companies can provide more reliable and uninterrupted power supply to their customers. In conclusion, power system reliability is of utmost importance, and reliability indices are just one of the many ways in which energy organizations measure their performance and strive for better reliability [18].

2.1. Modeling Techniques for Power System Reliability Analysis

Reliability analysis of power systems is crucial to ensure continuous electricity supply to consumers. One of the most effective methods for analyzing power system reliability is through modeling techniques. These techniques enable engineers to simulate various scenarios and identify potential issues that can impact system reliability. One commonly used modeling technique is Monte Carlo simulation. This approach involves randomly selecting values for various parameters within the model, such as failure rates and repair times, and running the simulation thousands of times to determine the probability of different outcomes. Another technique is the Markov model, which uses a series of states and transitions to represent the system's behavior over time. Using data that reflects real-world conditions is essential to obtaining accurate results. This includes historical data on equipment failures, weather patterns, and other relevant variables. Additionally, considering the impact of external factors like natural disasters and human error is crucial.

Engineers can gain a better understanding of the system's behavior and identify potential areas for improvement by using modeling techniques for power system reliability analysis. With this information, electricity distribution companies can make informed decisions about maintenance programs, system upgrades, and other measures to increase reliability and reduce downtime.

In conclusion, power system reliability is highly important, and modeling techniques are valuable tools for assessing and improving reliability [19].

2.2. Maintenance Strategies to Improve Power System Reliability

Power systems are integral to any industrial or residential operation, and like all machinery, they require regular maintenance to ensure their reliability and efficiency. In this article, we will discuss some of the best maintenance strategies

that can help improve power system reliability. First and foremost, regular inspections and checks should be conducted to identify potential issues before they become serious problems. This includes monitoring voltage levels, assessing the condition of cables, and checking for signs of wear or damage. Secondly, implementing a preventive maintenance program can help minimize downtime and prevent unexpected power interruptions. This program may include tasks such as cleaning, lubrication, and tightening loose connections. Investing in modern technologies like sensors and remote monitoring systems is another strategy that can help detect potential problems before they escalate. Lastly, training employees in proper handling and maintenance procedures can reduce the risk of human error and contribute to the long-term reliability of the power system. In conclusion, prioritizing regular maintenance using these strategies can lead to enhanced power system reliability, reduced downtime, and increased productivity. Ensuring the optimal performance of the system is crucial for overall operations, making regular maintenance a top priority [20].

2.3. Mathematical Modeling in Transmission and Distribution Systems

In power systems, the fundamental objective is to efficiently deliver electrical energy from generation sources to consumption points. This electrical transmission is typically accomplished through high-voltage transmission lines, which play a critical role in the process. The equivalent circuit illustrated in Figure 1 serves as a mathematical representation of a transmission line, a vital component of power systems [21]. This circuit comprises various elements:

- **VS (Voltage Source):** This represents the voltage supplied to the transmission line, usually originating from power plants or distribution centers.
- **R (Resistance):** It signifies the resistance of the transmission line, which can lead to energy losses, particularly over longer distances.
- **XL (Inductive Reactance):** This component depicts the inductive reactance in the transmission line, representing its interaction with inductive loads.
- **XC (Capacitive Reactance):** XC represents the capacitive reactance in the transmission line, symbolizing its interaction with capacitive loads.
- **VR (Receiver Voltage):** VR denotes the voltage at the receiver end of the transmission line.

The relationships between these components are expressed mathematically as follows:

- **Total Impedance (Z) Relationship:** $Z = R + jX$ (Here, 'j' represents the complex unit.)
- **Active Power (P) Relationship:** $P = \frac{|VR|^2}{R} - \frac{|VS|^2}{R}$
- **Reactive Power (Q) Relationship:** $Q = \frac{|VR|^2}{X} - \frac{|VS|^2}{X}$
- **Phase Angle (δ) Relationship:** $\delta = \tan^{-1} \left(\frac{|VR| \sin \delta - |VS| \sin 0}{|VR| \cos \delta - |VS| \cos 0} \right)$

These equations mathematically describe the behavior of transmission lines during the transmission of electrical energy.

These mathematical models are used in the analysis, design, and operation of power systems. Electrical engineers employ these models to optimize the performance of power systems and ensure the efficient transmission of electrical power [22].

3. MATERIAL AND METHOD

In power systems, the primary purpose of transmission lines is to deliver the generated electricity to consumers. The equivalent circuit of an electrical transmission line between two buses is depicted in Figure 1 [23, 24]. In this configuration, it represents VS as the source voltage, R as resistance, XL as inductive reactance, XC as capacitive reactance, and VR as the receiver voltage. The impedance and active-reactive power relationships associated with this electrical transmission line are provided in Equations. In these equations, Z represents the total impedance, P represents active power, Q represents reactive power, and δ represents the phase angle between the source and receiver voltages.

Expanding the existing distribution network is a comprehensive problem that involves making strategic decisions such as whether to add new lines, whether existing lines need to be upgraded, whether new transformers are needed, where to install new transformers, what capacity the transformers should have, whether old transformers need strengthening, where to install various types of distributed generation sources, and how much electricity from which sources should be supplied to specific consumption points. Distribution Network Expansion Problem (DNEP) is a complex problem, especially in a NP-Hard structure, and integrating distributed generation further complicates the problem [25]. Therefore, developing efficient mathematical models is crucial to achieve the best (optimal) results in a shorter time.

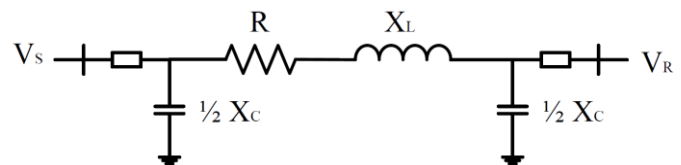


Figure 1. Equivalent circuit of an electrical transmission line between two busbars

The most commonly used network structure in distribution networks is the radial network [26]. An example of a radial network structure is provided in Figure 2. Radial networks, also known as branched networks, have a tree-like structure and do not allow closed loops. In this type of network, customers receive energy from a single distribution center and line. The radial network structure is often preferred because it is cost-effective and simple.

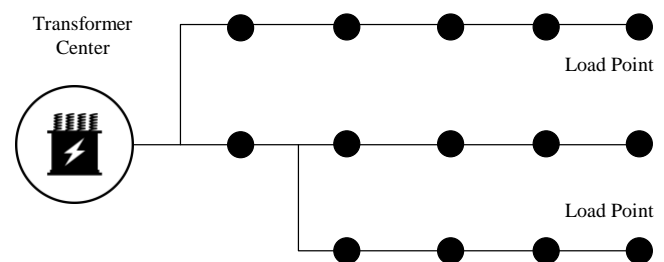


Figure 2. Radial network example as a Distribution Network Model

The choice of conductor material, length, and topology of transmission lines used in the construction of transmission lines can significantly impact the power system. Their reactive power characteristics, XC for capacitance, and XL for inductance, depend on the design. When a transmission line is loaded below its normal rating, it behaves capacitive, while when loaded above its normal rating, it behaves inductively. Using the equations, it is possible to determine the direction and magnitude of active-reactive power flow between two buses. The length and structure of the transmission line affect its capacity to carry both active and reactive power. Furthermore, changes in the quantity of active and reactive power can lead to variations in voltage levels and phase angles at the buses. In order to establish a radial structure, there should be one input for each demand node, and for demand nodes with no requests (if any), there should be at most one input. Constraints for this situation can be formulated as follows eq. 1 and eq. 2 [27].

$$\sum_{l \in L} \sum_{i \in \Omega} \sum_{k \in K} y_{ijkt}^t = 1 \forall j \in \Omega, \forall t \in T \quad (1)$$

$$\sum_{l \in L} \sum_{i \in \Omega} \sum_{k \in K} y_{ijkt}^t \leq 1 \forall j \in \Omega, \forall t \in T \quad (2)$$

When these constraints are considered alongside the network flow constraint, they are sufficient to establish a classic radial configuration. Due to the flow constraint, nodes require energy input, and consequently, they will connect to the single energy point, which is the transformer center. However, these constraints alone are not sufficient to ensure radially. When distributed generation sources are installed, nodes can create a disconnected loop in the network to receive energy from that source, and the connection to the transformer center may not occur. An example of a network that could result when the above constraints are applied is provided in the diagram. In this diagram, the Distributed Generation at each node is providing energy to the node. The input constraints for each node have been met, and a disconnected network segment has formed, not connecting to the transformer center. The distribution network can be expressed as a rooted tree with the transformer center considered as the root node [28]. When there are multiple transformer centers, it forms a forest structure. The formulation for the generalization of the Steiner tree problem is provided in constraints numbered in eq. 3-6 [29]. The network, denoted as G, is composed of the set of nodes V and edges E (G(V, E)). In the network, r represents the root node, and j represents the other nodes ($j \in V \setminus \{r\}$).

$$S_j = \begin{cases} 1, & \text{if } j \text{ point on tree} \\ 0, & \text{dd} \end{cases} \text{ and } S_r = 1 \text{ or } S_i \in \{0,1\} \quad (3)$$

$$X_e = \begin{cases} 1, & \text{if } e \text{ line on tree} \\ 0, & \text{dd} \end{cases} \text{ and } X_e \in \{0,1\} \quad (4)$$

$$\sum_{e \in E(U)} X_e \leq \sum_{i \in \frac{U}{K}} S_i \text{ for all } U \in V \text{ and } k \in U \quad (5)$$

In our problem, since there is no potential for all nodes in the network to be interconnected, the set $E(U)$ can be selected from the lines that can form sub cycles. This is because we have prior knowledge of the existing and potential lines in the network we are interested in. Therefore, unnecessary

calculations for lines that can never occur are avoided. Accurately determining the set $E(U)$ is crucial for reaching the correct result quickly. Taking into account certain characteristics of the problem and the model will greatly facilitate the determination of the set $E(U)$.

3.1. Key Factors Affecting Reliability of Power Systems: The Role of Transmission Lines and Network Design

In power systems, the primary purpose of transmission lines is to deliver generated electricity to consumers. The equivalent circuit of transmission lines is represented by the source voltage (VS), resistance (R), inductive reactance (XL), capacitive reactance (XC), and receiver voltage (VR). The total impedance (Z) of transmission lines and the relationships between active and reactive power are critical factors influencing the reliability of the system.

The Distribution Network Expansion Problem (DNEP) involves strategic decisions such as adding new lines, upgrading existing lines, and installing new transformers. The integration of distributed generation complicates this problem further. Developing effective mathematical models is crucial for achieving optimal results in a shorter time frame.

The most common structure in distribution networks is the radial network, which does not allow closed loops. In these networks, customers receive energy from a single distribution center. The radial structure is preferred due to its cost-effectiveness and simplicity.

The choice of materials, length, and topology of transmission lines significantly impacts the performance of the power system. When loaded below their normal rating, transmission lines exhibit capacitive behavior, while they behave inductively when loaded above their normal rating. Determining active and reactive power flows is essential for understanding variations in voltage levels and phase angles.

Two scenario studies investigate the effects of increases in active and reactive power consumption on network voltages:

Increase in Active Power Consumption: An increase in active power consumption negatively affects the voltage profile of the entire system.

Increase in Reactive Power Consumption: An increase in reactive power consumption has a more pronounced effect on the system's voltage stability, leading to lower voltage levels.

These studies provide valuable data for implementing necessary measures to enhance the reliability of the power system. In particular, the management of reactive power and the optimization of network structure are critical for improving the overall stability of the system.

3.2. Transmission Network Model: Single-Line Diagram

In this section, a portion of the existing electrical transmission system is discussed. The operating voltage in the created power system ranges from 380 kV to 34.5 kV. External grid connections at 380 kV are defined as external networks in the modeled system [30]. The power system consists of 5 buses, 3 transformers, and 2 transmission lines. The single-line diagram created in the DigSilent program is shown in Figure 3. The physical structure of the electrical transmission lines is overhead, and the cross-sectional areas of the conductors used may vary. Power system and model the transmission and

distribution networks within this system using the DigSilent program. Please note that the specifics of the transmission lines, transformers, and buses in the system can vary significantly based on the actual configuration and requirements of the power system being modeled.

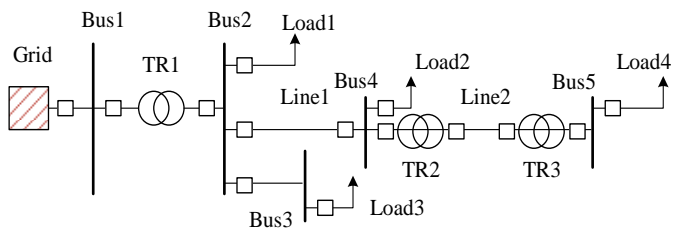


Figure 3. Single line diagram of the network modeled in the DigSilent program

In this section, simulation results using the DigSilent program are examined for several factors affecting voltage stability in a power system. Initially, the normal state of the network was determined. Subsequently, different scenario studies were configured by making changes to the network while considering the normal network state. Scenario Study-1 investigated the impact of an increase in active power consumption on bus voltages, while Scenario Study-2 examined the effect of an increase in reactive power consumption on the bus voltages on the consumer side.

3.3. Case Study-1: Increase in Active Power Consumption

In the normal network state, Bus 6 operates at 34.5 kV voltage level with a 10 MW load. To determine the effect of only the active power, the active power of Load 4 was increased while keeping the reactive power constant. Table 1 illustrates the changes in bus voltages in per-unit values corresponding to the increased active power values. Figure 3 shows the active power-voltage curve. It is observed that an increase in active power consumption leads to a decrease in bus voltages. An increase in active power consumption at a single point in the power system alters the voltage profile of the entire system. Specifically, the bus where consumption has increased is more affected. Table 1 presents the loading capacities of the lines resulting from the increase in active power, and Figure 4 shows the variation curves. For example, when the active power is 50 MW, the loading capacity of Line 2 has increased by approximately 7%. An increase in active power consumption has increased the loading capacities of the lines. Additionally, calculations were made based on simulation results for active powers of 10 MW and 50 MW. The results reveal the transmitted active power between Bus 4 and Bus 5, along with the loading capacity of Line 2.

TABLE I. Active power, voltage and line loading values in Case Study-1

Component	Bus 1	Bus 2	Bus 3	Bus 4	Bus 5	Line 1	Line 2
Capacity							
10 MW	1,000	0,996	0,995	0,99	0,98	7,87	32,5
20 MW	1,000	0,995	0,994	0,98	0,98	8,09	35,7
30 MW	1,000	0,995	0,994	0,98	0,98	8,32	39,0
40 MW	1,000	0,994	0,993	0,98	0,98	8,55	42,5
50 MW	1,000	0,993	0,992	0,98	0,97	8,81	46,2

For the case where the active power is 10 MW, the P value is obtained as 10.1MW, while the Loading ratio value is obtained as 10.34 MVA. On the other hand, for the case where the active power is 50 MW, the P value is obtained as 50.4MW, while the loading rate is obtained as 33.45%.

3.4. Case Study-2: Increase in Reactive Power Consumption

In this study, the reactive power consumption at Bus 6 has been increased, and the changes in bus voltages have been examined. Only the effect of reactive power has been considered to determine, assuming active power is constant. Table 2 shows the bus voltages for increasing reactive power values. Figure 5 depicts the reactive power-voltage curve. It is observed that the increase in reactive power consumption leads to a decrease in bus voltages. Especially, the voltage of the bus with higher reactive power consumption is more affected. In Case Study 2, the voltage levels are lower. For example, when the active power at Bus 6 is 50 MW, the bus voltage is 0.89 pu, whereas it drops to 0.65 pu when the active power is 50 MVar. Therefore, the change in reactive power has a greater impact on the system's voltage stability. Additionally, calculations have been made based on simulation results for the cases where reactive power is 10 MVar and 50 MVar. When we examine the transfer of reactive power between Bus 5 and Bus 6, it is seen that the transmitted reactive power values exceed the desired reactive power value. The reason for this is that the increase in reactive power component increases the capacitive reactance losses on the transmission line. For the case of 10 MVar of reactive power, the Q value is obtained as 14.3 MVar. For the case of 50 MVar of reactive power, the Q value is obtained as 79.7 MVar.

TABLE II. Active power, voltage and line loading values in Case Study-1

Component	Bus 1	Bus 2	Bus 3	Bus 4	Bus 5
Capacity					
10 MVar	1,000	0,99	0,99	0,98	0,98
20 MVar	1,000	0,99	0,99	0,98	0,97
30 MVar	1,000	0,99	0,99	0,98	0,96
40 MVar	1,000	0,99	0,98	0,97	0,95
50 MVar	1,000	0,98	0,98	0,97	0,94

The increase in active power leads to a decrease in voltage levels at Bus 6. This drop poses a threat to system reliability, as low voltage levels can adversely affect the operation of electrical equipment and lead to failures. A reliable system must maintain specific voltage ranges.

When the active power reaches 50 MW, the loading capacity of Line 2 increases by 7%. While this indicates an increase in the system's carrying capacity, it must be monitored carefully to avoid overloading. Otherwise, excessive loading can weaken the reliability of the lines and increase the risk of outages.

An increase in reactive power consumption results in a further decline in bus voltages. The drop in voltage at Bus 6 from 0.89 pu to 0.65 pu indicates a disruption in the reactive power balance. Effective reactive power management is critical for voltage stability; poor management can threaten system reliability.

The increase in reactive power transfer raises capacitive reactance losses in transmission lines and leads to exceeding desired values. Such losses can negatively impact overall system reliability and may cause performance issues in the long run.

The effects of both active and reactive power increases on voltage stability play a crucial role in reliability analysis. Careful management of voltage levels and loading capacities is essential for ensuring system reliability. A reliable electrical grid must maintain both active and reactive power balance to minimize the risks of outages and failures.

4. CONCLUSIONS AND SUGGESTIONS

This study aims to examine an existing power system and model the transmission and distribution networks within this system using the DigSilent program. Furthermore, it seeks to investigate the effects of different scenario studies on network voltage. In the context of the scenario analyses conducted, the impacts of active and reactive power increases on voltage stability were initially evaluated. Active power represents the electrical energy generation within the energy system, whereas reactive power is necessary for voltage control and balancing inductive loads. Therefore, the balanced distribution of these two power components is critically important for ensuring voltage stability. Additionally, the influence of transmission line lengths on voltage levels was also examined. Long transmission lines play a crucial role in transporting electrical energy to remote regions, but their length can increase inductive reactance, leading to voltage drops. To address this issue, it is recommended to use series capacitors on long transmission lines or apply transposition procedures to the lines. Series capacitors are used to balance inductive reactance and prevent voltage drops, while transposition balances the inductive effects of the lines, thereby enhancing voltage stability. Lastly, it should be noted that transformer tap settings can be effectively utilized for voltage control, and this study can serve as instructional material in undergraduate education. Transformers are employed to adjust and maintain voltage levels within the energy system, and this study provides a valuable knowledge resource on voltage management in energy systems for students and professionals in the energy sector.

In a normal state, Bus 6 operates at a voltage level of 34.5 kV with a load of 10 MW. When the active power is increased, it is observed that bus voltages decrease, particularly affecting the bus where consumption has increased. For instance, when the active power reaches 50 MW, the loading capacity of Line 2 increases by approximately 7%.

Similarly, when reactive power consumption is increased, a further drop in bus voltages occurs. The voltage at Bus 6 drops from 0.89 pu at 50 MW of active power to 0.65 pu at 50 MVar of reactive power. Reactive power transfer analyses reveal that the transmitted values exceed the desired amounts, attributed to increased capacitive reactance losses in the transmission lines. In conclusion, both active and reactive power increases significantly impact voltage stability.

REFERENCES

- [1] Medjoudj R, Aissani D, Haim KD. (2013). Power customer satisfaction and profitability analysis using multi-criteria decision making methods. *International Journal of Electrical Power and Energy Systems*, 45(1):331-339. DOI: 10.1016/j.ijepes.2012.08.062
- [2] Van Castaren J. (2000), Reliability assessment in electrical power systems: The Weibull-Markov stochastic model. *IEEE Transactions on Industry Applications*. 2000;36(6)
- [3] Medjoudj R, Aissani D, Boubakeur A, Haim KD. (2009), Interruption modeling in electrical power distribution systems using Weibull-Markov model. *Proceedings of the Institution of Mechanical Engineers (IMEchE), Part O: Journal of Risk and Reliability*. 01-06-2009;223:145-157.
- [4] Iberraken F, Medjoudj R, Medjoudj R, Aissani D. (2015), Combining reliability attributes to maintenance policies to improve high-voltage oil circuit breaker performances in the case of competing risks. *Proceedings of the Institution of Mechanical Engineers, Part O: Journal of Risk and Reliability* 2015. DOI:10.1177/1748006X15578572
- [5] Kishore, T.S and Singal, S.K. (2014), Optimal economic planning of power transmission lines: A review, *Renewable and Sustainable Energy Reviews*, vol. 39, pp. 949–974
- [6] Huang, Y. (2014), Electricity distribution network planning considering distributed generation, *KTH School of Electrical Engineering, MSc Thesis*
- [7] Orfanos, G.A. Georgilakis P.A and Hatziaargyriou, N.D, (2013), Transmission expansion planning of systems with increasing wind power integration, *IEEE Transactions on Power Systems*, vol.28, no.2, pp.1355-1362
- [8] IEEE Standard for Interconnecting Distributed Resources with Electric Power Systems, *IEEE Std 1547*, 2003.
- [9] Li, F. Song J. and Wang, M. (2011), A study on Statcom for voltage stability of wind power system, *IEEE International Conference on Mechatronic Science, Electric Engineering and Computer*, 19-22 August, 2011, Jilin, China.
- [10] Ertay, M.M. ve Aydoğmuş Z. (2010), Statcom ile bir enerji iletim sisteminde gerilim kontrolü, *Dumlupınar Üniversitesi Fen Bilimleri Enstitüsü Dergisi*, syf. 91-105, sayı 21.
- [11] Goa C. and Redfern M.A. (2010), A review of voltage control techniques of networks with distributed generations using on-load tap changer transformers, *IEEE 45th International Power Engineering Conference*, pp. 1-6, 31 August-3 September 2010, Cardiff, Wales.
- [12] Aydın, F., Uyaroğlu, Y. ve Yalçın M.A., (2009) Enerji iletim sistemlerinde seri kapasitörlerin gerilim kararlılığı açısından sistem büyümelerine etkileri, 3. Enerji Verimliliği ve Kalitesi Sempozyumu, 21-22 Mayıs 2009, Kocaeli, Türkiye.
- [13] Yalçınöz T., Altun H. ve Karadal H., (2004), Farklı topolojiye sahip MLP yapay sinir ağları ile enerji sistemlerinde gerilim kararlılığı analizi, *Uluslararası Yapay Zeka ve Yapay Sinir Ağları Türk Sempozyumu*, pp. 547-554, 10-11 Haziran 2004, İzmir, Türkiye.
- [14] Deveraj D. and Jeevajyothi R., (2011), Impact of wind turbine systems on power system voltage stability, *IEEE International Conference on Computer, Communication and Electrical Technology*, pp. 411-416, 18-19 March 2011, Tamilnadu
- [15] Shah R., Mithulananthan N., Bansal R.C., Lee K.Y. and Lomi A. (2011). Power system voltage stability as affected by large-scale PV penetration, *IEEE International Conference on Electrical Engineering and Informatics*, pp. 1-6, 17-19 July 2011, Bandung, Indonesia
- [16] Elma İ. ve Yılmaz O. (2012). Güneydoğu Anadolu bölgesi gerilim çökme problemlerinin değerlendirilmesi, *Elektrik-Elektronik ve Bilgisayar Mühendisliği Sempozyumu*, 29 Kasım - 01 Aralık 2012, Bursa, Türkiye.
- [17] Tur, M. R., Shobole, A., Wadi, M., & Bayindir, R. (2017). Valuation of reliability assessment for power systems in terms of distribution system, A case study. In 2017 IEEE 6th International Conference on Renewable Energy Research and Applications (ICRERA) (pp. 1114-1118)
- [18] Tur M.R. (2021), Deployment of reserve requirements into the power systems considering the cost, lost, and reliability parameters based on sustainable energy. *International Journal of Electrical Engineering & Education*, 58(2):621-639. doi:10.1177/0020720920983535
- [19] Hossain, E., Tür, M. R., Padmanaban, S., Ay, S., & Khan, I. (2018). Analysis and mitigation of power quality issues in distributed generation systems using custom power devices. *IEEE Access*, 6, 16816-16833.
- [20] Wadi, M, Baysal, M., Shobole, A., & Tur M.R. (2020). Historical and monte carlo simulation-based reliability assessment of power distribution systems. *Sigma Journal of Engineering and Natural Sciences*, 38(3), 1527-1540.

- [21] Duncan G.J, Overbye, T.J, Sarma, M.S, (2017), Power System Analysis and Design, Cengage Learning, ISBN: 978-1305632134
- [22] Krause, P., Wasynczuk, O., Sudhoff, S.D., Pekarek, S., (2002), Analysis of Electric Machinery and Drive Systems, Wiley, ISBN: 978-0471143260
- [23] Gridley J.H. (1967), Principals of Electrical Transmission Lines in Power and Communication, Pergamon Press, London, England.
- [24] Miller R.H. and Malinowski J.H., (1993), Power System Operation, McGraw Hill Inc., New York, USA.
- [25] M. H. Mondol, M. R. Tür, S. P. Biswas, M. K. Hosain, S. Shuvo and E. Hossain, "Compact Three Phase Multilevel Inverter for Low and Medium Power Photovoltaic Systems," in IEEE Access, vol. 8, pp. 60824-60837, 2020, doi: 10.1109/ACCESS.2020.2983131.
- [26] Prakash, K., Lallu, A., Islam, F. R., ve Mamun, K. A. (2016). Review of power system distribution network architecture. In 2016 3rd Asia-Pacific World Congress on Computer Science and Engineering, 124-130. doi: <https://doi.org/10.1109/APWC-on-CSE.2016.030>
- [27] Muñoz-Delgado, G., Contreras, J. ve Arroyo, J. M. (2015). Joint expansion planning of distributed generation and distribution networks. IEEE Transactions on Power Systems, 30(5), 2579-2590. doi: <https://doi.org/10.1109/TPWRS.2014.2364960>
- [28] Koutsoukis, N. C., Georgilakis, P. S. ve Hatziargyriou, N. D. (2017). Multistage coordinated planning of active distribution networks. IEEE Transactions on Power Systems, 33(1), 32-44. doi: <https://doi.org/10.1109/TPWRS.2017.2699696>
- [29] Tur, M. R. (2022). Investigation of Optimum Reserve Capacity Requirement in Ancillary Services with Extreme Learning Machine. Electric Power Components and Systems, 49(20), 1555-1566.
- [30] R. Bayindir, M. Yesilbudak and U. Cetinkaya, "Load and short-circuit analyses of the electricity transmission system for industry regions in Ankara," 2015 International Conference on Renewable Energy Research and Applications (ICRERA), Palermo, Italy, 2015, pp. 1243-1247, doi: 10.1109/ICRERA.2015.7418607.

BIOGRAPHIES

Mehmet Rıda Tür received the B.S. degree from the Marmara University, Department of Electrical in 2005, M.S. degree from the Fırat University, Department of Electrical and Electronics Engineering in 2010, and Ph.D. degree from the Yıldız Technical University, Department of Electrical Engineering in 2018. His main areas of interest are protection-reliability, power systems quality, power systems economics, renewable energy systems and smart grids.

Research Article

Design of A Novel IoT Based Mobile ECG Data Transmission System using ESP8266

Harun Sumbul^{1*} ^{1*}Ondokuz Mayıs University, Yesilyurt D.C. Vocational School, Tekkekoy, Samsun, Turkey. (e-mail: harun.sumbul@omu.edu.tr).

ARTICLE INFO

Received: Jun., 05. 2024

Revised: Nov., 10. 2024

Accepted: Jan, 15. 2025

Keywords:

ECG

SMTP

ESP8266

Telemonitoring

IoT

Corresponding author: *Harun Sumbul*

ISSN: 2536-5010 / e-ISSN: 2536-5134

DOI: <https://doi.org/10.36222/ejt.1496616>

ABSTRACT

The Covid-19 pandemic, declared a global pandemic by the World Health Organization, has adversely affected nearly everyone physically, mentally, and socially. During this period, an increase in cardiovascular diseases has been observed, attributed to factors such as changes in dietary habits, physical inactivity due to staying at home, increased consumption of frozen processed food, psychological stress, lack of social interaction, and consequently, rising alcohol and tobacco consumption. This has led to a significant increase in cardiologists' workload and a shift from traditional technologies to remote patient monitoring models.

In this context, remote Electrocardiogram (ECG) monitoring-based approaches have become widely used in recent years for the detection of heart diseases, owing to their reliability and non-invasive nature.

This study introduces an SMTP-based tele-monitoring approach that facilitates remote monitoring of ECG signals and supports a medical simulator, aiming to alleviate the workload of healthcare professionals. The primary objective of this research is to develop a wireless monitoring framework for ECG signals, aiming to enhance patient monitoring and safety, reduce the workload of healthcare providers, and ensure equitable access to healthcare services. Our research focuses on implementing a portable, real-time, and cost-effective ECG monitoring system.

1. INTRODUCTION

COVID-19 can significantly impact patients' cardiovascular systems. Mortality from COVID-19 is strongly associated with cardiovascular disease, diabetes, and hypertension [1]. COVID-19 has the potential to cause heart failure, and cases of severe myocarditis with reduced systolic function have been reported following COVID-19 [2, 3]. Post-COVID patients have exhibited myocardial deformation and reduced heart rate variability, which have subsequently increased the burden of ventricular arrhythmias [4].

The workload of cardiologists has significantly increased, particularly in the post-COVID era, accompanied by a rise in the number of monitored cardiac patients. Certain cardiac patients require periodic electrocardiogram (ECG) examinations, which contributes to hospital overcrowding. ECG signals, providing critical information about heart function, are widely utilized in the medical field to assess cardiovascular health and to monitor patients' treatment progress regularly [5]. Usually, the amplitude of the ECG signal peaks at approximately 1 millivolt (mV). It exhibits a distinctive waveform pattern consisting of P-QRS-T waves, as depicted in Figure 1 [6].

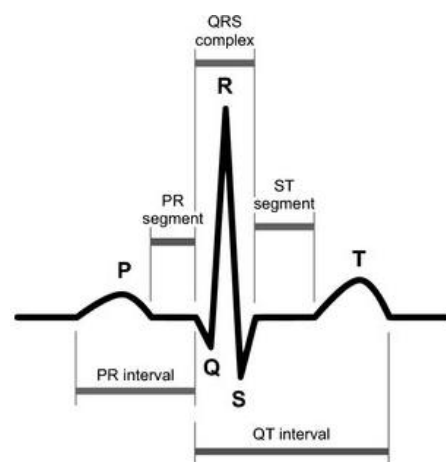


Figure 1. Standard pattern of a PQRST complex in ECG waveforms

The ECG waveform exhibits a characteristic pattern that repeats periodically. This pattern allows physicians to visually analyze the ECG and extract valuable information based on the observed morphological shape. The "normal" rhythm of the heart, known as sinus rhythm, represents the physiological activation of the atria followed by the ventricles, initiated by the sinus node. In adults at rest, sinus rhythm typically exhibits

a regular heart rate ranging from 60 to 80 beats per minute. On the ECG, sinus rhythm is characterized by a sequence of P-waves representing atrial activity, followed by ventricular activity indicated by the QRS complex and T-wave. Any disturbances or delays observed in this pattern can provide crucial information about the presence of cardiovascular disease (CVD). If the waveform deviates from the expected healthy morphology, it indicates the presence of an anomaly related to cardiovascular diseases, leading to the classification of the signal as arrhythmia. The ECG is extensively utilized in diverse medical contexts, playing a critical role in diagnosing various conditions such as chest pain, tachycardia, bradycardia, hypertension, hypotension, myocardial injury, atrial fibrillation, ventricular fibrillation, and more.

Based on the most recent research conducted by the World Health Organization (WHO), CVD has emerged as a major cause of worldwide fatalities. Recent studies suggest that a substantial portion, around 90%, of CVD cases, including conditions like arrhythmia, ischemia, ventricular hypertrophy, bundle branch block, and myocardial infarction, could be prevented through effective preventive measures [7,8]. Therefore, ECG recording is mandatory both at the time of the attack and during routine periods (especially for heart patients). Since this class of patients is generally elderly, it is vital that patients can transmit the ECG data they take from home to doctors remotely without going to the hospital. This will both reduce hospital density and provide patients with the opportunity to access treatment on equal terms. This study focused on normal ECK and several major forms of arrhythmia, which are summarized below:

Atrial Fibrillation Coarse: AF stands as the most prevalent form of cardiac arrhythmia. It can be identified on the surface ECG by two types: fine (AfibF) and coarse (AfibC). Fibrillatory waves may be observed, which can be categorized as either AfibF (amplitude < 0.5mm) or AfibC (amplitude > 0.5mm). AfibC is distinguished by the absence of P waves and the presence of fibrillary waves. In some cases, the fibrillary waves may be very fine and difficult to recognize in certain leads. In such situations, the absence of P waves and a completely irregular RR interval can indicate the presence of underlying atrial fibrillation [9].

Atrial Fibrillation Fine: These waves are typically associated with impaired atrial function, such as enlarged atrial size and reduced left atrial appendage flow. It is crucial to acknowledge that in certain cases, fine V-fib can bear a resemblance to asystole on a defibrillator or cardiac monitor that is set to a low gain [10, 11].

Bradycardia: Bradycardia is identified by a heart rate that is below 60 beats per minute (bpm). It is important to note that bradycardia can pose a life-threatening condition if the heart is unable to maintain a rate that efficiently circulates oxygen-rich blood throughout the body [12].

Tachycardia: Tachyarrhythmia refers to a heart rate that surpasses the normal resting rate. In adults, a resting heart rate above 100 beats per minute is generally classified as tachycardia. It is important to note that heart rates higher than the resting rate can be either normal, such as during exercise, or abnormal, indicating underlying electrical abnormalities within the heart [13].

Ventricular Fibrillation: Ventricular Fibrillation is the ventricular counterpart of atrial fibrillation. In Vfib, the ventricles of the heart contract in a completely asynchronous

and disorganized manner, leading to the absence of effective cardiac systole. The ECG recording of Vfib displays irregular, chaotic, and rapid ventricular activity, resulting in an oscillatory appearance. It is a life-threatening condition that requires immediate medical intervention, such as defibrillation, to restore a normal heart rhythm [14].

Regular surveillance of ECG readings assumes a pivotal function in the effective management of CVDs. By enabling continuous monitoring, it becomes possible to improve the diagnosis, control, and prevention of CVDs. In fact, ECG signals often provide more precise and accurate information compared to radiological images. Researchers are actively exploring new technologies in ECG monitoring systems to develop more efficient and effective solutions. Significant efforts have been dedicated to monitoring ECG waves for the diagnosis of arrhythmia [15, 16]. Nevertheless, there is a clear demand for the development of intelligent, energy-efficient, and cost-effective ECG tele-monitoring systems that can aid healthcare professionals and be used by individuals for preliminary checks.

This study aims to bridge this gap by introducing a novel system for detecting cardiovascular diseases. The suggested framework utilizes contemporary advancements like SMTP, telemonitoring, IoT and cloud computing to deliver a cost-effective, interconnected, and encouraging solution for ECG monitoring.

2. MATERIAL AND METHOD

This study employed a professional ECG simulator to generate normal sinus beat signals as well as various rhythm disturbance signals. These signals were then transmitted to a receiver using the SMTP Protocol. An interface software was developed using the C# programming language to visualize the data for analyzing and interpreting the received signals. The proposed framework of the ECG data transmission system, based on a microcontroller (ESP8266), is illustrated in Figure 2, providing an overview of the system architecture.

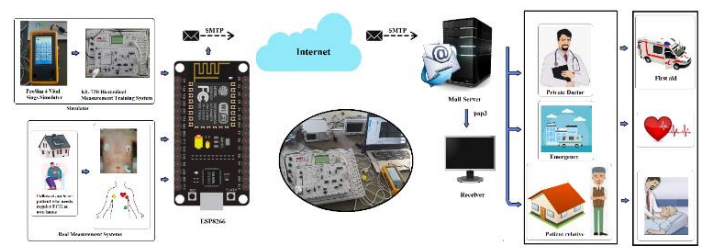


Figure 2. The architecture of the proposed study

In the implemented system, instead of using real patient data, signals were generated from the ProSim Vital Signs Simulator (v4), a professional ECG simulator device. This approach allowed for data augmentation and the inclusion of various patient scenarios, saving time and resources. The simulator data closely resemble real patient data, providing a reliable input for the system. The recorded and transmitted subsystem is responsible for transmitting the simulated ECG signals to the receiving party. The results are then presented to the doctor for evaluation and decision-making. It's important to note that the

final decision ultimately rests with the doctors in the decision-making process.

2.1. ECG data generation subsystem

The ECG data employed in this research was generated utilizing the ProSim 4 Vital Signs Patient Simulator (ProSim™ 4), a meticulously calibrated and manufactured device developed by Fluke Biomedical, headquartered in Cleveland, OH, USA. This device is commonly utilized for calibration purposes in medical devices such as bedside monitors. The ECG simulator operates by producing a 60 ms 1 mV square wave format at 2 Hz. It is a professional-grade device extensively employed in the biomedical field for generating ECG data [17, 18]. However, since the Simulator does not have a built-in data transfer function, the generated ECG data was transferred to a computer using the KL-730 Biomedical Measurement Training System. These devices were briefly introduced in this section to provide an understanding of the system's development and highlight the transition to a cloud-based framework.

KL-730 presents Bio-electronics sensors that are widely utilized and beneficial for students studying electronics and biomedical fields. Additionally, KL-730 gathers all the necessary equipment for measuring various body signals and performing experiments related to 12 different types. KL-730 consists of twelve modules, which encompass the measurement of ECG signals [19]. The System can establish a connection with the computer through a USB port, enabling seamless integration with the Simulator. Through the integration of these two devices, a system for generating ECG data has been created, allowing for the practical production and transfer of various types of ECG data to the computer. The ECG data generation system is illustrated in Figure 3.

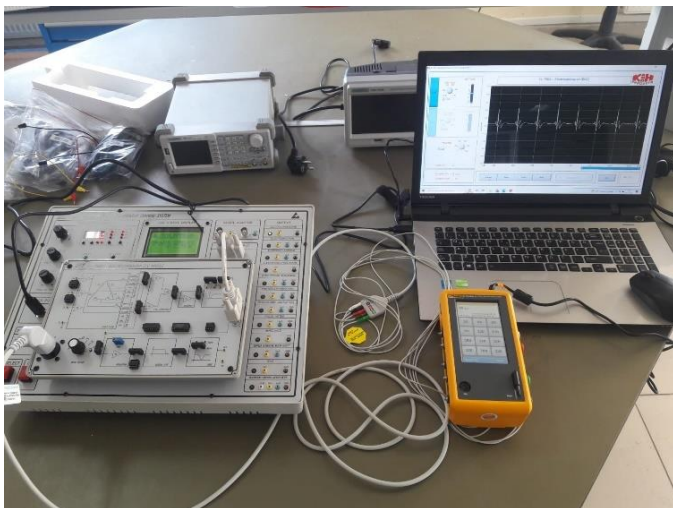


Figure 3. The ECG data generation system

2.2. Generating ECG Dataset

Cardiac arrhythmias are among the most common diseases that affect the heart rhythm. However, before discussing arrhythmias, it is important to understand the characteristics of the normal rhythm, also known as sinus rhythm. In a state of rest, the heart typically beats between 60 and 80 times per minute, which is referred to as the pulse or heartbeat.

Arrhythmias can manifest in various forms, including accelerated heart rate (tachycardia), slowed heart rate (bradycardia), or irregular heart rhythm. In the study, 6 types of ECG data (normal beats and arrhythmias) were generated by using ECG data generation subsystem and transmitted to test the performance of the system and whether there is any loss in the transmitted data. A total of 446 data were produced for use in short-term ECG transmission, and a total of 6,894 data were produced for long-term ECG transmission, thus creating a database. Sample ECG data graphs produced by the simulator to be transmitted to the receiver module are shown in Figure 4.

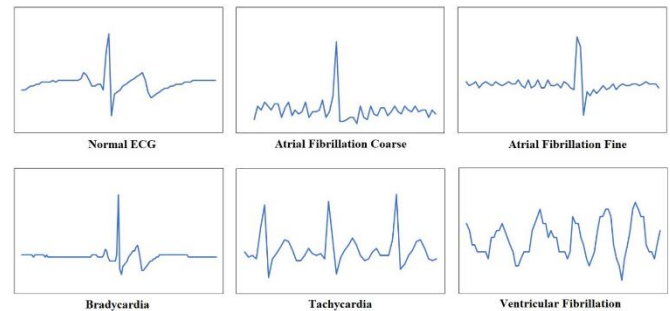


Figure 4. Short-term ECG signal patterns

2.3. Data transmission using Smtip protocol

The Internet of Things (IoT) is a concept that allows different devices to communicate with each other over networks such as the Internet and Bluetooth, and to have the ability to collect, process and share data [20]. In this way, communication between devices becomes easier and efficiency increases. IoT is a technology that is used in many sectors and has an impact on many areas of our lives. There are important studies on monitoring important medical data such as ECG and EEG with IoT [21, 22].

ESP8266 was configured and connected to the internet with the objective of transmitting the real-recording. The Simple Mail Transfer Protocol (SMTP) has been employed for email transmission due to its simplicity, reliability, flexibility, and security mechanisms. SMTP server is responsible for launching the SMTP protocol and delivering email messages. The Outlook SMTP server was selected for implementation due to its ability to handle large volumes of emails without performance issues and excellent support from Microsoft [23]. ECG data, saved in (.csv) format, was appended to an email message through the email client software.

2.4. Pseudocode

Pseudocode serves as a fundamental tool in the realm of computer science and software engineering. It provides a structured format for explaining the logic of an algorithm or program, bridging the gap between natural language and programming languages. Pseudocode can be defined as a structured textual representation of an algorithm that outlines its logic without adhering to the syntax of any specific programming language. Its primary purpose is to describe what a piece of code should accomplish rather than precisely how it should be implemented. This language-independent nature of pseudocode facilitates clearer communication among developers and analysts, allowing them to focus on the logic of algorithms rather than language-specific syntax. Below are the

Pseudocode codes of the software codes of the embedded system in the developed system.

BEGIN

SETUP:

Initialize Serial communication
Connect to Wi-Fi network
Configure input and output pins

LOOP:

READ ECG signal from simulator device
APPLY filters to clean the signal
CONVERT analog signal to digital (ADC)
STORE digital data in FLASH memory
IF time to send data:

SEND data to doctor using communication protocol

(SMTP)

END IF

WAIT for next reading interval

END

2.5. ECG feature extraction

The feature extraction phase plays a crucial role in capturing the distinctive information from physiological signals and representing it concisely. By extracting relevant features from significant waveform patterns, the ECG signal is analyzed to detect and classify various cardiac conditions [24]. In this research, the Pan-Tompkins algorithm was employed to perform feature extraction on ECG data [25,26]. The Pan-Tompkins algorithm was utilized in order to calculate the time interval between consecutive R peaks. This time duration between R peaks plays a crucial role in the early detection of cardiovascular disorders, providing valuable information for diagnosis. The RR interval refers to the time duration between two consecutive beats, specifically the distance from one R peak to the R peak of the following beat, which could be either its precursor or successor. Feature extraction algorithms that have shown the highest accuracies in existing literature encompass features extracted from both the time/frequency domain and characteristics related to the RR interval [27]. While the RR interval may vary among individuals without heart disease, it tends to be relatively consistent. However, in individuals with heart conditions such as tachycardia or bradycardia, the RR interval can become irregular, displaying intermittent periods of very short or very long durations [28]. Figure 5 illustrates the block diagram of the Pan and Tompkins Algorithm employed in the study.

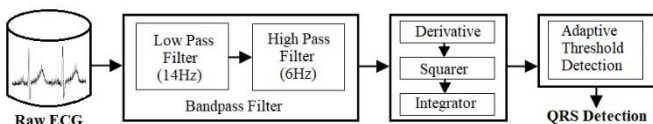


Figure 5. Pan and Tompkins Algorithm block diagram

3. EXPERIMENTAL RESULTS

An interface was developed in C# program in order to monitor and analyze the data. The interface screen is seen in Figure 6. The short-term ECG patterns produced from the simulator is as follows; 72 for normal ECG; 58 for Atrial Fibrillation Coarse; 60 for Atrial Fibrillation Fine; 135 for Bradycardia; 49 for Tachycardia and 72 for Ventricular

Fibrillation. A total of 446 data were transmitted to the receiver via SMTP protocol and visualized in the developed interface. The Long-term ECG patterns produced from the simulator is as follows; 72 for normal ECG; 1149 for Atrial Fibrillation Coarse; 1149 for Atrial Fibrillation Fine; 1149 for Bradycardia; 1149 for Tachycardia and 1149 for Ventricular Fibrillation. A total of 6.894 data were transmitted to the receiver via SMTP protocol and visualized in the developed interface.

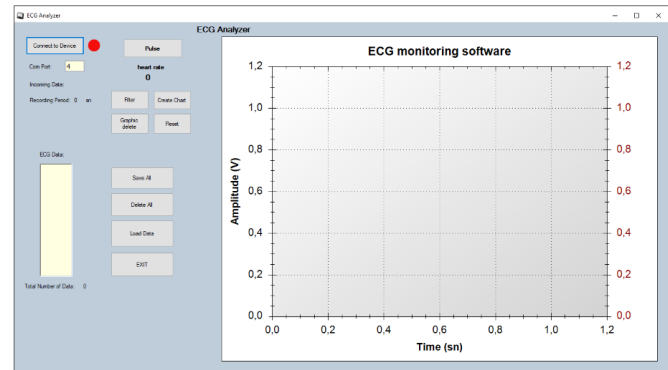
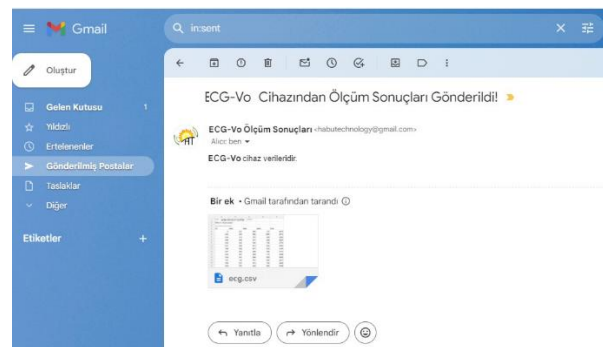
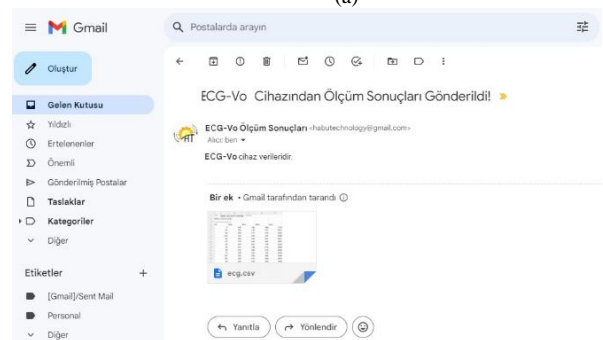


Figure 6. The improved interface screen

The email was directed to the designated recipient (like doctor) and transmitted utilizing the SMTP Protocol. ECG records sent via Gmail using the SMTP protocol with a duration of approximately 7 seconds, as shown in Fig. 7.



(a)



(b)

Figure 7. Transmission (a) and received (b) of signal using SMTP

ECG signals generated from the simulator were transmitted through the system and were successfully reconstructed through the developed interface. Accordingly, the ECG images of the 6 signals received are seen in Figure 8.

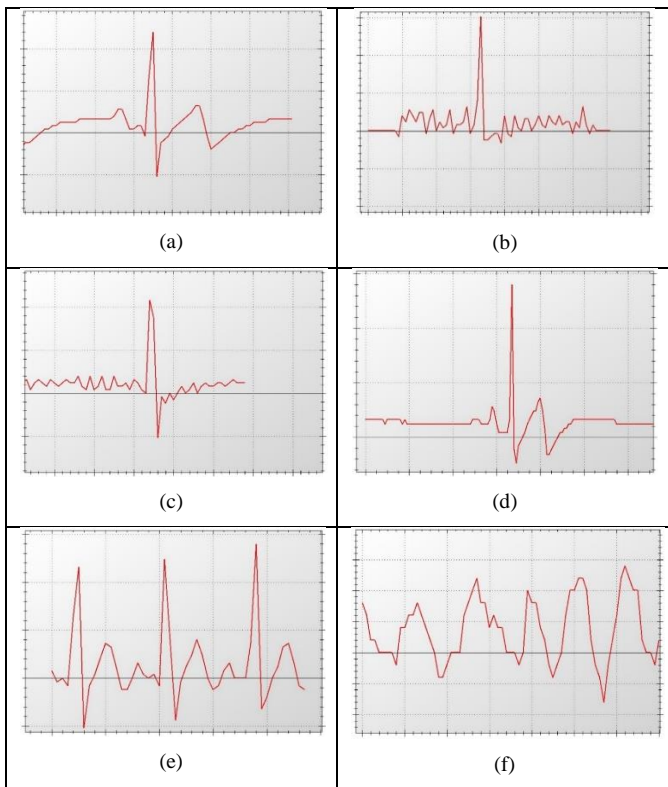


Figure 8. Short-term ECG signal patterns, (a) Normal, (b) Atrial Fibrillation Coarse, (c) Atrial Fibrillation Fine, (d) Bradycardia, (e) Tachycardia, (f) Ventricular Fibrillation

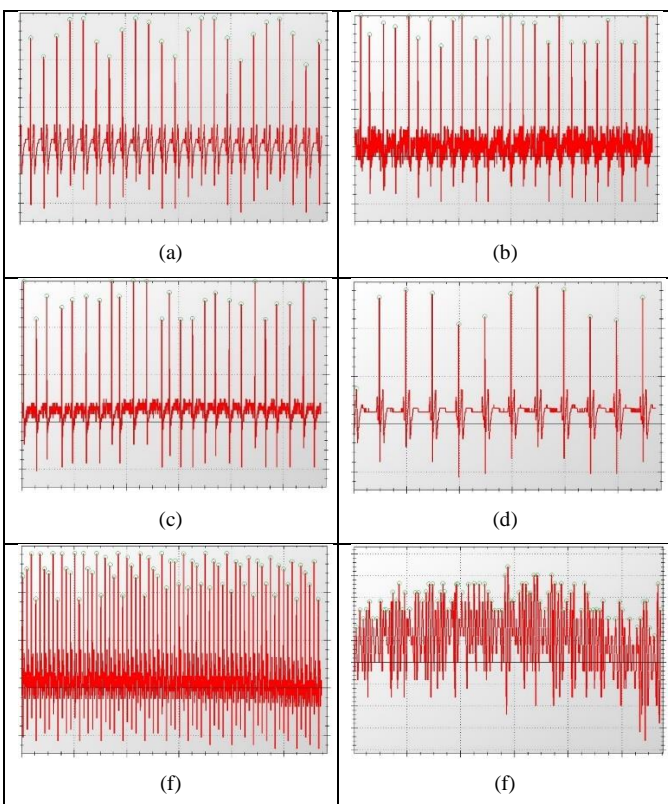


Figure 9. Long-term ECG signal patterns, (a) Normal, (b) Atrial Fibrillation Coarse, (c) Atrial Fibrillation Fine, (d) Bradycardia, (e) Tachycardia, (f) Ventricular Fibrillation

Long-term recordings were created for ECG classes and the Pan-Tompkins algorithm was applied to these signals. The

purpose of using the Pan-Tompkins algorithm is; is to measure the time between successive R peaks. The time from one R peak to the next R peak provides important data for the early diagnosis of cardiovascular diseases. Although this period is generally not the same in normal people, it is close to each other. In people with heart disease such as Tachycardia or Bradycardia, it may occur irregularly, with very short intervals or very long intervals. Figure 9 shows the ECG signal with the Pan-Tompkins algorithm applied. As can be seen, the R-R intervals have been marked successfully.

The integration of mobile devices for vital sign monitoring by healthcare professionals can offer significant benefits to both patients and doctors. The developed prototype in this study is not only cost-effective but also capable of real-time operation and robust performance. It can be utilized for experimental research and data collection of ECG signals. The reduced costs associated with this prototype can also facilitate and encourage further research in this field.

The number of Short-Term ECG signal patterns is given in Table 1.

Normal	Atrial Fibrillation Coarse	Atrial Fibrillation Fine	Brady cardia	Tachy cardia	Ventricular Fibrillation
72	58	60	135	49	72

4. DISCUSSION

Cardiovascular disease currently ranks as the leading cause of mortality. The ECG analysis serves as the predominant method for detecting these diseases by capturing cardiac activity through medical monitoring technology. However, the reliance on experts to analyze vast amounts of ECG data can strain medical resources significantly. Nevertheless, traditional methods possess limitations such as manual feature recognition, complex models, and lengthy training times. In this research paper, a data transmission system has been developed that can be used to transmit the ECG signals taken by heart patients at home to their doctors without the need to go to the hospital. Although there are medical data measurement and transfer systems in the literature using microcontrollers such as Arduino, our approach is more professional and more applicable.

5. CONCLUSIONS

Arrhythmia, a chronic cardiovascular disorder with potentially fatal consequences, presents a significant challenge when using ECG signals for detection. An accurate architecture capable of identifying abnormal ECG signals plays a crucial role in providing early and accurate diagnoses for patients. This study introduces a comprehensive framework that automates the collection of ECG signals, transmitting via SMTP, analysis via the developed interface and presentation of results, thereby enhancing the diagnostic efficiency of doctors. In this state, the system has successfully transmitted ECG data. In future studies, a system design that will measure real ECG data will be integrated into this study. Thus, it is planned to produce an integrated device. Additionally, the developed system is intended to be implemented in hospitals to address any potential practical usage side effects, will making it a valuable tool in clinical settings.

ACKNOWLEDGEMENT

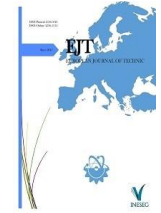
The research conducted in this study received support from the Coordinatorship of Ondokuz Mayıs University's Scientific Research Projects in Samsun, Turkey. The project was identified by the project number PYO.YMY.1908.22.004. This study competed as a finalist in the TEKNOFEST 2023 Artificial Intelligence in Health Competition in the University and Above Level Medical Technologies Category.

REFERENCES

- [1] Chang, Wei-Ting et al., Cardiac Involvement of COVID-19: A Comprehensive Review, *The American Journal of the Medical Sciences*, 361 (2021), 1, pp.14-22. DOI: <https://doi.org/10.1016/j.amjms.2020.10.002>
- [2] Xu, Z. · Shi, L. · Wang, Y., Pathological findings of COVID-19 associated with acute respiratory distress syndrome *Lancet Respir Med*. 8 (2020), pp.420-422, DOI: 10.1016/S2213-2600(20)30076-X
- [3] Chen, T. Wu, D. Chen, H., Clinical characteristics of 113 deceased patients with coronavirus disease 2019: retrospective study, *BMJ*. 2020; 368:m1091, DOI: 10.1136/bmj.m1295
- [4] Hamdy RM, Samy M, Mohamed HS. Clinical utility of ambulatory ECG monitoring and 2D-ventricular strain for evaluation of post-COVID-19 ventricular arrhythmia. *BMC Cardiovasc Disord*. (2024) 16;24(1):429. DOI:10.1186/s12872-024-03982-0.
- [5] Singh, A.K., Krishnan, S. ECG signal feature extraction trends in methods and applications. *BioMed Eng OnLine* 1, (2023), 22. DOI:10.1186/s12938-023-01075-1
- [6] Hernando-Ramiro, C., Lovisoló, L., Cruz-Roldán, F. et al. Matching Pursuit Decomposition on Electrocardiograms for Joint Compression and QRS Detection. *Circuits Syst Signal Process* 38(2019), pp.2653–2676. DOI:10.1007/s00034-018-0986-2
- [7] Xie, J., Peng, L., Wei, L. et al. A signal quality assessment–based ECG waveform delineation method used for wearable monitoring systems. *Med Biol Eng Comput* 59(2021), pp.2073–2084. DOI:10.1007/s11517-021-02425-8
- [8] Aziz, S., Ahmed, S. & Alouini, MS. ECG-based machine-learning algorithms for heartbeat classification. *Sci Rep* 11, 18738 (2021). DOI:10.1038/s41598-021-97118-5
- [9] Finotti, E.; Quesada, A.; Ciaccio, E.J.; Garan, H.; Hornero, F.; Alcaraz, R.; Rieta, J.J. Practical Considerations for the Application of Nonlinear Indices Characterizing the Atrial Substrate in Atrial Fibrillation. *Entropy* (2022), 24, 1261. DOI:10.3390/e24091261
- [10] Liu, C., Tai, M., Hu, J. et al. Application of smart devices in investigating the effects of air pollution on atrial fibrillation onset. *npj Digit. Med*. 6, 42 (2023). DOI:10.1038/s41746-023-00788-w
- [11] O. Aligholipour and M. Kuntalp, "Clustering of Paroxysmal Atrial Fibrillation (PAF) and non-PAF subjects based on arrhythmia-free records," 2018 Electric Electronics, Computer Science, Biomedical Engineering's Meeting (EBBT), Istanbul, Turkey, (2018), pp. 1-5, DOI: 10.1109/EBBT.2018.8391425.
- [12] Wang, J., Wang, X., Liu, H. et al. Effect of butorphanol on visceral pain in patients undergoing gastrointestinal endoscopy: a randomized controlled trial. *BMC Anesthesiol* 23, 93 (2023). DOI:10.1186/s12871-023-02053-9.
- [13] Solis, A., Shimony, J., Shinawi, M. et al. Case report: malignant hypertension associated with catecholamine excess in a patient with Leigh syndrome. *Clin Hypertens* 29, 7 (2023). DOI:10.1186/s40885-022-00231-4.
- [14] Lange, T., Backhaus, S.J., Schulz, A. et al. Cardiovascular magnetic resonance-derived left atrioventricular coupling index and major adverse cardiac events in patients following acute myocardial infarction. *J Cardiovasc Magn Reson* 25, 24 (2023). DOI:10.1186/s12968-023-00929-w.
- [15] Atamanyuk, I., Kondratenko, Y., Havrysh, V. et al. Computational method of the cardiovascular diseases' classification based on a generalized nonlinear canonical decomposition of random sequences. *Sci Rep* 13, 59 (2023). DOI:10.1038/s41598-022-27318-0
- [16] Ahmet Reşit Kavsaoğlu, Eftal Şehirli, A novel study to classify breath inhalation and breath exhalation using audio signals from heart and trachea, *Biomedical Signal Processing and Control*, 80(2023), Part 1, 104220, DOI:10.1016/j.bspc.2022.104220
- [17] Xie, J., Peng, L., Wei, L. et al. A signal quality assessment–based ECG waveform delineation method used for wearable monitoring systems. *Med Biol Eng Comput* 59(2021), pp.2073–2084. DOI:10.1007/s11517-021-02425-8
- [18] Luo Brooke, McLoone Melissa, Rasooly Irit R., Craig Sansanee, Muthu Naveen, Won James, Ruppel Halley, Bonafide Christopher P., ANALYSIS: Protocol for a New Method to Measure Physiologic Monitor Alarm Responsiveness, *Biomedical Instrumentation & Technology*, 54:6 (2020), pp.389-396, DOI:10.2345/0899-8205-54.6.389
- [19] Murat Alan, M. Caner Akuner, Kalen Berry, Erkan Kaplanoglu, Correlation Between ECG and Heart Sound, 2020 SoutheastCon, Raleigh, NC, USA, 2020, pp. 1-4, Date of Conference: 28-29 March 2020, Conference Location: Raleigh, NC, USA, DOI: 10.1109/SoutheastCon44009.2020.9249693.
- [20] Demir, A.K., & Abut, F.. Grid ağ topolojilerinde CoAP ve CoCoA tıkanıklık kontrol mekanizmalarının karşılaştırılması. *Gümüşhane Üniversitesi Fen Bilimleri Dergisi*, (2018), pp.53-60. DOI:10.17714/gumusfenbil.436056
- [21] Sümbül, H.. Deneyap kart kullanarak pozisyonel uyku apnesi tespiti ve IoT uygulaması. *Gümüşhane Üniversitesi Fen Bilimleri Dergisi*, 13(4) (2023), pp.1033-1045. DOI:10.17714/gumusfenbil.1262913
- [22] Çiftçi, B., Şen, Z., & Akkaş, M. (2021). Nesnelerin İnterneti Tabanlı Kablosuz Taşınabilir EKG Cihazı. *Avrupa Bilim Ve Teknoloji Dergisi*(26), 91-95. DOI:10.31590/ejosat.949795
- [23] Saeed, I. M., Eltaema, M. A., Eldie, G. A. S., H Mohamed, H. O., T. Ahmed and M. E. S. Hamad, "Development of 3-Channel 12-Lead ECG Monitoring Device with Telemedicine Integration using AD8232," 2023 International Conference on Computer and Applications (ICCA), Cairo, Egypt, 2023, pp. 1-8, DOI: 10.1109/ICCA59364.2023.10401513.
- [24] ZhaoYang Ge, Huiqing Cheng, Zhuang Tong, Ning Wang, Adi Alhudhaif, Fayadh Alenezi, Haiyan Wang, Bing Zhou, Zongmin Wang, ECG-MAKE: An ECG signal delineation approach based on medical attribute knowledge extraction, *Information Sciences* 637 (2023) 118978, DOI:10.1016/j.ins.2023.118978
- [25] Neri L, Oberdier MT, Augello A, Suzuki M, Tumarkin E, Jaipalli S, Geminiani GA, Halperin HR, Borghi C. Algorithm for Mobile Platform-Based Real-Time QRS Detection. *Sensors*. 2023; 23(3):1625. DOI:10.3390/s23031625
- [26] Liu Feifei, Wei Shoushui, Li Yibin, Jiang Xinge, Zhang Zhimin, Zhang Ling, Liu Chengyu, the accuracy on the common pan-tompkins based QRS detection methods through low-quality electrocardiogram database *J. Med. Imag. Health Inform.*, 7 (5) (2017), pp. 1039-1043, DOI: 10.1166/jmih.2017.2134
- [27] Eduardo José da S. Luz, William Robson Schwartz, Guillermo Cámara-Chávez, David Menotti, "Ecg-based heartbeat classification for arrhythmia detection: A survey," *Computer methods and programs in biomedicine*, 127 (2016), pp. 144–164, DOI:10.1016/j.cmpb.2015.12.008
- [28] Abdioğlu, S., Acar, B. & Kavsaoğlu, A.R. Kablosuz EKG cihazı tasarımı ve sinyal işleme teknikleri kullanılarak özneliklerin değerlendirilmesine yönelik web sitesi tasarımı. *Avrupa Bilim ve Teknoloji Dergisi*, 26 (2021), pp.144-150, DOI: 10.31590/ejosat.951988.

BIOGRAPHIES

Harun SÜMBÜL received B.S. degree in Electronic sciences from the Selçuk University, Konya, Turkey, in 2008, the M.S. degree from the Selçuk University from Electrical and Electronics Engineering, Konya, Turkey, in 2011, and received the Ph.D. degree in electrical and electronics engineering from Karabük University, Karabük, Turkey. His primary areas of research are biomedical engineering and biomedical signal processing. He is currently a Lecturer at the Yeşilyurt Demir Çelik Vocational School, department of biomedical device technologies at Ondokuz Mayıs University, Turkey.



Research Article

Some Numerical Techniques for Solution of Nonlinear Regularized Long Wave Equation

İhsan Çelikkaya^{1*} ¹Batman University, Department of Mathematics, 72100, Batu Raman, Batman, Turkey. (e-mail: ihsan.celikkaya@batman.edu.tr).

ARTICLE INFO

Received: Feb., 21. 2024

Revised: Dec., 02. 2024

Accepted: Jan, 08. 2025

Keywords:

RLW equation
Richardson extrapolation
Strang algorithm
Ext4 algorithm
Ext6 algorithm
Solitary waves

Corresponding author: *Ihsan Celikkaya*

ISSN: 2536-5010 / e-ISSN: 2536-5134

DOI: <https://doi.org/10.36222/ejt.1440941>

ABSTRACT

In this study, numerical solutions of the one-dimensional Regularized Long Wave (RLW) equation have been investigated. For this purpose, the RLW equation is divided into two sub equations, one linear and the other nonlinear, according to the time term. Then, algebraic equation systems have been obtained by writing the derivative approximations obtained with the help of cubic trigonometric B-spline base functions and Crank-Nicolson finite difference approximations to the derivatives in each sub-equation. To obtain numerical solutions of the RLW equation, these systems are solved the Strang splitting algorithm, Ext4, and Ext6 techniques created by Richardson extrapolation of the Strang algorithm have used to increase the accuracy of the solutions. In order to investigate the effectiveness of these methods, single solitary wave motion and the interaction of two solitary waves problems, which are most commonly used in the literature, have been taken into consideration. In addition, the stability analysis of the Strang algorithm have been investigated by the von Neumann method.

1. INTRODUCTION

In science, nonlinear partial differential equations often represent wave events that are motivated by certain physical initial/boundary conditions [1]. In recent times, solitary waves, especially soliton waves, have become both experimental and theoretically very interesting and outstanding. A soliton is a very special type of solitary wave, which has a continuous form, can be placed in a region and interaction with another soliton, and can be separated unchanged without a change of phase [11]. In this paper we examine the RLW equation in the following form as

$$U_t + U_x + \varepsilon U U_x - \mu U_{xxt} = 0, \quad (1)$$

$U \rightarrow 0$ when $x \rightarrow \pm\infty$. Where t is the time, x is the position coordinate, $U(x, t)$ is the wave height (amplitude), and ε and μ are the positive parameters.

The RLW equation was first appeared when calculating the development of the "undular bore" problem by Peregrine [2]. The RLW is a nonlinear dispersive wave equation which is a more conventional than the KdV equation in observing the wave phenomena. This equation is most commonly used in order to model physical phenomena such as pressure waves in liquid-gas bubble mixtures, longitudinal dispersive waves in elastic rods, ion-acoustic waves in plasma, thermally excited phonon packets in low temperature nonlinear crystals, shallow water waves and plasma waves [2,31].

Several researchers have solved the RLW equation using various methods and techniques. Among others, Rasoulizadeh

et al. [3] developed a method for the numerical solution of the RLW equation by means of an implicit method based on the - weighted and finite difference methods. Oruç et al. [4] obtained the numerical solutions of the RLW equation using Strang splitting approach combined with Chebyshev wavelets. Irk et al. [5] used quartic trigonometric B-spline finite element method to solve the RLW equation numerically. Yağmurlu and Karakaş in the papers [6] and [7] applied the trigonometric cubic B-spline collocation method to get numerical solution of the equal width equation and modified equal width wave equation. Kutluay et al. [8] used cubic hermite B-spline collocation method to solve modified equal width wave equation. Kutluay et al. [9] utilized a robust quantic hermite collocation method for the numerical solution of the one dimensional heat equation. for Dağ et al. [10] applied a collocation method based on the trigonometric cubic B-spline function to obtain numerical solutions of the RLW equation. Kutluay [40] and Esen [25] solved the equation using both finite difference and finite elements method. Mei and Chen [30] used explicit multistep method. Gardner et al. [29] solved the regularized long wave equation numerically by Galerkin method with quadratic B-spline finite elements. Dağ et al. [31] obtained numerical solution of the RLW equation using a splitting up technique and both quadratic and cubic B-splines. Saka and Dağ [32] developed a new algorithm based on the collocation method using splitting. Oruç et al. [38] utilized Haar wavelet method and Islam and et al. [41] presented a meshfree technique using the radial basis functions (RBFs) in order to obtain the numerical solutions of the equation.

Moreover; Dağ et al. in the papers [23] and [28] developed cubic B-spline collocation and quintic B-Spline Galerkin finite element methods for obtaining numerical solutions of the present equation. Besides, while Zaki [26] applied a combination of the splitting method and cubic B-spline finite elements, and Raslan [39] used cubic B-spline collocation method for approximate solutions of the equation.

2. Formulation of Splitting Methods

One way of dealing with complex problems is "divide and conquer". In the context of evolution type equations, the operator splitting idea has been a very successful approach. The underlying idea behind such an approach is that all model evolution operators are formally written as the sum of the evolution operators for each term that is being modeled. In other words, when one splits the model into a series of sub-equations, simpler and more practical algorithms for each sub-equation occur. Then the applied numerical method is applied to each sub-problem and numerical schemes are obtained and these schemes are combined by operator splitting [13]. We are going to dwell on the situation in which we have the following the Cauchy problem

$$\frac{dU(t)}{dt} = AU(t) + BU(t), t \in [0, T], U(0) = U_0. \quad (2)$$

Where, an initial function $U_0 \in X$ is given, A and B are assumed to be a bounded linear operator in the Banach space X together with $A, B : X \rightarrow X$. There is also a norm associated with the space X denoted by $\|\cdot\|_X$, and if both A and B are matrixes, then it is called Euclidean norm [14].

2.1. Strang splitting algorithm

In splitting methods, the given equation is generally divided into several parts and each part is solved separately, independently of the main equation, over $[t_n, t_{n+1}]$ time intervals. Such methods are generally called time splitting or fractional step methods [15]. Strang [12] has proposed a symmetrizing splitting scheme

$$\begin{aligned} \frac{dU^*}{dt} &= AU^*, U^*(0) = U_0, \text{ on } \left[0, \frac{\Delta t}{2}\right] \\ \frac{dU^{**}}{dt} &= BU^{**}, U^{**}(0) = U^*\left(\frac{\Delta t}{2}\right), \text{ on } [0, \Delta t] \quad (3) \\ \frac{dU^{***}}{dt} &= AU^{***}, U^{***}(0) = U^{**}(\Delta t), \text{ on } \left[0, \frac{\Delta t}{2}\right] \end{aligned}$$

where the final values are obtained by $U^{***}(\Delta t/2)$. This scheme is called $(A - B - A)$ and the scheme $(B - A - B)$ can be derived in a similar manner. This scheme has a local splitting error

$$le = \left[e^{A\frac{\Delta t}{2}} e^{B\Delta t} e^{A\frac{\Delta t}{2}} - e^{(A+B)\Delta t} \right] \quad (4)$$

$$= O(\Delta t) \quad (5)$$

is a second-order scheme and is used in practice for many applications [20].

2.2. Construction of Ext4 and Ext6 algorithms

In extrapolation techniques, a simple low-order method (basic method) is applied for different time steps t . Then, higher order methods are obtained by taking an appropriate combination of the results [21]. Now let's explain how to obtain a higher order R method. To do this, let $R(t)$ be an approximation to R with step length t when $t \rightarrow 0, R(t) \rightarrow R$ and let's assume

$$R(\Delta t) = R + a_2\Delta t^2 + a_4\Delta t^4 + a_6\Delta t^6 + \dots \quad (6)$$

If the time step t is divided into k substeps then the basic method is applied k times [22, 16], i.e.

$$\left(R\left(\frac{\Delta t}{k}\right) \right)^k = R\left(\frac{\Delta t}{k}\right) \circ R\left(\frac{\Delta t}{k}\right) \circ R\left(\frac{\Delta t}{k}\right) \dots \circ R\left(\frac{\Delta t}{k}\right).$$

In this study, the Strang method is used as the basic method to obtain **Ext4** and **Ext6** techniques. To obtain the **Ext4** method, the expressions $R(t)$ and $R\left(\frac{\Delta t}{2}\right)$ are used in (6)

$$R(\Delta t) = R + a_2\Delta t^2 \quad (7)$$

$$R\left(\frac{\Delta t}{2}\right) = R + a_2\frac{\Delta t^2}{4}. \quad (8)$$

If a_2 is eliminated in the equations (7) and (8) and necessary operations performed for R

$$R = \frac{4}{3}\left(R\left(\frac{\Delta t}{2}\right)\right)^2 - \frac{1}{3}R(\Delta t) + O(\Delta t^4) \quad (9)$$

If the approximation (9) is applied to Strang's algorithm $S_{\Delta t} = e^{A\frac{\Delta t}{2}} e^{B\Delta t} e^{A\frac{\Delta t}{2}}$, **Ext4** algorithm is obtained as follows

$$\begin{aligned} \text{Ext4} &= \frac{4}{3}\left(S_{\frac{\Delta t}{2}}\right)^2 - \frac{1}{3}S_{\Delta t} \\ &= \frac{4}{3}\varphi_{\frac{\Delta t}{4}}^{[A]} \circ \varphi_{\frac{\Delta t}{2}}^{[B]} \circ \varphi_{\frac{\Delta t}{2}}^{[A]} \circ \varphi_{\frac{\Delta t}{2}}^{[B]} \circ \varphi_{\frac{\Delta t}{4}}^{[A]} - \frac{1}{3}\varphi_{\frac{\Delta t}{2}}^{[A]} \circ \varphi_{\Delta t}^{[B]} \circ \varphi_{\frac{\Delta t}{2}}^{[A]}, \end{aligned}$$

where $\varphi_{\Delta t}$ is a numerical method. Similarly, the following equations are used to obtain the **Ext6** method

$$R(\Delta t) = R + a_2\Delta t^2 + a_4\Delta t^4 \quad (10)$$

$$R\left(\frac{\Delta t}{2}\right) = R + a_2\frac{\Delta t^2}{4} + a_4\frac{\Delta t^4}{4} \quad (11)$$

$$R\left(\frac{\Delta t}{3}\right) = R + a_2\frac{\Delta t^2}{9} + a_4\frac{\Delta t^4}{81} \quad (12)$$

If the necessary operations are performed for R after a_2 and a_4 are eliminated in the equations (10), (11), (12)

$$R = \frac{81}{40}R\left(\frac{\Delta t}{3}\right)^3 - \frac{16}{15}R\left(\frac{\Delta t}{2}\right)^2 + \frac{1}{24}R(\Delta t) + O(\Delta t^6). \quad (13)$$

If the approximation (13) is applied to Strang's algorithm $S_{\Delta t} = e^{A\frac{\Delta t}{2}} e^{B\Delta t} e^{A\frac{\Delta t}{2}}$, **Ext6** algorithm is obtained as follows

$$\begin{aligned} \text{Ext6} &= \frac{81}{40}\left(S_{\frac{\Delta t}{3}}\right)^3 - \frac{16}{15}\left(S_{\frac{\Delta t}{2}}\right)^2 + \frac{1}{24}S_{\Delta t} \\ &= \frac{81}{40}\varphi_{\frac{\Delta t}{6}}^{[A]} \circ \varphi_{\frac{\Delta t}{3}}^{[B]} \circ \varphi_{\frac{\Delta t}{3}}^{[A]} \circ \varphi_{\frac{\Delta t}{3}}^{[B]} \circ \varphi_{\frac{\Delta t}{3}}^{[A]} \circ \varphi_{\frac{\Delta t}{3}}^{[B]} \circ \varphi_{\frac{\Delta t}{6}}^{[A]} \\ &\quad - \frac{16}{15}\varphi_{\frac{\Delta t}{4}}^{[A]} \circ \varphi_{\frac{\Delta t}{2}}^{[B]} \circ \varphi_{\frac{\Delta t}{2}}^{[A]} \circ \varphi_{\frac{\Delta t}{2}}^{[B]} \circ \varphi_{\frac{\Delta t}{4}}^{[A]} + \frac{1}{24}\varphi_{\frac{\Delta t}{2}}^{[A]} \circ \varphi_{\Delta t}^{[B]} \circ \varphi_{\frac{\Delta t}{2}}^{[A]}. \end{aligned}$$

Since these methods contain negative coefficients, it is not known exactly they are stable for what kind of problems. However, it has been shown by Dia and Schatzman [16] that the **Ext4** technique is stable with dimensional splitting for linear parabolic problems at finite time intervals.

3. Method of Solution

To examine the numerical behavior of the RLW equation (1), the solution domain is constrained on a closed interval $[a, b]$. The homogenous boundary conditions

$$U(a, t) = 0, U(b, t) = 0, t \geq 0 \quad (14)$$

$$U_x(a, t) = 0, U_x(b, t) = 0$$

and the initial condition

$$U(x, 0) = f(x), a \leq x \leq b$$

are taken as stated above, and $f(x)$ is a predefined function. Let us assume that the space solution domain is $[a, b]$ and a uniform discretization of this domain by the nodal points x_m , $m = 0, 1, \dots, N$, is given by $a = x_0 < x_1 < \dots < x_N = b$. Dividing the solution region into elements of equal length ensures that the calculated error norms are smaller. If we define the distance between two consecutive points as $h = x_{m+1} - x_m$ and $T_m(x)$, $m = -1(1)N + 1$, then trigonometric cubic B-spline functions on the domain $[a, b]$ can be expressed in terms of nodal points x_m as follows

$$T_m(x) = \frac{1}{r} \begin{cases} p^3(x_{m-2}), & x \in [x_{m-2}, x_{m-1}] \\ p(x_{m-2})(p(x_{m-2})q(x_m) + q(x_{m+1})p(x_{m-1})) \\ + q(x_{m+2})p^2(x_{m-1}), & x \in [x_{m-1}, x_m] \\ q(x_{m+2})(p(x_{m-1})q(x_{m+1}) + q(x_{m+2})p(x_m)) \\ + p(x_{m-2})q^2(x_{m+1}), & x \in [x_m, x_{m+1}] \\ q^3(x_{m+2}), & x \in [x_{m+1}, x_{m+2}] \\ 0, & \text{otherwise} \end{cases} \quad (15)$$

as stated by [17, 18]. Where $p(x_m) = \sin(\frac{x-x_m}{2})$, $q(x_m) = \sin(\frac{x_m-x}{2})$ and $r = \sin(h/2)\sin(h)\sin(3h/2)$. It is obvious that the set $\{T_{-1}(x), T_0(x), \dots, T_{N+1}(x)\}$ constitutes a base on the domain $[a, b]$. If we assume that the function $U(x, t)$ is defined on the domain $[a, b]$, then the function $U(x, t)$ can be approximated as follows in terms of trigonometric cubic B-spline functions and time dependent parameters $\delta_m(t)$ as follows

$$U(x, t) \cong \sum_{m=-1}^{N+1} \delta_m(t) T_m(x). \quad (16)$$

Where time-dependent parameters $\delta_m(t)$ are going to be determined using the Eq. (1) and its auxiliary conditions. Since the Eq. (1) contains the terms U, U' and U'' , we need the values of U , its first and second order derivatives in terms of trigonometric cubic B-spline functions. Using the approximations (15) and (16), the nodal values of U, U' and U'' are obtained in terms of the time-dependent parameters $\delta_m(t)$ as follows

$$\begin{aligned} U_m &= U(x_m) = \alpha_1 \delta_{m-1} + \alpha_2 \delta_m + \alpha_1 \delta_{m+1}, \\ U'_m &= U'(x_m) = \beta_1 \delta_{m+1} - \beta_1 \delta_{m-1}, \\ U''_m &= U''(x_m) = \gamma_1 \delta_{m-1} + \gamma_2 \delta_m + \gamma_1 \delta_{m+1}, \end{aligned} \quad (17)$$

with the coefficients

$$\begin{aligned} \alpha_1 &= \frac{\sin^2(\frac{h}{2})}{\sin(h)\sin(\frac{3h}{2})}, \alpha_2 = \frac{2}{1 + \cos(2h)}, \\ \beta_1 &= -\frac{3}{4\sin(\frac{3h}{2})}, \gamma_2 = \frac{3\cos^2(\frac{h}{2})}{\sin^2(\frac{h}{2})(2 + 4\cos(h))}, \\ \gamma_1 &= \frac{3(1 + 3\cos(h))}{16\sin^2(\frac{h}{2})(2\cos(\frac{h}{2}) + \cos(\frac{3h}{2}))}. \end{aligned}$$

Where ' and '' denote the first and second order derivatives with respect to the space variable x , respectively.

The time split RLW equation is taken as follows

$$U_t - \mu U_{xxt} + U_x = 0 \quad (18)$$

$$U_t - \mu U_{xxt} + \varepsilon U U_x = 0. \quad (19)$$

If the values of U_m, U'_m and U''_m at nodal points x_m are used in (18) and (19) and basic necessary operations are performed, we obtain the following first order ordinary differential equation systems

$$\begin{aligned} \alpha_1 \dot{\delta}_{m-1} + \alpha_2 \dot{\delta}_m + \alpha_1 \dot{\delta}_{m+1} - \mu(\gamma_1 \dot{\delta}_{m-1} + \gamma_2 \dot{\delta}_m + \gamma_1 \dot{\delta}_{m+1}) \\ + \beta_1 (\delta_{m+1} - \delta_{m-1}) = 0, \end{aligned} \quad (20)$$

$$\begin{aligned} \alpha_1 \dot{\delta}_{m-1} + \alpha_2 \dot{\delta}_m + \alpha_1 \dot{\delta}_{m+1} - \mu(\gamma_1 \dot{\delta}_{m-1} + \gamma_2 \dot{\delta}_m + \gamma_1 \dot{\delta}_{m+1}) \\ + \varepsilon z_m \beta_1 (\delta_{m+1} - \delta_{m-1}) = 0, \end{aligned} \quad (21)$$

where $\dot{\cdot}$ denotes derivation with respect to t and the value of z_m is taken as follows for linearization process

$$z_m = \alpha_1 \delta_{m-1} + \alpha_2 \delta_m + \alpha_1 \delta_{m+1}.$$

Instead of the parameter $\delta_m, \frac{\delta_m^{n+1} + \delta_m^n}{2}$ is written and instead of time-varying parameters $\dot{\delta}_m, \frac{\delta_m^{n+1} - \delta_m^n}{\Delta t}$ is written in Eqs. (20) and (21), the following equations

$$\begin{aligned} \alpha_1 \delta_{m-1} + b_1 \delta_m + c_1 \delta_{m+1} \\ = c_1 \delta_{m-1} + b_1 \delta_m + a_1 \delta_{m+1}, \end{aligned} \quad (22)$$

$$\begin{aligned} \alpha_2 \delta_{m-1} + b_2 \delta_m + c_2 \delta_{m+1} \\ = c_2 \delta_{m-1} + b_2 \delta_m + a_2 \delta_{m+1} \end{aligned} \quad (23)$$

$$a_1 = \alpha_1 - \mu\gamma_1 - \frac{\beta_1 \Delta t}{2}, b_1 = \alpha_2 - \mu\gamma_2,$$

$$c_1 = \alpha_1 - \mu\gamma_1 + \frac{\beta_1 \Delta t}{2}, a_2 = \alpha_1 - \mu\gamma_1 - \frac{\varepsilon z_m \beta_1 \Delta t}{2},$$

$$b_2 = \alpha_2 - \mu\gamma_2, c_2 = \alpha_1 - \mu\gamma_1 + \frac{\varepsilon z_m \beta_1 \Delta t}{2}$$

are obtained. The equations given in (22) and (23) consist of $(N + 1)$ equations and $(N + 3)$ unknown j parameters. Using the boundary conditions $U(a, t) = 0$ and $U(b, t) = 0$, we obtain the following equalities for parameters δ_{-1} and δ_{N+1}

$$\delta_{-1} = \frac{\alpha_2}{\alpha_1} \delta_0 - \delta_1, \delta_{N+1} = -\delta_{N-1} - \frac{\alpha_2}{\alpha_1} \delta_N. \quad (24)$$

If the parameters δ_{-1} and δ_{N+1} are eliminated from systems (22) and (23) using identities (24), $(N + 1) \times (N + 1)$ dimensional tridiagonal band matrix systems are obtained. A unique solution of these systems can be obtained using the Thomas algorithm. In order to solve these systems, it is necessary to use δ_m^0 initial parameters in (22) and (23) after the initial parameters $U(x, 0) = f(x)$ are obtained. If we call (22) and (23) systems A and B respectively, then the results will be obtained using the splitting scheme $(A - B - A)$ as stated in (3).

3.1. Initial Condition

The initial vector δ_m^0 will be formed using the initial condition $U(x, 0) = f(x)$ as follows

$$\begin{aligned}
 U(x_i, 0) &= U_N(x_i, 0), i = 0(1)N \\
 U_m &= \alpha_1 \delta_{m-1}^0 + \alpha_2 \delta_m^0 + \alpha_1 \delta_{m+1}^0, m = 0(1)N \\
 U_0 &= \alpha_1 \delta_{-1}^0 + \alpha_2 \delta_0^0 + \alpha_1 \delta_1^0 \\
 U_1 &= \alpha_1 \delta_0^0 + \alpha_2 \delta_1^0 + \alpha_1 \delta_2^0 \\
 &\vdots \\
 U_N &= \alpha_1 \delta_{N-1}^0 + \alpha_2 \delta_N^0 + \alpha_1 \delta_{N+1}^0.
 \end{aligned} \quad (25)$$

This system consists of $(N + 1)$ equations and $(N + 3)$ unknown δ_m^0 parameters. The parameters δ_{-1}^0 and δ_{N+1}^0 are calculated from (25) using the boundary conditions $U'_N(a, 0) = 0$ and $U'_N(b, 0) = 0$

$$\beta_1 \delta_1^0 - \beta_1 \delta_{-1}^0 = 0, \beta_1 \delta_{N+1}^0 - \beta_1 \delta_{N-1}^0 = 0.$$

Now, newly obtained $(N + 1) \times (N + 1)$ dimensional solvable matrix is obtained for δ_m^0 parameters.

$$\begin{bmatrix} \alpha_2 & 2\alpha_1 & 0 & & & \\ \alpha_1 & \alpha_2 & \alpha_1 & & & \\ & & \ddots & & & \\ & & & \alpha_1 & \alpha_2 & \alpha_1 \\ & & & & 2\alpha_1 & \alpha_2 \end{bmatrix} \begin{bmatrix} \delta_0^0 \\ \delta_1^0 \\ \vdots \\ \delta_{N-1}^0 \\ \delta_N^0 \end{bmatrix} = \begin{bmatrix} U_0 \\ U_1 \\ \vdots \\ U_{N-1} \\ U_N \end{bmatrix}.$$

3.1. Von Neumann Stability Analysis

The (22) and (23) numerical schemes have been considered by the Fourier von Neumann [19] method. In this method $\delta_m^n = \xi^n e^{i\beta m h}$ is taken, where $i = \sqrt{-1}$, β is mode number, ξ is amplification factor and h is the space step in the method. In Eq. (1) in the term uu_x , since we take $u = z_m$ for linearization purpose, it will behave as a local constant. Let us assume that the amplification factors related to the schemes in (22) and (23) be ρ_A and ρ_B , respectively. If we write $\delta_m^n = \xi_{A/2}^n e^{i\beta m h}$ in Eq.(22), we obtain

$$\rho_A \left(\frac{\xi^{n+1/2}}{\xi^n} \right) = \frac{X - iY}{X + iY'}$$

$$X = b_1 + (c_1 + a_1) \cos \beta h, Y = (c_1 - a_1) i \sin \beta h.$$

Thus, since $\left| \rho_A \left(\frac{\xi^{n+1/2}}{\xi^n} \right) \right| \leq 1$ is valid, the linearized scheme is unconditionally stable. In a similar way, if we take $\delta_m^n = \xi_B^n e^{i\beta m h}$ in Eq. (23), we obtain $\left| \rho_B \left(\frac{\xi^{n+1}}{\xi^n} \right) \right| \leq 1$. Since the scheme (3) is as follows

$$\begin{aligned}
 \rho_S(\xi) &= \rho_A^{n+1/2} \rho_B^{n+1} \rho_A^{n+1/2}, \\
 |\rho_S(\xi)| &\leq \left| \rho_A \left(\frac{\xi^{n+1/2}}{\xi^n} \right) \right| \left| \rho_B \left(\frac{\xi^{n+1}}{\xi^n} \right) \right| \left| \rho_A \left(\frac{\xi^{n+1/2}}{\xi^n} \right) \right| \leq 1
 \end{aligned}$$

the solution for Eq. (1) obtained using Strang splitting scheme is unconditionally stable.

4. Numerical Examples and Their Results

We have considered two test problems to observe the effectiveness of the method. The solution of each problem with cubic B-spline collocation method gives $(N + 1) \times (N + 1)$ tridiagonal band matrix systems which can be

easily and effectively solved by Thomas algorithm. In order to see the difference between numerical solution and analytic solution, we have used the error norms defined as to measure the difference and thus to see how well the wave position and amplitude estimate of the method are

$$L_2 = \sqrt{h \sum_{j=1}^N [U_j^{exact} - U_j]^2}, L_\infty = \max_j |U_j^{exact} - U_j|.$$

The RLW equation given in (1) satisfies three invariants known as mass, momentum and energy given as follows

$$\begin{aligned}
 I_1 &= \int_{-\infty}^{+\infty} U dx \approx h \sum_{j=1}^N U_j^n, \\
 I_2 &= \int_{-\infty}^{+\infty} [U^2 + \mu(U_x)^2] dx \approx h \sum_{j=1}^N [(U_j^n)^2 + \mu((U_x)_j^n)^2], \\
 I_3 &= \int_{-\infty}^{+\infty} [U^3 + 3U^2] dx \approx h \sum_{j=1}^N [(U_j^n)^3 + 3(U_j^n)^2]. \quad (26)
 \end{aligned}$$

4.1. Single Solitary Movement

Analytical solution for single soliton wave solution of RLW equation is

$$U(x, t) = 3c \sec h^2[k(x - x_0 - vt)]$$

Where $k = \frac{1}{2} \left(\frac{\varepsilon c}{\mu(1+\varepsilon c)} \right)$, $v = 1 + \varepsilon c$ is wave velocity and $3c$ is wave amplitude. The following initial

$$U(x, 0) = 3c \sec h^2[k(x - x_0)]$$

and the boundary conditions

$$U(a, t) = U(b, t) = 0$$

are used at the boundaries. Analytic values of the invariants for this problem are

$$I_1 = \frac{6c}{k}, I_2 = \frac{12c^2}{k} + \frac{48kc^2\mu}{5}, I_3 = \frac{36c^2}{k} \left(1 + \frac{4c}{5} \right) \quad (27)$$

given by Zaki [26]. In order to be able to make a comparison with previous studies, all calculations were taken as $\varepsilon = 1, \mu = 1, x_0 = 0$ and $\Delta t = 0.1$. In Table 1, the values of the error norms L_2, L_∞ and the invariant values calculated with the $S_{\Delta t}$, **Ext4** and **Ext6** techniques are given at different times in the region $-40 \leq x \leq 60$. As it is clearly seen from Table 1, the invariants remain almost the same as time progresses. Moreover, the error norms L_2, L_∞ calculated by **Ext4** and **Ext6** are smaller than those with $S_{\Delta t}$. In Table 2, several comparisons have been made with some of those in the literature at time $t = 20$ for the values of $c = 0.03, h = 0.1, 0.125$. As can be clearly seen from Table 2, the results obtained with $S_{\Delta t}$, **Ext4** and **Ext6** techniques are in good harmony with other results found in the literature. Figure 1 and 2 show 2 and 3 dimensional behavior of the numerical solution and the exact solution. As can be clearly seen from Figure 1 and 2, $S_{\Delta t}$, **Ext4** and **Ext6** techniques preserve the physical structure of the problem quite well.

Table 1: A comparison of the invariants and error norms calculated at various times for values of $h = 0.1, 0.125, \Delta t = 0.1, c = 0.1, \varepsilon = \mu = 1$ in the region $-40 \leq x \leq 60$ for single solitary wave.

h	Time	Method	I_1	I_2	I_3	$L_2 \times 10$	$L_\infty \times 10$
0.125	$t = 0$	$S_{\Delta t}$	3.979927	0.810462	2.579007	0.00000	0.00000
		Ext4	3.979927	0.810462	2.579007	0.00000	0.00000
		Ext6	3.979927	0.810462	2.579007	0.00000	0.00000
	$t = 4$	$S_{\Delta t}$	3.979953	0.810462	2.579007	0.29086	0.79795
		Ext4	3.979953	0.810463	2.579008	0.28673	0.78652
		Ext6	3.979999	0.810480	2.579066	0.28705	0.76386
	$t = 8$	$S_{\Delta t}$	3.979971	0.810462	2.579007	0.58210	1.62771
		Ext4	3.979971	0.810463	2.579008	0.57383	1.60407
		Ext6	3.980062	0.810498	2.579124	0.57354	1.55669
	$t = 12$	$S_{\Delta t}$	3.979984	0.810462	2.579007	0.87407	2.47927
		Ext4	3.979984	0.810463	2.579008	0.86164	2.44339
		Ext6	3.980121	0.810516	2.579183	0.85984	2.36902
	$t = 16$	$S_{\Delta t}$	3.979986	0.810462	2.579007	1.16709	3.34710
		Ext4	3.979986	0.810463	2.579008	1.15046	3.29862
		Ext6	3.980169	0.810533	2.579241	1.14629	3.19580
	$t = 20$	$S_{\Delta t}$	3.979962	0.810463	2.579007	1.46140	4.22716
		Ext4	3.979962	0.810463	2.579008	1.44054	4.16731
		Ext6	3.980190	0.810551	2.579299	1.43318	4.03364
0.1	$t = 4$	$S_{\Delta t}$	3.979954	0.810462	2.579007	0.18742	0.51431
		Ext4	3.979954	0.810463	2.579008	0.18665	0.51186
		Ext6	3.979954	0.810463	2.579008	0.18397	0.50423
	$t = 8$	$S_{\Delta t}$	3.979973	0.810462	2.579007	0.37508	1.04901
		Ext4	3.979973	0.810463	2.579008	0.37353	1.04404
		Ext6	3.979973	0.810463	2.579008	0.36816	1.02848
	$t = 12$	$S_{\Delta t}$	3.979988	0.810462	2.579007	0.56319	1.59752
		Ext4	3.979988	0.810463	2.579008	0.56085	1.59032
		Ext6	3.979988	0.810463	2.579008	0.55278	1.56656
	$t = 16$	$S_{\Delta t}$	3.979993	0.810462	2.579007	0.75197	2.15660
		Ext4	3.979993	0.810463	2.579008	0.74883	2.14697
		Ext6	3.979993	0.810463	2.579008	0.73803	2.11515
	$t = 20$	$S_{\Delta t}$	3.979970	0.810462	2.579007	0.94157	2.72364
		Ext4	3.979970	0.810463	2.579008	0.93764	2.71180
		Ext6	3.979970	0.810463	2.579008	0.92410	2.67198

Table 2: A comparison of the invariants and error norms calculated at $t = 20$ for values of $h = 0.1, 0.125, \Delta t = 0.1, c = 0.03, \varepsilon = \mu = 1$ in the region $-40 \leq x \leq 60$ for single solitary wave.

h	Method	I_1	I_2	I_3	$L_2 \times 10$	$L_\infty \times 10$
0.1	$S_{\Delta t}$	2.109485	0.12730	0.388807	0.67947641	0.248333660
	Ext4	2.109485	0.127303	0.388807	0.67959141	0.248317182
	Ext6	2.109480	0.127302	0.388805	0.67885613	0.248300644
	[24](SBCM1)	2.10904	0.12730	0.38881	0.556	0.419
	[24](SBCM2)	2.10904	0.12730	0.38881	0.556	0.419
	[29]	2.1050	0.12730	0.38880	0.563	0.432
	[32]	2.10948	0.12730	0.38880	0.651	0.432
	[26]	2.10760	0.127302	0.38879	0.41652	0.23197
	$S_{\Delta t}$	2.109003	0.127302	0.388806	0.64278799	2.19097274
	Ext4	2.109003	0.127302	0.388806	0.64057300	2.19069041
0.125	Ext6	2.108997	0.127302	0.388804	0.64176027	2.19050366
	[24](SBCM1)	2.10849	0.12730	0.38881	0.444	0.419
	[24](SBCM2)	2.10849	0.12730	0.38881	0.444	0.419
	[31]	2.10471	0.12730	0.38880	0.538	0.198
	[32]	2.10902	0.12731	0.38881	0.547	0.432
	[26]	2.10741	0.12723	0.38856	0.242	0.125

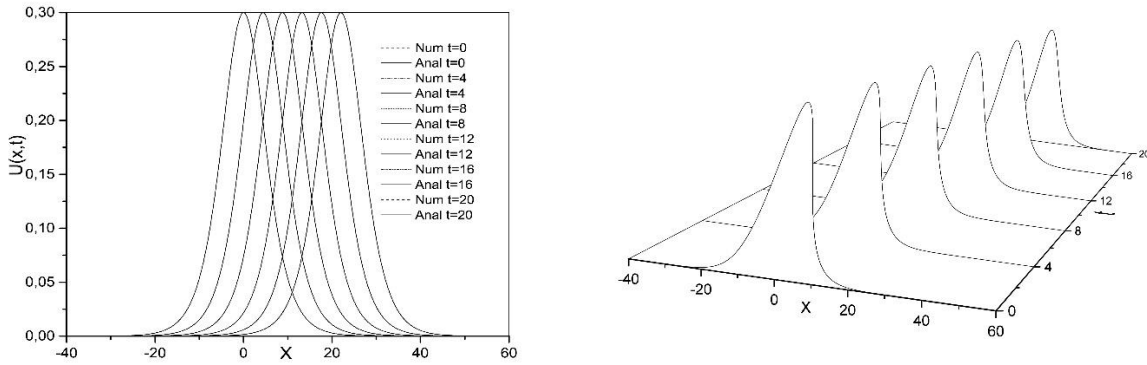


Figure 1. Physical behavior of the single solitary wave for $c = 0.1$.

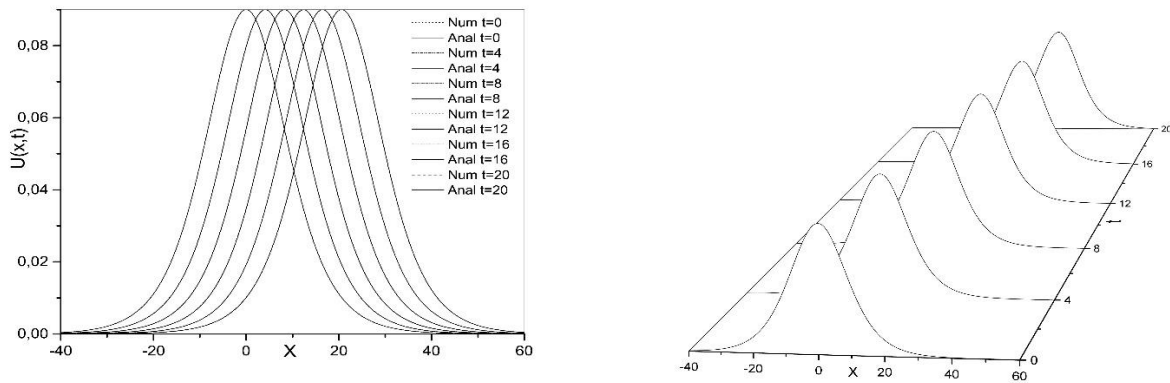


Figure 2. Physical behavior of the single solitary wave for $c = 0.03$.

Table 3: The invariants of the interaction problem and comparison with those in Ref. [40, 39]

method	t	0	4	8	16	20	25
$S_{\Delta t}$	I_1	37.91652	37.91702	37.91732	37.91764	37.91761	37.91769
	I_2	120.5228	120.5244	120.5081	120.4223	120.5126	120.5273
	I_3	744.0812	744.0866	744.0760	743.9454	744.0848	744.0999
Ext4	I_1	37.91648	37.91697	37.91721	37.91740	37.91744	37.91747
	I_2	120.5234	120.5258	120.5117	120.4292	120.5298	120.5551
	I_3	744.0813	744.0921	744.1171	744.1573	744.2281	744.3226
Ext6	I_1	37.91648	37.91719	37.91763	37.91800	37.91821	37.91851
	I_2	120.5234	120.5258	120.5101	120.4258	120.5159	120.5301
	I_3	744.0813	744.0920	744.1042	744.1249	744.1126	744.1141
[40]	I_1	37.91648	37.91697	37.91719	37.91740	37.91744	37.91745
	I_2	120.3515	120.3584	120.3570	120.3886	120.3599	120.3595
	I_3	744.0814	744.0110	743.8679	742.4889	743.8638	744.0085
[39]	I_1	37.91652	37.91170	37.85975	37.52916	37.64730	38.05010
	I_2	120.5228	121.1602	119.7317	119.4185	119.8041	119.8355
	I_3	744.0815	736.9443	728.5173	725.8399	727.1948	727.4392

4.2. Interaction of Two Solitary Waves

An interaction problem is that the boundary condition is taken as $U \rightarrow 0$ when $x \rightarrow \pm\infty$ and the initial condition is taken as follows

$$U(x, 0) = \sum_{j=1}^2 3A_j \operatorname{sech}^2[k_j(x - x_j)]$$

where $A_j = \frac{4k_j^2}{1-4k_j^2}$, $j = 1, 2$. In order to observe this interaction problem, we worked within the region $0 \leq x \leq 120$ and with the parameters $x_1 = 15$, $x_2 = 35$, $k = 0.4$, $k_2 = 0.3$, $\varepsilon = 1$, $\mu = 1$, $h = 0.3$ and $\Delta t = 0.1$. To observe the problem of the interaction, the small waves amplitude is calculated as 1.6869 at $t = 25$, $x = 70.2$ and the large waves amplitude is calculated as 5,3456 at $x = 87$. In Figure 3, the interaction and separation of two solitary waves is demonstrated using the numerical results calculated with the **Ext6** technique. As can

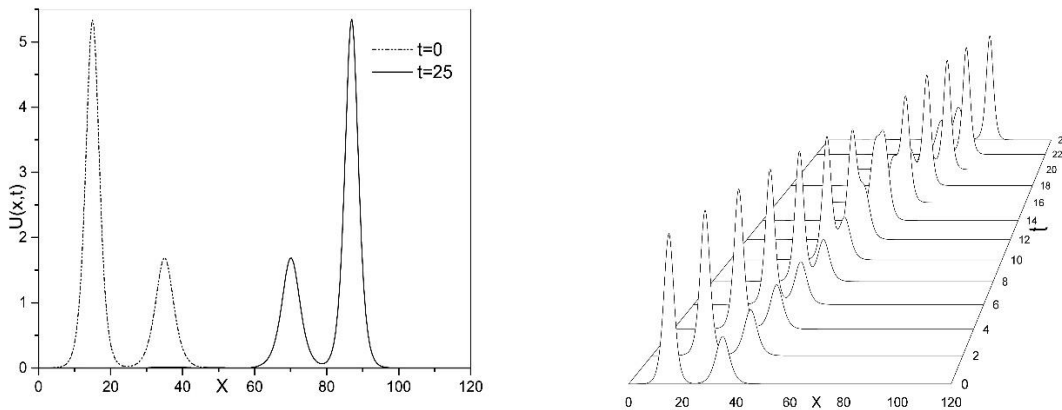


Figure 3. Physical behavior of the interaction of two solitary waves.

5. Conclusions

In this study, the trigonometric cubic B-spline collocation method is used with some splitting techniques for the numerical solutions of the regularized long wave equation. **Ext4** and **Ext6** techniques have been constructed using the Strang splitting algorithm. The results obtained with all three techniques have compared with each other and with some studies in the literature. It has been seen that the numerical

interaction of two solitary waves, the wave with the larger amplitude is placed at $x_1 = 15$ and the smaller one at $x_2 = 35$. Since the speed of the wave with the larger amplitude is also higher, it is observed that it catches the smaller wave and leaves it behind as time progresses. After the

be seen from Table 3, the invariants are calculated with $S_{\Delta t}$, **Ext4** and **Ext6** techniques remain almost constant throughout the calculations and the results are in good agreement with those in Refs. [40, 39].

results calculated with $S_{\Delta t}$, **Ext4** and **Ext6** techniques preserve the physical structure of the problems and the calculated error norms L_2 , L_∞ are small enough. As a result, it can be said that $S_{\Delta t}$, **Ext4** and **Ext6** techniques are effective techniques to improve the numerical results of partial differential equations

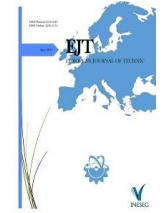
REFERENCES

- [1] Jain, P. C., Shankar, R., and Singh, T. V. (1993). Numerical Solution Of Regularized Long-Wave Equation. Communications in Numerical Methods in Engineering, 9, 579-586.
- [2] Peregrine, D. H. (1966). Calculations of the development of an undular bore. J. Fluid Mech., 25(2), 321-330
- [3] Rasoulizadeh, M. N., Nikan, O., and Avazzadeh, Z. (2020). The impact of LRBFFD on the solutions of the nonlinear regularized long wave equation. Mathematical Sciences, 15, 365-376.
- [4] Oruç, Ö., Esen, A., and Bulut, F. (2020). A Strang Splitting Approach Combined with Chebyshev Wavelets to Solve the Regularized Long-Wave Equation Numerically. Mediterr. J. Math., 17, 140
- [5] Irk, D., Keskin Yıldız, P., and Zorşahin Görgülü, M. (2019). Quartic trigonometric B-spline algorithm for numerical solution of the regularized long wave equation. 43, 112-125.
- [6] Yağmurlu, N. M., and Karakaş, A. S. (2020). Numerical solutions of the equal width equation by trigonometric cubic B-spline collocation method based on Rubin-Graves type linearization. Numerical Methods for Partial Differential Equations, 36(5), 1170-1183.
- [7] Yağmurlu, N. M., and Karakaş, A. S. (2022). A novel perspective for simulations of the MEW equation by trigonometric cubic B-spline collocation method based on Rubin-Graves type linearization. Computational methods for Differential Equations, 10(4), 1046-1058
- [8] Kutluay, S., Yağmurlu, N. M., and Karakaş, A. S. (2024). A novel perspective for simulations of the Modified Equal-Width Wave equation by cubic Hermite B-spline collocation method. Wave Motion, 129, 103342.
- [9] Kutluay, S., Yağmurlu, N. M., and Karakaş, A. S. (2024). A Robust Quintic Hermite Collocation Method for One-Dimensional Heat Conduction Equation. Journal of Mathematical Sciences and Modelling, 7(2), 82-89.
- [10] Dağ, I., Irk, D., Kaçmaz, O., and Adar, N. (2016). Trigonometric B-spline collocation algorithm for solving the RLW equation. Applied and Computational Mathematics, 15(1), 96-105.
- [11] N.G. Chegini A. Salaripناه · R. Mokhtari, D. Isvand. Numerical solution of the regularized long wave equation using nonpolynomial splines, Nonlinear Dyn 69 (2012) 459-471.
- [12] Strang, G. (1968). On The Construction and Comparison Of Difference Schemes. SIAM J. Numer. Anal., 5(3), 506-517.
- [13] Holden, H., Karlsen, K. H., Lie, K. A., & Risebro, N. H. (2010). Splitting Methods for Partial Differential Equations with Rough Solutions. European Mathematical Society.
- [14] Geiser, J. (2011). Iterative Splitting Methods for Differential Equations. CHAPMAN & HALL/CRC. Numerical Analysis and Scientific Computing. London
- [15] Hundsdorfer, W., & Verwer, J. (2003). Numerical Solution of Time-Dependent Advection-Diffusion-Reaction Equations (First Edition). Springer-Verlag Berlin Heidelberg, New York.
- [16] Dia, B. O., & Schatzman, M. (1996). Commutateurs De Certains Semi-Groupes Holomorphes Et Applications Aux Directions Alternees. Math. Modelling Num. Anal., 30(3), 343-383.
- [17] Walz, G. (1997). Identities for trigonometric B-splines with an application to curve design. BIT, 37, 189-201.
- [18] Koch, P. E. (1988). Multivariate trigonometric B-splines. J. Approx. Theory, 54, 162-168.
- [19] VonNeumann, J. and Richtmyer, R. D. (1950). A Method for the Numerical Calculation of Hydrodynamic Shocks, J. Appl. Phys., 21, 232-237.
- [20] Sportisse, B. (2000). An Analysis of Operator Splitting Techniques in the Stiff Case. Journal of Computational Physics 161, 140-168.
- [21] Blanes, S., Casas, F., and Ros, J. (1999). Extrapolation Of Symplectic Integrators. Celest. Mech. & Dyn. Astron., 75, 149-161.

- [22]Blanes, S., and Casas, F. (2016). A Concise Introduction to Geometric Numerical Integration. CRC Press LLC.
- [23]Dağ, I., Saka, B., and Irk, D. (2004). Application of cubic B-splines for numerical solution of the RLW equation. Applied Mathematics and Computation, 159, 373–389.
- [24]Saka, B., Şahin, A., and Dağ, I. (2011). B-Spline Collocation Algorithms for Numerical Solution of the RLW Equation. Numerical Methods for Partial Differential Equations, 27(3), 581-607.
- [25]Esen, A., and Kutluay, S. (2006). Application of a lumped Galerkin method to the regularized long wave equation. Applied Mathematics and Computation, 174, 833–845.
- [26]Zaki, S.I. (2001). Solitary waves of the splitted RLW equation. Computer Physics Communications, 138, 80–91.
- [27]Doğan, A. (2002). Numerical solution of RLW equation using linear finite elements within Galerkin's method. Applied Mathematical Modelling, 26, 771–783.
- [28]Dağ, I., Saka, B., and Irk, D. (2006). Galerkin method for the numerical solution of the RLW equation using quintic B-splines. Journal of Computational and Applied Mathematics, 190, 532–547.
- [29]Gardner, L. R. T., Gardner, G. A., & Dağ, I. (1995). A B-spline finite element method for the regularized long wave equation. Commun Numer Meth Eng.,11, 59–68.
- [30]Mei, L., & Chen, Y. (2012). Explicit multistep method for the numerical solution of RLW equation. Applied Mathematics and Computation, 218, 9547–9554.
- [31]Dağ, I., Doğan, A., and Saka, B. (2003). B-Spline Collocation Methods For Numerical Solutions Of The Rlw Equation. International Journal of Computer Mathematics, 80(6), 743-757
- [32]Saka, B., and Dağ, I. (2005). A collocation method for the numerical solution of the RLW equation using cubic B-spline basis. Arab J Sci Eng., 30, 39–50.
- [33]Saka, B., and Dağ, I. (2008). A numerical solution of the RLW equation by Galerkin method using quartic B-splines. Communications in Numerical Methods In Engineering, 24, 1339–1361.
- [34]Dağ, I., and Özer, M. N. (2001). Approximation of the RLW equation by the least square cubic B-spline Finite element method. Applied Mathematical Modelling, 25, 221–231.
- [35]Saka, B., Dağ, I., & Doğan, A. (2004). Galerkin method for the numerical solution of the RLW equation using quadratic B-splines. International Journal of Computer Mathematics, 81(6), 727–739
- [36]Mokhtari, R., and Mohammadi, M. (2010). Numerical solution of GRLW equation using Sinc-collocation method. Computer Physics Communications, 181, 1266–1274.
- [37]Saka, B., and Dağ, I. (2007). Quartic B-Spline Collocation Algorithms for Numerical Solution of the RLW Equation. Numerical Methods for Partial Differential Equations, 23(3), 731-751.
- [38]Oruç, O., Bulut, F., and Esen, A. (2016). Numerical Solutions of Regularized Long Wave Equation by Haar Wavelet Method. Mediterr. J. Math., 13, 3235–3253.
- [39]Raslan, K.R. (2005). A computational method for the regularized long wave (RLW) equation. Applied Mathematics and Computation, 167, 1101–1118
- [40]Kutluay, S., and Esen, A. (2006). A Finite Difference Solution of The Regularized Long-Wave Equation. Mathematical Problems in Engineering, 2006, 1–14.
- [41]Islam, S. L., Haq, S., and Ali, A. (2009). A meshfree method for the numerical solution of the RLW equation. Journal of Computational and Applied Mathematics, 223, 997–1012.

BIOGRAPHIES

İhsan Çelikkaya received his B.Sc. degree in mathematics from Atatürk University, Turkey in 2008, the M.Sc. degree in applied mathematics from İstanbul Beykent University, and Ph.D. degree in applied mathematics from Malatya İnönü University. He is working as an assistant professor at Batman University.



Research Article

Eye State Classification from Electroencephalography (EEG) Signals Using the Extra Trees Classifier Algorithm

Suleyman Dal^{1*} ^{1*} Batman University, Rectorate, Energy Coordination Office, Batman, Turkey. (e-mail: suleyman.dal@batman.edu.tr).

ARTICLE INFO

Received: May., 22. 2025

Revised: Jun., 08. 2025

Accepted: Jun., 12. 2025

Keywords:

Electroencephalography

Extra Trees Classifier

Eye State

Machine Learning

Corresponding author: *Suleyman Dal*

ISSN: 2536-5010 / e-ISSN: 2536-5134

DOI: <https://doi.org/10.36222/ejt.1704397>

ABSTRACT

This study aims to automatically classify the eye openness state (open/closed) of individuals from electroencephalography (EEG) signals. In the classification process, based on the knowledge that EEG signals reflect short-term cognitive states, the EEG Eye State dataset is used. The dataset contains 14,980 samples from 14 EEG channels and the eye state is labelled according to the binary classification problem. Within the scope of the preprocessing steps for the data, the scaling process was performed and then the classification model was created. In the modelling process, the Extra Trees Classifier (ETC) algorithm, which is an ensemble learning method based on decision trees, was preferred. The performance of the model was evaluated by 10-fold cross-validation method; accuracy, precision, sensitivity and F1 score metrics were calculated at each layer. The findings revealed that the model performed well in all metrics. In particular, the highest F1 score was achieved in Fold 1, and the width of the area under the ROC curve (AUC) confirmed the discriminative power of the model. In addition, in the feature importance analysis, it was observed that the signals obtained from occipital and parietal regions contributed more to the classification process. The results show that traditional machine learning algorithms, together with appropriate preprocessing strategies, can produce effective classification outputs on EEG data. This study contributes to the academic literature on EEG-based eye state detection and provides a meaningful basis for applications such as human-computer interaction, attention monitoring systems and neurocognitive assessment.

1. INTRODUCTION

Electroencephalography (EEG) is a neurophysiological recording method that measures the voltage changes in electrical signals that occur due to neuronal activity of the brain with high temporal resolution through (non-invasive) electrodes placed on the scalp [1-3]. The ability to examine EEG signals in more depth with analytical and signal processing methods has led to a significant increase in studies on human cognitive processes, moods and behavioral patterns in recent years; in this context, many studies have been carried out in the literature [2, 4, 5]. In this context, automatic classification of an individual's eye-openness state (eyes open or closed) over EEG signals is not only capturing a physiological response; it is of vital importance in attention level monitoring, driver drowsiness detection, state of consciousness tracking, personal identity verification, monitoring the sleep-wake cycle of infants, epileptic seizure detection and various clinical evaluation scenarios [6-10].

Eye state is not only a short-term motor response associated with the visual system, but also an important cognitive indicator that affects the dynamic structure of brain networks

[4]. In particular, it is known that micro-movements such as blinking cause a dipole movement in the vertical direction with the electrical charge separation caused by the interaction between the cornea and the eyelid. This effect is observed as a positive wave lasting approximately 100 milliseconds in EEG recordings and is most prominently observed in the frontopolar region [11]. The meaningful analysis of such signals makes EEG-based eye state classification a high-potential application area both in neurocognitive research and in the design of real-time human-machine interfaces [12].

EEG signals provide an important biological data source for classification-based analyses because they have high temporal resolution and contain electrical patterns directly related to cognitive states [4,13]. Thanks to these features, many cognitive parameters such as an individual's mental state, emotional state or motor responses can be modelled through EEG signals by means of various algorithms [13, 14]. In this context, especially machine learning methods are effectively used in automatic classification processes by analysing the structural complexity of EEG data [15]. Recent studies have shown that various machine learning algorithms have been

successfully applied to classify the open/closed eye state with EEG data [12,16]. The aim of this study is to classify the eye openness state (eyes open or closed) of individuals with high accuracy using EEG signals. For this purpose, the UCI EEG Eye State dataset was used in the experimental analyses [17]. The dataset consists of 14,980 samples and 15 features and contains eye state labels corresponding to EEG signals recorded at different time intervals. This time series data is a widely referenced source in the literature for the evaluation of EEG-based classification algorithms.

In this study, Extra Trees Classifier (ETC) method was applied to develop an effective model in terms of classification accuracy, sensitivity to class balance and computational efficiency. Extra Trees algorithm is an ensemble learning method consisting of randomised decision trees and attracts attention with its fast-training process and high accuracy potential, especially in high-dimensional data sets [18, 19]. The model used in the study was first trained by eliminating missing values and performing the necessary normalisation operations in the dataset and then tested with 10-fold cross-validation method. The results obtained show that the developed model exhibits high success in eye state classification. These results suggest that traditional machine learning methods, when applied with careful data preprocessing and feature management, can provide an effective alternative to more complex and computationally costly classification models in terms of both accuracy and computational efficiency. In addition, this study aims to make both academic and practical contributions by providing a faster, simpler and feasible alternative to the computationally expensive models in the literature for eye state detection based on EEG signals.

The remaining sections of the paper are structured as follows: In the second section, current approaches and related works in the literature on eye state classification based on EEG signals are comprehensively reviewed. In the third section, the EEG Eye State dataset used in the study, the data preprocessing steps, and the methods applied in the classification process are presented in detail. In the fourth section, the modelling process performed using the Extra Trees Classifier algorithm and the metrics and results used to evaluate the success of the model are shared. In the fifth section, the feature importance levels of the classification model are analysed, and the relative contributions of the EEG channels are interpreted. In the sixth section, the study is discussed comprehensively in the light of the findings obtained; finally, in the seventh section, general conclusions are given and suggestions for future studies are presented.

2. LITERATURE RESEARCH

Classification of eye-openness state from EEG signals is considered as an important research area in many application areas such as human-computer interaction, driver attention systems and cognitive state analyses. In studies conducted in this direction, the effects of various machine learning modelling approaches on the classification performance of EEG-based signals have been extensively investigated. Hasan et al. (2021) proposed an ensemble model consisting of multilayer artificial neural networks to classify eye opening state using EEG signals, and obtained 89.2% accuracy and 91.24% F-measure in their experiments on the UCI EEG Eye State dataset. The study revealed that the proposed approach is effective not only in terms of classification accuracy but also in

terms of its suitability for real-time applications [20]. Similarly, Jayadurga et al. (2024) compared various ensemble learning algorithms based on bagging and boosting on EEG data and stated that Bagged k-NN model offers the best results in terms of classification performance. In addition, the XGBoost algorithm was effective in increasing the interpretability of the model thanks to its capacity to evaluate feature importance levels. The study reveals that ensemble-based approaches provide high performance and stable solutions for EEG-based eye state classification [21].

Xiao et al. (2023) proposed a model based on continuous wavelet transform (CWT) and an improved convolutional neural network (CNN) for the classification of eye openness state from EEG signals. In this study, variational mode decomposition (VMD) algorithm is used for signal preprocessing, CWT method is used for time-frequency feature extraction, and then classification is performed with a CNN model developed with residual connections and attention mechanisms. Experiments on the UCI EEG Eye State dataset show that the proposed method provides high accuracy and generalisation. This study makes an important contribution to improve the classification performance of deep learning architectures by obtaining two-dimensional visual representation from EEG signals [22]. In another study, Hasan Adil et al. proposed a simple but effective machine learning approach using the K-Nearest Neighbour (KNN) algorithm for the classification of eye openness status based on EEG signals. The signals obtained with Emotiv EPOC EEG device were manually labelled with video support and used in model training. The KNN algorithm yielded successful results in terms of accuracy and classification performance, while attracting attention with its low processing time. The study shows that simple machine learning algorithms can provide a powerful alternative for EEG-based classification problems when configured correctly [23].

Fikri et al. (2021) systematically examined the opportunities and main challenges of machine learning and deep learning approaches for eye movement classification. In particular, the study comparatively analysed the methods used for the detection of basic eye movement events such as saccade, fixation and smooth pursuit, highlighting the limitations of threshold-based methods and emphasising the potential of machine learning algorithms and recent deep learning architectures in this field. The models in the literature are evaluated in terms of classification performance, interpretability, data balance and real-time application compatibility, and the limitations encountered at the application level such as data labelling processes, parametric adjustments and generalisation problems are discussed. In this respect, the study provides a useful resource for comparing the methods used in classification applications with eye movement data and understanding the methodological trends [24].

Although studies on eye state classification with EEG signals have an important place in the literature, there are also many studies for different purposes using EEG signals. In this context, EEG-based approaches have been successfully used in various applications such as epileptic seizure detection, mood analysis and mental state classification. Alkhaldi et al. (2024) presented a comprehensive review of the role of artificial intelligence and remote health applications in EEG-based epilepsy management. In the study, it was reported that algorithms such as CNN, SVM, Random Forest and stacking showed high performance in areas such as epileptiform activity

classification, seizure prediction and surgical prediction. It was also emphasised that tele-EEG systems and AI-supported mobile applications offer significant advantages, especially in regions where access to healthcare services is limited. This study demonstrates the increasing impact of AI-based models in the diagnosis and treatment of epilepsy at the literature level [25].

Gaddanakeri et al. (2024) compared CNN and LSTM based deep learning models on DEAP dataset for emotion recognition with EEG signals. As a result of the preprocessing and modelling processes applied, it is stated that the LSTM architecture captures time-dependent patterns more successfully and provides superiority in classification performance. The study shows that deep learning is an effective method in EEG-based emotion recognition [26]. In this study by Wei-Yang Yu et al. (2024), a multi-model machine learning approach was developed by combining EEG signals and genetic data in the classification of Alzheimer's disease (AD). Within the scope of the study, both EEG-based biomarkers and a large number of single nucleotide polymorphisms (SNPs) and polygenic risk scores (PRS) were evaluated. Three different algorithms (SVM, Random Forest and XGBoost) were compared in the developed model and it was reported that the best performance was obtained with SVM. Significant differences were observed between AD patients and healthy individuals, especially in parameters such as EEG power, sample entropy and phase locking value (PLV). The findings reveal that the combination of EEG and genetic data provides an effective solution for early diagnosis of Alzheimer's disease and higher classification accuracy [27].

3. MATERIAL AND METHOD

3.1. Material

In this study, the open-access EEG Eye State dataset created by Oliver Roesler at Baden-Württemberg Cooperative State University was used in the analyses for the classification of individuals' eye openness state from electroencephalography (EEG) signals [17].

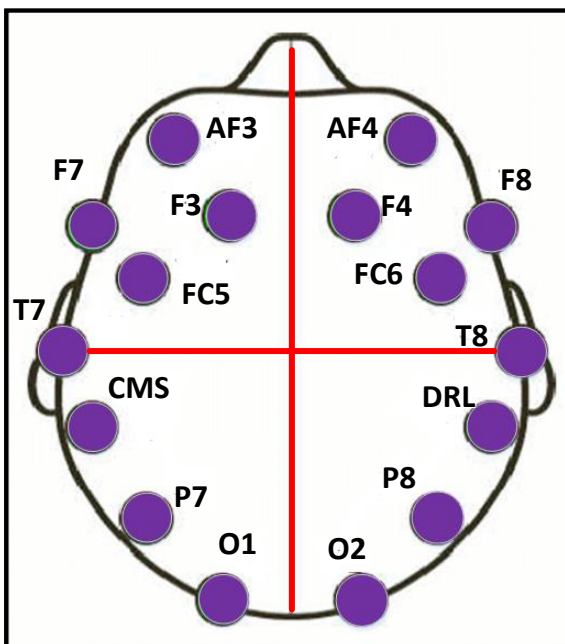


Figure 1. Electrode positions of the 14-channel Emotiv EPOC EEG system.

The dataset consists of observations matching EEG signals with the open or closed eyes of individuals and is suitable for binary classification problem. The target variable eyeDetection represents the closed eyes with a value of 0 and the open eyes with a value of 1. Accordingly, the target variable in the dataset consists of two categories and the number of samples corresponding to the moments when the eyes are closed is 8,257 and the number of samples corresponding to the moments when the eyes are open is 6,723. The dataset consists of 14,980 observations and 15 columns in total. The first 14 columns reflect the instantaneous values of EEG signals obtained from different electrodes. These signals were recorded using the Emotiv EPOC EEG headset and the electrodes used cover the following channels: AF3, F7, F3, FC5, T7, P7, O1, O2, P8, T8, FC6, F4, F8 and AF4. The electrodes were placed in different regions of the brain, allowing data collection from the frontal, temporal, parietal and occipital lobes. This placement structure is visually presented in Figure 1.

3.2. Method

Data Preparation and Pre-processing: The EEG Eye State dataset used in this study is structured in ARFF (Attribute-Relation File Format) format. ARFF is a file format that is widely preferred especially in machine learning applications and contains both attribute definitions and data. This structure allows the features in the dataset and the target variable to be explicitly defined, ensuring data integrity. The dataset was imported in the appropriate format to enable the analysis and modelling processes to be carried out in the Python environment and then converted to DataFrame format using the pandas library. Thanks to this transformation, the data has been made flexible and suitable for processing in order to perform statistical analyses, select attributes and apply classification models.

Feature and Label Separation: Feature and label separation, which is one of the basic steps of the data preprocessing process, is a critical stage in terms of structuring machine learning algorithms. In this study, the variables in the EEG Eye State dataset are divided into two groups as independent variables (features) and dependent variables (target labels). The feature set (X) consists of numerical values corresponding to 14 different electrode channels from which EEG signals are obtained. These channels were recorded by electrodes placed in the frontal, temporal, parietal and occipital regions of the brain. The target variable (y) is called eyeDetection and is a binary classification variable representing the closed eyes with the label 0 and the open eyes with the label 1. This distinction enabled the model to predict eye state only from the explanatory variables and allowed the learning process of the algorithms to be structured correctly.

Feature and Label Separation: The first step in the data preprocessing process is the systematic separation of the explanatory variables and the target variable. In this study, numerical data representing EEG signals are set as independent variables (X), while the target variable eyeDetection is separated as dependent variable (y). The independent variable set contains the signals of 14 different electrode channels recorded by the EEG device, and the classification model is enabled to learn over these multidimensional data. The target variable contains the binary class information indicating whether the eyes are open (1) or closed (0).

Feature Scaling (Standard Scaler): Scaling is a critical part of the modelling process in order to increase the effectiveness of machine learning algorithms and to balance the effect of attributes on the model. In this context, the Standard Scaler method used in this study is a preprocessing technique that aims to fit the data into a standard distribution by setting the mean of each attribute equal to zero and the standard deviation equal to one. Thanks to this standardisation process expressed in Equation 1, the model is able to evaluate all variables at the same level of importance without discriminating between attributes of different scales. Thus, over-sensitivities and attribute biases that can be seen especially in distance and weight-based algorithms are prevented. The Standard Scaler application both increases the overall accuracy of the model and makes the training process more stable and faster [28].

$$X_{scaled} = \frac{X - mean(X)}{std(X)} \quad (1)$$

X_{scaled} represents scaled data with mean 0 and standard deviation 1, where X is the data value, $mean(X)$ is the mean of the dataset and $std(X)$ is the standard deviation of the dataset.

4. MODELLING AND EVALUATION

4.1. Extra Trees Classifier

In this study, the Extra Trees Classifier (ETC) algorithm was preferred in the modelling phase for classifying the eye-opening status of individuals from EEG signals. ETC is a classifier that stands out among tree-based ensemble learning methods and is known for its high level of randomness. The algorithm is based on the ‘Extremely Randomised Trees’ approach developed by Geurts et al [29]. This method is based on the collective construction of decision trees and the combination of the predictions obtained from these trees by majority voting. The difference of the Extra Trees Classifier from traditional methods such as Random Forest is that not only the attributes but also the split points are randomised. In addition, the entire training data is used in the construction of the model without bootstrap sampling, thus providing diversity among the trees and increasing the generalisation capacity of the model. This high level of randomisation strategy reduces the variance of the model and limits the risk of overfitting. At the same time, the no-sampling approach provides more balanced learning by reducing the systematic bias [30].

The ETC model used in this study was trained with an ensemble of 100 decision trees. This number of trees was chosen to improve both the stability of the model and the classification performance. A large number of trees improves decision reliability and supports overall accuracy, especially for biosignals that may contain noise such as EEG. A visual representation of the general operation of the model is presented in Figure 2. Among the hyperparameters of the algorithm, variables such as the number of trees, minimum sample size and the number of random features to be evaluated at the node are critical factors that directly affect the decision diversity and generalisation performance in the learning process. On the other hand, since the node splitting process is randomised due to the structure of ETC, the computational cost remains low, which makes the method a computationally efficient solution. Thanks to these features, Extra Trees

Classifier is considered as a powerful, fast and balanced learning tool for binary classification problems such as eye state in high-dimensional, multivariate and structurally complex EEG data.

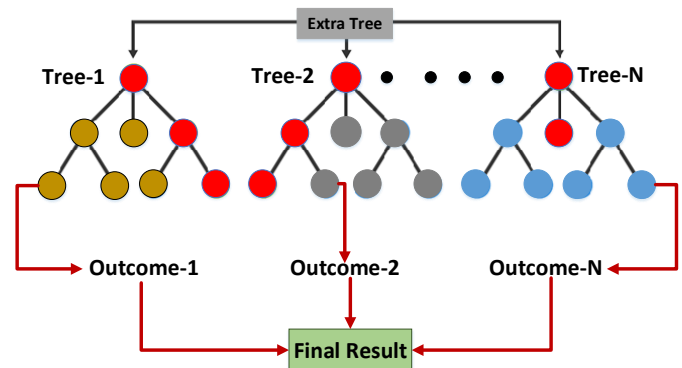


Figure 2. Extra Trees Classifier

4.2. Evaluation Metrics

Cross Validation: In this study, the 10-Fold Cross-Validation method was used to reliably assess the generalisability of the classification model. This method allows the model to be tested independently in each subset by dividing the entire dataset into ten subgroups of approximately equal size, thus providing more robust and statistically significant performance measures. The StratifiedKFold approach was adopted in the cross-validation process. This method stabilises the validation process of the model in data sets with class imbalance, by preserving the class distribution proportionally in each layer and enables the evaluation criteria to be calculated fairly across classes.

Performance Evaluation Metrics: The success level of the classification model developed in this study is evaluated with basic performance measures that are widely used in classification problems and are considered statistically significant. These metrics quantitatively reveal both the overall and class-based discrimination capacity of the model and allow inferences to be made regarding the practical applicability of the model.

Accuracy: Accuracy is a key indicator of success that expresses the overall accuracy of the classification model. It is calculated as the ratio of the number of data correctly classified by the model out of all instances to the total number of instances. Since this metric includes correct predictions in both positive and negative classes, it is a holistic evaluation measure that reflects the overall classification competence of the model. Accuracy is calculated as the ratio of the sum of True Positive (TP) and True Negative (TN) predictions, plus false positive (FP) and false negative (FN) predictions, to the total number of samples. In Equation 2, the accuracy measure is expressed mathematically [28].

$$Accuracy = \frac{TP + TN}{TP + TN + FP + FN} \quad (2)$$

Precision: Precision is an evaluation metric that expresses the proportion of samples that the model predicts belong to the positive class that are actually positive. This metric is especially critical in cases where the model has a high tendency to generate false positives (FP). This is because it reflects the level of accuracy in the model's positive forecasts and reveals its forecast reliability. In other words, it measures how many of the samples that the model marks as ‘‘positive’’ class actually

belong to that class. In Equation 3, the Precision criterion is expressed mathematically [28].

$$Precision = \frac{TP}{TP + FP} \quad (3)$$

Recall: Recall is one of the key classification metrics that measures the model's ability to recognize true positive examples. In other words, it refers to the proportion of all instances belonging to the positive class that the model correctly classifies as positive. This metric plays a decisive role, especially in applications where it is critical to reduce the number of False Negative (FN), i.e. missed positive examples. The sensitivity value is expressed mathematically in equation 4 [28].

$$Recall = \frac{TP}{TP + FN} \quad (4)$$

F1-Score: The F1 score is a composite metric that quantitatively reflects the balance between the precision and recall metrics of a classification model. By taking the harmonic mean of both values, this metric summarizes in a single value both the model's ability to detect true positives and its success in avoiding false alarms. Especially in datasets with imbalance between classes, where general measures of success such as accuracy can be misleading, the F1 score provides a more accurate representation of the model's true performance. Due to its computational methodology, the F1 score can reach high values not only with high precision or high sensitivity, but by optimizing both together. As such, it is one of the key success indicators of choice, especially in scenarios where both false positive (FP) and false negative (FN) results are critical (e.g. medical diagnostics, security systems, fraud detection). The F1 score is mathematically formulated in equation 5 [28,31].

$$F1\ Score = 2 \times \frac{Precision \times Recall}{Precision + Recall} \quad (5)$$

This ratio takes a value between 0 and 1, with a value closer to 1 indicating that the model has a strong balance in terms of both precision and sensitivity. Therefore, the F1 score is considered as an indispensable performance criterion for the reliability and application success of classification systems.

Receiver Operating Characteristic Curve (ROC): It is an evaluation tool that visualizes the extent to which the model can correctly distinguish the positive class depending on the classification thresholds in binary classification problems. The ROC curve shows the relationship between the model's True Positive Rate (TPR), or sensitivity, and False Positive Rate (FPR). These two ratios change as the threshold is varied, and the ROC curve graphically presents the discrimination performance of the model across this variability. The points on the curve represent the behaviour of the model at different thresholds, while the Area Under the Curve (AUC) is a singular metric that summarizes the overall classification ability of the model. The AUC value ranges between 0 and 1, with values close to 1 indicating that the model can distinguish between positive and negative classes with high accuracy. AUC value: 0.5 means performance equivalent to random guessing and 1.0 means excellent classification performance. In this context, ROC-AUC analysis offers a more robust and reliable metric to assess the true discrimination capacity of the model, especially

in scenarios where classical metrics such as accuracy can be misleading, especially in the presence of class imbalance [28].

Confusion Matrix: The Complexity Matrix is a fundamental evaluation tool that allows analysing the performance of classification models not only in terms of overall accuracy, but also in terms of class-based patterns of success and error. This structure details the classification process by comparing the predictions produced by the model with the actual class labels through four main components: True Positive (TP), False Positive (FP), True Negative (TN) and False Negative (FN). These four components categorically reflect both the model's accuracy and its tendency to be wrong at the class level. Especially in binary classification problems, the structure of this matrix is usually 2x2 in size, allowing a direct comparison of the performance of the model for different classes [28].

The complexity matrix is the main data source for calculating not only overall accuracy but also important derivative metrics such as precision and recall. In this respect, the complexity matrix provides the opportunity to analyse the decision quality of the model in more detail, especially in data sets with class imbalance or in clinical, financial or security-based applications where certain classes (e.g. positive class) are more critical. It also provides a more comprehensive perspective on what types of errors the model is prone to make and the operational consequences of these errors in the application domain. Thus, not only quantitative success but also qualitative evaluation becomes possible [31].

5. FEATURE IMPORTANCE

In order to increase the interpretability of machine learning models and to quantitatively reveal which variables contribute more to the classification process, feature importance ranking was performed in this study. This analysis allows for a more transparent evaluation of not only the output of the model but also the decision-making process [32,33]. Especially when working with multidimensional and structurally complex data such as biological signals, knowing the relative importance levels of attributes plays a critical role in understanding the internal logic of the model and increasing its interpretability [34]. In this study, attribute importance scores are computed from the decision trees of the Extra Trees Classifier algorithm using a model-based approach. This method statistically evaluates the contribution of the EEG data obtained from each electrode channel to the classification decision. Due to the natural structure of tree-based algorithms, direct interaction between features is taken into account and the features that contribute the most to the learning process of the model are ranked according to their relative weights.

6. RESULT AND DISCUSSION

6.1 Result

This study aims to classify the eye openness (open/closed) of individuals using the EEG Eye State dataset, which is made openly available by Baden-Württemberg Cooperative State University through the UCI Machine Learning Repository. The dataset consists of a total of 14,980 observations corresponding to 14 channels of EEG signals recorded at different time points; each sample is labeled in a binary classification format according to whether the eyes are open (1) or closed (0). In the modeling process, Extra Trees Classifier (ETC), an ensemble learning algorithm based on decision trees, was used and the

classification performance of this model, which was configured with 100 trees, was analysed based on various criteria.

In order to evaluate the generalizability and stability of the model, the Stratified 10-Fold Cross-Validation method was used and key performance metrics such as accuracy, precision, recall and F1 score were calculated for each layer. According to the results presented in Table 1, the model performed consistently above 90% in all layers, especially in layer 1 (Fold 1), where the F1 score of 0.9521 was the highest among all layers. This result indicates that the model maximizes the model's ability to predict the positive class both accurately and consistently in this layer. Overall, the average accuracy of the model is 0.9511, average precision is 0.9645, average sensitivity is 0.9252 and average F1 score is 0.9444. These metrics reveal that the model performs a high performance and reliable classification by balancing between classes. In particular, the high average F1 score shows that the model is able to distinguish both positive and negative classes in a balanced way and exhibits a stable behavior in decision processes.

TABLE 1
CROSS-VALIDATION PERFORMANCE METRICS

Fold	Accuracy	Precision	Recall	F1 Score
1	0.9579	0.9736	0.9315	0.9521
2	0.9526	0.9574	0.9360	0.9466
3	0.9566	0.9691	0.9330	0.9507
4	0.9526	0.9659	0.9271	0.9461
5	0.9506	0.9614	0.9271	0.9439
6	0.9473	0.9640	0.9167	0.9397
7	0.9493	0.9571	0.9286	0.9426
8	0.9426	0.9666	0.9034	0.9339
9	0.9526	0.9703	0.9227	0.9459
10	0.9493	0.9599	0.9257	0.9425

Feature importance evaluation, which is used to analyse which features are more decisive in the classification decisions of the model, plays an important role in making the internal decision structure of the model more transparent and interpretable. In this context, the relative importance scores calculated by the Extra Trees Classifier algorithm over the decision trees are analysed. As presented in Table 2, the attributes that the model gives the most weight in the classification process are the data belonging to the O1 and P7 electrodes. The fact that these two channels stand out with importance scores of 0.1154 and 0.1000, respectively, indicates that the EEG signals obtained from the occipital (O1) and parietal (P7) regions have high discriminative power in distinguishing the eye-opening status.

TABLE 2
FEATURE IMPORTANCE SCORES

Feature	Importance Score
O1	0.1154
P7	0.1000
F7	0.0857
F8	0.0782
AF3	0.0772
AF4	0.0761
FC6	0.0650
FC5	0.0617
F4	0.0614
T7	0.0587
T8	0.0583
F3	0.0571
O2	0.0568
P8	0.0482

Moreover, channels such as F7, AF3 and AF4, which correspond to the frontal region, ranked high with scores of 0.0857, 0.0772 and 0.0761, respectively, suggesting that the model also considers frontal lobe activities as an important determinant in the decision-making process. This supports that brain regions associated with visual attention, eye movements and cortical activation processes are critical for the detection of eye openness via EEG signals. Channels with low importance scores, such as O2, P8 and F3, contributed less to the model's classification process, which may be instructive for future regional analyses in relation to the topographic distribution and signal characteristics of the data.

In order to visually and statistically evaluate the classification performance of the model, the Receiver Operating Characteristic (ROC) curve was analysed. The ROC curve shows the accuracy of the model at different thresholds, indicating the extent to which the positive class is correctly separated. As presented in Figure 3, the ROC curve for Fold 1 clearly shows that the model has a high discriminative power, with its structure almost leaning towards the upper left corner. The Area Under Curve (AUC) value was calculated as 0.9926 in this sample. This value indicates that the classification performance is almost perfect, confirming that the model works with both high accuracy and low false positive rate. In this context, the obtained ROC curve and AUC score show that the model is highly successful not only in terms of average metrics but also in terms of its sensitivity in class discrimination. As the reduction of false positives is critical, especially in biomedical classification problems, this result supports the suitability of the model for practical applications.

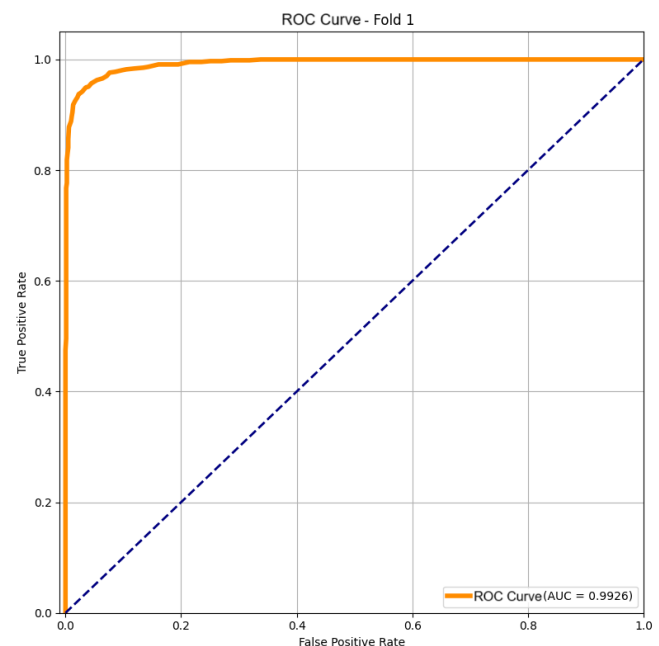


Figure 3. ROC Curve and AUC Value for Fold 1

In order to further analyse the classification performance of the model, the confusion matrix for Fold 1 is examined. As presented in Figure 4, the four main components of the model's correct and incorrect classifications are clearly visible. The model produced 809 True Negative and 17 False Positive predictions for the negative class (label 0), which represents when the eyes are closed. On the other hand, 626 True Positive and 46 False Negative predictions were made for the positive

class (label 1). According to these results, the model was able to discriminate both classes with high accuracy and demonstrated its discriminative power by making very low false positive predictions, especially for the negative class. The relatively high number of false negatives (FN = 46) suggests that the model is more cautious when classifying the positive class (eyes open). This distribution reveals that the model exhibits a balancing structure that contributes to its overall performance and keeps the misclassification rates to a minimum. Hence, these findings from the confusion matrix are consistent with previous performance metrics and ROC analysis, numerically confirming the model's consistent success in class discrimination.

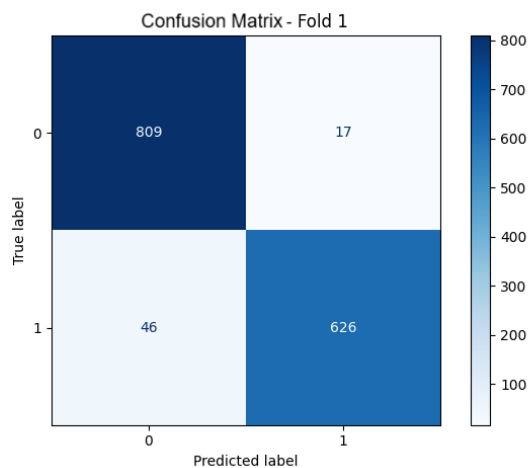


Figure 4. Confusion Matrix for Fold 1

6.2 Discussion

In this study, it is aimed to classify the eye openness state (open/closed) of individuals using EEG signals. For this purpose, the EEG Eye State dataset was used; the dataset contains 14,980 observations labelled for binary classification, consisting of 14 attributes in total. In the modelling process, data normalization was applied, and all variables were evaluated on the same scale. In the classification phase, the Extra Trees Classifier (ETC) algorithm, an ensemble method based on decision trees, was preferred and the model was tested with a 10-fold cross-validation method. The model gave consistent results in each fold and demonstrated an overall successful classification performance. In particular, Fold 1 showed the highest success in terms of F1 score.

The ROC curve of the model shows that the classification sensitivity is high, while the confusion matrix reveals low levels of misclassifications. Moreover, the feature importance analysis shows that the model gives more weight to some EEG channels in the classification process. This supports the effect of topographical diversity of EEG signals on classification success. However, the study also has some limitations. Since the dataset used was obtained from a single group of participants, it may be limited in terms of generalizability. In addition, only one basic machine learning algorithm was used for classification, and different model comparisons were not included. The lack of integration of deep learning or other signal processing techniques may have limited the ability of the method to recognize more complex patterns. In these respects, the study has demonstrated the effectiveness of machine learning methods in EEG-based eye state classification, but it is recommended to be supported by studies with larger

participant profiles, different algorithms and multiple data sources.

7. CONCLUSION AND FUTURE STUDIES

In this study, we aim to automatically classify the eye openness state (open/closed) of individuals from EEG signals and develop a machine learning model on the EEG Eye State dataset. In the modelling process, the Extra Trees Classifier method, an ensemble learning algorithm based on decision trees, was preferred and the performance of the model was analysed in detail by applying 10-fold cross-validation on the dataset. The findings show that the model offers a consistent classification success. In particular, the highest success in terms of F1 score was observed in Fold 1, while the ROC curve and confusion matrix revealed that the model has a strong discrimination ability in terms of both sensitivity and specificity. Feature importance analysis revealed that some EEG channels play more decisive roles in the classification process, emphasizing the contribution of regional EEG activity to classification success. These findings suggest that traditional machine learning algorithms, when combined with appropriate preprocessing techniques and balanced modelling strategies, can provide effective solutions to classification problems based on biological signals such as EEG.

Despite the findings of this study, some limitations need to be addressed in future research. First of all, since the dataset used was obtained from a single device and under limited conditions, the generalizability of the model should be re-evaluated with EEG data collected from different populations and conditions. Furthermore, comparative performance analysis of different machine learning algorithms (e.g. LightGBM, XGBoost) and deep learning-based models (e.g. CNN, LSTM) can be performed to reveal more robust classification structures. On the other hand, this line of research can be further deepened by extending studies such as time series-based feature extraction, advanced filtering techniques for signal noise removal, and classification of cognitive states other than eye state. In particular, the development of low latency and high accuracy models for real-time applications will contribute to practical applications such as EEG-based human-computer interfaces and driver attention systems.

REFERENCES

- [1] Piatek, Ł., Fiedler, P., & Haueisen, J. (2018). Eye state classification from electroencephalography recordings using machine learning algorithms. *Digital Medicine*, 4(2), 84-95.
- [2] Bharati, S., Podder, P., & Raihan-Al-Masud, M. (2018, November). EEG eye state prediction and classification in order to investigate human cognitive state. In 2018 International Conference on Advancement in Electrical and Electronic Engineering (ICAEEE) (pp. 1-4). IEEE.
- [3] Nilashi, M., Abumalloh, R. A., Ahmadi, H., Samad, S., Alghamdi, A., Alrizq, M., ... & Nayer, F. K. (2023). Electroencephalography (EEG) eye state classification using learning vector quantization and bagged trees. *Heliyon*, 9(4).
- [4] Ketu, S., & Mishra, P. K. (2022). Hybrid classification model for eye state detection using electroencephalogram signals. *Cognitive Neurodynamics*, 16(1), 73-90.
- [5] Saeid Sanei, Jonathon A. Chambers, "EEG Signal Processing," John Wiley & Sons, 2013.
- [6] Peter Wolf (M.D.), "Epileptic Seizures and Syndromes: With Some of Their Theoretical Implications," John Libbey Eurotext, 1994.
- [7] Aleksandar Čolić, Oge Marques, Borko Furht, "Driver Drowsiness Detection: Systems and Solutions," Springer, 2014.

- [8] Mardi Z, Ashtiani SNM, Mikaili M (2011) EEG-based drowsiness detection for safe driving using chaotic features and statistical tests. *J Med Signals Sens* 1(2):130
- [9] Khurram I,Qazia, H.K.Lama, BoXiao, Gaoxiang Ouyang, XunheYinc, "Classification of epilepsy using computational intelligence techniques", *CAAI Transactions on Intelligence Technology*, Volume 1, Issue 2, Pages 137-149, April 2016.
- [10] Correa AG, Orosco L, Laciari E (2014) Automatic detection of drowsiness in EEG records based on multimodal analysis. *Med Eng Phys* 36(2):244–249.
- [11] Sanei, S., & Chambers, J. A. (2013). *EEG signal processing*. John Wiley & Sons.
- [12] Laport, F., Castro, P. M., Dapena, A., Vazquez-Araujo, F. J., & Iglesia, D. (2020, August). Study of machine learning techniques for eye state detection. In *Proceedings (Vol. 54, No. 1, p. 53)*. MDPI.
- [13] Mumtaz W, Ali SSA, Yasin MAM, Malik AS (2018) A machine learning framework involving EEG-based functional connectivity to diagnose major depressive disorder (MDD). *Med Biol Eng Comput* 56(2):233–246
- [14] Zhang T, Chen W, Li M (2019) Classification of inter-ictal and ictal EEGs using multi-basis MODWPT, dimensionality reduction algorithms and LS-SVM: a comparative study. *Biomed Signal Process Control* 47:240–251.
- [15] Chatterjee R, Maitra T, Islam SH, Hassan MM, Alamri A, Fortino G (2019a) A novel machine learning based feature selection for motor imagery EEG signal classification in Internet of medical things environment. *Future Gener Comput Syst* 98:419–434
- [16] Gajbhiye, P., Singh, V., Saharan, S., & Joshi, S. (2024). Artificial neural network-based classification of eye states using electroencephalogram signals: a comparative analysis of algorithms and artifact removal techniques. In *Artificial Intelligence: A tool for effective diagnostics* (pp. 5-1). Bristol, UK: IOP Publishing.
- [17] O. Roesler, "UCI Machine Learning Repository [EEG Eye State]," *Baden-Wuerttemberg Cooperative State University (DHBW)*, Stuttgart, Germany, 2013. [Online]. Available: <https://archive.ics.uci.edu/ml/datasets/EEG+Eye+State>
- [18] Keerthi Latha, C. V., & Kezia Joseph, M. (2024, June). Enhancing Depression Detection Using EEG Signals Through Adaptive Feature Weighting in Extra Trees Classifier. In *International Conference on Frontiers of Intelligent Computing: Theory and Applications* (pp. 583-592). Singapore: Springer Nature Singapore.
- [19] Shafique, R., Mehmood, A., & Choi, G. S. (2019). Cardiovascular disease prediction system using extra trees classifier. *Res. Sq*, 11, 51.
- [20] Hassan, M. M., Hassan, M. R., Huda, S., Uddin, M. Z., Gumaei, A., & Alsanad, A. (2021). A predictive intelligence approach to classify brain-computer interface based eye state for smart living. *Applied Soft Computing*, 108, 107453.
- [21] Jayadurga, N. P., Chandralekha, M., & Saleem, K. (2024, May). Leveraging Ensemble Techniques for Enhanced Eye State Classification with EEG Data. In *2024 2nd International Conference on Advancement in Computation & Computer Technologies (InCACCT)* (pp. 570-576). IEEE.
- [22] Xiao, Q., Yang, M., & Yuan, K. (2023). Eye state recognition based on continuous wavelet transform and improved convolutional neural network.
- [23] Adil, S. H., Ebrahim, M., Raza, K., & Ali, S. S. A. (2018, August). Prediction of eye state using knn algorithm. In *2018 International Conference on Intelligent and Advanced System (ICIAS)* (pp. 1-5). IEEE.
- [24] Fikri, M. A., Santosa, P. I., & Wibirama, S. (2021, October). A review on opportunities and challenges of machine learning and deep learning for eye movements classification. In *2021 IEEE International Biomedical Instrumentation and Technology Conference (IBITeC)* (pp. 65-70). IEEE.
- [25] Alkhaldi, M., Joudeh, L. A., Ahmed, Y. B., & Husari, K. S. (2024). Artificial intelligence and telemedicine in epilepsy and EEG: A narrative review. *Seizure: European Journal of Epilepsy*, 121, 204-210.
- [26] Gaddanakeri, R. D., Naik, M. M., Kulkarni, S., & Patil, P. (2024, April). Analysis of EEG signals in the DEAP dataset for emotion recognition using deep learning algorithms. In *2024 IEEE 9th International Conference for Convergence in Technology (I2CT)* (pp. 1-7). IEEE.
- [27] Yu, W. Y., Sun, T. H., Hsu, K. C., Wang, C. C., Chien, S. Y., Tsai, C. H., & Yang, Y. W. (2024). Comparative analysis of machine learning algorithms for Alzheimer's disease classification using EEG signals and genetic information. *Computers in Biology and Medicine*, 176, 108621.
- [28] Hazar, Y., & Ertuğrul, Ö. F. (2025). Process management in diabetes treatment by blending technique. *Computers in Biology and Medicine*, 190, 110034.
- [29] Geurts, P., Ernst, D., & Wehenkel, L. (2006). Extremely randomized trees. *Machine learning*, 63, 3-42.
- [30] Hussein, N., & Zeebaree, S. R. (2024). Performance Evaluation of Extra Trees Classifier by using CPU Parallel and Non-Parallel Processing. *The Indonesian Journal of Computer Science*, 13(2).
- [31] A. G'eron, *Hands-on Machine Learning with Scikit-Learn, Keras, and TensorFlow*, O'Reilly Media, Inc, 2022.
- [32] M.A. Jamil, S. Khanam, Influence of One-Way ANOVA and Kruskal–Wallis Based Feature Ranking on the Performance of ML Classifiers for Bearing Fault Diagnosis, *Journal of Vibration Engineering & Technologies*, 2023, pp. 1–32.
- [33] A. Al Imran, A. Rahman, H. Kabir, M.S. Rahim, The impact of feature selection techniques on the performance of predicting Parkinson's disease, *Int. J. Inf. Technol. Comput. Sci.* 10 (11) (2018) 14–29.
- [34] N. Silpa, V.M. Rao, M.V. Subbarao, R.R. Kurada, S.S. Reddy, P.J. Uppalapati, An enriched employee retention analysis system with a combination strategy of feature selection and machine learning techniques, in: *2023 7th International Conference on Intelligent Computing and Control Systems (ICICCS)*, IEEE, 2023, May, pp. 142–149.

BIOGRAPHIES

Süleyman Dal Dr. Lecturer. Assist. Süleyman Dal is an academic specialised in the field of electrical and electronics engineering. He completed his undergraduate education at Çukurova University, Department of Electrical and Electronics Engineering in 2018, completed his master's degree at Batman University, Institute of Science and Technology in 2020, and completed his doctorate education at the Institute of Graduate Studies of the same university in 2021. He is currently working as a Dr. Lecturer in the Energy Coordination Department within the Batman University Rectorate. His research interests include machine learning, signal processing and optimisation algorithms.

Research Article

An Investigation into The Utilization of a Biodiesel Fuel Blend Supplemented with $Mn(NO_3)_2$ Additives in a CI Engine

Tarhan Tan¹ , Selman Aydin^{2*} ¹ Department of Automotive Engineering, Institute of Graduate Studies Batman University, Batman, Turkey. (e-mail: otomotiv_213372@hotmail.com)^{2*} Vocational High School of Technical Sciences, Department of Mechanical and Metal Technology, Batman University, Batman, Turkey. (e-mail: selman.aydin@batman.edu.tr)

ARTICLE INFO

Received: May., 30. 2024

Revised: Oct., 02. 2024

Accepted: Jan., 07. 2025

Keywords:

Diesel engine
Waste vegetable oils biodiesel
Combustion
Energy
 $Mn(NO_3)_2$ additive
Emission

*Corresponding author: [Selman Aydin](mailto:Selman.Aydin@batman.edu.tr)

ISSN: 2536-5010 / e-ISSN: 2536-5134

DOI: <https://doi.org/10.36222/ejt.1491374>

ABSTRACT

As it is known, due to the fact that petrol has a limited reserve, the search for renewable energy has an important place in all world states (by researchers). In this perspective, it was aimed to investigate the effect of a manganese standard solution for the improvement of combustion and other properties of biodiesel fuel. The experimental fuels had been created as follows: DF (diesel fuel), B25 (a blend of 25% biodiesel and 75% DF), and Mn100B25 (a blend of 25% biodiesel, 75% DF, and 100 ppm of $Mn(NO_3)_2$ additive). During the examination of the experimental fuels, the Mn100B25 fuel exhibited a decrease in density, viscosity, cetane index, and flash point compared to the B25 fuel. However, there was a slight improvement in the calorific value of the Mn100B25 fuel. The combustion and emission parameters were empirically investigated in a compression ignition (CI) engine operating at various load conditions and constant engine speeds. The analysis of the experimental data revealed that the Mn100B25 fuel exhibited the highest values for cylinder gas pressure, average gas pressure, and net heat release at the 6 bar bmep parameter. During analyzing the emission values, it emerged that the HC emissions of Mn100B25 fuel types exhibited 14.28% lower values compared to DF fuel under the 4 bar bmep conditions. At 4 bar bmep and 6 bar bmep, the CO emission values for DF and Mn100B25 fuels were the same; however, the emission value for B25 fuel was lower than that of the other two fuel types. As a result, it was observed that positive results were obtained by adding a mixture of biodiesel and manganese standard solution to the biodiesel fuel blend at a certain rate. As a result, it was observed that biodiesel and manganese standard solution blend can be used as an alternative fuel by adding to diesel fuel at certain ratios.

1. INTRODUCTION

Energy is the most important factor that human beings need to meet their needs. Due to the ever-increasing world energy demand, industrialization and rapid population growth, the need for energy is increasing day by day and the growing energy demand deficit is growing [1]. Various studies have been carried out to investigate the feasibility of using cleaner [2-4] and renewable fuel alternatives to reduce the unfavorable impact of engine exhaust emissions on the environment. While coal, oil and natural gas were mostly used as fossil resources in the past, today more renewable and transformable energy resources such as wind, solar, hydraulic, biomass etc. are produced and consumed. In addition, biodiesel, which is one of the renewable energy

sources [5-6], has advantages such as the fact that it can be used without making any changes in the structure of the diesel engine, its cetane number is high, its flash point is low, it is safer to transport and store compared to diesel fuel, and it reduces exhaust emission values [7-8]. Apart from its advantages, the disadvantages of biodiesel fuel compared to diesel fuel in terms of its thermal value, viscosity, cold flow property and freezing point have led researchers to develop it with various nanoparticles [9-10]. Although hybrid and electric vehicles are being studied intensively in the coming years, the need for an alternative renewable energy source to diesel fuel is indispensable for heavy vehicles with diesel engines that need power and torque requirements [11]. Keskin et al. reported [12] that methyl esters were produced from fatty acids and the resin acids were reacted with NiO

and MnO_2 at certain ratios for the production of metallic fuel additives in order to improve the values that may occur in diesel fuel. To prepare each metallic fuel additive test fuels, a mixture of 60% biodiesel and 40% diesel fuel was made and 8 $\mu\text{mol/l}$ and 12 $\mu\text{mol/l}$ of additives were added. The metallic additives added to biodiesel fuel improved the pour point and viscosity values and reduced CO emissions by 64.28% and smoke opacity by 30.91% in the exhaust emission gases of biodiesel fuels. It was observed that NO_x emissions were generally low in biodiesel fuel. Gürü et al. Used [13] organic compounds of Mg, Ca, Cu and Mn as fuel additives. In the experiments, manganese-containing fuel additive has a better effect on diesel fuel compared to other metallic additives. While 54 $\mu\text{mol Mn/l}$ additive, which was determined as the rate to be used, decreased the freezing temperature of diesel fuel by 12.4 °C, manganese additive used at the same rate increased the cetane number from 46.22 to 48.24. O_2 and CO emissions decreased by 0.2% and 14%, respectively.

In the literature research, the use of biodiesel obtained from waste frying oil in diesel engines needs to be improved due to deterioration in performance and combustion parameters compared to diesel fuel. Therefore, in this study, the manganese standard solution additive ($Mn(NO_3)_2$) was added to biodiesel and diesel fuel blends, and the resulting blends were tested in a CI engine to investigate the changes in combustion and emission parameters as well as the chemical and physical properties of the blended fuels.

2. MATERIALS AND METHODS

2.1. The test equipment and methodology

Experimental studies were carried out in the workshop of Batman University Automotive Engineering Department. Biodiesel was produced from waste frying oil by transesterification method [14]. B25 and Mn100B25 fuel blends were obtained with biodiesel fuel produced by standard methods. For combustion parameters and emission values, cylinder gas pressure, net heat release, pressure increase rate, average gas temperature, cumulative heat release and NO_x , CO, CO_2 , HC emission values of DF, B25 and Mn100B25 fuels were tested in the experimental engine setup shown in Figure 1 and compared graphically in results and discussion section.

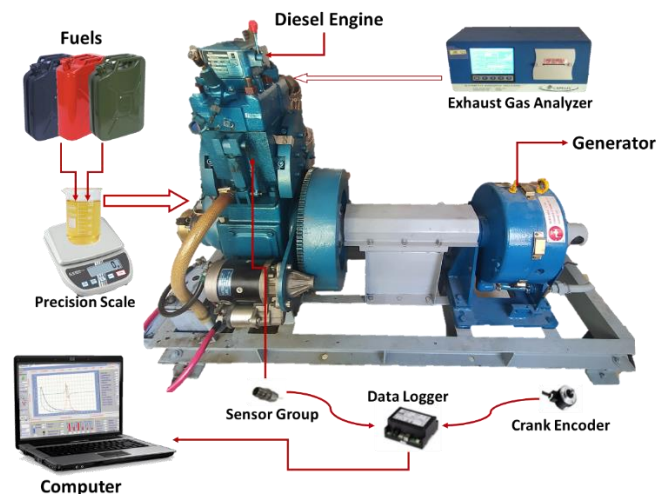


Figure 1. Schematic view of the experimental engine

The technical specifications of the diesel engine used for the determination of combustion and emission values are given in TABLE I. The combustion values of the test fuels in the diesel research engine were taken at 2 bar bmep, 4 bar bmep and 6 bar bmep parameters and under the same experimental conditions.

TABLE I. THE TECHNICAL SPECIFICATIONS OF THE TEST CI ENGINE

Engine Brand and Type	Kirloskar TVI
Bore / Stroke	87 / 110 mm
Compression ratio	17.5:1
Total displacement	0.66 liter
Connecting rod length	234 mm
Brake power	5.2 kW @ 1500 rpm

In this study, ICEngineSoft_9.0 computer program was used for combustion data. ICEngineSoft_9.0 application simultaneously transfers the data received from the engine to the computer. For the emission values in the experimental studies NO_x , CO, CO_2 and HC exhaust emission values of three different fuels were measured by testing DF, B25 and Mn100B25 fuel blends at 2 bar bmep, 4 bar bmep and 6 bar bmep parameters with CAPELEC brand CAP 3200 model exhaust gas device. Technical specifications of the diesel emission device are shown in TABLE II.

TABLE II. SENSITIVITY AND LIMITS OF MEASUREMENT

Parameter	limits of measurement	Precision
Engine speed	0-12000 rpm	$\pm 0.1\%$
Pressure sensor	0-200 bar	$\pm 0.5\%$
NO_x	0-10000 ppm	± 1 ppm
CO_2	0-21.0%	$\pm 0.1\%$
CO	0-10%	$\pm 0.001\%$
HC	0-20000 ppm	± 1 ppm

2.1. Test Fuels and Manganese Additives

Mn compounds in solid form on earth are found in more than 300 minerals and the most commercially used compound is manganese dioxide (MnO_2). Manganese dioxide is used between 78-85% in the battery industry and 74-84% in the chemical industry. The density value of the additive used is 1.014 gr/cm^3 , which is slightly higher than the density value of diesel and biodiesel. In the literature studies, it has been observed that Mn-based additive acts as a combustion enhancer, increases the cetane number and accordingly reduces the freezing point. In addition, the manganese additive improved the disadvantages of biodiesel fuel such as high viscosity and density and low heating value. Commercially available Sigma-Aldrich brand sodium hydroxide and decanol brand 99% purity methyl alcohol were used. For biodiesel production, 0.5% sodium hydroxide (NaOH) catalyst and 20% methyl alcohol (CH_3OH) were used in 1 liter of waste frying oil [14]. For fuel analysis, B100, B25 and Mn100B25 fuels were analyzed by TÜBİTAK Marmara Research Center (MAM) and viscosity, density, flash point, freezing point, cetane index and lower heating value parameters were analyzed separately for each fuel in accordance with the standards and the results are given in TABLE III.

TABLE III. PHYSICAL AND CHEMICAL PROPERTIES OF THE TEST FUELS USED IN THE EXPERIMENTS

Parameter	DF	Biodiesel	B25	Mn100B25	Analysis method
Viscosity (mm ² /s, at 40°C)	2.895	5.292	3.344	3.291	ASTM D 445
Density (kg/m ³ , at 15°C)	832	890.8	848.6	846.4	ASTM D 4052
Flash point (°C)	---	165.5	70.5	68.5	ASTM D 93
Cetane Number	52.78	53.7	53.6	53.3	EN ISO 4264
LHV (kJ/kg)	43850	39.34	43.67	43.83	ASTM D 240

3. RESULTS AND DISCUSSIONS

3.1. Cylinder Gas Pressure and Net Heat Release

The variations of CGP with respect to °CA at constant engine speed at 1500 rpm for 2 bar bmep, 4 bar bmep and 6 bar bmep parameters of three different loads types used for test fuels are given in Fig. 2. When the 6 bar bmep parameter, which has the highest °CA, is examined, it is found that the highest CGP increase values are Mn100B25, B25, DF fuels and their values are 74.62 °CA, 73.28 °CA, 72.78 °CA bar, respectively.

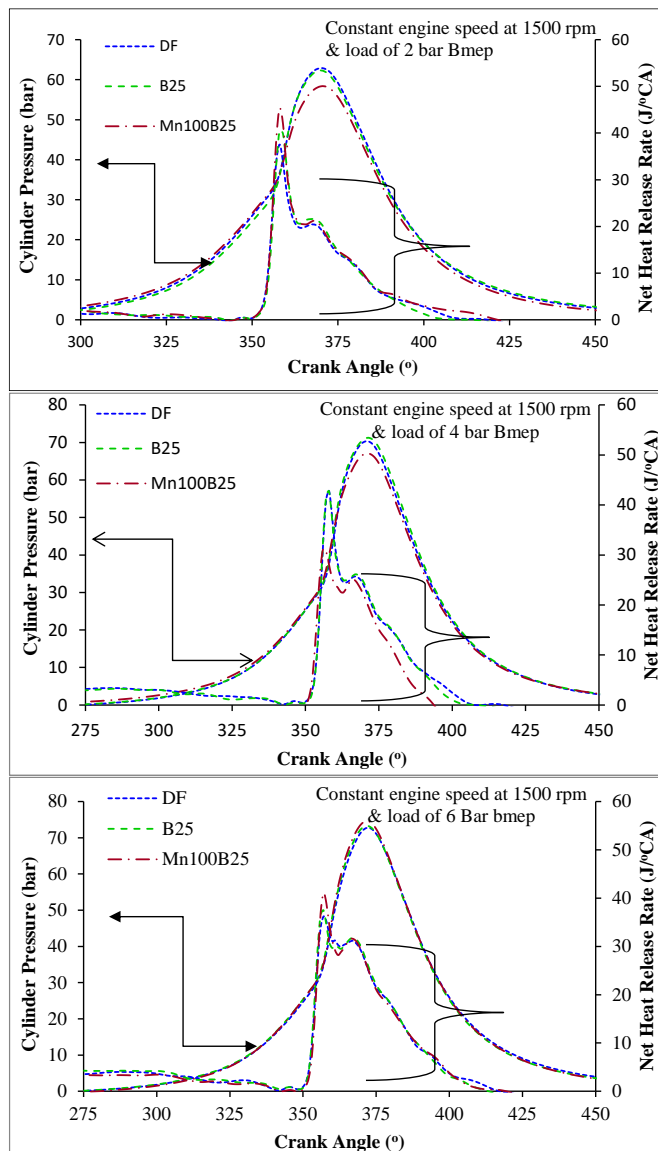


Figure 2. Cylinder gas pressure and net heat release rate curves under varying loads

The difference in CGP between Mn100B25 and DF values is 2.46%. When all the figures are analyzed, it is observed that as the engine parameter is increased, the fuel ratio sent to the cylinder will increase and the CGP will also increase. At 6 bar bmep, the CGP of Mn100B25 fuel are higher than diesel fuel, which is thought to be due to the fuel mixture ratio and the increase in the thermal value of the manganese additive.

The variations of the net HRR of the test fuels at 2 bar bmep, 4 bar bmep and 6 bar bmep parameters at constant 1500 rpm in terms of J/° with respect to °CA are given in in Fig. 3. When the 6 bar bmep parameter, which has the highest °CA, is examined, it is seen that Mn100B25, B25 and DF fuels have the highest HRR values at 357 J/° and their values are 41.05 J/°, 37.5 J/° and 36.19 J/°, respectively. The difference in HRR between Mn100B25 and DF fuel values is 11.83%. The high value in Mn100B25 fuel is due to the high amount of fuel burned per cycle due to the increase in the parameter amount [15]. Since the manganese additive added to the Mn100B25 fuel increases the calorific value of the fuel, the HRR was high at 6 bar bmep parameter.

3.2. Pressure Increase Rate and Mean Gas Temperature

The variations of the MGT of the test fuels with respect to the °CA at 2 bar bmep, 4 bar bmep and 6 bar bmep parameters and at constant 1500 rpm are given in Fig. 3. When the 6 bar bmep parameter is examined, it is seen that the highest values of the MGT at 380 K are Mn100B25, DF and B25 fuels and their values are 1624.07 K, 1600.48 K and 1588.75 K, respectively. The difference between the highest Mn100B25 fuel and DF fuel, which has the closest values, is 1.45%. Biodiesel fuel has a lower heating value than diesel fuel. The addition of manganese additive to Mn100B25 fuel increased its calorific value and increased the MGT. In addition, the decrease in density value was effective in increasing the MGT by increasing the flame intensity [16]. Changes in the rate of pressure rise (RPR) increase according to crankshaft angle (bar/°) at low, medium and high loads and at constant 1500 rpm for test fuels are given in Figure 4. When the figures are examined, it is observed that as the engine parameter is increased, the amount of fuel sent to the cylinder will increase and therefore the cylinder pressure increase rates increase. The highest-pressure increase rates were observed for B25 fuel at 2 bar bmep, DF fuel at 4 bar bmep and Mn100B25 fuel at 6 bar bmep. The sudden pressure increase of B25 fuel at 2 bar bmep depends on the cetane number of the fuel, the temperature and pressure of the air taken into the cylinder due to the long ignition delay. At 6 bar bmep, as the engine parameter increases, it can be said that a more controlled combustion occurs as a result of

the decrease in the rate of pressure increase between the fuels and the shortening of the ignition delay time [17].

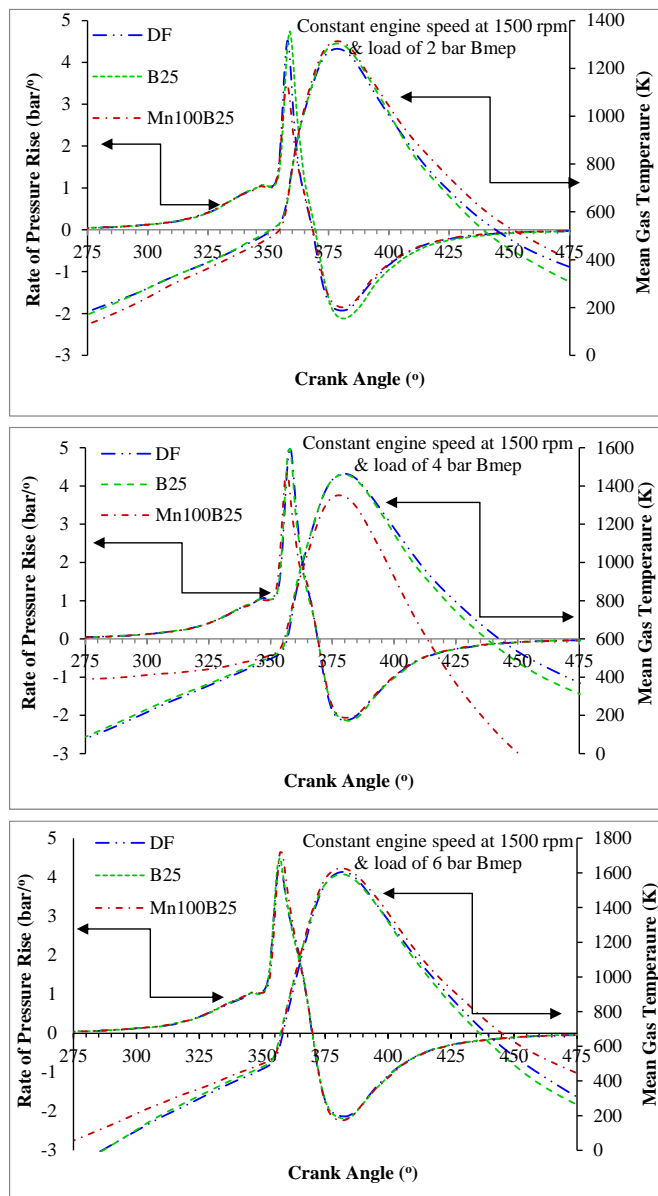


Figure 3. The mean gas temperature curves and rate of pressure rise curves under varying loads

3.3. Cumulative Heat Release

The cumulative heat release (CHR) changes for the test fuels at constant 1500 rpm and different engine parameters at low, medium and high loads, with respect to °CA are given in Figure 4. Once the figures are examined, the CHR increased with the increase in the engine parameter, but the difference between the heat release values decreased gradually. Mn100B25 at 2 bar bmep, DF fuel has the highest cumulative heat release at 4 bar bmep and 6 bar bmep. The high CHR value of B25 and Mn100B25 fuel values can be said to be the high oxygen content in biodiesel fuel and the effect of manganese additive on cetane number [18]. It is thought that the high values CHR in the low load parameters are due to the high amount of oxygen in the biodiesel fuel, the Mn additive used and the effect on the cetane number. The high cumulative heat release value of B25 and Mn100B25 fuel values can be attributed to the high oxygen content in biodiesel fuel and the effect of manganese additive on cetane number [18].

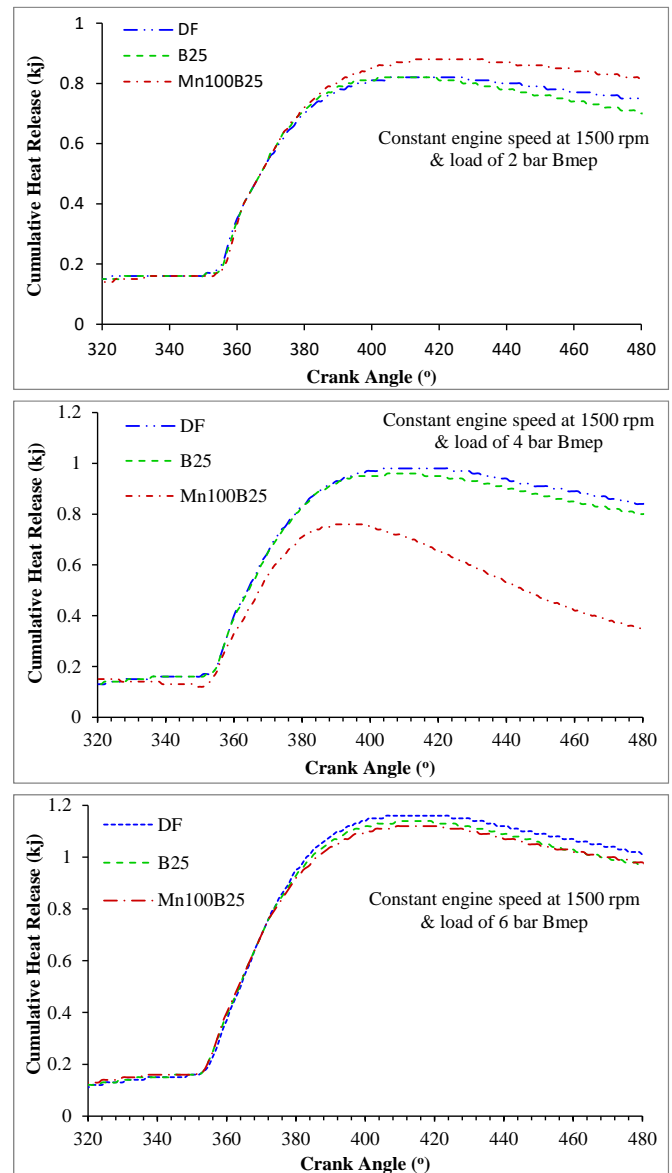


Figure 4. The cumulative heat release curves under varying loads

3.4. NOx Emission

At temperatures above 1600 °C reached in in-cylinder combustion, nitrogen oxides are formed by the reaction of nitrogen in the air with oxygen, provided that there is sufficient time. In the case of a lean mixture, nitrogen oxide emissions will decrease as the internal temperature of the cylinder will decrease with the amount of gas reacting. In addition, nitrogen oxides can cause lung diseases, respiratory infections and damage to vegetation [16]. The NOx emission values of different fuel types at different engine parameters are shown graphically in Figure 5. When all fuel types are examined, the emission values, which are at minimum levels at low loads, increase in NOx emission values with gradual increase in engine parameters. According to the 2 bmep parameters, Mn100B25 emission value has the highest NOx emission value with 161 ppm and 144 ppm, Mn100B25 emission value has 141 ppm, DF emission value has the lowest NOx emission value with 133 ppm. The fact that diesel fuel emits less emissions compared to biodiesel fuel blended fuels, the increase in fuel consumption due to the increase in the value of the bmep

parameter and the increase in the in-cylinder temperature with expanding combustion increased NO_x emissions.

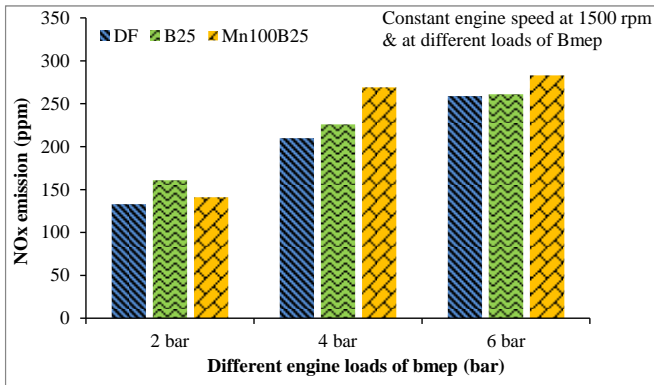


Figure 5. The variation of NO_x emissions under varying loads for test fuels

3.5. CO Emission

The presence of CO emissions in combustion products is due to the lack of sufficient oxygen in the environment. If the amount of air in the air-fuel mixture is low, the amount of O₂ in the combustion reaction will be insufficient, and not all of the fuel carbon will be converted into CO₂ and remain as CO [19]. The CO emission values of different fuel types at different engine parameters (idle, low, medium and high) are shown graphically in Fig. 6. When all fuel types are analyzed, while CO emission values of all fuels are equal in the idle parameter, DF and B25 fuel values remain equal in the low parameter, while there is a slight increase in the Mn100B25 value. In the medium and high parameters, the CO emission values of DF and Mn100B25 fuels were equal to each other, while the emission value of B25 fuel remained below the two fuel types. It can be said that the oxygen content in biodiesel fuel is effective in reducing CO emission gases [20-22].

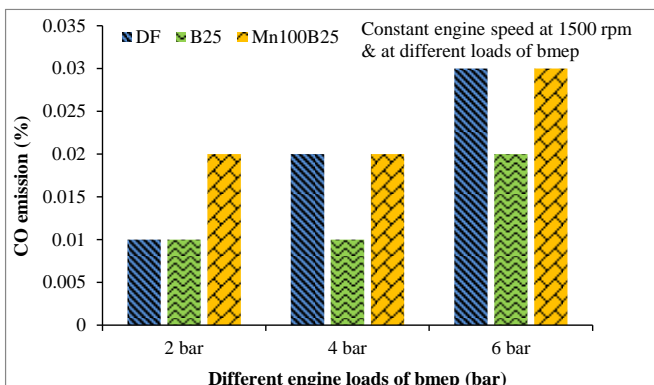


Figure 6. The variation of CO emissions under varying loads for test fuels

3.6. CO₂ Emission

Carbon dioxide is the combustion product of fuels containing carbon molecules in their structure, which combines with oxygen and combusts completely in the combustion chamber [16]. The CO₂ emission values of different fuel types at different engine parameters are shown graphically in Fig. 7. When all fuel types are examined, while the CO₂ emission values of all fuels are equal at idle parameter, an increase in all CO₂ emission values is observed due to the increase in engine parameters. At high load, B25 and Mn100B25 fuel

emission values were equal values while DF emission value remained at 8.33% lower levels. With the increased amount of parameters, the emission values increased in direct proportion to the load due to the conversion of more CO emissions into CO₂ emissions with improvements in combustion with more air intake into the combustion chamber.

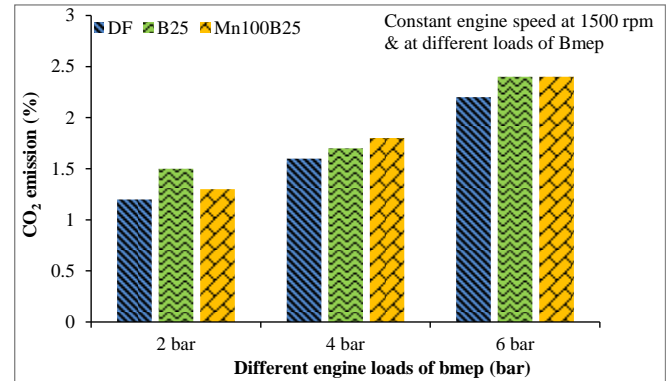


Figure 7. The variation of CO₂ emissions under varying loads for test fuels

3.7. HC emission

The presence of HC emissions in the exhaust gases is due to incomplete combustion of the fuel. It is a situation where the combustion reaction slows down due to the air-fuel mixture ratios being too rich or too lean and the combustion cannot be completed [19]. The HC emission values of different fuel types at different engine parameters (low, medium and high) are shown graphically in Fig. 8. When all fuel types are analyzed, it is seen that the in-cylinder temperature does not occur sufficiently with the increase of the parameter and accordingly the combustion efficiency does not increase sufficiently, which increases the HC emissions [23]. At medium and high fuel parameters, B25 and Mn100B25 fuel emission values are lower than DF fuel and B25 has the lowest emission values, which depends on the amount of oxygen in biodiesel fuel and diesel-biodiesel fuel blend ratios [24].

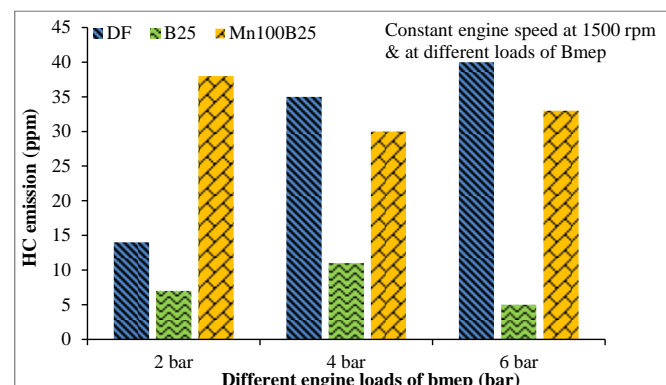


Figure 8. The variation of HC emissions under varying loads for test fuels

4. CONCLUSION

Due to the dwindling oil reserves in the world, the search for renewable fuels for internal combustion engines has led to a growing interest in biodiesel. In order to improve the chemical and physical properties such as calorific value,

viscosity, and freezing point, which are among the disadvantages of biodiesel fuel, it has prompted researchers to use various additives. In this study, biodiesel fuel blend was blended with nanoparticles, and after physical and chemical analysis, combustion parameters and emission values were tested in a diesel research engine. In the experimental study with Mn100B25, B25, and DF test fuels, the following results were generally determined.

- The additive decreased the viscosity, flash point, cetane number and density of Mn100B25 fuel. It slightly increased the freezing point and calorific value.
- When the cylinder gas pressures of three different fuels are compared, the highest cylinder gas pressure was observed in Mn100B25 fuel at 6 bar bmep, which has the highest crankshaft angle, and the difference in cylinder gas pressure between Mn100B25 and DF fuels is 2.46%.
- Crankshaft angles were close to each other and the highest average gas temperature at 6 bar bmep was found for Mn100B25 fuel. The difference in cylinder gas pressure between Mn100B25 and DF fuels is 1.45%. The high average gas temperature in Mn100B25 fuel is thought to be due to density and calorific value.
- The highest net heat release was determined with Mn100B25 fuel at 6 bmep. The difference in net heat release between Mn100B25 and DF fuel values is 11.83%. The manganese additive added to Mn100B25 fuel was found to increase the calorific value of the fuel.
- It is thought that the high values at idle and low parameters in cumulative heat release, the high amount of oxygen in biodiesel fuel and the additive used have an effect on the cetane number.

- An increase in NO_x emission values was also observed with the increase in bmep value. At 2 bar and 6 bar bmep parameters, NO_x emission values increased the least from 33 to 259 ppm, respectively.
- The fact that diesel fuel emits less emissions than biodiesel fuel blended fuels can be said to be due to the in-cylinder temperature and the oxygen content in the biodiesel content.

As a result of the studies, manganese standard solution additive [Mn(NO₃)₂] added to biodiesel-diesel fuel blends obtained from waste vegetable oil improved the important chemical and physical properties of the blended fuels and the combustion parameters were generally parallel to the diesel fuel curves. It was determined that biodiesel-diesel fuel blends with Mn(NO₃)₂ additive can be used in diesel engines without any modification.

Abbreviations

CGP	Cylinder gas pressure, bar
CHR	Cumulative heat release
CI	Compression ignition
Mn100B25	25% (in vol.) biodiesel, 75% DF (in vol.) and 100 ppm M(NO ₃) ₂
HC	Hydrocarbon
HRR	Heat release rate, J/°
MGT	Mean gas temperature, K
DF	Diesel fuel
°CA	Crank angle degree

Acknowledgements

Data in this research are part of the results of the M.Sc. thesis project by Batman University Institute of Graduate Studies with Thesis Number of 750900. The research was performed at the Engine Research Laboratory, University of Batman, Batman, Turkey.

REFERENCES

- [1] Keskin, A. 2005. Tall oil based biodiesel and fuel additive production and their effects on diesel engine performance, PhD Thesis, Gazi University Institute of Science and Technology, Ankara.
- [2] Aydın, A., Kayri, İ., & Aydın, H. 2023. Electrical and thermal performance enhancement of a photovoltaic thermal hybrid system with a novel inner plate-finned collective cooling with different nanofluids, *International Journal of Green Energy*, 21 (3), 555-569.
- [3] Cengiz, M., Kayri, İ., & Aydın, H. 2024. A collated overview on the evaporative cooling applications for photovoltaic modules. *Renewable and Sustainable Energy Reviews*, 197, 114393.
- [4] Kayri, İ. 2023. The effects of coolant mass flow rate and atmospheric indicators in a PV/T system with experimental and ANN's models. *Sustainable Energy, Grids and Networks*, 36, 101189.
- [5] Şener, Ramazan. 2022. Ducted Fuel Injection: Numerical Study of Soot Formation and Oxidation Using Detailed Soot Modeling Approach in a Compression Ignition Engine at Different Loads. *Journal of the Brazilian Society of Mechanical Sciences and Engineering* 44 (1):45.
- [6] Erdoğan, S., Balki M. K., Aydın S., Sayın C. 2020. Performance, Emission and Combustion Characteristic Assessment of Biodiesels Derived from Beef Bone Marrow in a Diesel Generator. *Energy* 207, 118300.
- [7] Yaşar, F. 2020. Comparison of Fuel Properties of Biodiesel Fuels Produced from Different Oils to Determine the Most Suitable Feedstock Type. *Fuel*, 264:116817.
- [8] Sundus, F., Fazal, M. A., Masjuki, H. H., 2017. Tribology with biodiesel, a study on enhancing biodiesel stability and its fuel properties, *Renewable and Sustainable Energy Reviews*, 70, 399-412.
- [9] Çılğın, E. 2024. Investigation of the effects of single and double-walled carbon nanotube utilization on diesel engine combustion, emissions, and performance. *Case Studies in Thermal Engineering*, 57, 104282.
- [10] Deviren, H., Çılğın, E., & Aydın, S. 2023. Study on using nano magnesium oxide (MNMgO) nanoparticles as fuel additives in terebinth oil biodiesel blends in a research diesel engine. *Energy Sources, Part A: Recovery, Utilization, and Environmental Effects*, 45(4):12181-12200.
- [11] Aydın, S. 2020. Detailed evaluation of combustion, performance and emissions of ethyl proxitol and methyl proxitol-safflower biodiesel blends in a power generator diesel engine *Fuel*, 270 (2020), p. 117492.
- [12] Keskin, A., Gürü, M., Altıparmak, D., 2007. Biodiesel production from tall oil with synthesized Mn and Ni based additives: Effects of the Additives on Fuel Consumption and Emissions, *Fuel*, 86(7-8): 1139-1143.
- [13] Çelikten, İ. ve Gürü, M., 2011. Petrodizel ve kanola biyodizeli performans ve emisyon kriterlerinin mangan esaslı katkı maddeleriyle geliştirilmesi, *Gazi Üniversitesi Mühendislik Mimarlık Fakültesi Dergisi* Cilt: 26, No: 3, 643-648.
- [14] Behcet R., Aydın S., İlkilic C., 2011. Production of biodiesel from safflower oil. *Energy Education Science & Technology, Part A: Energy Science and Research*, 27(2):295-300.
- [15] Yağız, S., 2019. Investigation of the possibilities of using cotton oil and waste cotton oil biodiesel as fuel in a diesel engine generator, Master's Thesis, Batman University Institute of Science and Technology, Batman.
- [16] Heywood, J., 1988. Internal combustion engine fundamentals, Macgraw-Hill Book Company, New York.
- [17] Safgönül, B., Ergeneman, M., Arslan, E., Soruşbay, C., 2008. Internal combustion engines, Birsan publishing house, İstanbul.
- [18] Aksoy, F. and Yılmaz, E., 2019. Investigation of combustion and performance characteristics of a direct injection diesel engine operating with 10% fish oil biodiesel - 90% diesel fuel blend, *Gazi University Journal of Science and Technology, GU J Sci, Part C*, 7(1): 12-24.
- [19] Ergeneman, M., Mutlu, M., Kutlar, O. A., Arslan, H., 1997. Exhaust pollutants from vehicles, Birsan Publishing House, İstanbul, 4-15.
- [20] Beyaz, M., Aydın S., Şener R., and Sayın C. 2023. Effects of Ethyl Proxitol (1-Ethoxy-2-Propanol) Additive on Combustion and Emission Characteristics of Biodiesel Blends. *Biofuels*, 14:8, 817-824.

- [21] Seraç, M. R., Aydın, S., Sayın C. 2020. Comprehensive evaluation of performance, combustion, and emissions of soybean biodiesel blends and diesel fuel in a power generator diesel engine, *Energy Sources, Part A: Recovery, Utilization, and Environmental Effects*, 42:18, 2316-2331.
- [22] Şahin, S., 2021. Determination of the effects of some additives added to diesel and safflower biodiesel blends on fuel properties, engine performance and emission values, PhD Thesis, Selçuk University Institute of Science and Technology, Konya, 124-137.
- [23] Öztürk, E. Y., Altinkurt, D. M., Türkcen, A., 2020. Experimental investigation of combustion, performance and emission characteristics of a diesel engine using diesel-biodiesel-isobutanol triple blends, *Journal of Fuels, Fire and Combustion in Engineering*, 8, 56-66.
- [24] Aydın, S. 2020. Comprehensive analysis of combustion, performance and emissions of power generator diesel engine fueled with different source of biodiesel blends. *Energy* 205:118074.

BIOGRAPHIES

Tarhan TAN was born in 1985 in Diyarbakır/Turkey. I received my primary, secondary and high school education in Mersin/Turkey. I graduated from Dicle University Batman Faculty of Education Automotive Teaching Department in 2009. I graduated from Batman University Institute of Science and Engineering Automotive Engineering in 2022. I have been working as a civil servant in a public institution since 2012.

Selman Aydın was born in Batman, Turkey. Between 2000 and 2004, he graduated from the Dicle University Technical Education Faculty Automotive Teaching B.Sc. program. In 2008, he started his M.Sc. degree at Firat University Institute of Science and Technology, Department of Mechanical Education/Automotive. In 2010, he graduated with an M.Sc. degree. In 2010, he started his Ph.D. at Marmara University Institute of Science and Technology, Department of Mechanical Education. In 2014, he graduated with a Ph.D. Between 2012 and 2015, he worked as a lecturer at Hakkari University, Department of Mechanical Engineering/Automotive. In 2015, he began working as an assistant professor in the Batman University Faculty of Technology's Department of Automotive Engineering. In 2020, he was named an associate professor in automotive engineering. Batman University Vocational High School of Technical Sciences appointed him as an associate professor in 2021. He is currently an associate professor in the same unit. Major research interests are internal combustion engines, engine dynamics, alternative fuels, fuel cells, and automotive engineering. He has published more than 50 papers in international and national journals and conferences.

Research Article

The Potential of Transformer-Based Models for Automated Lung Cancer Detection from CT Scans

Oguzhan Katar^{1*}, Tulin Ozturk², Ozal Yildirim¹¹Department of Software Engineering, Firat University, Elazig, Turkey. (e-mail: okatar@firat.edu.tr) (e-mail: ozalyildirim@firat.edu.tr)²Department of Radiology, Fethi Sekin City Hospital, Elazig, Turkey. (e-mail: tulin58@hotmail.com).

ARTICLE INFO

Received: Nov., 09. 2024

Revised: Mar., 28. 2025

Accepted: May., 12. 2025

Keywords:

Lung cancer
Transformer models
CT imaging
Diagnosis
Deep learningCorresponding author: *Oguzhan Katar*

ISSN: 2536-5010 / e-ISSN: 2536-5134

DOI: <https://doi.org/10.36222/ejt.1582121>

ABSTRACT

Lung cancer is the most common type of cancer worldwide and the leading cause of cancer-related deaths. Early diagnosis and treatment can significantly increase the survival rate of this disease. Radiological methods used in the diagnosis of lung cancer, especially Computed Tomography (CT) imaging, allow tumors to be detected more precisely. However, manual analysis of these images is time consuming and error prone due to human factors. In this study, we compared the potential of three different transformer-based state-of-the-art models (ViT, DeiT and Swin Transformer) for automatic lung cancer detection. We collected 690 CT images including small cell lung cancer (SCLC), non-small cell lung cancer (NSCLC) and normal findings from a local hospital. Each image was carefully reviewed and labeled by our expert radiologist, and these labeled images were used to train the models. The ViT, DeiT and Swin Transformer models achieved accuracy rates of 91.3%, 84.1% and 80.4% respectively on the test samples. This study shows that the use of transformer-based models for lung cancer classification is promising in overcoming the difficulties in manual analysis.

1. INTRODUCTION

Lung cancer is the most common type of cancer and the leading cause of cancer-related deaths worldwide [1]. According to the GLOBOCAN database, approximately 2.09 million new cases were reported in 2018, with around 1.76 million deaths attributed to the disease [2]. In recent years, both incidence and mortality rates have risen sharply [3].

Lung cancer is classified into two main types: Non-Small Cell Lung Cancer (NSCLC) and Small Cell Lung Cancer (SCLC) [4]. NSCLC accounts for 80%–85% of cases and includes three subtypes: adenocarcinoma, squamous cell carcinoma, and large cell carcinoma [5]. SCLC, on the other hand, represents about 10%–15% of cases. Although survival rates vary by clinical stage, the overall 5-year survival rate remains low at approximately 22% [6].

Radiological imaging methods are frequently used to detect lung cancer early [7]. Chest radiography is one of the most basic methods [8]. It is both low-cost and widely used. However, the tumor's size and location can cause issues. It might be missed or mistaken for other lung diseases [9]. Due to these disadvantages, detecting small lesions or early-stage tumors on chest radiography is very challenging [10].

Computed tomography (CT) is a more sensitive method for lung cancer diagnosis [11]. It allows comprehensive volumetric images to be captured in a single breath-hold [12].

By scanning the lungs in thin sections, CT can detect both small nodules and the extent of tumor spread [13]. Several studies have shown that low-dose CT detects more nodules and early-stage lung cancers compared to chest radiography [14, 15]. However, interpreting lung CT scans is a particularly intensive task. It requires extensive experience to assess the malignancy risk accurately [16]. Without such experience, the risk of misinterpretation can increase, affecting the accuracy of diagnosis.

To reduce these risks, deep learning-based computer-aided diagnosis (CAD) systems have been developed [17, 18]. These AI-powered systems enhance diagnostic efficiency, potentially reducing the workload on radiologists [19]. Li et al. introduced the Reconstruction-Assisted Feature Coding Network (RAFENet) model [20]. This model automatically classifies adenocarcinoma and squamous cell carcinoma in CT images. In their study, CT images from the Cancer Imaging Archive (TCIA) were utilized. Due to hardware limitations, each CT slice was cropped into a 128×128 pixel patch centered on the target structure. An early stopping function was used during training to stop the process if validation accuracy didn't improve within 10 epochs. RAFENet achieved a classification accuracy of 79.70% on the test set. Pang et al. developed a model based on densely connected convolutional neural networks (CNNs) to automatically classify adenocarcinoma, squamous cell

carcinoma, and large cell carcinoma in CT images [21]. They used real patient data collected from Shandong Provincial Hospital for training and validation. Since the dataset was limited, they applied data augmentation techniques such as rotation, translation, and transformation to increase the variability in the training data. The model achieved an accuracy of 89.85% in detecting lung cancer. Han et al. employed the VGG-16 architecture for automatic classification of adenocarcinoma and squamous cell carcinoma [22]. Their model was trained using a dataset collected from Peking University Cancer Hospital. The dataset was split using a 10-fold cross-validation approach. The VGG-16 model reached an accuracy of 84.10% on the test set. Chaunzwa et al. also proposed a VGG-16 based model for classifying adenocarcinoma and squamous cell carcinoma from CT images [23]. The model was trained using a private dataset collected from 311 early-stage NSCLC patients treated at Massachusetts General Hospital. The model achieved an AUC of 0.71 ($p = 0.018$) in classifying these cancer types. Zhao et al. proposed a Vision Transformer-based (ViT) model for the classification of NSCLC subtypes [24]. Their model was trained on CT images obtained from the TCIA. To optimize performance, images were resized to 224×224 pixels before being fed into the network. A data augmentation strategy, including rotation and flipping, was applied to improve generalization. The model was trained using a cross-entropy loss function, and an adaptive learning rate scheduler was employed. Experimental results demonstrated that the ViT model achieved a classification accuracy of 86.00%. Venkatesh et al. proposed a hybrid deep learning model for lung cancer detection, combining patch processing with CNN-based classification [25]. Using CT images from the LIDC and Kaggle datasets, the model automatically distinguishes between benign and malignant lung nodules. By extracting relevant features through CNN, the approach achieved an impressive classification accuracy of 99.96%.

The experimental findings of these studies show that deep learning architectures hold great potential for automatically classifying NSCLC subtypes. However, these studies focus solely on NSCLC detection and exclude SCLC and normal findings. While NSCLC makes up about 85% of lung cancer cases, models that only detect this class are not enough. A reliable decision support system should also accurately classify SCLC and normal cases. However, we have not come across a publicly available lung CT dataset containing NSCLC, SCLC and normal images labelled for training deep learning models. In addition, when the studies are analyzed, it is seen that most of them use CNN-based architectures for lung cancer detection. However, CNNs heavily depend on local receptive fields and pooling operations, which limits their ability to capture long-range dependencies within an image. This limitation makes it harder to fully understand the input and identify complex relationships between different regions of the image. In contrast, transformer-based models, which use self-attention mechanisms to capture interactions between distant image regions, have the potential to enhance the accuracy of lung cancer classification.

In this study, we compared the performance of transformer-based architectures for automatic lung cancer classification from CT images. Specifically, we evaluated three models commonly used in image classification: ViT, data-efficient image transformers (DeiT), and Swin Transformer. For this study, we collected a private lung cancer dataset, which includes CT images of patients with SCLC, NSCLC and normal findings. Then we trained each model

with equal hyper-parameters. Using the weights obtained as a result of training, we examined the computational and statistical performance of the models on the test samples.

The main contributions of this study are as follows:

- We provided a thorough comparison of three state-of-the-art transformer-based models for the task of lung cancer classification from CT images.
- We applied the transformer-based models to a real world lung cancer dataset.
- We compared the computational efficiency of the models and assessed their potential for integration into diagnostic processes.
- Our work contributes to the growing field of CAD by showcasing the potential of transformer-based models.

2. MATERIAL AND METHODS

In this study, we utilized three different deep learning models for lung cancer classification. Our approach includes a pre-processing stage where input CT images are divided into patches that these models can process. Specifically, we used 16×16 pixel patches for ViT and DeiT, while the Swin Transformer operates with 4×4 pixel patches. Each model leverages a transformer-based architecture to extract features from the images, and classifies them into one of three categories: SCLC, NSCLC, or normal. To evaluate and compare the performance of these models, we analyzed confusion matrices, training and validation curves, and epoch-based duration. The block diagram of our used framework is given in Figure 1.

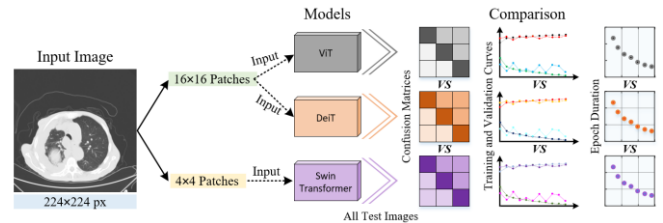


Figure 1. The block diagram of our framework.

2.1. Lung cancer CT dataset

In this study, we collected a private dataset with the approval of the non-interventional ethics committee from Firat University (Approval Number: 2024/13-38). The dataset contains 690 CT images, showing either lung cancer (SCLC or NSCLC) or normal findings. These scans were taken at Elazig Fethi Sekin City Hospital between 2020 and 2024. All CT scans were performed using a Philips Ingenuity-128 CT device. Our expert radiologist carefully reviewed and labeled each image. For images labeled as SCLC or NSCLC, a biopsy result confirmed the diagnosis.

TABLE I
DETAILS OF THE LUNG CANCER CT DATASET

Class	Label	Image Resolution	Number of Images	Percentage
Cancer	SCLC	768×768×3	125	54,35 %
	NSCLC	768×768×3	250	
Normal	Normal	768×768×3	315	45,65 %

CT images without finding of lung cancer were labeled as normal. The dataset comprises 125 images of SCLC, 250

images of NSCLC, and 315 images with no pathological findings. The SCLC and NSCLC images include diverse tumor sizes, locations, and densities to ensure clinical variability. Normal images include patients with no signs of nodules, masses, or other abnormalities. Further details about the dataset are given in Table 1.

2.2. Transformer-based image classification models

In recent years, transformer-based models have gained significant popularity in computer vision studies [26, 27]. These models have the ability to capture long-distance dependencies thanks to their self-attention mechanisms [28]. This capability sets them apart from traditional CNNs. In this study, we employed three different transformer-based models. Each of these models can be summarized as follows.

In 2020, Dosovitskiy et al. introduced the ViT model, which marked a significant step in applying transformer-based architectures to image classification [29]. Unlike CNNs, ViT divides input images into fixed-size patches. These patches are treated like tokens in natural language processing tasks. Each patch is linearly embedded and passed through several layers of self-attention [30]. The model uses a specialized classification token (CLS token) to summarize the information gathered from the patches. The output of this token is converted into a class prediction through a small multilayer perceptron (MLP) using a tanh activation function in a single hidden layer.

The DeiT model, developed by Touvron et al. in 2021, aims to make transformer-based architectures for image classification more efficient [31]. Similar to ViT, DeiT divides the input images into fixed-size patches and treats these patches as tokens. These patches are placed linearly and then passed through self-attention layers. One of the most important features of DeiT is that it uses a teacher model to improve performance even with less data. This approach, called knowledge distillation, involves transferring knowledge from a larger and well-trained teacher model to a smaller student model [32]. The model trained on a larger dataset not only provides accurate predictions, but also valuable information about the relationships between different classes. This additional information allows DeiT to be trained more efficiently even with limited data.

In 2021, Liu et al. proposed the Swin Transformer model, which builds on transformer-based architectures for image classification [33]. This model addresses some of the challenges seen in ViT. While ViT processes an entire image at once, the Swin Transformer divides the image into fixed-size patches called windows. Self-attention is applied within each window, focusing on local regions, which reduces the computational load. To connect information between windows, the model uses a shifting window mechanism that shifts the windows at different layers, allowing the model to gather features from across the image [34]. Swin Transformer also uses a hierarchical structure, where the patch size increases as the network progresses, letting it capture both detailed and broader features. This multi-scale processing helps the model handle both fine and coarse information effectively.

2.3. Evaluation metrics

We used confusion matrix based metrics to evaluate the performance of the models. Confusion matrix is a simple table showing the relationship between the actual and predicted classes. This matrix contains the number of true predictions

and false predictions. These situations are represented by 4 different elements. In a multi-class study, these elements are usually evaluated separately for each class. These elements can be summarized as follows.

- True Positive (TP): The number of images whose labels are correctly predicted from the samples belonging to the target class.
- True Negative (TN): The number of images whose labels are correctly predicted from samples of classes other than the target class.
- False Positive (FP): The number of images whose labels are predicted as the target class although their actual labels are different from the target class.
- False Negative (FN): The number of predicted images with labels different from the target class.

When measuring the classification performance of deep learning models, four main metrics are typically used. Accuracy (Acc) measures how correctly the model predicts across all test data. It is calculated using Equation 1.

$$Acc = \frac{TP + TN}{TP + FP + FN + TN} \quad (1)$$

Precision (Pre) assesses how accurate the model is in its positive classifications. It is calculated using Equation 2.

$$Pre = \frac{TP}{TP + FP} \quad (2)$$

Recall (Rec) evaluates how well the model identifies true positives. It is calculated using Equation 3.

$$Rec = \frac{TP}{TP + FN} \quad (3)$$

F-1 score provides a balance between precision and recall by calculating their harmonic mean. It is calculated using Equation 4.

$$F1 = \frac{2 \times Pre \times Rec}{Pre + Rec} \quad (4)$$

3. EXPERIMENTS

In this section, we present our experimental setup and results. First, we describe the training scenario and pre-processing steps. Next, we detail the training and testing processes of the models used in the study. Finally, we compare the performance of the models using various metrics.

3.1. Experimental setup

In this study, we evaluated the performance of transformer-based models for classifying lung cancer from CT images. Each model was initialized with pre-trained weights. We fine-tuned these models on our lung cancer dataset. Randomly selected samples from the classes in our dataset are given in Figure 2.

The models were trained to classify the CT images into one of three categories: SCLC, NSCLC, or normal. The collected CT images were first resized to a resolution of 224×224 pixels. The dataset samples are randomly divided as follows: 60% for training, 20% for validation, and 20% for

testing. The distribution of the dataset samples is given in Table 2.

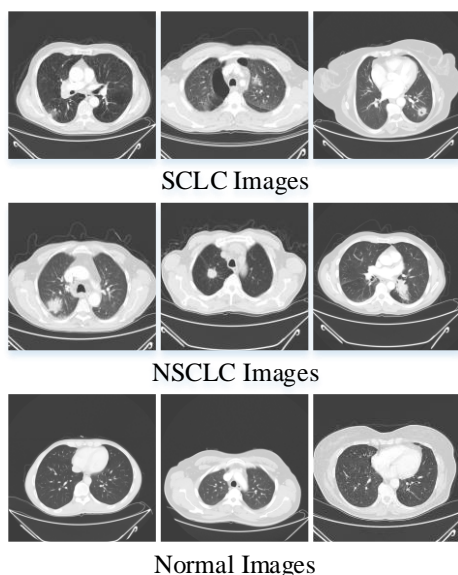


Figure 2. Randomly selected samples from our dataset.

TABLE II

THE DISTRIBUTION OF THE DATASET SAMPLES

Image Type	Resolution	Number of Train Images	Number of Validation Images	Number of Test Images
PNG	224×224×3	SCLC=75	SCLC=25	SCLC=25
		NSCLC=150	NSCLC=50	NSCLC=50
		Normal=189	Normal=63	Normal=63

All models were implemented using the PyTorch framework (version 2.2.1). The training pipeline was managed using timm. We used the AdamW optimizer with an initial learning rate of 0.00002. A batch size of 16 was used for training. Each model was trained for a maximum of 100 epochs. Early stopping function was used to prevent overfitting. The patience value was set to five, and validation loss was monitored at the end of each epoch. The performance of each model was evaluated using confusion matrix-based metrics. All experimental studies were carried out on RTX 4090 24 GB GPU.

3.2. Results

This section presents the experimental results of transformer-based models for lung cancer classification. The

evaluation includes accuracy, precision, recall, F1-score, and computational efficiency. A summary of the model-specific training processes is provided below.

The training loss of the ViT model decreased steadily. It dropped from 1.12 in the first epoch to 0.14 in the final epoch (14th epoch). Training accuracy improved significantly, rising from 47.8% at the beginning to 93.4% in the final epoch. This shows that the model adapted well to the training data, and the learning process was successful. The continuous decrease in training loss correlated with an increase in accuracy. Accuracy, which started at lower levels, increased rapidly as the loss decreased. Validation loss followed a similar trend. It dropped from 1.07 at the beginning to 0.37 in the final epoch. Validation accuracy improved from 60.1% to 86.9%. Training times ranged between 3.03 and 3.23 seconds per epoch, while validation times were approximately 0.60 to 0.68 seconds. The training and validation curves, along with the epoch-based time plot for the ViT model, are shown in Figure 3.

The DeiT model also showed good results. Training loss decreased from 1.00 in the first epoch to 0.20 by the final epoch (29th epoch). Training accuracy rose from 49.8% to 93.7%. The decrease in training loss was in line with the increase in accuracy. Although accuracy was low at first, it improved as the losses decreased. Validation loss showed a similar pattern. It dropped from 0.94 at the beginning to 0.34 by the final epoch. Validation accuracy increased from 64.5% in the first epoch to 85.5% by the end of training. This indicates that the model performed well on unseen data. Training times ranged from 3.05 to 3.61 seconds per epoch, while validation times were approximately 0.64 to 0.72 seconds. The training and validation curves, along with the epoch-based time plot for the DeiT model, are shown in Figure 4.

The Swin Transformer model also demonstrated effective learning. Training loss decreased from 1.02 in the first epoch to 0.38 by the final epoch (21st epoch). Training accuracy improved from 46.9% to 84.7%. Validation loss followed a similar pattern. Validation accuracy increased from 56.5% in the first epoch to 85.5% by the final epoch. Training times averaged between 2.35 and 2.76 seconds per epoch, while validation times were approximately 0.53 to 0.58 seconds. The training and validation curves, along with the epoch-based time plot for the Swin Transformer model, are shown in Figure 5.

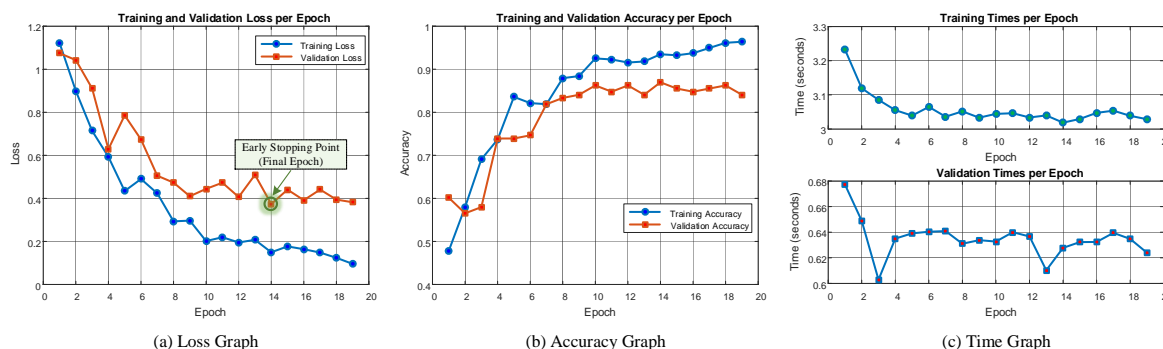


Figure 3. The performance of ViT Model: (a) Loss Graph, (b) Accuracy Graph and (c) Time Graph

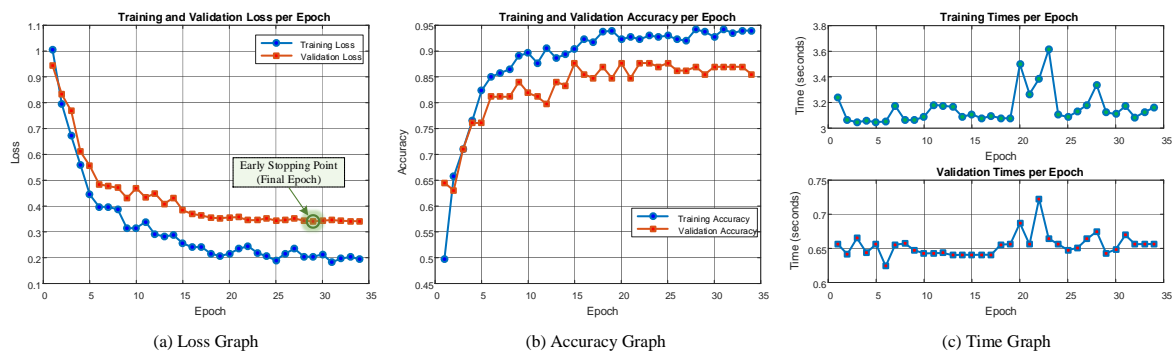


Figure 4. The performance of DeiT Model: (a) Loss Graph, (b) Accuracy Graph and (c) Time Graph

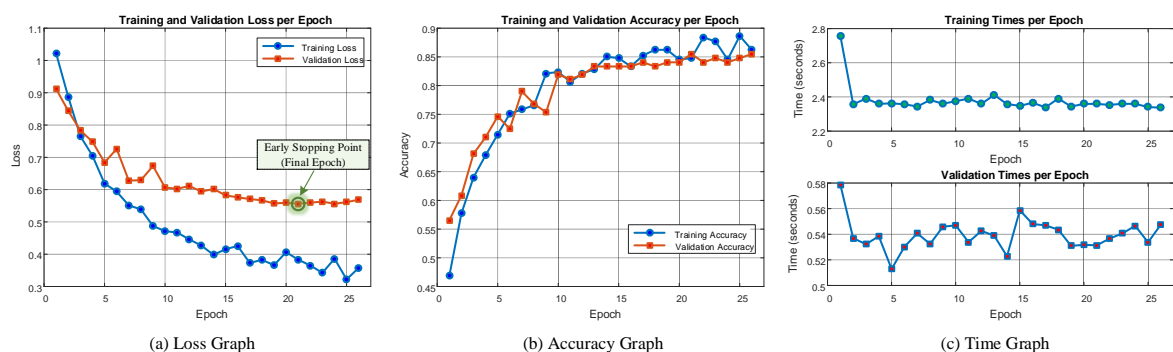


Figure 5. The performance of Swin Transformer Model: (a) Loss Graph, (b) Accuracy Graph and (c) Time Graph

The performance of all models during the training and validation processes was generally successful. After completing these processes, each model was evaluated using the test images. The confusion matrices, generated from the predictions of each model on the test samples, are shown in Figure 6.

The DeiT model performed well in the Normal class with 90.5% (57/63) prediction rate. However, it achieved 82% prediction rate (41/50) in the NSCLC class, with slightly more errors in this category. In the SCLC class, it performed worse, with a prediction rate of 72% (18/25). The NSCLC class was the most difficult for this model, as some samples were misclassified as Normal.

The Swin Transformer model had the highest prediction rate in the Normal class, achieving 95.2% (60/63). However, its performance was lower in the NSCLC class, with 74% prediction rate (37/50), and even lower in the SCLC class, at 56% (14/25). Misclassifications were particularly notable in the NSCLC class, with many samples predicted as Normal. The prediction rate in the SCLC class was also the lowest among the three models.

Table 3 shows in detail the performance of each model on the test samples.

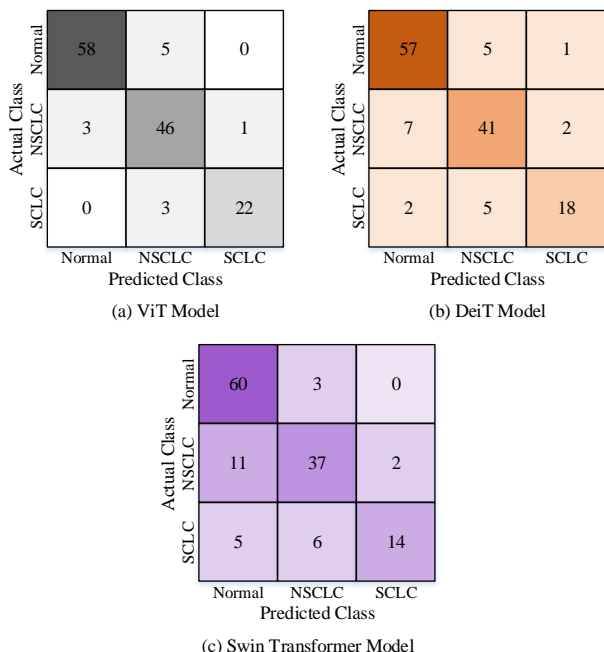


Figure 6. Lung cancer classification results: (a) ViT Model, (b) DeiT Model and (c) Swin Transformer Model.

The ViT model achieved a high prediction rate of 92.1% (58/63) in the Normal class. It correctly predicted 92% (46/50) in the NSCLC class and 88% (22/25) in the SCLC class. The model's biggest challenge was misclassifying some Normal samples as NSCLC. Additionally, several SCLC samples were predicted as NSCLC.

TABLE III
DETAIL THE PERFORMANCE OF EACH MODEL

Model	Class	Pre (%)	Rec (%)	F-1 (%)	Acc (%)
ViT	Normal	95.08%	92.06%	93.55%	91.30%
	NSCLC	85.19%	92.00%	88.46%	
	SCLC	95.65%	88.00%	91.67%	
DeiT	Normal	86.36%	90.48%	88.37%	84.06%
	NSCLC	80.39%	82.00%	81.19%	
	SCLC	85.71%	72.00%	78.26%	
Swin Transformer	Normal	78.95%	95.24%	86.33%	80.43%
	NSCLC	80.43%	74.00%	77.08%	
	SCLC	87.50%	56.00%	68.29%	

4. DISCUSSION

The experimental results highlight the impressive ability of transformer-based models to effectively classify lung cancer from CT images. Among these models, ViT stood out, delivering the highest overall performance, especially in classifying NSCLC and SCLC cases. Its balanced accuracy across all three classes reflects its strong generalization

capability. However, minor misclassifications were observed, particularly between NSCLC and SCLC. The DeiT model, while performing well, showed slightly lower accuracy than ViT, particularly in distinguishing NSCLC from SCLC and normal cases. The Swin Transformer, on the other hand, achieved the best performance in classifying normal cases but faced challenges in accurately differentiating between NSCLC and SCLC.

These differences in performance can be attributed to several factors. From an architectural standpoint, ViT uses global self-attention mechanisms that allow it to capture long-range dependencies across the image, which is particularly effective for capturing complex patterns in medical imaging. DeiT, uses distillation-based training that can slightly limit its capacity in fine-grained classification. Swin Transformer adopts a hierarchical structure with shifted windows, which is more efficient but may lose some global contextual information potentially affecting performance on subtle differences between cancer subtypes.

While the results are promising, several challenges remain. Dataset size and class imbalance continue to impact the models' performance. Transformer-based architectures require larger, more balanced datasets to improve robustness and prevent overfitting. Integrating widely-used public datasets, such as LIDC-IDRI, could further enhance the models' performance.

As for the practical application of these models in clinical settings, we emphasize their potential to significantly reduce the workload of radiologists and assist in early diagnosis. The ViT model, with its strong generalization ability, offers a promising path toward faster, more accurate diagnoses. By automating the classification process, these models not only reduce the time and effort needed for manual analysis but also enable earlier detection, ultimately facilitating quicker treatment decisions. However, while these models show strong performance, their computational demands present a challenge for seamless integration into clinical workflows. The memory and processing power required by transformer-based models, particularly ViT, could limit their real-time application. Moreover, the need for thorough validation, regulatory approval, and interpretability further complicates clinical integration. Despite this, the continued advancement of hardware capabilities and optimization techniques such as model pruning, quantization, and distributed computing suggests that these models can be adapted for practical use in clinical environments. In future work, we aim to explore various model optimization strategies to improve inference times and reduce memory consumption, making these transformer-based models even more suitable for integration into clinical practice. Furthermore, explainability methods will be investigated to ensure that predictions are interpretable and clinically trustworthy.

5. CONCLUSION

This study demonstrated the potential of transformer-based models, specifically ViT, DeiT, and Swin Transformer, for lung cancer classification from CT images. These models were evaluated on a private dataset with images of NSCLC, SCLC, and normal lung. Their performance was compared using accuracy, precision, recall, and F1-score. The results showed that all three models were effective in detecting lung cancer. Each model excelled in different aspects. The ViT model

achieved the highest overall accuracy. It showed strong performance across all categories, particularly in the Normal and NSCLC classes. The DeiT model also performed well, but it struggled more in the SCLC class. The Swin Transformer achieved the highest prediction rate for the Normal class. However, it had weaker results in distinguishing between NSCLC and SCLC. Despite their success, there is room for improvement, particularly in increasing the classification accuracy for more aggressive cancer types like SCLC. Future research could focus on improving the generalization of these models by incorporating larger and more diverse datasets. Additionally, hybrid approaches that combine the strengths of CNNs and transformers could be explored to enhance performance further.

ACKNOWLEDGEMENT

This study was supported by Scientific Research Projects Unit of Firat University (FUBAP) under the Grant Number TEKF.24.42. The authors thank to FUBAP for their supports

REFERENCES

- [1] A. Leiter, R. R. Veluswamy, and J. P. Wisnivesky, "The global burden of lung cancer: current status and future trends," *Nat. Rev. Clin. Oncol.*, vol. 20, no. 9, pp. 624–639, Sep. 2023, doi: 10.1038/s41571-023-00798-3.
- [2] F. Bray, J. Ferlay, I. Soerjomataram, R. L. Siegel, L. A. Torre, and A. Jemal, "Global cancer statistics 2018: GLOBOCAN estimates of incidence and mortality worldwide for 36 cancers in 185 countries," *CA. Cancer J. Clin.*, vol. 68, no. 6, pp. 394–424, Nov. 2018, doi: 10.3322/caac.21492.
- [3] Y. Fang et al., "Burden of lung cancer along with attributable risk factors in China from 1990 to 2019, and projections until 2030," *J. Cancer Res. Clin. Oncol.*, vol. 149, no. 7, pp. 3209–3218, Jul. 2023, doi: 10.1007/s00432-022-04217-5.
- [4] M. Kriegsmann et al., "Deep Learning for the Classification of Small-Cell and Non-Small-Cell Lung Cancer," *Cancers (Basel)*, vol. 12, no. 6, p. 1604, Jun. 2020, doi: 10.3390/cancers12061604.
- [5] L. E. L. Hendriks et al., "Non-small-cell lung cancer," *Nat. Rev. Dis. Prim.*, vol. 10, no. 1, p. 71, Sep. 2024, doi: 10.1038/s41572-024-00551-9.
- [6] R. L. Siegel, K. D. Miller, H. E. Fuchs, and A. Jemal, "Cancer statistics, 2022," *CA. Cancer J. Clin.*, vol. 72, no. 1, pp. 7–33, Jan. 2022, doi: 10.3322/caac.21708.
- [7] S. J. Adams, E. Stone, D. R. Baldwin, R. Vliegthart, P. Lee, and F. J. Fintelmann, "Lung cancer screening," *Lancet*, vol. 401, no. 10374, pp. 390–408, Feb. 2023, doi: 10.1016/S0140-6736(22)01694-4.
- [8] R. Nooreldeen and H. Bach, "Current and Future Development in Lung Cancer Diagnosis," *Int. J. Mol. Sci.*, vol. 22, no. 16, p. 8661, Aug. 2021, doi: 10.3390/ijms22168661.
- [9] J. Kim and K. H. Kim, "Role of chest radiographs in early lung cancer detection," *Transl. Lung Cancer Res.*, vol. 9, no. 3, pp. 522–531, Jun. 2020, doi: 10.21037/tlcr.2020.04.02.
- [10] B. Philip et al., "Current investigative modalities for detecting and staging lung cancers: a comprehensive summary," *Indian J. Thorac. Cardiovasc. Surg.*, vol. 39, no. 1, pp. 42–52, Jan. 2023, doi: 10.1007/s12055-022-01430-2.
- [11] H. L. Lancaster, M. A. Heuvelmans, and M. Oudkerk, "Low-dose computed tomography lung cancer screening: Clinical evidence and implementation research," *J. Intern. Med.*, vol. 292, no. 1, pp. 68–80, Jul. 2022, doi: 10.1111/joim.13480.
- [12] M. A. Thanoon, M. A. Zulkifley, M. A. A. Mohd Zainuri, and S. R. Abdani, "A Review of Deep Learning Techniques for Lung Cancer Screening and Diagnosis Based on CT Images," *Diagnostics*, vol. 13, no. 16, p. 2617, Aug. 2023, doi: 10.3390/diagnostics13162617.
- [13] E. W. Zhang et al., "Characteristics and Outcomes of Lung Cancers Detected on Low-Dose Lung Cancer Screening CT," *Cancer Epidemiol. Biomarkers Prev.*, vol. 30, no. 8, pp. 1472–1479, Aug. 2021, doi: 10.1158/1055-9965.EPI-20-1847.
- [14] K.-L. Huang, S.-Y. Wang, W.-C. Lu, Y.-H. Chang, J. Su, and Y.-T. Lu, "Effects of low-dose computed tomography on lung cancer screening: a systematic review, meta-analysis, and trial sequential analysis," *BMC*

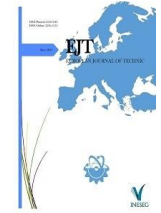
- Pulm. Med., vol. 19, no. 1, p. 126, Dec. 2019, doi: 10.1186/s12890-019-0883-x.
- [15] E. F. Patz, E. Greco, C. Gatsonis, P. Pinsky, B. S. Kramer, and D. R. Aberle, "Lung cancer incidence and mortality in National Lung Screening Trial participants who underwent low-dose CT prevalence screening: a retrospective cohort analysis of a randomised, multicentre, diagnostic screening trial," *Lancet Oncol.*, vol. 17, no. 5, pp. 590–599, May 2016, doi: 10.1016/S1470-2045(15)00621-X.
- [16] S. J. van Riel et al., "Observer variability for Lung-RADS categorisation of lung cancer screening CTs: impact on patient management," *Eur. Radiol.*, vol. 29, no. 2, pp. 924–931, Feb. 2019, doi: 10.1007/s00330-018-5599-4.
- [17] S. H. Hosseini, R. Monsefi, and S. Shadroo, "Deep learning applications for lung cancer diagnosis: A systematic review," *Multimed. Tools Appl.*, vol. 83, no. 5, pp. 14305–14335, Jul. 2023, doi: 10.1007/s11042-023-16046-w.
- [18] R. Javed, T. Abbas, A. H. Khan, A. Daud, A. Bukhari, and R. Alharbey, "Deep learning for lung cancer detection: a review," *Artif. Intell. Rev.*, vol. 57, no. 8, p. 197, Jul. 2024, doi: 10.1007/s10462-024-10807-1.
- [19] J. V. Naga Ramesh, R. Agarwal, P. Deekshita, S. A. Elahi, S. H. Surya Bindu, and J. S. Pavani, "Application of Several Transfer Learning Approach for Early Classification of Lung Cancer," *EAI Endorsed Trans. Pervasive Heal. Technol.*, vol. 10, Mar. 2024, doi: 10.4108/eetpht.10.5434.
- [20] H. Li, Q. Song, D. Gui, M. Wang, X. Min, and A. Li, "Reconstruction-Assisted Feature Encoding Network for Histologic Subtype Classification of Non-Small Cell Lung Cancer," *IEEE J. Biomed. Heal. Informatics*, vol. 26, no. 9, pp. 4563–4574, Sep. 2022, doi: 10.1109/JBHI.2022.3192010.
- [21] S. Pang, Y. Zhang, M. Ding, X. Wang, and X. Xie, "A Deep Model for Lung Cancer Type Identification by Densely Connected Convolutional Networks and Adaptive Boosting," *IEEE Access*, vol. 8, pp. 4799–4805, 2020, doi: 10.1109/ACCESS.2019.2962862.
- [22] Y. Han et al., "Histologic subtype classification of non-small cell lung cancer using PET/CT images," *Eur. J. Nucl. Med. Mol. Imaging*, vol. 48, no. 2, pp. 350–360, Feb. 2021, doi: 10.1007/s00259-020-04771-5.
- [23] T. L. Chaunzwa et al., "Deep learning classification of lung cancer histology using CT images," *Sci. Rep.*, vol. 11, no. 1, p. 5471, Mar. 2021, doi: 10.1038/s41598-021-84630-x.
- [24] A. Fanizzi et al., "Comparison between vision transformers and convolutional neural networks to predict non-small lung cancer recurrence," *Sci. Rep.*, vol. 13, no. 1, p. 20605, 2023, doi: 10.1038/s41598-023-48004-9.
- [25] C. Venkatesh et al., "A hybrid model for lung cancer prediction using patch processing and deeplearning on CT images," *Multimedia Tools and Applications*, vol. 83, no. 15, p. 43931-43952, 2024, doi: 10.1007/s11042-024-19208-6.
- [26] R. Azad et al., "Advances in medical image analysis with vision Transformers: A comprehensive review," *Med. Image Anal.*, vol. 91, p. 103000, Jan. 2024, doi: 10.1016/j.media.2023.103000.
- [27] A. Parvaiz, M. A. Khalid, R. Zafar, H. Ameer, M. Ali, and M. M. Fraz, "Vision Transformers in medical computer vision—A contemplative retrospection," *Eng. Appl. Artif. Intell.*, vol. 122, p. 106126, Jun. 2023, doi: 10.1016/j.engappai.2023.106126.
- [28] A. M. Hafiz, S. A. Parah, and R. U. A. Bhat, "Attention mechanisms and deep learning for machine vision: A survey of the state of the art," *Jun. 2021*.
- [29] A. Dosovitskiy et al., "An Image is Worth 16x16 Words: Transformers for Image Recognition at Scale," *Oct. 2020*.
- [30] O. Katar and O. Yildirim, "An Explainable Vision Transformer Model Based White Blood Cells Classification and Localization," *Diagnostics*, vol. 13, no. 14, p. 2459, Jul. 2023, doi: 10.3390/diagnostics13142459.
- [31] H. Touvron, M. Cord, M. Douze, F. Massa, A. Sablayrolles, and H. Jegou, "Training data-efficient image transformers & distillation through attention," in *Proceedings of the 38th International Conference on Machine Learning*, M. Meila and T. Zhang, Eds., in *Proceedings of Machine Learning Research*, vol. 139, PMLR, Oct. 2021, pp. 10347–10357. [Online]. Available: <https://proceedings.mlr.press/v139/touvron21a.html>
- [32] G. Habib, T. J. Saleem, and B. Lall, "Knowledge Distillation in Vision Transformers: A Critical Review," *Feb. 2023*.
- [33] Z. Liu et al., "Swin transformer: Hierarchical vision transformer using shifted windows," in *Proceedings of the IEEE/CVF international conference on computer vision*, 2021, pp. 10012–10022.
- [34] J. Huang et al., "Swin transformer for fast MRI," *Neurocomputing*, vol. 493, pp. 281–304, Jul. 2022, doi: 10.1016/j.neucom.2022.04.051.

BIOGRAPHIES

Oguzhan Katar was born in Elazığ, Türkiye, in 1997. He received the B.Sc. and M.Sc. degrees in computer engineering from Firat University, Elazığ, in 2019 and 2022, respectively, where he is currently pursuing the Ph.D. degree in software engineering. His research interests include machine learning, deep learning, and image processing.

Tulin Ozturk graduated from Firat University Faculty of Medicine. She received radiology training at Firat University Radiology Clinic. She currently works as an associate professor at the Radiology clinic of the University of Health Sciences. She has published over 30 papers in journals. She main research interests include abdominal radiology and oncological radiology.

Ozal Yildirim received the Ph.D. degree in electrical and electronic engineering from Firat University, Türkiye. He is currently an Associate Professor in software engineering with Firat University. He has published over 60 papers in international refereed journals and conference proceedings. His main research interests include deep learning and medical signal and image processing.



Research Article

Prediction and Optimization of Tensile Strength Values of 3D Printed PLA Components with RSM, ANOVA and ANN Analysis

Fuat Kartal^{1*} , Arslan Kaptan²

^{1*} Kastamonu University, Faculty of Engineering and Architecture, Department of Mechanical Engineering, 37150, Kastamonu, Turkey. (e-mail: fkartal@kastamonu.edu.tr).

² Sivas Cumhuriyet University, Sivas Vocational School of Technical Sciences, Department of Motor Vehicles and Transportation Technologies, 58140 Sivas, Turkey. (e-mail: akaptan@cumhuriyet.edu.tr).

ARTICLE INFO

Received: Oct.,5. 2024
Revised: Mar., 5. 2025
Accepted: Apr., 12. 2025

Keywords:

Response surface methodology
Analysis of variance
Tensile strength
Artificial neural networks
Fused deposition modeling
3D printing
PLA components
Process optimization

Corresponding author: *Fuat Kartal*

ISSN: 2536-5010 / e-ISSN: 2536-5134

DOI: <https://doi.org/10.36222/ejt.1561857>

ABSTRACT

This study evaluates the comparative effectiveness of Response Surface Methodology (RSM), Analysis of Variance (ANOVA), and Artificial Neural Networks (ANN) in predicting and optimizing the tensile strength of 3D-printed PLA components. Key process parameters—including layer thickness, infill density, print speed, temperature, and build orientation—were systematically varied to analyze their impact on tensile strength. The results indicate that RSM and ANOVA offer higher prediction accuracy compared to ANN, with lower deviation rates (0.65%, 0.18%, and 3.43% for RSM; 0.20%, 0.12%, and 3.25% for ANOVA) versus ANN (5.93%, 3.88%, and 6.26%). The analysis revealed that layer thickness plays the most significant role in tensile strength, followed by temperature, infill density, build orientation, and print speed. The optimal combination of parameters—0.20 mm layer thickness, 50% infill density, 50 mm/s print speed, 220°C nozzle temperature, and 90° build orientation—yielded a maximum tensile strength of 55.506 MPa. These findings highlight the importance of parameter optimization in improving the mechanical properties of FDM-printed components. The study provides valuable insights for enhancing the reliability and efficiency of additive manufacturing processes, paving the way for future research on hybrid modeling techniques and alternative material applications.

1. INTRODUCTION

Additive Manufacturing (AM), commonly known as 3D printing, has emerged as a transformative technology, revolutionizing traditional manufacturing across various industries. This layer-by-layer fabrication technique offers unparalleled design freedom, reduced material waste, and enhanced production efficiency, making it highly attractive for industrial applications in aerospace, automotive, biomedical, and consumer goods sectors [1-3]. Among the diverse AM technologies, Fused Deposition Modeling (FDM) has gained significant popularity due to its cost-effectiveness, ease of use, and compatibility with a wide range of thermoplastic materials [4,5]. FDM operates by extruding thermoplastic filament through a heated nozzle, which solidifies to form a structurally sound component. Despite its advantages, achieving high mechanical performance in FDM-printed components remains a challenge, as their properties are heavily influenced by multiple process parameters.

1.1 Importance of Process Parameters in FDM

The mechanical properties of FDM-printed parts, such as tensile strength, stiffness, toughness, and fatigue resistance, are significantly affected by process parameters, including layer thickness, infill density, print speed, temperature, and build orientation [6-9]. Numerous studies have investigated the optimization of these parameters to enhance part quality. For instance, Zhou et al. (2018) found that infill density and printing pattern strongly influence the tensile strength of PLA components [10], while Gebisa and Lemu (2018) analyzed how factors such as air gap, raster angle, and contour width affect the mechanical properties of ULTEM 9085 parts [11]. Christiyan et al. (2016) reported that lower printing speed and reduced layer thickness improve both tensile and flexural strength in 3D-printed ABS composites [12]. These studies emphasize the need for a systematic approach to parameter optimization in FDM processes.

1.2 Statistical and Computational Approaches for Optimization

Traditional optimization techniques, such as Design of Experiments (DOE), Response Surface Methodology (RSM), and Analysis of Variance (ANOVA), have been widely used

to model the effects of process parameters on mechanical properties [13-15]. These methods provide statistically significant insights by identifying key factors and their interactions. More recently, Artificial Neural Networks (ANN) have gained attention as an advanced computational technique capable of handling complex, nonlinear relationships between process parameters and material properties [16,17]. While ANN models offer high predictive accuracy, their effectiveness in comparison to statistical methods like RSM and ANOVA remains an area of active research.

1.3 Research Gap and Objective

Although previous studies have explored the relationship between FDM parameters and mechanical performance, comparative analyses of RSM, ANOVA, and ANN in predicting and optimizing tensile strength remain limited. Most existing works focus on either experimental testing or individual modeling approaches, without a direct comparison of their accuracy and applicability. This study aims to fill this gap by systematically evaluating the predictive performance of RSM, ANOVA, and ANN in modeling the tensile strength of FDM-printed PLA components. The key objectives of this research are:

To assess the influence of critical FDM parameters (layer thickness, infill density, print speed, temperature, and build orientation) on tensile strength.

To compare the accuracy of RSM, ANOVA, and ANN in predicting mechanical properties.

To determine the optimal set of printing parameters that maximizes tensile strength.

By integrating statistical and computational methodologies, this study provides valuable insights into the optimization of FDM processes, enabling the production of high-performance

3D-printed components with enhanced reliability and efficiency. The findings contribute to the broader field of additive manufacturing, guiding future research on hybrid modeling techniques and alternative material applications.

2. MATERIALS AND METHODS

Tensile test specimens were fabricated using 1.75 mm diameter PLA plus filaments, chosen for their high tensile strength, excellent printability, and biomedical potential. Specimens were designed in SolidWorks 2015 to conform to ASTM D638 Type IV standards and printed using an Ender 3 S1 Pro printer with CURA 5.3.0 slicing software. Key process parameters—layer thickness, infill density, print speed, temperature, and build orientation—were varied at three levels (Table 1), resulting in 27 experiments to optimize the balance between prediction accuracy and cost-efficiency (Table 2). Mechanical testing was performed on a Shimadzu Autograph AGS-X universal testing machine, with tensile tests conducted at a speed of 4 mm/min, recording ultimate load and deformation values to analyze mechanical properties (Figure 1.a and b). Statistical analyses, including ANOVA, were executed in Minitab 17.0 to evaluate the effects and significance of process parameters on tensile strength. Additionally, an ANN model with a 5-input layer, 10 hidden neurons, and a single output layer was trained in MATLAB R2015a, using 70% of the data for training, 15% for validation, and 15% for testing, achieving accurate tensile strength predictions. RSM was employed to model and optimize the effects of process parameters on tensile strength, using experimental data to develop a predictive model for optimization. This integrative approach, combining statistical and mathematical techniques with advanced modeling, facilitated a comprehensive analysis and accurate prediction of tensile strength in 3D printed PLA components.

TABLE 1.

PROCESS PARAMETERS THEIRS LEVEL AND VALUES (FIXED TYPE)

	Layer Thickness (mm)	Infill Density (%)	Print Speed (mm/s)	Temperature (°C)	Build Orientation (°)
Levels	3	4	3	3	3
Values	0,20 0,25 0,30	20 30 40 50	30 40 50	200 210 220	0 45 90

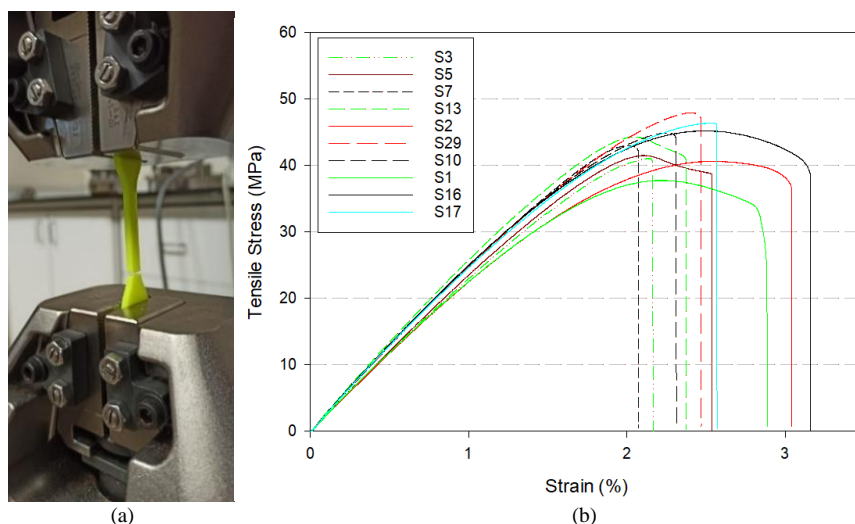


Figure 1. (a) Tensile testing (b) Tensile test results

TABLE 2.

EXPERIMENTAL DESIGN AND LAYOUT

No	Layer Thickness (mm)	Infill Density (%)	Print Speed (mm/s)	Temperature (°C)	Build Orientation (°)
1	0,2	20	30	200	0
2	0,2	20	40	210	45
3	0,2	20	50	220	90
4	0,2	30	30	200	45
5	0,2	30	40	210	90
6	0,2	30	50	220	0
7	0,2	40	30	200	90
8	0,2	40	40	210	0
9	0,2	40	50	220	45
10	0,2	50	30	200	0
11	0,2	50	40	210	45
12	0,2	50	50	220	90
13	0,25	20	30	210	90
14	0,25	20	40	220	0
15	0,25	20	50	200	45
16	0,25	30	30	210	0
17	0,25	30	40	220	45
18	0,25	30	50	200	90
19	0,25	40	30	210	45
20	0,25	40	40	220	90
21	0,25	40	50	200	0
22	0,25	50	30	210	90
23	0,25	50	40	220	0
24	0,25	50	50	200	45
25	0,3	20	30	220	45
26	0,3	20	40	200	90
27	0,3	20	50	210	0
28	0,3	30	30	220	90
29	0,3	30	40	200	0
30	0,3	30	50	210	45
31	0,3	40	30	220	0
32	0,3	40	40	200	45
33	0,3	40	50	210	90

3. RESULTS

The tensile test results from 33 different process parameter combinations were comprehensively analyzed to evaluate the predictive accuracy and optimization capability of Response Surface Methodology (RSM), Analysis of Variance (ANOVA), and Artificial Neural Networks (ANN) for FDM-printed PLA components. By comparing experimental tensile strength values with predicted outcomes, error rates were calculated, enabling a rigorous validation of each model.

3.1. ANOVA results

Table 3 shows the ANOVA results for the model. The ANOVA analysis revealed that all selected parameters—layer thickness, infill density, print speed, temperature, and build orientation—have a statistically significant effect on tensile strength ($p < 0.05$ for all factors). Among these parameters, layer thickness emerged as the most dominant factor, followed by build orientation, temperature, and infill density. The high adjusted R^2 (99.60%) and R^2 (99.01%) values indicate a strong predictive fit, confirming that the selected variables accurately model the tensile strength of 3D-printed components (Figure 2).

TABLE 3.

ANOVA (ANALYSIS OF VARIANCE)

Source	DF	Adj SS	Adj MS	F-Value	P-Value
Model	5	622,431	124,486	1157,97	0,000
Linear	5	622,431	124,486	1157,97	0,000
Layer Thickness (mm)	1	441,517	441,517	4106,99	0,000
Infill Density (%)	1	77,935	77,935	724,95	0,000
Print Speed (mm/s)	1	33,806	33,806	314,46	0,000
Temperature (°C)	1	50,617	50,617	470,84	0,000
Build Orientation (degree)	1	71,437	71,437	664,51	0,000
Error	27	2,903	0,108		
Total	32	625,333			

UTS= $-10.35+93.77\times\text{Layer Thickness}+0.14618\times\text{Infill Density}-0.12421\times\text{Print Speed}+0.15198\times\text{Temperature}+0.04012\times\text{Build Orientation}$

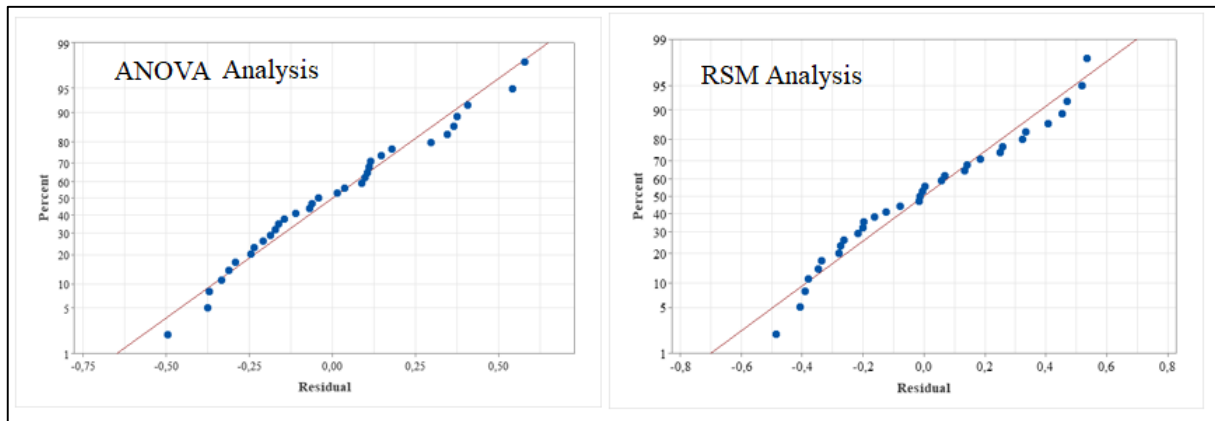


Figure 2. Normal probability plot of residuals for ultimate tensile strength

3.2. Pareto analysis

Figure 3 illustrates the Pareto chart of standardized effects, providing a visual representation of the magnitude of influence of each parameter on tensile strength. Layer thickness dominates the tensile strength response, followed by temperature, infill density, build orientation, and print speed. This analysis highlights which parameters should be prioritized for optimizing mechanical performance in FDM printing.

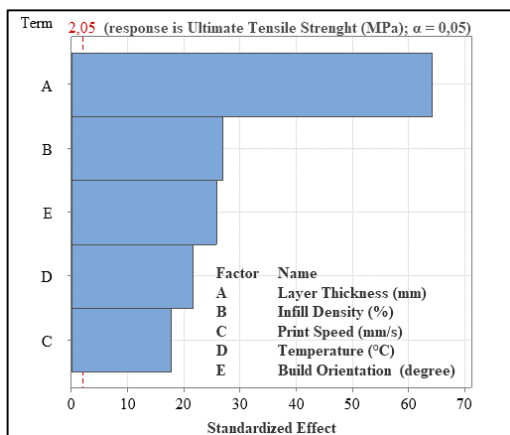


Figure 3. Pareto chart of the standardized effects of parameters

3.3. ANN prediction method

An ANN model with a 5-input layer, 10 hidden neurons, and a single output layer was trained and tested using a 70%-15%-15% data split. The ANN model successfully predicted tensile strength but exhibited slightly higher error rates compared to RSM and ANOVA. Despite its strong correlation coefficients ($R > 0.92$), the ANN's prediction errors were more pronounced for certain parameter combinations, indicating that while ANN is effective for nonlinear datasets, RSM and ANOVA remain more reliable for FDM-printed tensile strength predictions (Figure 4 and Figure 5).

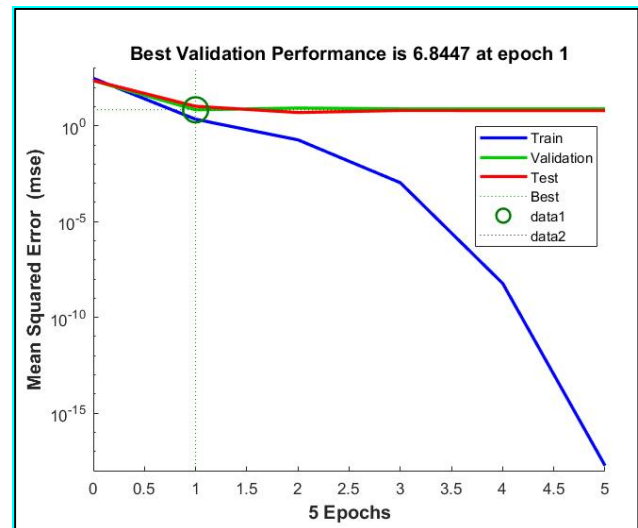


Figure 4. Changes of performance function in training phase of training, validation and test data

3.4. Comparison of methods

A comparative evaluation of actual tensile strength values vs. predicted values (Table 4) confirmed that RSM and ANOVA outperformed ANN in accuracy. RSM showed the lowest deviation percentages (0.65%, 0.18%, 3.43%), followed closely by ANOVA (0.20%, 0.12%, 3.25%), whereas ANN had higher deviation percentages (5.93%, 3.88%, 6.26%). This highlights the importance of selecting the appropriate predictive technique based on specific conditions and parameters, with statistical models proving superior for tensile strength optimization.

3.5. Validation parameters

The correlation matrix (Figure 6) was used to assess the relationship between process parameters and tensile strength. Layer thickness had the highest positive correlation (0.79) with tensile strength, confirming its dominance in mechanical performance. Temperature (0.29) and build orientation (0.34) positively influenced tensile strength, supporting findings from ANOVA. Print speed (-0.20) showed a slight negative correlation, indicating that excessive speed may weaken layer bonding. These results validate that layer thickness,

temperature, and build orientation should be the primary focus when optimizing FDM-printed mechanical properties.

3.6. Correlation analysis and correlation matrix for evaluation methods

The validation parameters provide the test results of tensile strength and predicted values for different values of new process parameters (Table 5). These validation examples were conducted to examine the effects of parameters such as Layer Thickness, Infill Density, Print Speed, Temperature, and Build Orientation. Samples were produced and tensile strength was tested while keeping these values constant. The "Tensile Test" column in the table represents the actual test results, while the "Predicted by RSM," "Predicted by ANOVA," and "Predicted by ANN" columns indicate the predicted tensile strength values. The deviation percentage of these predicted values from the actual test results is also calculated. This deviation percentage indicates how much the predicted value deviates from the actual test result. Thus, it can be observed how close the predictions are to the actual test results. In the first example, the value predicted by the RSM method shows a deviation of 0.65% compared to the actual test result. The ANOVA method exhibits a deviation of 0.20%, while the ANN method shows a deviation of 5.93%. In this case, the RSM and ANOVA methods make predictions closer to the actual test result, while the ANN method shows a slightly higher deviation. In the second example, the value predicted by the RSM method exhibits a deviation of 0.18%, the ANOVA method shows a deviation of 0.12%, and the ANN method exhibits a deviation of 3.88%. Here again, the RSM and ANOVA methods make predictions closer to the actual test result, while the ANN method shows a slightly higher deviation. In the third example, the value predicted by the RSM method exhibits a deviation of 3.43%, the ANOVA

method shows a deviation of 3.25%, and the ANN method exhibits a deviation of 6.26%. In this case, the ANN method shows a higher deviation compared to the actual test result. In these experiments, tensile strength was measured using different parameter combinations. The predicted values were calculated using the RSM, ANOVA, and ANN methods. According to the analysis results, when comparing the actual tensile strength (Tensile Test) with the predicted values (Predicted by RSM, Predicted by ANOVA, and Predicted by ANN), the predictions generally yield results close to the actual values. However, in some experiments, the predictions show slight deviations from the actual values. These results indicate the effectiveness of the RSM, ANOVA, and ANN methods in predicting tensile strength. Table 5 provides an analysis of the experimental parameters and results, demonstrating which parameters affect tensile strength and how accurate the prediction methods are. This information serves as an important reference for material characterization and optimization of production processes.

Figure 6 shows a correlation matrix illustrating the relationships between various parameters and tensile strength. Layer thickness has the strongest positive correlation with tensile strength (0.79), indicating that increased layer thickness leads to higher tensile strength. Infill density shows a weak positive correlation (0.21), suggesting a slight increase in tensile strength with higher infill density. Print speed has a weak negative correlation (-0.20), indicating that higher speeds tend to reduce tensile strength. Temperature has a positive correlation (0.29), meaning higher temperatures generally improve tensile strength. Build orientation also has a positive correlation (0.34), showing that larger build orientation angles tend to increase tensile strength. Among the parameters studied, layer thickness has the most significant impact on tensile strength.

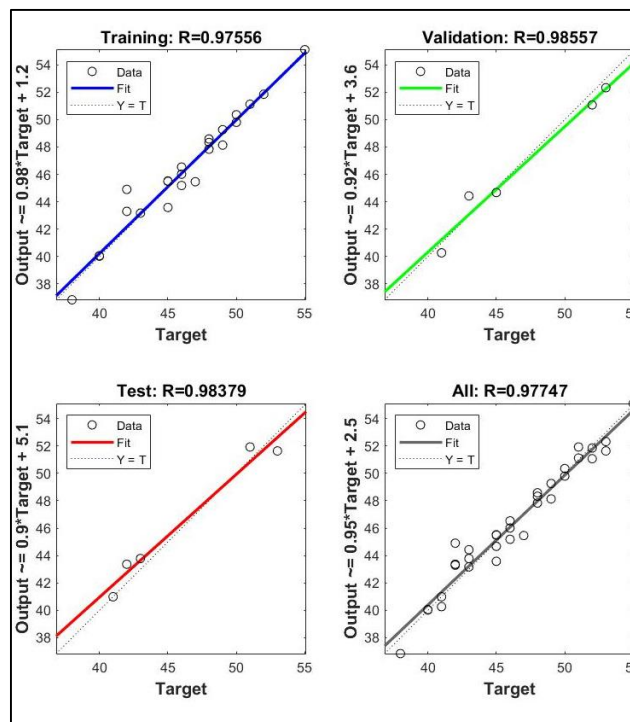


Figure 5. Regression curves of the results of training, validation, and testing data

TABLE 4.

ACTUAL (vs) PREDICTED RSM (vs) PREDICTED ANOVA (vs) PREDICTED ANN AND % OF ERROR

Exp No	Ultimate tensile Strength	Predicted by RSM	Predicted by ANOVA	Predicted by ANN	Error for RSM	Error for ANOVA	Error for ANN
	(MPa)	(MPa)	(MPa)	(MPa)	%	%	%
1	38,293	37,995	37,903	41,055	0,00541	0,09722	0,07248
2	40,834	40,078	40,236	39,523	-0,07792	-0,23611	-3,21541
3	42,537	42,161	42,069	42,999	-0,16126	-0,06944	-0,82333
4	41,551	41,262	41,162	44,989	-0,26190	-0,16204	-8,74304
5	43,285	43,345	43,495	42,295	-0,34524	-0,49537	2,23538
6	40,589	40,012	39,884	39,181	-0,01190	0,11574	-3,27008
7	45,789	44,529	44,421	45,488	0,47078	0,57870	-0,5647
8	41,002	41,196	41,310	40,791	-0,19589	-0,31019	-0,51613
9	43,438	43,279	43,144	41,386	-0,27922	-0,14352	-4,67721
10	42,901	42,380	42,292	46,037	-0,37987	-0,29167	-7,33214
11	45,606	44,463	44,625	44,530	0,53680	0,37500	-2,37682
12	47,516	46,547	46,458	45,978	0,45346	0,54167	-3,27761
13	48,818	47,814	47,819	47,674	0,18615	0,18056	-2,21562
14	45,269	44,481	44,653	45,185	0,51948	0,34722	-0,38324
15	42,239	42,004	41,986	43,233	-0,00433	0,01389	2,53419
16	46,968	45,665	45,634	46,058	0,33550	0,36574	-0,19479
17	48,189	47,748	47,912	48,176	0,25216	0,08796	-0,03116
18	45,207	45,272	45,245	46,237	-0,27165	-0,24537	-2,16132
19	49,937	48,932	48,894	48,074	0,06818	0,10648	-3,71934
20	51,839	51,015	51,171	50,066	-0,01515	-0,17130	-3,40579
21	43,158	43,122	43,060	44,130	-0,12229	-0,06019	-2,45991
22	52,384	52,199	52,208	49,350	-0,19913	-0,20833	-5,75819
23	49,357	48,866	49,042	49,496	0,13420	-0,04167	-0,27374
24	46,042	46,390	46,375	48,773	-0,38961	-0,37500	-6,15304
25	52,484	52,216	52,111	51,034	-0,21645	-0,11111	-2,69422
26	50,282	49,740	49,889	49,858	0,25974	0,11111	-0,08686
27	46,355	46,407	46,333	46,406	-0,40693	-0,33333	-0,09348
28	55,506	55,484	55,370	52,134	-0,48377	-0,37037	-6,10174
29	48,907	47,591	47,704	50,879	0,40909	0,29630	-4,2566
30	50,974	49,674	49,593	48,611	0,32576	0,40741	-4,54132
31	53,875	53,334	53,185	52,523	-0,33442	-0,18519	-2,61525
32	51,281	50,858	50,963	52,622	0,14177	0,03704	-2,55961
33	53,647	52,942	52,852	51,496	0,05844	0,14815	-4,07171

Figure 5. Regression curves of the results of training, validation, and testing data

Figure 7 shows a correlation matrix for four evaluation methods: Experimental Ultimate Tensile Strength, Prediction by RSM, Prediction by ANOVA, and Prediction by ANN. A correlation coefficient near 1 indicates a strong positive correlation. The analysis reveals that all methods are highly correlated. The correlation between Experimental Ultimate Tensile Strength and Prediction by RSM is extremely strong (0.994643), as is the correlation with ANOVA (0.994585),

indicating that RSM and ANOVA predictions closely match experimental values. The correlation with ANN, while still strong (0.922469), is slightly lower, suggesting that ANN predictions are less precise than RSM and ANOVA. These findings indicate that RSM and ANOVA provide more accurate predictions of tensile strength, though all three methods are effective in evaluating tensile strength in FDM-printed components.

TABLE 5

ANOVA (ANALYSIS OF VARIANCE)

No	Layer Thickness	Infill Density	Print Speed	Temperature	Build orientation	Tensile Test	Predicted by RSM	Predicted by ANOVA	Predicted by ANN
CODE	(mm)	(%)	(mm/s)	(°C)	(°)	(MPa)	(MPa)	(MPa)	(MPa)
1	0,25	55	10	200	45	38,187	Y1	Y2	Y3
2	0,18	65	20	210	0	40,963	38,464	38,276	40,386
3	0,38	75	30	220	90	41,112	41,038	41,381	42,757
							42,618	42,382	43,917

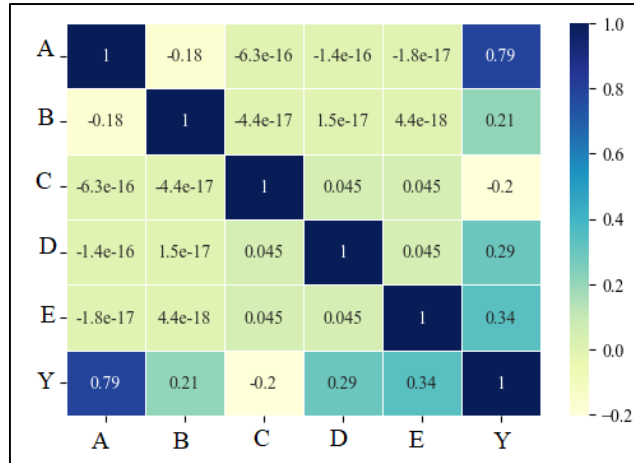


Figure 6. Correlation heatmap between the process parameters and the responses

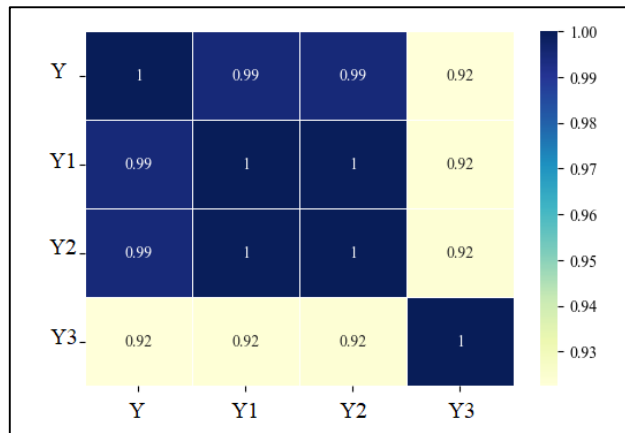


Figure 7. Correlation heatmap between the prediction methods.

3.7. Optimal parameters

The highest UTS value of 55.506 MPa was achieved in experiment no. 28, with the following optimal parameters: 0.20 mm layer thickness, 50% infill density, 50 mm/s print speed, 220°C nozzle temperature, and 90° build orientation. Thin layers ensured a homogeneous structure and enhanced interlayer bonding, while higher infill density provided increased material integrity. A 90° build orientation improved stress distribution, leading to enhanced mechanical strength. A nozzle temperature of 220°C optimized filament flow, minimizing internal voids. Using these parameters, an even higher UTS of 58.173 MPa was achieved in additional optimization trials.

3.8. SEM Analysis

Scanning Electron Microscope (SEM) images (Figure 9) revealed critical insights into fracture behavior. Higher nozzle temperatures (220°C) improved layer adhesion, reducing microvoids. Optimal build orientation (90°) resulted in a more uniform failure pattern, indicating better stress distribution. Some surface irregularities were still observed, suggesting further improvements in extrusion parameters may enhance mechanical performance. The SEM analysis supports the conclusion that process parameter optimization significantly influences the microscopic structure and fracture behavior of FDM-printed PLA components.

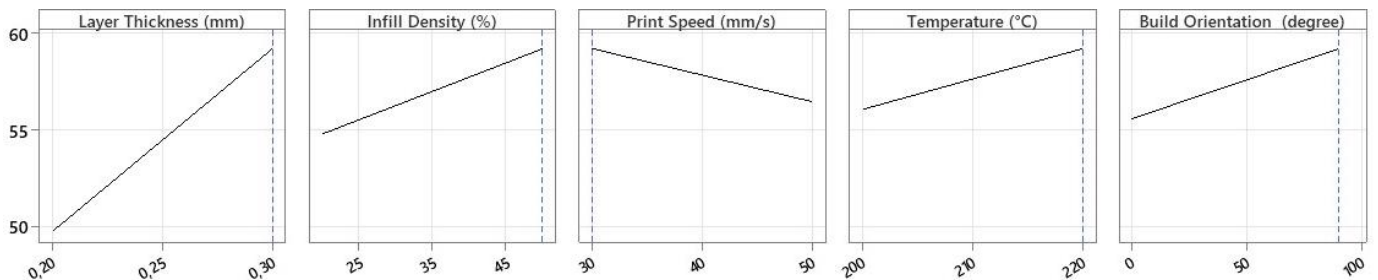


Figure 8. Optimal solution of parameters and their levels

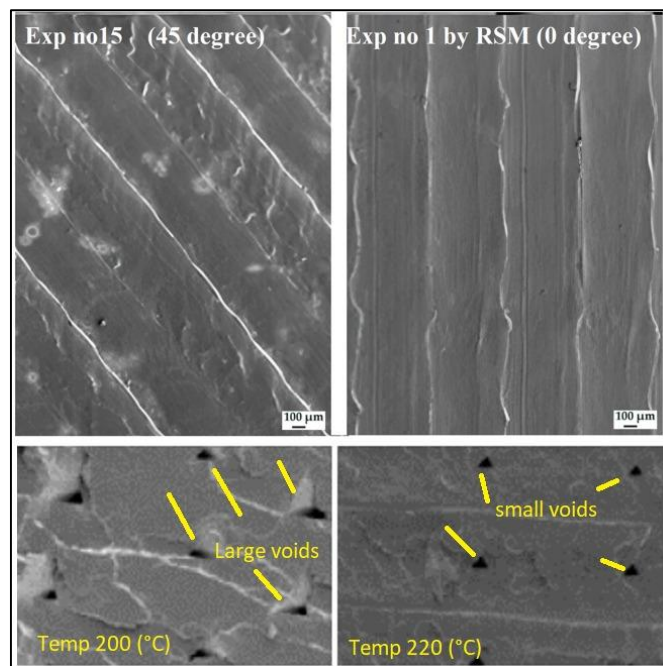


Figure 9. Side surface morphology of 3D printed tensile test specimens' PLA. Experiment No. 15 conducted at 45 degrees yielded a higher ultimate tensile strength compared to the predicted result for Experiment No. 1 by RSM conducted at 0 degrees.

4. DISCUSSIONS

The findings of this study confirm that Response Surface Methodology (RSM), Analysis of Variance (ANOVA), and Artificial Neural Networks (ANN) are effective methods for predicting the ultimate tensile strength (UTS) of FDM-printed PLA components. However, RSM and ANOVA demonstrated superior accuracy, achieving higher correlations with experimental results (97.5% and 98.6%, respectively) and lower error rates (2.5% and 1.4%) compared to ANN. Although ANN exhibited a slightly higher correlation (99.2%), its error rate (0.8%) was higher, suggesting greater deviations in certain cases. The strong statistical foundation of RSM and ANOVA allows for precise modeling of process parameters and their interactions, making them highly reliable for optimizing FDM processes. While ANN provides flexibility in handling complex and nonlinear datasets, it exhibited higher deviations, highlighting the necessity of further refinement or hybrid modeling techniques to enhance predictive accuracy. The analysis revealed that layer thickness was the most influential factor in determining tensile strength, consistent with previous research indicating that thinner layers contribute to improved interlayer bonding and superior mechanical properties. Temperature was also a significant parameter, enhancing material adhesion and minimizing voids, thereby improving overall strength. Infill density and build orientation had moderate effects, suggesting that further refinement of these parameters can enhance part durability. Print speed had the least impact within the tested range, indicating that its role in tensile strength optimization is relatively minor compared to other parameters. These results have important implications for the additive manufacturing industry, as optimizing key process parameters can lead to stronger, more reliable, and higher-performance 3D-printed components, particularly in aerospace, automotive, and biomedical applications. Future research should explore hybrid modeling approaches that integrate RSM, ANOVA, and ANN to leverage the strengths of both statistical and computational techniques. Studies such as those by Deshwal et al. (2020) demonstrate the potential of genetic algorithm-

assisted ANN (GA-ANN) for mechanical property enhancement, while research by Tura et al. (2022) and Saad et al. (2021) highlights the significance of raster angle and print speed optimization. Additionally, work by Giri et al. (2021) on build orientation and Zhou et al. (2017, 2019) on fibril formation and compatibilizers provide valuable insights into further improving material performance. This study underscores the effectiveness of RSM and ANOVA as robust tools for optimizing FDM-printed tensile strength, with ANN serving as a complementary approach. The integration of optimized process parameters—layer thickness, infill density, print speed, temperature, and build orientation—significantly improves the mechanical performance of 3D-printed parts, reinforcing their suitability for industrial applications and advancing the potential of additive manufacturing technologies.

5. CONCLUSION

This study provides a comprehensive comparison of Response Surface Methodology (RSM), Analysis of Variance (ANOVA), and Artificial Neural Networks (ANN) in predicting and optimizing the tensile strength of FDM-printed PLA components. The findings indicate that RSM and ANOVA outperform ANN in predictive accuracy, as evidenced by their lower deviation rates (0.65%, 0.18%, and 3.43% for RSM; 0.20%, 0.12%, and 3.25% for ANOVA) compared to ANN (5.93%, 3.88%, and 6.26%). The strong correlation between predicted and experimental values highlights the robustness of RSM and ANOVA in modeling the effects of key process parameters, including layer thickness, infill density, print speed, temperature, and build orientation. Among these, layer thickness was identified as the most influential factor, followed by temperature, infill density, build orientation, and print speed. The study confirmed that an optimal combination of process parameters—0.20 mm layer thickness, 50% infill density, 50 mm/s print speed, 220°C nozzle temperature, and 90° build orientation—significantly enhances tensile strength, with a maximum recorded value of 55.506 MPa. The results

reinforce that statistical modeling techniques (RSM and ANOVA) provide reliable and precise predictions, making them highly suitable for optimizing mechanical properties in additive manufacturing applications. The integration of these approaches into the FDM process contributes to the development of higher-performance, more durable, and industrially viable 3D-printed components. Future research should explore the application of these methodologies to different thermoplastic and composite materials, as well as investigate hybrid modeling approaches that integrate machine learning techniques with statistical optimization to further enhance accuracy and efficiency in additive manufacturing processes. The findings of this study provide valuable insights into process parameter optimization, enabling sustainable and efficient manufacturing practices, thereby contributing to the continuous advancement of FDM technology in industrial applications such as aerospace, automotive, and biomedical engineering.

6. LIMITATIONS AND FUTURE RESEARCH

While this study successfully demonstrates the effectiveness of RSM, ANOVA, and ANN in predicting and optimizing the tensile strength of FDM-printed PLA components, certain limitations should be acknowledged.

- **Material Selection Constraint:** This research focuses solely on PLA, which, while widely used in FDM, may not represent the mechanical behavior of other thermoplastics such as ABS, PETG, or Nylon. Future studies should explore these materials to assess the generalizability of the findings.
- **Parameter Range Limitations:** The study considers five process parameters, but additional factors, such as raster angle, cooling rate, and extrusion width, could further influence mechanical properties. Expanding the parameter space in future research could yield more robust optimization strategies.
- **Comparative Modeling Enhancements:** While RSM and ANOVA exhibited superior predictive accuracy, ANN's potential for handling highly nonlinear relationships suggests that hybrid approaches (e.g., Genetic Algorithm-assisted ANN, Deep Learning-based models) should be explored to further enhance prediction reliability.
- **Industrial Validation:** The findings are based on laboratory-scale experiments, and their applicability to real-world industrial scenarios remains to be tested. Future research should focus on validating these results in large-scale manufacturing environments to ensure practical implementation.

ACKNOWLEDGEMENT

We would like to thank Kastamonu University Scientific Research Coordinatorship for supporting this study with project number KÜ-BAP01/2023.

REFERENCES

- [1] A.J. Sheoran, H. Kumar, "Fused Deposition modeling process parameters optimization and effect on mechanical properties and part quality: Review and reflection on present research". *Mater. Today Proc.*, 2019, 10, 14. <https://doi.org/10.1016/j.matpr.2019.11.296>
- [2] A. Pandžić, D. Hodžić, E. Kadrić, "Experimental Investigation on Influence of Infill Density on Tensile Mechanical Properties of Different FDM 3D Printed Materials". *TEM Journal*, 2021, 10(3). <https://doi.org/10.18421/TEM103-25>
- [3] V. Wankhede, D. Jagetiya, A. Joshi, R. Chaudhari, "Experimental investigation of FDM process parameters using Taguchi analysis". *Mater. Today Proc.*, 2019, 27, 2117–2120. <https://doi.org/10.1016/j.matpr.2019.09.078>
- [4] M. Algarni, S. Ghazali, "Comparative study of the sensitivity of PLA, ABS, PEEK, and PETG's mechanical properties to FDM printing process parameters". *Crystals*, 2021, 11.8: 995. <https://doi.org/10.3390/cryst11080995>
- [5] A. Milovanović, A. Sedmak, A. Grbović, Z. Golubović, G. Mladenović, K. Čolić, M. Milošević, "Comparative analysis of printing parameters effect on mechanical properties of natural PLA and advanced PLA-X material". *Procedia Struct. Integr.*, 2020, 28, 1963–1968. <https://doi.org/10.1016/j.prostr.2020.11.019>
- [6] G.C. Onwubolu, F. Rayegani, "Characterization and Optimization of Mechanical Properties of ABS Parts Manufactured by the Fused Deposition Modelling Process". *Hindawi*, 2014, 1–13. <http://dx.doi.org/10.1155/2014/598531>
- [7] H.B. Mamo, A.D. Tura, A.J. Santhos, N. Ashok, D.K. Rao, "Modeling and analysis of flexural strength with fuzzy logic technique for a fused deposition modeling ABS components". *Mater. Today Proc.*, 2022, 57, 768–774. <https://doi.org/10.1016/j.matpr.2022.02.306>
- [8] S. Wang, Y. Ma, Z. Deng, S. Zhang, J. Cai, "Effects of fused deposition modeling process parameters on tensile, dynamic mechanical properties of 3D printed polylactic acid materials". *Polym. Test.*, 2020, 86, 106483. <https://doi.org/10.1016/j.polymertesting.2020.106483>
- [9] J. Lluch-Cerezo, R. Benavente, M.D. Meseguer, S.C. Gutiérrez, "Study of samples geometry to analyze mechanical properties in Fused Deposition Modeling process (FDM)". *Procedia Manuf.*, 2019, 41, 890–897. <https://doi.org/10.1016/j.promfg.2019.10.012>
- [10] Y.G. Zhou, J.R. Zou, H.H. Wu, B.P. Xu, "Balance between bonding and deposition during fused deposition modeling of polycarbonate and acrylonitrile-butadiene-styrene composites". *Polymer Composites*, 2019, 41(1), 60-72. <https://doi.org/10.1002/pc.25345>
- [11] A.W. Gebisa, H.G. Lemu, "Influence of 3D printing FDM process parameters on tensile property of ULTEM 9085". *Procedia Manufacturing*, 2019, 30, 331-338. <https://doi.org/10.1016/j.promfg.2019.02.047>
- [12] K.I. Byberg, A.W. Gebisa, H.G. Lemu, "Mechanical properties of ULTEM 9085 material processed by fused deposition modeling". *Polymer Testing*, 2018, 72, 335-347. <https://doi.org/10.1016/j.polymertesting.2018.10.040>
- [13] K.P. Motaparti, G. Taylor, M.C. Leu, K. Chandrashekara, J. Castle, M. Matlack, "Experimental investigation of effects of build parameters on flexural properties in fused deposition modelling parts". *Virtual and Physical Prototyping*, 2017, 12(3), 207-220. <https://doi.org/10.1080/17452759.2017.1314117>
- [14] K.J. Christiyan, U. Chandrasekhar, K. Venkateswarlu, "A study on the influence of process parameters on the Mechanical properties of 3D printed ABS composite". In *IOP conference series: materials science and engineering*, IOP Publishing, 2016, 114, 1, 012109. <https://doi.org/10.1088/1757-899X/114/1/012109>
- [15] X. Zhou, S.J. Hsieh, C.C. Ting, "Modelling and estimation of tensile behaviour of polylactic acid parts manufactured by fused deposition modelling using finite element analysis and knowledge-based library". *Virtual and Physical Prototyping*, 2018, 13(3), 177-190. <https://doi.org/10.1080/17452759.2018.1442681>
- [16] A.W. Gebisa, H.G. Lemu, "Investigating effects of fused-deposition modeling (FDM) processing parameters on flexural properties of ULTEM 9085 using designed experiment". *Materials*, 2018, 11(4), 500. <https://doi.org/10.3390/ma11040500>
- [17] M.H. Hsueh, C.J. Lai, S.H. Wang, Y.S. Zeng, C.H. Hsieh, C.Y. Pan, W.C. Huang, "Effect of printing parameters on the thermal and mechanical properties of 3d-printed PLA and PETG, using fused deposition modeling". *Polymers*, 2021.a, 13(11), 1758. <https://doi.org/10.3390/polym13111758>
- [18] E.U. Enemuoh, S. Duginski, C. Feyen, V.G. Menta, "Effect of process parameters on energy consumption, physical, and mechanical properties of fused deposition modeling". *Polymers*, 2021, 13(15), 2406. <https://doi.org/10.3390/polym13152406>

- [19] M.H. Hsueh, C.J. Lai, K.Y. Liu, C.F. Chung, S.H. Wang, C.Y. Pan, Y.S. Zeng, "Effects of printing temperature and filling percentage on the mechanical behavior of fused deposition molding technology components for 3D printing". *Polymers*, 2021, 13(17), 2910. <https://doi.org/10.3390/polym13172910>
- [20] C. Patil, P.D. Sonawane, M. Naik, D.G. Thakur, "Finite element analysis of flexural test of additively manufactured components fabricated by fused deposition modelling". In *AIP Conference Proceedings AIP Publishing*, December, 2020, 2311, 1. <https://doi.org/10.1063/5.0034306>
- [21] R. Srinivasan, T. Pridhar, L.S. Ramprasad, N.S. Charan, W. Ruban, "Prediction of tensile strength in FDM printed ABS parts using response surface methodology (RSM)". *Materials Today: Proceedings*, 2020, 27, 1827-1832. <https://doi.org/10.1016/j.matpr.2020.03.788>
- [22] S. Deshwal, A. Kumar, D. Chhabra, "Exercising hybrid statistical tools GA-RSM, GA-ANN and GA-ANFIS to optimize FDM process parameters for tensile strength improvement". *CIRP Journal of Manufacturing Science and Technology*, 2020, 31, 189-199. <https://doi.org/10.1016/j.cirpj.2020.05.009>
- [23] A.D. Tura, H.G. Lemu, H.B. Mamo, "Experimental investigation and prediction of mechanical properties in a fused deposition modeling process". *Crystals*, 2022, 12(6), 844. <https://doi.org/10.3390/cryst12060844>
- [24] M.S. Saad, A. Mohd Nor, M.Z. Zakaria, M.E. Baharudin, W.S. Yusoff, "Modelling and evolutionary computation optimization on FDM process for flexural strength using integrated approach RSM and PSO". *Progress in Additive Manufacturing*, 2021, 6, 143-154. <https://doi.org/10.1007/s40964-020-00157-z>
- [25] J. Giri, P. Shahane, S. Jachak, R. Chadge, P. Giri, "Optimization of FDM process parameters for dual extruder 3d printer using artificial neural network". *Materials Today: Proceedings*, 2021, 43, 3242-3249. <https://doi.org/10.1016/j.matpr.2021.01.899>
- [26] Y.G. Zhou, B. Su, L.S. Turng, "Deposition-induced effects of isotactic polypropylene and polycarbonate composites during fused deposition modeling". *Rapid Prototyping Journal*, 2017, 23(5), 869-880. <https://doi.org/10.1108/RPJ-12-2015-0189>

BIOGRAPHIES

Fuat Kartal received his BS and MS degrees from Kocaeli University, Department of Mechanical Education in 2006 and 2009, respectively, and his PhD from Karabük University, Institute of Science in 2015. He also completed his BS degree in Mechanical Engineering at Karabük University in 2020. His research interests include additive manufacturing, computer-aided design, and manufacturing. During his career, he worked at Kastamonu University, Machinery and Metal Technologies program between 2008 and 2015. Since 2015, he has been working as an Associate Professor at Kastamonu University, Department of Mechanical Engineering. He teaches and conducts research on 3D printers, mechanical design, abrasive waterjet machining, and pressure vessels. He has published more than 60 research articles. He has published several books chapter and frequently gives invited keynote lectures at international conferences.

Arslan Kaptan received his BS and MS degrees in Mechanical Education from Kocaeli University in 2004 and 2006, respectively, and his PhD degree from the Institute of Science at the same university in 2015. Additionally, he completed his undergraduate degree in Mechanical Engineering at Sivas Cumhuriyet University in 2019. His research interests include additive manufacturing, computer-aided design and manufacturing. During his career, he worked at Gaziosmanpaşa University between 2007-2011 in the Motor Vehicles and Transportation Technologies program. He has been working as an Assistant Professor in the same department at Sivas Cumhuriyet University since 2011. He teaches and researches on 3D printers, abrasive waterjet machining and pressure vessels.

Research Article

The Investigation of the Weldability of Ti6Al4V Alloy with Different Stainless Steel Series Using Copper Interlayer via Friction Welding

Ertugrul Celik^{1*} ^{1*}Munzur University, Faculty of Engineering, Mechanical Engineering Department, Tunceli, Turkey. (e-mail: ecelik@munzur.edu.tr).

ARTICLE INFO

Received: Apr., 9. 2025
 Revised: Jan., 14. 2025
 Accepted: Dec., 17. 2024

Keywords:

Friction welding
 Stainless steel
 Ti6Al4V alloy
 Copper interlayer

Corresponding author: [Ertugrul Celik](mailto:Ertugrul.Celik@munzur.edu.tr)

ISSN: 2536-5010 / e-ISSN: 2536-5134

DOI: <https://doi.org/10.36222/ejt.1567815>

ABSTRACT

Friction welding is a solid-state welding method used for joining metals with different properties, providing minimal thermal deformation in welded joints. Based on this advantageous feature of friction welding, this study investigates the weldability of Ti6Al4V alloy with 316L, 316Ti, 310, 430, and 304 series stainless steels using a Cu powder interlayer. Following the experimental procedures, the microstructures of the materials were analyzed using SEM-EDX, their macrostructures were visually inspected for physical changes, microhardness measurements were taken, and tensile tests were performed. It was observed that the Cu powder interlayer significantly influenced the reactions and bonding between the materials, playing a crucial role in both microstructure and mechanical properties. In this study, successful joining results were achieved using the friction welding method, and the microstructural characteristics and mechanical performance of the welded joints were thoroughly evaluated. Upon examining the microhardness results, no significant variations in hardness values were observed on the Ti6Al4V side.

1. INTRODUCTION

Welding is a technique that permanently joins metallic and plastic materials, typically performed using heat, pressure, or a combination of both. Ideally, the materials should have similar melting points, and the surfaces should be clean. However, achieving these conditions can be challenging, which has led to the development of various welding methods. Welding techniques are classified into two main categories: fusion welding and solid-state welding. In fusion welding, the materials are melted using heat, while in solid-state welding, the materials are joined below their melting points [1]. Friction welding is an important solid-state welding technique that enables the joining of cylindrical parts by generating heat through friction. This method does not require filler materials or shielding gases and offers advantages such as low energy consumption, fast processing times, and the ability to join dissimilar materials [2-5].

Titanium and its alloys remain among the most widely used materials in biomedical applications due to their exceptional strength and biocompatibility [6,7]. Among titanium alloys, Ti6Al4V is a commonly preferred alloy belonging to the $\alpha+\beta$ alloy group, offering balanced properties through its aluminum and vanadium content [8]. This alloy is widely used in numerous industrial applications due to its advantages such as low density, high thermal stability,

excellent mechanical properties, effective corrosion resistance, and biocompatibility [9-11]. Ti6Al4V is frequently employed in fields such as jet engines, spacecraft, the automotive industry, and medical implants. However, the welding processes of titanium alloys carry risks of distortion and contamination due to high heat input. Specifically, the absorption of harmful gases in the weld seam of Ti6Al4V can lead to a reduction in mechanical properties. Friction welding offers an effective solution to mitigate these challenges, as its low heat input and controlled process can enhance weld quality and prevent gas absorption. Therefore, the potential advantages provided by friction welding in joining Ti6Al4V alloy play a noteworthy role [12].

Stainless steels offer a wide range of properties and applications, making them essential in industrial and engineering fields. 316L and 316Ti belong to the austenitic stainless steel category; 316L, with its low carbon content, provides superior performance in corrosive environments such as seawater, while 316Ti, with titanium addition, enhances stability and corrosion resistance at high temperatures [13]. 310 stainless steel is an austenitic alloy designed for high-temperature applications, known for its excellent heat resistance and oxidation resistance [14]. Ferritic 430 stainless steel is favored in less corrosive environments and decorative applications, while 304 stainless steel, the most

common type in the austenitic group, offers good general corrosion resistance and workability [15]. Each of these steel types serves a broad range of industrial applications by offering properties tailored to specific requirements.

In this context, Ünal et al. investigated the friction welding of AISI 430, AISI 440, and AISI 304 stainless steels with AISI 4340 steel and examined the fatigue strength of the materials after welding. The experiments were conducted using a continuous drive friction welding machine at different rotational speeds; the weld zones were examined using optical and scanning electron microscopes, while EDAX analyses and Vickers hardness measurements were performed. Fatigue tests were carried out on a rotating bending fatigue machine, and fracture surfaces were analyzed with SEM [16]. Ting et al. joined 304 stainless steel with Ti-15-3 titanium alloy using electron beam welding with a copper interlayer. The microstructures of the welded region were examined by optical microscopy, scanning electron microscopy, and X-ray diffractometry, and the mechanical properties were evaluated through tensile testing. The formation of $TiFe_2$ intermetallic phases on the stainless steel side and Ti-Cu and Ti-Fe-Cu layers on the titanium side was observed [17]. Turner and colleagues explored the weldability of titanium alloys using the linear friction welding method. They conducted experiments on Ti6Al4V alloy and evaluated heat transfer effects using thermocouples [18]. The experimental results were consistent with the modeling outcomes. Kumar and Balasubramanian studied the friction welding of SUS 304 HCU austenitic stainless steel pipes. In the welding process, using friction welding parameters, it was observed that the potential for eutectic formation of Cu at low temperatures was minimized [19].

In this study, the joining of Ti6Al4V alloy with 316L, 316Ti, 310, 430, and 304 stainless steels was performed. A precise direct-drive friction welding machine, where all welding parameters could be controlled via a PLC automation system, was utilized. In preliminary trials, several attempts without using an interlayer resulted in failure, prompting the re-evaluation of Ti6Al4V alloy's weldability with the use of an interlayer. The method employed involved filling 4 mm diameter holes drilled into the surface of the material to be welded with powdered Cu, which served as the interlayer. This approach led to successful joining results. Copper powder was used as the interlayer, and the powder was compressed into the hole created in the material with a specialized punch. Since the powder was secured to the stationary side of the welding machine, no material loss occurred. The welded joints were evaluated through microstructural characterization, tensile tests, microhardness measurements, and SEM-EDS analyses.

2. MATERIAL AND METHOD

The samples used in the experiments were commercially procured. The device utilized for the welding process was specifically designed for this purpose. All welding parameters could be controlled through a touchscreen interface on the PLC unit. The mechanical structure of the friction welding device is divided into three main sections: the drive area, the movable area, and the pressure area. These sections are bolted onto a single piece made of St52 material, which is 50 mm thick, to prevent vibrations. The welded samples and the welding process parameters are presented in Table 1.

TABLE I

WELDED SAMPLES AND WELDING PROCESS PARAMETERS

Welded Pairs/dönm	Interlayer Materials	Friction Time (sn)	Forging Time (sn)	Friction Pressure (MPa)	Forging Pressure (MPa)	Rotational Speed (dev/dk)
Ti6Al4V-316L	Cu	5	15	100	250	2850
Ti6Al4V-316Ti	Cu	5	15	100	250	2850
Ti6Al4V-310	Cu	7	15	75	175	1800
Ti6Al4V-430	Cu	7	15	75	175	1800
Ti6Al4V-304	Cu	11	15	75	175	1800

Commercially obtained rods with a diameter of 8 mm and a length of 3 meters were cut to a length of 30 mm using a precision sample cutting device and subjected to turning operations on a lathe to achieve a smooth joint. Holes with a diameter of 4 mm and a depth of 2 mm were drilled into the samples to be joined with the Ti6Al4V alloy on the lathe. Copper powder was placed in these holes as an interlayer using a special pressing apparatus, and a drop of alcohol was applied to each powder to prevent scattering. During welding, the Ti6Al4V sample was placed in the rotating section, while the other material was positioned in the fixed section. Figure 1 shows the friction welding machine used in the experiment. European Journal of Technique, European Journal of Technique, European Journal of Technique, European Journal of Technique, European Journal of Technique, European Journal of Technique, European Journal of Technique, European Journal of Technique, European Journal of Technique, European Journal of Technique [2-6].



Figure 1. Friction Welding Machine Used in the Experiment

After the samples were placed, the welding process was carried out, and they were reduced to suitable sizes for metallographic analysis. Subsequently, the samples were subjected to cold mounting and prepared for microstructure and microhardness examinations. The samples were polished sequentially with water sandpapers numbered 180 to 2000 and then polished with 1 μ m and 3 μ m paste. After polishing, the surfaces were cleaned with ethyl alcohol. Chemical etching was performed for 30 seconds using different etchants on the Ti6Al4V and stainless steel samples. The welded samples were prepared for scanning electron microscopy and energy-dispersive X-ray spectroscopy (EDX), and microhardness measurements were conducted using the Vickers method. Hardness values were measured at ten different points horizontally with 0.5 mm spacing, focusing on the center of the weld zone. Tensile specimens were prepared according to ASTM E 8M-04 standards, and tensile tests were performed using a "AG-IC SHIMADZU" device with a capacity of 100 kN. Tensile strength, percentage elongation, and stress values were measured using the TRAPEZIUM-X software.

3. RESULTS AND DISCUSSION

The Ti6Al4V alloy has been successfully joined with 316L, 316Ti, 310, 430, and 304 materials. The macrostructure, microhardness, tensile tests, as well as SEM and EDX analyses of the obtained welded samples have been thoroughly examined. The results of these analyses are presented below.

3.1. Macrostructure Investigations

Macrostructure images of the welded samples are presented in Figure 2. The macro and cross-sectional images of the samples welded using a copper interlayer for AISI 316L-Ti6Al4V alloys have also been analyzed. In these samples, the neck region was observed in the Ti6Al4V alloy, resulting in a length reduction of 5.08% after welding. The cross-sectional images clearly show that the welding process was successfully carried out and that the deformation of the weld interzone was evident. The macrostructure images of the samples welded with AISI 316Ti and Ti6Al4V alloys reveal that the neck region is located within the Ti6Al4V alloy, with a length reduction of 6.1%. This situation reflects the influence of the physical properties of the Ti6Al4V alloy and the applied welding parameters. In the macrostructure images obtained from the friction welding of AISI 310 and Ti6Al4V alloys, it

can be seen that the joining process was successfully executed, with the neck region forming on the Ti6Al4V alloy side. The length reduction resulting from the welding process was measured to be approximately 2.5%. Upon examining the cross-sectional images, it was observed that the deformed area was limited and that the copper interlayer diffused throughout the weld zone. Similarly, the welded samples of AISI 430 and Ti6Al4V alloys using a copper interlayer were also investigated. A successful welding operation was observed in these samples, and the macrostructure analysis indicated that the neck region was on the AISI 430 side, with a length reduction of 3% occurring after welding. The cross-sectional image clearly illustrates the deformation of the weld zone and the diffusion of the copper interlayer throughout the weld section. Finally, macro and cross-sectional photographs of the friction welding processes of AISI 304 and Ti6Al4V alloys using a copper interlayer have been examined. In cases where the friction time was 5 seconds, the welding process was unsuccessful; however, at 11 seconds and a rotational speed of 1800 RPM, the welding operation successfully facilitated the joining of the materials. The neck region formed in the Ti6Al4V alloys after welding, with a length reduction measured at 0.89%. The cross-sectional images indicate that the structure of the spot hole was preserved due to minimal deformation observed on the AISI 304 side, resulting in a robust joint region.

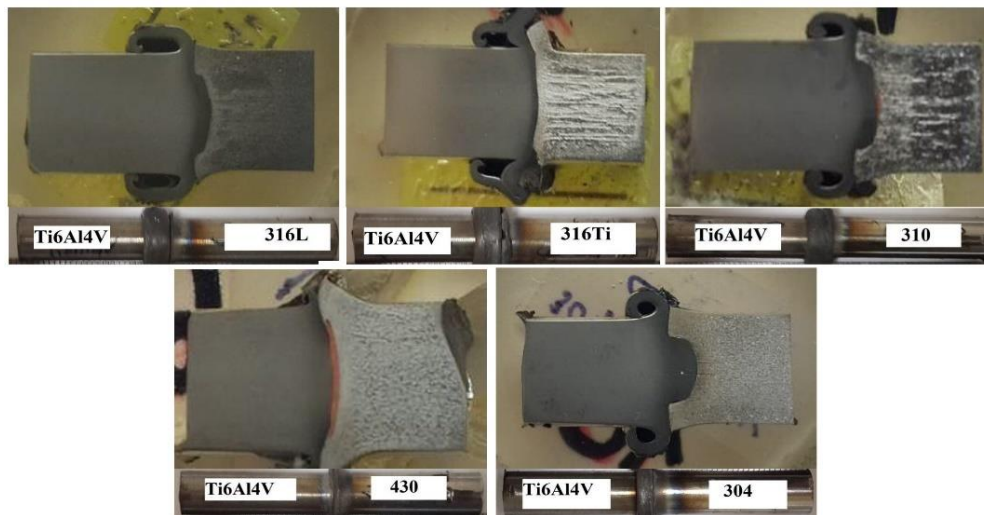


Figure 2. Macrostructure Images of Welded Samples

3.2. Microhardness Measurement Results

Figure 3 presents the microhardness profiles of weld samples using a Cu interlayer. In the Ti6Al4V-316L weld, it is observed that while there is no significant change in the hardness values on the Ti6Al4V side, a notable decrease is observed on the 316L side towards the weld interface. This reduction in hardness is attributed to the elevated temperatures in the weld region, which relieve internal stresses within the material [20,21]. Conversely, in the microhardness graph of the weld process using a Cu interlayer for the 316Ti and Ti6Al4V alloys, the hardness on the Ti6Al4V side remains relatively stable up to the fusion zone, with an average value of approximately 310 HV. However, the 316Ti side exhibits an increase in hardness values up to a distance of 3 mm from the fusion zone, rising from 212.2 HV to 266.8 HV. This increase is linked to the reduction of internal stresses facilitated by the heat in the weld zone, which enhances hardness. Despite

these differing trends in hardness, the underlying cause appears to be similar—both phenomena are related to the thermal influence on internal stresses within the material. Therefore, a more nuanced reinterpretation is required to accurately reflect the relationship between thermal effects and hardness variations in the weld region. In the welding process between the 430 and Ti6Al4V alloys, no significant change in hardness values was observed, which is attributed to the low heat input in the fusion zone. The highest hardness value measured on the AISI 430 side was 238 HV, while on the Ti6Al4V side, it was 324 HV. The microhardness values in the welding process between AISI 304 and Ti6Al4V alloys did not exhibit a significant change. The interlayer hardness could not be measured due to the thin section thickness at the weld interface. The highest hardness value measured on the AISI 304 side was 330 HV, and 358 HV on the Ti6Al4V side.

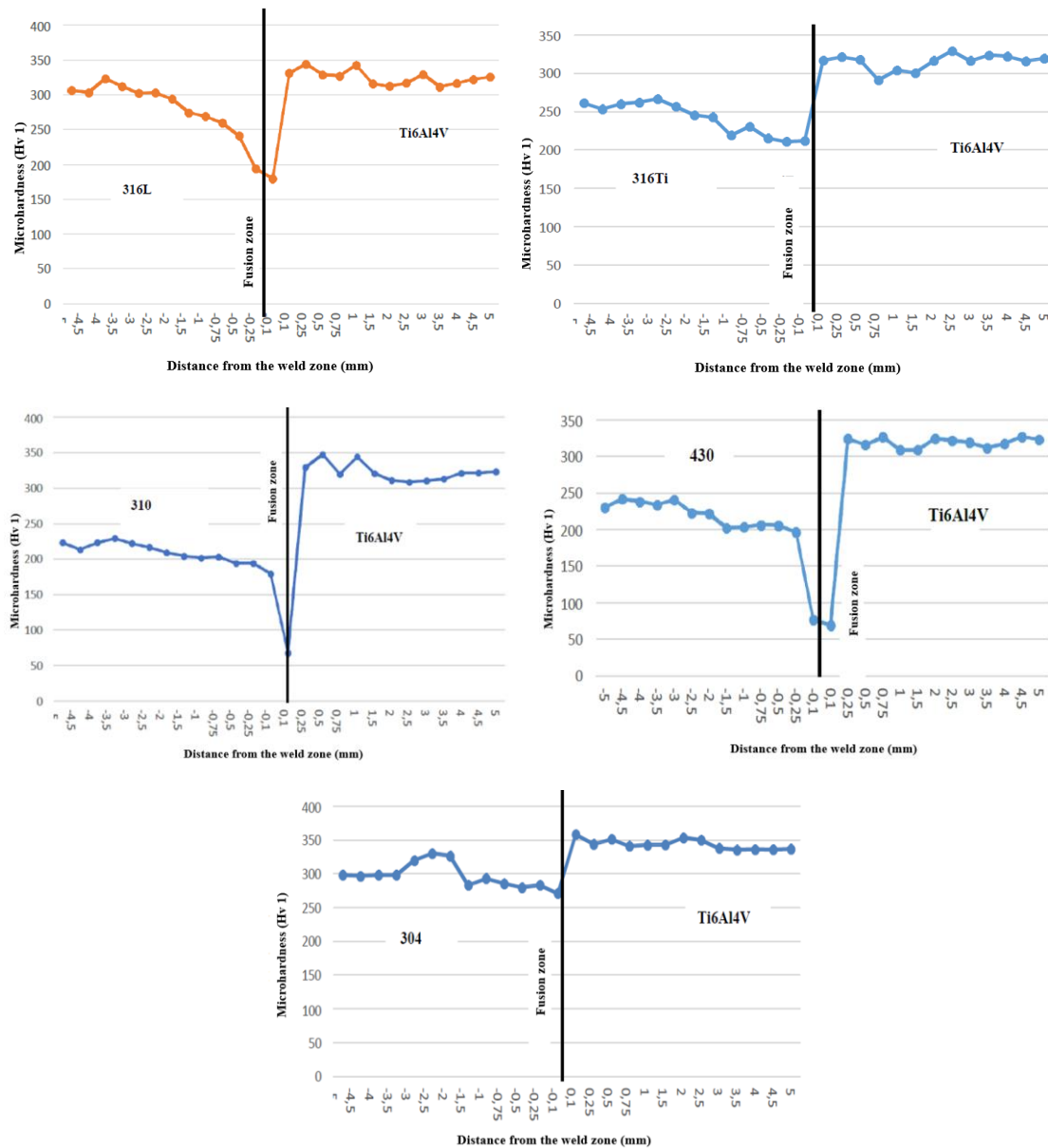


Figure 3. Microhardness Measurement Graphs of Welded Samples

3.3. Tensile Test Analysis

Figure 4 presents the tensile strength of samples welded using a copper interlayer. It has been observed that the elastic deformation of the 316L-Ti6Al4V materials is approximately 42 MPa, followed by a fracture occurring at 291 MPa, with a material elongation of 3.5%. The tensile strength exceeds that of the copper interlayer, which has a tensile strength of 200 MPa. This phenomenon is primarily associated with the low heat input during the welding process. Low heat input reduces the material's overall thermal exposure. It facilitates rapid cooling, promoting the formation of a finer microstructure and enhancing tensile strength. Therefore, although both rapid cooling and low heat input contribute to the outcome, the main factor responsible for the increase in tensile strength is the low heat input, which controls the cooling rate and improves material properties. [21-22]. According to the tensile graph of samples welded with Cu interlayer using 316Ti and Ti6Al4V alloys, the material exhibits an elastic strain value of 45 MPa, and the fracture strength is measured to be approximately 320 MPa, with an elongation of 4.6%. The

tensile strength surpasses the tensile strength of copper, which is 200 MPa. In the average tensile strength graph of the Ti6Al4V alloy with a value of 310, the material exhibits elastic behavior up to approximately 45 MPa, followed by fracture at 440 MPa in the interfacial region, with a 5.5% elongation. This value exceeds the tensile strength of copper, which is 220 MPa, due to the interlayer thickness of approximately 200 μm and the substantial cross-sectional thickness. The friction welding process has enhanced the tensile strength, primarily due to the effects of friction time and consolidation pressure. Friction time allows for more heat generation and material softening, promoting better interfacial bonding, while consolidation pressure ensures proper contact and densification of the material, further improving the mechanical properties. In the tensile graph of the 430 and Ti6Al4V alloy, the material exhibits elastic properties up to approximately 40 MPa, followed by a fracture occurring around 230 MPa, with an elongation of 3.1%. The tensile strength exceeds the tensile strength of the copper interlayer, which is 200 MPa; this is attributed to the significant interlayer thickness and the uniform distribution of the interlayer across the cross-section. The average

tensile graph of the Ti6Al4V alloy with 304 shows elastic properties up to approximately 40 MPa, after which a fracture occurs at 187 MPa, resulting in an elongation of 2.8%. This value is below the tensile strength of copper,

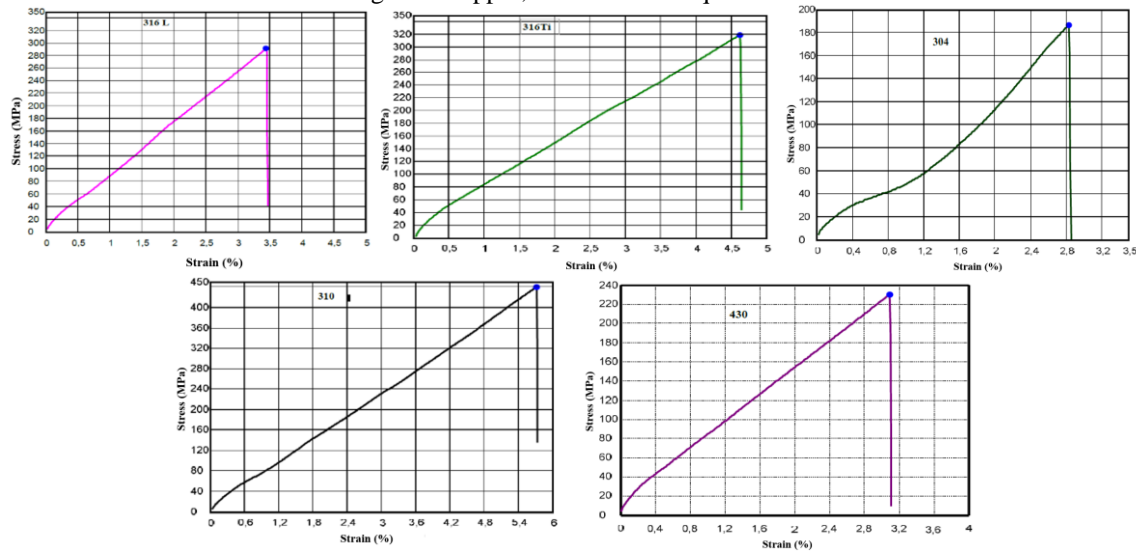
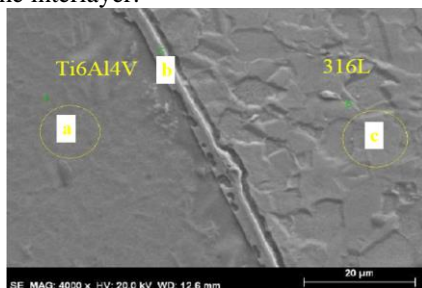


Figure 4. Tensile Test Graphs of Samples Joined Using Cu Interlayer

3.4. Microstructural Analyses

Figure 5 presents the SEM images and EDX analyses of the welded materials. Upon examining the SEM images of the 316L and Ti6Al4V samples, it was observed that the weld zone exhibited a smooth and homogeneous distribution along a consistent line. Furthermore, it was determined that a thin layer, approximately 5 μm thick, was formed in the weld interfacial region. The EDX results of the samples indicated that the highest proportions of elements in the weld interfacial region were 28.64% Ti, 40.04% Fe, and 13.45% Cu (Figure 5). This indicates that solid-state diffusion of atoms occurred from the weld pairs towards the interlayer.



Element	a region (% wt.)	b region (% wt.)	c region (% wt.)
Ti	90.15	28.64	-
Al	5.97	1.16	-
V	3.88	-	-
C	-	0.02	0.03
Si	-	0.53	0.77
Cr	-	8.09	17.44
Fe	-	40.04	69.42
Ni	-	5.72	10.07
Mn	-	1.54	2.27
Cu	-	13.45	-

Figure 5. SEM Images and EDX Results of 316L-Ti6Al4V Welded Samples

which is 220 MPa, due to the interlayer thickness being approximately 20 μm . European Journal of Technique, European Journal of Technique, European Journal of Technique.

In the SEM analyses conducted on the joining of 316Ti and Ti6Al4V alloys using a copper interlayer, it was observed that the bonding region was distinctly visible across the entire surface. The interfacial thickness in this region was measured to be 15 microns (Figure 6).

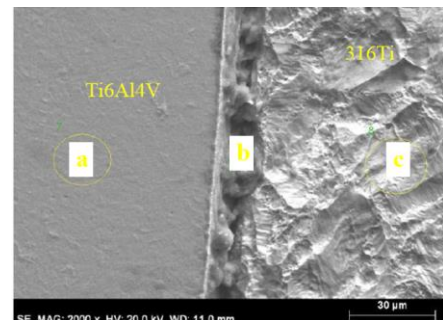
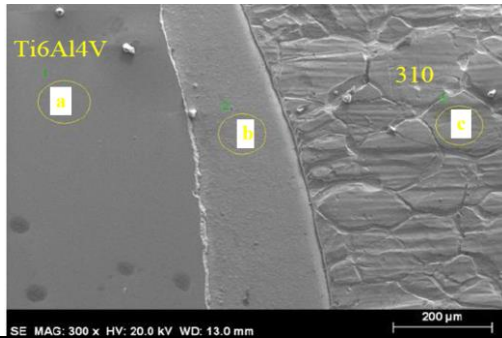


Figure 6. SEM Image of 316Ti-Ti6Al4V Welded Samples

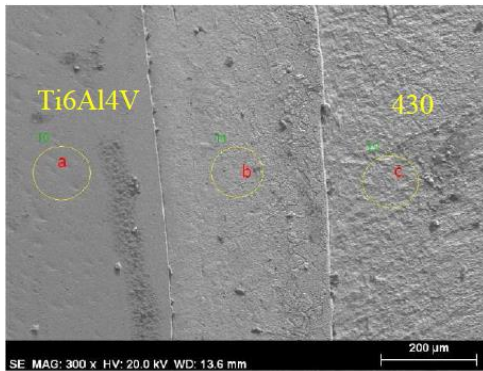
The SEM images of the samples welded with a copper interlayer using the 310 and Ti6Al4V alloys demonstrate that the welding process was successful and that the copper interlayer formed uniformly and homogeneously (Figure 7). Additionally, the SEM photograph indicates that the thickness of the interfacial layer is approximately 200 μm . Upon examining the EDX analyses, it was concluded that due to the width of the weld interfacial thickness, only 100% Cu atoms are present, suggesting that diffusion may occur at the contact areas.



Element	a region (% wt.)	b region(% wt.)	c region (% wt.)
Ti	90.15	-	-
Al	5.97	-	-
V	3.88	-	-
C	-	-	0.24
Si	-	-	0.63
Cr	-	-	21.87
Fe	-	-	57.50
Ni	-	-	17.82
Mn	-	-	1.94
Cu	-	100	-

Figure 7. SEM Images and EDX Results of 310-Ti6Al4V Welded Samples

Upon examining the SEM images of the samples welded using a copper interlayer with the 430 and Ti6Al4V alloys, it was observed that the welding process was successful and that the weld region exhibited a smooth and homogeneous distribution along its length (Figure 8). The SEM images clearly demonstrate that the thickness of the weld interfacial region occupies a broad area with a thickness of 350 μm at the bonding region. Furthermore, EDX analyses revealed that due to the considerable thickness of the weld interfacial region, only the copper phase was present in the area.



Element	a region (% wt.)	b region (% wt.)	c region (% wt.)
Ti	90.15	-	-
Al	5.97	-	-
V	3.88	-	-
C	-	-	0.11
Si	-	-	0.57
Cr	-	-	15.82
Fe	-	-	82.53
Ni	-	-	0.97
Mn	-	-	-
Cu	-	100	-

Figure 8. SEM Images and EDX Results of 430-Ti6Al4V Welded Samples

Upon examining the SEM images of the 304 and Ti6Al4V alloys, it was observed that the weld region

formed around the drilled pin hole. The welding process was carried out uniformly across the cross-section, and the interfacial thickness was measured to be approximately 30 microns (Figure 9).

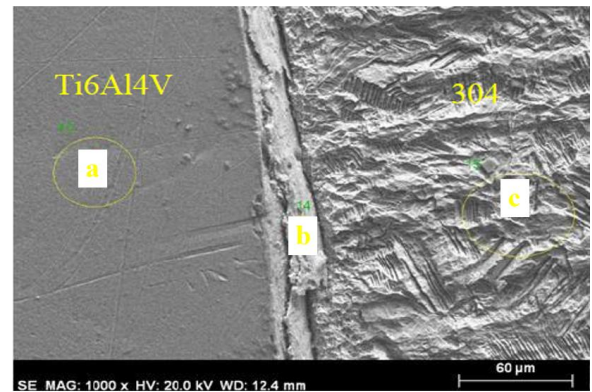


Figure 9. SEM Images of 304-Ti6Al4V Welded Samples

4. CONCLUSION

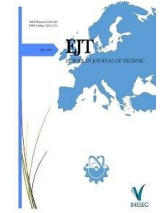
The results obtained from friction welding processes conducted using a Cu interlayer in various metal alloys have been examined in detail. The findings of the research are summarized below:

- In both macro and microstructural evaluations, it was observed that the interlayer formed uniformly across the weld surface in all joining operations without any discontinuities.
- The interlayer thicknesses of the welded samples were determined to be 5 μm for 316L, 15 μm for 316Ti, 200 μm for 310, 350 μm for 430, and 30 μm for 304.
- It was found that the tensile strengths of the materials were consistent with the tensile strength of the interlayer used. The highest elongation and tensile strength were measured at 5.5% elongation and 440 MPa for the 310 stainless steel-Ti6Al4V alloy pair.
- In the microhardness analyses, no significant change in hardness values was observed in the Ti6Al4V portion. This can be attributed to the limited heat input into the material due to the neck formation occurring on the titanium side, which prevented a temperature-dependent reduction in hardness values. Additionally, microstructural changes in the heat-affected zone and the stability of the material's crystal structure may have contributed to the preservation of hardness by limiting the effects of high temperatures. These mechanisms play a crucial role in explaining the relationship between heat input and hardness.

REFERENCES

- [1] Çiğdem, M., 2006. Manufacturing Methods, Çağlayan Publishing House, Istanbul, pp. 161-207.
- [2] Kırık I., Ozdemir N., Sarsılmaz F., 2012. Microstructure and Mechanical Behavior of Friction Welded AISI 2205/AISI 1040 Steel Joints. *Materials Testing*, 54: 683-687.
- [3] Lucas W., 1971. Process Parameters and Friction Welds. *Met. Cons. and British Welding Journal*, 71: 293-297.
- [4] Çalgülü U., Orhan A., Gür A.K., 2007. The Effect of Environmental Speed on Microstructural Properties in AISI 420/AISI 1010 Steel Couples Joined by Friction Welding Method. *Firat University Journal of Science and Engineering*, 19: 583-592.
- [5] Kaluç E., 2004. *Welding Technology Handbook*. MMO Publications, Ankara, pp. 356-358.
- [6] Islak, S., Houssain, H., Emin, N., Yazar, H., Danacı, H.C., & Koç, V., 2024. Microstructural, mechanical, and biocompatibility properties of Ti-Cu/B4C composites for biomedical applications. *Materials Chemistry and Physics*, 319, 129417.
- [7] Abd-Elaziem, W., Darwish, M. A., Hamada, A., & Daoush, W. M., 2024. Titanium-Based alloys and composites for orthopedic implants applications: A comprehensive review. *Materials & Design*, 112850.
- [8] Köse, C., & Karaca, E., 2017. Robotic Nd:YAG Fiber Laser Welding of Ti-6Al-4V Alloy, *Metals*, Vol: 7, pp: 1-11.
- [9] Kahraman, N., 2007. The Influence of Welding Parameters on the Joint Strength of Resistance Spot-Welded Titanium Sheets. *Mater.Des.*, Vol: 28, pp: 420-427.
- [10] Çalgülü, U., 2016. The Weldability of Ti6Al4V Alloy Using Silver Interlayer via Diffusion Welding, *Dicle University Engineering Journal*, Vol: 7, pp: 577-586.
- [11] Yıldız, A., Kaya, Y., & Kahraman, N., 2016. Joint Properties and Microstructure of Diffusion-Bonded Grade 2 Titanium to AISI 430 Ferritic Stainless Steel Using Pure Ni Interlayer, *Int J Adv Manuf Technol.*, Vol: 86, pp: 1287-1298.
- [12] Dikbaş, H., & Katı, N., 2015. The Investigations of the Weldability of Ti6Al4V Alloy at 1800W Welding Power in PTA Welding, *Dicle University Faculty of Engineering, Engineering Journal*, Vol: 6, pp: 19-30.
- [13] Smith, J., 2022. Corrosion Resistance of Austenitic Stainless Steels. *Journal of Material Science*, 58(3), 789-803.
- [14] Jones, M., Williams, A., & Chen, L., 2021. High-Temperature Performance of Stainless Steels: An Overview. *Materials Performance*, 60(7), 112-123.
- [15] Brown, T., & Taylor, R., 2020. The Versatility of 304 Stainless Steel in Various Industrial Applications. *Engineering Materials*, 47(5), 45-56.
- [16] Ünal, E., 2003. Investigating the Fatigue Strength of Friction Welded AISI 4340 Steel and Stainless Steels, F.Ü. Graduate Thesis, Elazığ.
- [17] Ting, W. A. N. G., Zhang, B. G., Chen, G. Q., Feng, J. C., & Qi, T. A. N. G., 2010. Electron Beam Welding of Ti-15-3 Titanium Alloy to 304 Stainless Steel with Copper Interlayer Sheet. *Transactions of Nonferrous Metals Society of China*, 20(10), 1829-1834.
- [18] Turner, R., Gebelin, J.C., Ward, R.M., Reed, R.C., 2011. Linear Friction Welding of Ti-6Al-4V: Modeling and Validation. *Acta Materialia*, 59, pp: 3792-3803.
- [19] Kumar, M.V., Balasubramanian, V., 2013. Microstructure and Tensile Properties of Friction Welded SUS 304HCu Austenitic Stainless Steel Tubes. *International Journal of Pressure Vessels and Piping*, 113, pp: 25-31.
- [20] Çelik, E., Tunç, B., 2024. The Role of Cu and Ni Interlayers in the Friction Welding of Ti6Al4V-Inconel 600 Materials. *Munzur 6th International Applied Sciences Congress, Tunceli*, pp: 226-236.
- [21] Çelik, E., Tunç, B., 2024. Effect of Different Interlayers (Cu, Ni, and MX-1480) on the Friction Welding of Ti6Al4V Alloy and AISI 316 Steel. *Al Farabi 12th International Scientific Research and Innovation Congress, Kazakhstan*, pp: 664-675.
- [22] Batı, S., Kılıç, M., Kırık, İ. 2016. Friction Welding of Dissimilar AISI 304 And AISI 8640 Steels. *European Journal of Technic*, Vol: 6, pp: 79-86.

Ertuğrul Çelik obtained BSc in the Metal Teaching Department, Technical Education Faculty Firat University in 2003. He received the BSc., and MSc. diploma in this field from the Firat University in 2006 and 2009 respectively, and PhD degrees. In 2009 he joined the Faculty of Mechanical Engineering, Istanbul Technical University as assistant professor, He received the title of associate professor in 2018 and still works as an academician at Munzur University.



Research Article

Sentiment Analysis in Turkish Using Language Models: A Comparative Study

Mert Incidelen^{1*}, Murat Aydoğan²¹Firat University, Artificial Intelligence and Data Engineering Department, Elazig, Turkey. (e-mail: mincidelen@firat.edu.tr).²Firat University, Software Engineering Department, Elazig, Turkey. (e-mail: m.aydogan@firat.edu.tr).

ARTICLE INFO

Received: Jun., 23. 2025

Revised: Jun., 8. 2025

Accepted: Nov, 27. 2024

Keywords:

Turkish Sentiment Analysis
Language Models (LMs)
Natural Language Processing (NLP)

Corresponding author: *Mert Incidelen*

ISSN: 2536-5010 / e-ISSN: 2536-5134

DOI: <https://doi.org/10.36222/ejt.1592448>

ABSTRACT

Sentiment analysis is a natural language processing (NLP) task that aims to automatically identify positive, negative and neutral emotions in texts. Agglutinative languages such as Turkish pose challenges for sentiment analysis due to their complex morphological structure. Traditional methods are inadequate for detecting sentiment in texts. Language models (LMs), on the other hand, achieve successful results in sentiment analysis as well as in many other NLP tasks thanks to their ability to learn context and structural features of the language. In this study, XLM-RoBERTa, mBERT, BERTurk 32k, BERTurk 128k, ELECTRA Turkish Small and ELECTRA Turkish Base models were fine-tuned using the Turkish Sentiment Analysis – Version 1 (TRSAv1) dataset and the performances of the models were compared. The dataset consists of 150,000 texts containing user comments on e-commerce platforms. The classes have a balanced distribution for positive, negative and neutral classes. The fine-tuned models are evaluated using the test set with metrics such as accuracy, precision, recall and F1 score. The findings show that models customized for the Turkish language exhibit better performance in emotion detection compared to multilingual models. The BERTurk 32k model achieved strong results with an accuracy of 83.69% and an F1 score of 83.65%, while the BERTurk 128k model followed closely with an accuracy of 83.68% and an F1 score of 83.66%. On the other hand, the XLM-RoBERTa model, a multilingual model, delivered competitive performance with an accuracy of 83.27% and an F1 score of 83.22%.

1. INTRODUCTION

In recent years, with the rise of internet usage, there has been a significant increase in text data [1]. A significant portion of this data consists of social media posts, customer comments on e-commerce sites, news sites, and content on similar sources. The need to interpret and analyze such a large amount of text data has increased the importance of natural language processing (NLP) techniques and the interest in this field. Today, social media platforms are commonly used to share personal thoughts and feelings, while e-commerce sites allow customers to express product-related experiences [2,3]. Analysis of data on these platforms has the potential to provide valuable insights into understanding the needs of individuals and societies, as well as predicting future trends. Sentiment analysis, an NLP task that focuses on detecting positive, negative, and neutral emotions in texts, is a crucial area of research in this context. Sentiment analysis is widely accepted as an effective method for addressing important issues, such as determining marketing strategies and making strategic decisions, by governments. In recent years, advancements in sentiment analysis methods have significantly increased interest in this field [4,5].

Before language models (LMs), sentiment analysis methods were divided into machine learning and lexical-based approaches. Machine learning-based approaches consist of various techniques such as Naive Bayes, Support Vector Machines (SVM), and Decision Trees. In these methods, machine learning algorithms are trained on a given labeled dataset and perform classification on texts [6]. Lexical-based methods, on the other hand, analyze the emotional words in the text and assign scores. These approaches use a pre-created dictionary to determine whether the words in the text contain emotions. Thus, a sentiment score is calculated according to the number of words [7]. Ahmad et al. [8] used the SVM algorithm for sentiment analysis with tweets and found that the performance varies depending on the characteristics of the dataset, and it is especially successful in neutral sentiment classification. Dhaoui et al. [9] compared the performance of lexical-based and machine learning-based approaches using social media comments. They observed that combining both methods improved the performance in sentiment analysis. Onan [10] performed sentiment analysis on Turkish tweets using Naive Bayes, SVM, and Logistic Regression methods. In the study, it was revealed that Naive Bayes method gave more successful results than other machine learning approaches.

Traditional approaches are limited in terms of context understanding and vocabulary, as they cannot go beyond the words in the predefined list. Machine learning and lexical based methods may exhibit limited performance depending on the size and diversity of the data. The emergence of LMs with the introduction of the Transformer architecture has led to significant improvements for NLP tasks. LMs can learn the context and relationships between words in texts thanks to the large corpora and self-attention mechanism used during their pre-training [11]. This contextual information enables the accurate analysis of sentence structure. The representations learned by the models can be fine-tuned for development purposes for specific domains and tasks. Thus, LMs can be adapted for tasks in various domains. These pre-trained models have been successfully applied to a wide range of NLP tasks such as text classification [12], machine translation [13], text summarization [14] and question-answer systems [15]. Unlike traditional methods, LMs have the potential to exhibit high performance with fine-tuning, even with imbalanced or complex datasets. This is particularly advantageous for low-resource languages. The contextual capabilities of LMs increase their performance in NLP tasks. Tan et al. [16] proposed a model that combines Transformer architecture with recurrent neural network architecture for sentiment analysis. This model has a hybrid structure with Robustly Optimized Bidirectional Encoder Representations from Transformers Pretraining Approach (RoBERTa) and Long Short-Term Memory (LSTM) approaches that have Bidirectional Encoder Representations from Transformers (BERT) structure. The proposed approach exhibited superior performance on IMDb, Twitter US Airline Sentiment and Sentiment140 datasets by combining the strong contextual ability of RoBERTa with the ability of LSTM to capture long dependencies. Arroni et al. [17] developed a simple model that uses the Transformer architecture's self-attention mechanism to analyze the sentiment of tweets about hotels. The model aims to classify tweets about hotels according to their sentiments. The study revealed that Transformer-based LMs are more effective than traditional methods. Khan et al. [18] fine-tuned the Multilingual BERT (mBERT) model for Urdu, a low-resource language, by comparing traditional methods with deep learning methods. The findings from the study revealed that the contextual capabilities of the BERT model outperformed other traditional methods. mBERT stood out as an effective model, especially for low-resource languages. Yürütücü and Demir [19] performed sentiment analysis using tweets about COVID-19. In the study, LMs and Naive Bayes method were compared for sentiment analysis. Higher accuracy sentiment detection was achieved with the BERT-based model compared to the Naive Bayes method. The results of the study showed that the BERT-based model performed successfully in capturing contextual information compared to traditional methods. Köksal and Özgür [20] created an original dataset consisting of tweets for Turkish sentiment analysis. Using this dataset, BERTurk, mBERT and XLM-RoBERTa models were fine-tuned, and the performances of the models were compared. The best performance among the models was obtained with BERTurk.

The increasing importance of NLP tasks and sentiment analysis has necessitated the development of the capabilities of LMs and the evaluation of their performance. The success of LMs in NLP tasks and sentiment analysis varies depending on many factors. These factors include the structural complexity

of the model used, the size and quality of the corpora used in pre-training, grammatical features, and syntactic structure. There are challenges for NLP tasks and sentiment analysis in low-resource languages compared to models in resource-rich languages, such as English [21]. Turkish is also among the low-resource languages. The agglutinative structure of Turkish causes roots and suffixes to combine in different ways, providing a flexible structure. In particular, the fact that the subject and predicate can be in different places in the sentence makes the language complex in terms of syntax. Therefore, in the analysis of the performance of Turkish LMs, this unique structure of the language must be considered. Considering the agglutinative structure and contextual diversity of Turkish, using models to grasp the structure of the language and to perform tasks such as sentiment analysis is a difficult but necessary goal. Models have the potential to exhibit superior performance even in a low-resource language such as Turkish, provided that the size and diversity of the corpora are provided in the pre-training. The performance of the models depends on their ability to grasp the structural and grammatical features of the language.

This study examines the performance of LMs for sentiment analysis. The limited contextual representation and inadequacy of traditional methods highlight the potential of LMs in this field. Evaluating the performance of these models in low-resource languages plays a critical role in the development of NLP studies in these languages. The aim of this study is to examine the performance of XLM-RoBERTa, mBERT, BERTurk 32k, BERTurk 128k, Efficiently Learning an Encoder that Classifies Token Replacements Accurately (ELECTRA) Turkish Small and ELECTRA Turkish Base models in the Turkish sentiment analysis task and to contribute to the development of methods that will provide higher performance for Turkish. In addition, it is aimed to obtain important findings on how to make fine-tuning processes more effective in accordance with the language structure of Turkish and to provide guidance on how these models can be adapted sensitively to the linguistic features of Turkish. The key contributions of this study are as follows:

- A comparative evaluation of LMs on Turkish sentiment analysis.
- Performance benchmarking on a balanced and representative Turkish dataset.
- Analysis of monolingual vs. multilingual model performance.
- Interpretation of model outputs across sentiment classes.
- Recommendations for fine-tuning strategies in morphologically rich, low-resource languages like Turkish.

This study consists of five main sections. In the first section, the background of the study, previous studies, motivation and objectives are presented. In the second section, details about the dataset used in the study and details of the LMs compared are given. In the third section, the experimental setup is explained, information about the fine-tuning process and the metrics used to evaluate the model performances are given. In the fourth section, the findings obtained from the experiments, the comparison of the models and the detailed evaluation of their performance are included. In the fifth section, a general evaluation of the study is made, the main findings are summarized and suggestions for future studies are presented.

2. MATERIAL AND METHOD

This section outlines the dataset and models utilized in the study. First, the TRSAv1 dataset is introduced in detail, followed by descriptions of the LMs and their fine-tuning procedures.

2.1. Dataset

Turkish Sentiment Analysis-Version 1 (TRSAv1) was used in this study [22]. The dataset serves as a comprehensive resource for evaluating sentiment analysis in Turkish. The TRSAv1 dataset contains 150,000 e-commerce reviews of products in the Turkish market from real users. These reviews consist of authentic comments expressing users' opinions about their shopping experiences and product quality. The comments in the dataset are categorized into three classes as positive, negative, and neutral. The number of comments in the classes shows a balanced distribution. Each class includes exactly 50,000 reviews, which were manually labeled using a custom-developed annotation tool. The dataset includes nearly 2 million words and more than 80,000 unique terms. Specifically, the positive class contains 717,674 words, the negative class 613,737, and the neutral class 583,541. This balanced dataset structure allows the models to measure their performance for different sentiment classes. The balanced distribution prevents models from overfitting or underfitting. Examples of the data in the classes in the dataset are given in Table 1.

TABLE I
EXAMPLES OF SENTIMENT CLASSES IN THE TRSAV1 DATASET

Sentiment Class	Example
Positive	“Saçlarda dökülmeyi belirgin derecede azaltıyor. Hem de yumuşacık yapıyor. Kendi yakın arkadaşlarıma dahi önerdiğim bir ürün”
Neutral	“Annem için aldım bakalım memnun kalacak mı boyutu normal”
Negative	“Çok kötü oyuncak gibi sakın almayın bir işe yaramaz”

A data preprocessing pipeline was applied to the dataset to ensure a cleaner input for the models and improve sentiment classification performance. In the data preprocessing phase, elements that could affect the accuracy of the models in the dataset were cleaned. Comments were cleaned by removing symbols such as emojis, hashtags, user mentions, and hyperlinks, which are known to introduce noise in sentiment prediction. As a result, the dataset was structured to be compatible with sentiment classification tasks.

2.2. Language Models

LMs are models trained with large text data that focus on understanding and reproducing the complex structure of human language in the field of NLP. These models learn the contextual structure of language in depth by using the self-attention mechanism in the Transformer architecture [23]. Thus, these models are versatile and applicable to a wide range of NLP

tasks. These models are typically trained in two stages. First, they undergo pretraining on large-scale corpora to learn general language representations. Then, they are fine-tuned on task-specific datasets to adapt to NLP applications and domains [24].

LMs can be pre-trained in multiple languages or customized in a single language. In this study, multilingual models, including Turkish and customized models for Turkish, were used. The models used in the study, their parameters and types are given in Table 2.

TABLE II
LANGUAGE MODELS

Model Name	Parameter Count	Language Type
<i>XLM-RoBERTa</i>	270M	Multilingual
<i>mBERT</i>	110M	Multilingual
<i>BERTurk 32k</i>	110M	Monolingual
<i>BERTurk 128k</i>	110M	Monolingual
<i>ELECTRA Turkish Small</i>	14M	Monolingual
<i>ELECTRA Turkish Base</i>	110M	Monolingual

XLM-RoBERTa: A multilingual model developed by Facebook AI and pre-trained with text data in more than 100 languages [25]. It is based on the RoBERTa architecture, an extended version of BERT [26]. XLM-Roberta's multilingual structure, including Turkish, provides successful results for different NLP tasks in different languages. In this study, this multilingual model is fine-tuned for Turkish sentiment analysis and its performance is analyzed.

mBERT: mBERT is a multilingual model based on the BERT architecture. The BERT model is based on Masked Language Modeling and Next Sentence Prediction techniques [24]. The multilingual version developed by Google can be widely used in text classification, sentiment analysis and other NLP tasks in different languages. In the pre-training process of the model, it was trained with text data in 104 different languages, including Turkish. mBERT's multilingual structure, including Turkish, allows it to be used in Turkish NLP tasks.

BERTurk: BERTurk is a BERT-based model trained on Turkish corpora, including news articles, Wikipedia, and OSCAR datasets. The BERTurk model has been specially developed for high performance on Turkish language tasks. The model is sensitive to the linguistic features and semantic details of Turkish. There are several versions of the BERTurk model with different vocabularies [27]. The 32k and 128k case versions of the BERTurk model, which have shown successful results in Turkish text-based tasks, are used in this study for fine-tuning the sentiment analysis task.

ELECTRA Turkish: ELECTRA Turkish is a customized version of the ELECTRA base model for Turkish. This model has been pre-trained with large Turkish texts and has a good command of the general structure of the Turkish language. ELECTRA is based on the Transformer architecture and uses the Replaced Token Detection technique. This method offers a pre-training process with a different approach than the masked

language model [28]. The ELECTRA model adapted for Turkish has the potential to exhibit high performance in Turkish NLP tasks. This model was fine-tuned for the sentiment analysis task in this study.

3. EXPERIMENTAL SETUP

In this section, the fine-tuning stage and evaluation metrics for the experimental setup of the study are explained. LMs pre-trained on large corpora were fine-tuned with the TRSAv1 dataset for sentiment analysis, and the results were evaluated. Figure 1 shows the pre-training, fine-tuning, and evaluation processes of the LMs.

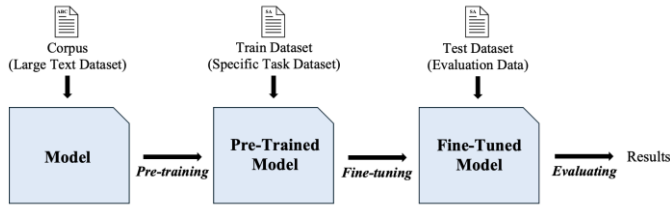


Figure 1. The Process of Pre-training, Fine-tuning, and Evaluation of LMs

3.1. Fine-Tuning

XLM-RoBERTa, mBERT, BERTurk 32k, BERTurk 128k, ELECTRA Turkish Small and ELECTRA Turkish Base models were fine-tuned with TRSAv1 dataset for Turkish sentiment analysis task. Fine-tuning is the process of customizing pre-trained models for specific NLP tasks. 80% of the dataset was allocated for training and 20% for testing. During data splitting, balanced representation of all sentiment classes was ensured to avoid class imbalance issues. Identical hyperparameter values were applied during fine-tuning to ensure fair comparison across models. The fine-tuning parameters, including the number of epochs, learning rate, and batch size, are presented in Table 3.

TABLE III
HYPERPARAMETER SETTINGS FOR FINE-TUNING

Hyperparameter	Assigned Value
Epoch	3
Batch Size	32
Learning Rate	3e-5

The fine-tuning of the models was conducted utilizing the Hugging Face Transformers library, a widely recognized toolset for NLP tasks, implemented in Python. An NVIDIA A100 graphics processing unit, with its high memory bandwidth and computational power, was utilized to accelerate the fine-tuning process. After the models were fine-tuned, their overall and class-based performances were evaluated with various metrics using the test dataset.

3.2. Evaluation Metrics

The commonly used metrics of accuracy, precision, recall and F1 score are used to evaluate fine-tuned models for sentiment analysis tasks. These metrics provide the opportunity to evaluate different performance aspects of the model in detail for each class in a classification problem. Thus, the

performance of the model for the problem can be analyzed in depth.

Accuracy: The ratio of samples correctly classified by the model to the total number of samples. The formula for the Accuracy metric is given in Equation 1.

$$Accuracy = \frac{TP + TN}{TP + TN + FP + FN} \quad (1)$$

Precision: The ratio of instances that the model correctly classifies as positive to the total number of instances that the model correctly classifies as positive. The formula for the metric is given in Equation 2.

$$Precision = \frac{TP}{TP + FP} \quad (2)$$

Recall: The ratio of samples correctly classified as positive by the model to the total number of true positive samples. The formula for the Recall metric is given in Equation 3.

$$Recall = \frac{TP}{TP + FN} \quad (3)$$

F1 Score: It is expressed as the harmonic mean of Precision and Recall metrics. Its formula is given in Equation 4.

$$F1\ Score = 2 \times \frac{Precision \times Recall}{Precision + Recall} \quad (4)$$

4. RESULTS and DISCUSSION

In this study, we comprehensively evaluate and compare the performance of fine-tuned LMs on a Turkish sentiment analysis task. This evaluation, which includes multilingual models designed in accordance with the linguistic features of Turkish, provides important insights into which model may be more effective in NLP tasks such as sentiment analysis. Table 4 shows the performance of the fine-tuned models in sentiment analysis.

TABLE IV
PERFORMANCE METRICS OF FINE-TUNED MODELS FOR TURKISH SENTIMENT ANALYSIS

Model	Accuracy (%)	Precision (%)	Recall (%)	F1 Score (%)
XLM-RoBERTa	83.27	83.30	83.27	83.22
mBERT	81.86	82.00	81.86	81.89
BERTurk 32k	83.69	83.68	83.69	83.65
BERTurk 128k	83.68	83.69	83.68	83.66
ELECTRA Turkish Small	81.84	81.87	81.84	81.80
ELECTRA Turkish Base	83.64	83.64	83.64	83.58

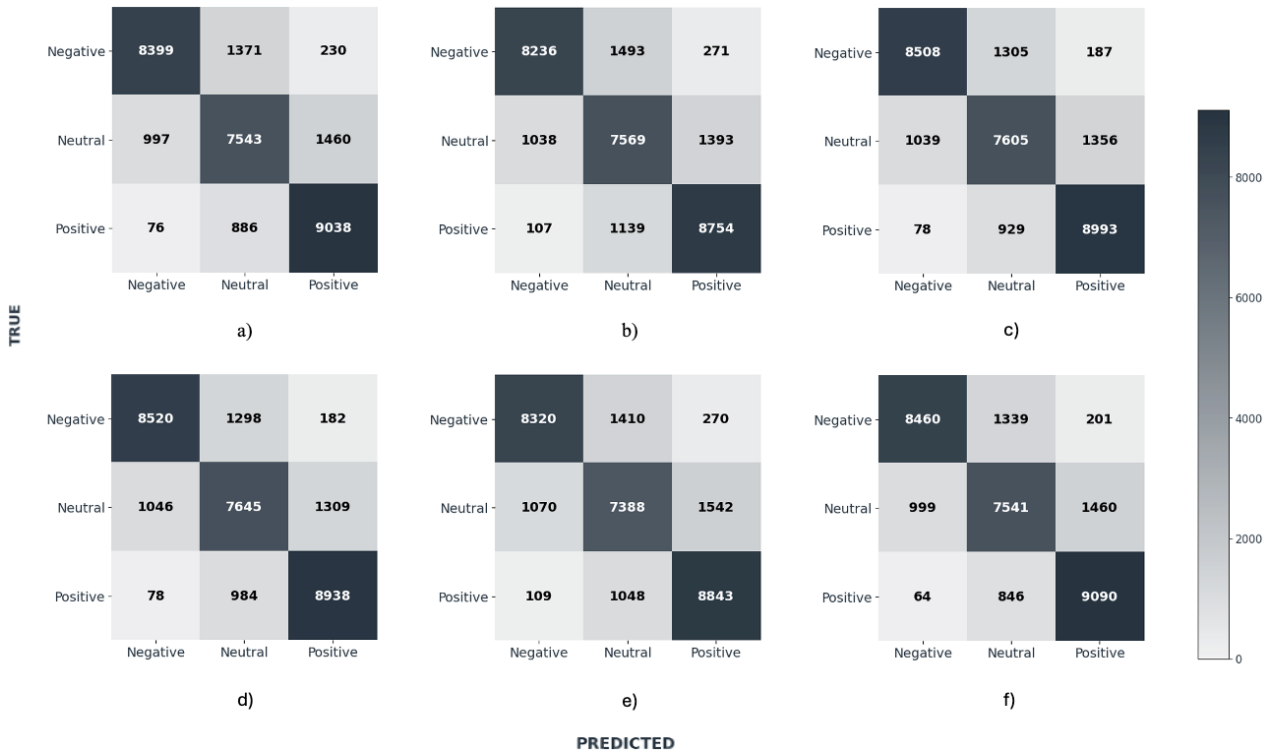


Figure 2. Confusion Matrices of Fine-Tuned Models: **a)** XLM-RoBERTa, **b)** mBERT, **c)** BERTurk 32k, **d)** BERTurk 128k, **e)** ELECTRA Turkish Small, **f)** ELECTRA Turkish Base

Among the models evaluated for Turkish sentiment analysis, BERTurk models were the most effective models. The BERTurk 32k model achieved an accuracy of 83.69% and an F1 score of 83.65%. Similarly, the BERTurk 128k model followed closely, with 83.68% accuracy and an F1 score of 83.66%. Pre-training on Turkish-specific data, which enables the models to effectively grasp the agglutinative and morphological nuances of the language, seems to be effective in Turkish NLP tasks. The ELECTRA Turkish Base model also performed commendably with an accuracy of 83.64% and an F1 score of 83.58%. These results demonstrate the robustness of monolingual models trained on Turkish data. However, the ELECTRA Turkish Small model with only 14 million parameters struggled to capture the rich contextual information of Turkish. Its lower performance with 81.84% accuracy and 81.80% F1 score can be attributed to its limited capacity to learn from data. Therefore, the model is less suitable for tasks involving complex language structures. The importance of model size and pre-training in achieving high performance in morphologically rich languages such as Turkish emerges.

Among the multilingual models, XLM-RoBERTa showed strong results with an accuracy of 83.27% and an F1 score of 83.22%. It performed particularly well in the positive and negative sentiment classes, demonstrating its ability to understand Turkish sentiment in these categories. However, as can be seen in Table 5, its performance in the neutral class was significantly weaker compared to the monolingual BERTurk model. This limitation suggests that despite its multilingual capabilities, XLM-RoBERTa struggles to fully adapt to Turkish-specific grammatical structures and nuanced expression of neutral sentiments. On the other hand, mBERT performed less effectively than the other models, achieving an accuracy of 81.86% and an F1 score of 81.89%. This suggests that its generalized multilingual architecture does not fully address the unique linguistic features of Turkish. Its lower

performance compared to monolingual models suggests that pre-trained LMs, especially for Turkish, have an advantage in understanding the articulatory and context-sensitive nature of the language. Table 5 shows the results of the fine-tuned models for different sentiment classes according to the precision, recall and F1 score metrics.

TABLE V
PERFORMANCE OF LMS ACROSS SENTIMENT CLASSES

Model	Class	Precision (%)	Recall (%)	F1 Score (%)
<i>XLM-RoBERTa</i>	Negative	88.67	83.99	86.27
	Neutral	76.97	75.43	76.19
	Positive	84.25	90.38	87.21
<i>mBERT</i>	Negative	87.79	82.36	84.99
	Neutral	74.20	75.69	74.94
	Positive	84.03	87.54	85.75
<i>BERTurk 32k</i>	Negative	88.39	85.08	86.71
	Neutral	77.29	76.05	76.67
	Positive	85.35	89.93	87.58
<i>BERTurk 128k</i>	Negative	88.35	85.20	86.74
	Neutral	77.01	76.45	76.73
	Positive	85.70	89.38	87.50
<i>ELECTRA Turkish Small</i>	Negative	87.59	83.20	85.34
	Neutral	75.04	73.88	74.45
	Positive	82.99	88.43	85.63
<i>ELECTRA Turkish Base</i>	Negative	88.84	84.60	86.67
	Neutral	77.53	75.41	76.46
	Positive	84.55	90.90	87.61

As seen in Figure 2, the confusion matrices show a high number of misclassifications in the neutral sentiment class, especially among multilingual models. A significant number of neutral examples were incorrectly predicted as positive. This indicates that the models have difficulty distinguishing subtle contextual cues that separate neutral from positive sentiment. Correct classification of neutral expressions in the Turkish sentiment analysis task is one of the biggest challenges. Neutral expressions can be perceived as positive or negative depending on the context, which can affect the classification performance of LMs. BERTurk models performed better in the neutral class compared to other models. This suggests that these monolingual models may have better learned the contextual diversity and grammatical features of Turkish. The other multilingual models performed inconsistently in the neutral class. This shows that multilingual models are generally less sensitive to context in languages with a suffixal structure such as Turkish. The suffixal structure of Turkish, the fact that word roots combine with different affixes to acquire new meanings, and the flexibility of sentence structure pose a significant challenge for LMs. In this context, the monolingual models analyzed are more successful than multilingual models in learning this complex structure. BERTurk models clearly show the advantage of being specially trained with Turkish data.

5. CONCLUSION

This study investigates the performance of LMs on Turkish sentiment analysis tasks. Different variations of the BERTurk and ELECTRA Turkish models, as well as the mBERT and XLM-RoBERTa multilingual models, were compared for the sentiment analysis task. The findings revealed that Turkish customized models such as BERTurk 32k, BERTurk 128k and ELECTRA Turkish Base were significantly more effective at capturing Turkish linguistic context. BERTurk variations have proven to be a strong choice for Turkish sentiment analysis tasks due to their consistent performance. While sentiment analysis is challenging with traditional methods and multilingual models due to the complex linguistic structure of Turkish, monolingual models managed to overcome these challenges and achieved high accuracy and F1 scores. These findings demonstrate the importance of models trained on language-specific data. The TRSAv1 dataset, featuring a balanced class structure and real user comments, was used in this study. These characteristics of the dataset enabled more accurate evaluation of the models. In this context, BERTurk models demonstrated better performance in the neutral class compared to other models. Although the multilingual models showed acceptable performance for the affirmative and negative classes, they were insufficient in capturing the context for the neutral class. This suggests that monolingual models may be more suitable for low-resource and agglutinative languages such as Turkish. By contrast, ELECTRA Turkish Small, with fewer parameters, was inadequate for handling the complex linguistic features of Turkish due to its limited capacity. Nevertheless, the results indicate that this model can be a viable option for non-critical applications due to its low hardware requirements and high speed. Conversely, the ELECTRA Turkish Base model performs close to the BERTurk models and has considerable success for Turkish sentiment analysis.

This study highlights the potential and limitations of LMs for low-resource and structurally ambiguous languages such as

Turkish. The success of models such as BERTurk has demonstrated the power of monolingual models. The success of these Turkish-specific models demonstrates their capabilities in NLP tasks such as language understanding and Turkish sentiment analysis. Future studies can improve model performance in Turkish and similar low-resource languages by investigating the effect of larger and more diverse datasets such as domain-specific texts. In this context, the findings of this study provide important findings and a roadmap for Turkish NLP tasks.

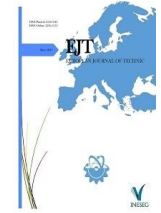
REFERENCES

- [1] I. Yaqoob, I. A. T. Hashem, A. Gani, S. Mokhtar, E. Ahmed, N. B. Anuar, and A. V. Vasilakos, "Big data: From beginning to future," *Int. J. Inf. Manage.*, vol. 36, no. 6, pp. 1231–1247, 2016.
- [2] S. Mittal, A. Goel, and R. Jain, "Sentiment analysis of E-commerce and social networking sites," in *Proc. 3rd Int. Conf. Comput. Sustainable Global Develop. (INDIACom)*, 2016, pp. 2300–2305.
- [3] M. Rodríguez-Ibáñez, A. Casáñez-Ventura, F. Castejón-Mateos, and P.-M. Cuenca-Jiménez, "A review on sentiment analysis from social media platforms," *Expert Syst. Appl.*, vol. 223, p. 119862, 2023.
- [4] M. Marong, N. K. Batcha, and R. Mafas, "Sentiment analysis in e-commerce: A review on the techniques and algorithms," *J. Appl. Technol. Innov.*, vol. 4, no. 1, p. 6, 2020.
- [5] M. Wankhade, A. C. S. Rao, and C. Kulkarni, "A survey on sentiment analysis methods, applications, and challenges," *Artif. Intell. Rev.*, vol. 55, no. 7, pp. 5731–5780, 2022.
- [6] A. P. Jain and P. Dandannavar, "Application of machine learning techniques to sentiment analysis," in *Proc. 2nd Int. Conf. Appl. Theor. Comput. Commun. Technol. (iCATccT)*, 2016, pp. 628–632.
- [7] C. S. G. Khoo and S. B. Johnkhan, "Lexicon-based sentiment analysis: Comparative evaluation of six sentiment lexicons," *J. Inf. Sci.*, vol. 44, no. 4, pp. 491–511, 2018.
- [8] M. Ahmad, S. Aftab, and I. Ali, "Sentiment analysis of tweets using SVM," *Int. J. Comput. Appl.*, vol. 177, no. 5, pp. 25–29, 2017.
- [9] C. Dhaoui, C. M. Webster, and L. P. Tan, "Social media sentiment analysis: Lexicon versus machine learning," *J. Consum. Market.*, vol. 34, no. 6, pp. 480–488, 2017.
- [10] A. Onan, "Sentiment analysis on Twitter messages based on machine learning methods," *Yönetim Bilişim Sistemleri Dergisi*, vol. 3, no. 2, pp. 1–14, 2017.
- [11] T. Wolf, L. Debut, V. Sanh, J. Chaumond, C. Delangue, A. Moi, P. Cistac, T. Rault, R. Louf, M. Funtowicz, et al., "Transformers: State-of-the-art natural language processing," in *Proc. 2020 Conf. Empirical Methods Natural Lang. Process.: System Demonstrations*, 2020, pp. 38–45.
- [12] R. Qasim, W. H. Bangyal, M. A. Alqarni, and A. A. Almazroi, "A fine-tuned BERT-based transfer learning approach for text classification," *J. Healthcare Eng.*, vol. 2022, no. 1, p. 3498123, 2022.
- [13] X. Zhang, N. Rajabi, K. Duh, and P. Koehn, "Machine translation with large language models: Prompting, few-shot learning, and fine-tuning with QLoRA," in *Proc. Eighth Conf. Mach. Transl.*, 2023, pp. 468–481.
- [14] H. Chouikhi and M. Alsuhaibani, "Deep transformer language models for Arabic text summarization: A comparison study," *Appl. Sci.*, vol. 12, no. 23, p. 11944, 2022.
- [15] S. Butt, N. Ashraf, M. H. F. Siddiqui, G. Sidorov, and A. Gelbukh, "Transformer-based extractive social media question answering on TweetQA," *Computación y Sistemas*, vol. 25, no. 1, pp. 23–32, 2021.
- [16] K. L. Tan, C. P. Lee, K. S. M. Anbananthen, and K. M. Lim, "RoBERTa-LSTM: A hybrid model for sentiment analysis with transformer and recurrent neural network," *IEEE Access*, vol. 10, pp. 21517–21525, 2022.
- [17] S. Arroni, Y. Galán, X. M. Guzmán Guzmán, E. R. Núñez Valdéz, A. Gómez Gómez, et al., "Sentiment analysis and classification of hotel opinions in Twitter with the transformer architecture," *Int. J. Interact. Multimedia Artif. Intell.*, 2023.
- [18] L. Khan, A. Amjad, N. Ashraf, and H.-T. Chang, "Multi-class sentiment analysis of Urdu text using multilingual BERT," *Sci. Rep.*, vol. 12, no. 1, p. 5436, 2022.
- [19] Ö. Y. Yürüttücü and Ş. Demir, "Ön eğitilmiş dil modelleriyle duygu analizi," *İstanbul Sabahattin Zaim Üniversitesi Fen Bilimleri Enstitüsü Dergisi*, vol. 5, no. 1, pp. 46–53, 2023.

- [20] A. Köksal and A. Özgür, "Twitter dataset and evaluation of transformers for Turkish sentiment analysis," in Proc. 29th Signal Process. Commun. Appl. Conf. (SIU), 2021, pp. 1–4.
- [21] S. Joshi, M. S. Khan, A. Dafe, K. Singh, V. Zope, and T. Jhamtani, "Fine tuning LLMs for low resource languages," in Proc. 5th Int. Conf. Image Process. Capsule Netw. (ICIPCN), 2024, pp. 511–519.
- [22] M. Aydoğan and V. Kocaman, "TRSAv1: A new benchmark dataset for classifying user reviews on Turkish e-commerce websites," J. Inf. Sci., vol. 49, no. 6, pp. 1711–1725, 2023.
- [23] A. Vaswani, "Attention is all you need," Adv. Neural Inf. Process. Syst., 2017.
- [24] J. Devlin, "BERT: Pre-training of deep bidirectional transformers for language understanding," arXiv preprint arXiv:1810.04805, 2018.
- [25] A. Conneau, "Unsupervised cross-lingual representation learning at scale," arXiv preprint arXiv:1911.02116, 2019.
- [26] Y. Liu, "RoBERTa: A robustly optimized BERT pretraining approach," arXiv preprint arXiv:1907.11692, vol. 364, 2019.
- [27] S. Schweter, BERTurk - BERT models for Turkish, version 1.0.0, Zenodo, Apr. 2020. [Online]. Available: <https://doi.org/10.5281/zenodo.3770924>. DOI: 10.5281/zenodo.3770924.
- [28] K. Clark, "ELECTRA: Pre-training text encoders as discriminators rather than generators," arXiv preprint arXiv:2003.10555, 2020.

Mert Incidelen was born in Elazığ, Turkey, in 1997. He completed his Bachelor's degree in Department of Computer Engineering at Firat University in 2021. Currently, he is pursuing a Master's degree in Software Engineering at Firat University. He served as a Research Assistant in the Department of Computer Engineering at Iğdır University between 2023 and 2024. Presently, he is a Research Assistant at Firat University in the Department of Artificial Intelligence and Data Engineering. His research interests include Natural Language Processing and Artificial Intelligence.

Murat Aydoğan obtained his Bachelor's degree from the Computer Education Program in the Department of Electronics and Computer Education at Firat University in 2011. He earned his Master's degree in Software Engineering from Firat University in 2014 and completed his Ph.D. in Computer Engineering at İnönü University in 2019. Since 2020, he has been working as an Assistant Professor in the Department of Software Engineering at Firat University. His research interests include Natural Language Processing, Artificial Intelligence, and Data Mining.



Research Article

Design and Implementation of an Individual Shooting Simulation System and Software

Yilmaz Vedat¹

¹Institute of Forensic Sciences, Gendarmerie and Coast Guard Academy, Ankara, Türkiye (e-mail: vylmz26@gmail.com).

ARTICLE INFO

Received: Dec., 04. 2024

Revised: Jan., 04. 2025

Accepted: Jan., 04. 2025

Keywords:

Shooting training
Security Technologies
Simulation Software
Law Enforcement

Corresponding author: Vedat
Yilmaz

ISSN: 2536-5010 / e-ISSN: 2536-5134

DOI: <https://doi.org/10.36222/ejt.1596034>

ABSTRACT

In this study, a software solution for the development of the Individual Shooting Simulation System is introduced. Shooting training for military and law enforcement is critical to mission effectiveness and safety. However, traditional shooting methods have physical, financial and safety limitations. The developed software offers a cost-effective solution to the user, thanks to its portable capabilities and user-friendly interface. The system includes laser-based targeting, image processing applications and real-time feedback. Designed in Python, the software offers easy installation and use with portable hardware. Tests have shown that the system is successful in terms of accuracy (± 1 pixels), speed (under 1 second processing time) and flexibility. Users and instructors expressed their satisfaction with the performance and ease of use of the system. Additionally, the system offers an effective learning environment for both individual and group training. In the future, it is aimed to implement the system in a wider application area with improvements such as artificial intelligence-supported image processing and mobile device compatibility. This study provides a solution that contributes to making shooting training safe, effective and accessible.

1. INTRODUCTION

All elements of the Armed Forces and the Gendarmerie General Command, the Directorate of Security and the Coast Guard Command, consisting of law enforcement forces, are of critical importance for the protection of the national economy and public order [1].

While the armed forces undertake the task of protecting the country against threats that could harm its sovereignty and territorial integrity, it plays a strategic role as a deterrent against possible external threats and, when necessary, as a striking force. Law enforcement forces, on the other hand, carry out their duty to ensure public security by ensuring social order, protecting the rights and freedoms of citizens, and fighting against crime and criminals. The fact that the personnel working in these institutions is effectively trained and equipped is the most fundamental element for the institutions responsible for security to fully fulfill their duties. The personnel to work in these institutions are selected and they begin training on weapons and weapon use simultaneously with the start of their training activities.

Shooting training ensures that Military and Law Enforcement personnel acquire the skills and weapon

knowledge they need to use their duty weapons effectively and minimize the risks that may arise during use [2].

Shooting training of these personnel is a critical process to improve target accuracy, increase their ability to make quick decisions to neutralize the target by shooting it from the desired point, and reinforce their safe gun use skills. This process ensures the success of personal effectiveness and tactical field operations to destroy the target in any operation.

Traditional shooting training is a process that starts from the theory of basic gun use, continues with the introduction of weapons, and ends with the use of real bullets in the final stage. In this process, the safety rules against accidents and aiming principles for duty weapons are explained theoretically and they are informed before the actual shooting [3].

In this process, both physical conditions and ammunition costs prevent the trained personnel from providing sufficient practical training. Traditional training has many limitations, including security and shooting areas. Limitations such as preparing targets before shooting in open shooting areas or closed ranges, preparing physical security and protective measures for both the shooter and other observers, bringing and distributing ammunition also increase the duration of the training. Additionally, any carelessness during shooting may result in accidental injury or death [4].

Personnel who are not properly or sufficiently trained may cause an unexpected accident when using weapons or shooting to neutralize the target. This means the mission fails. For this reason, it is very important to properly and fully train military personnel authorized to use weapons and law enforcement personnel fighting crime and criminals.

Simulation-based shooting training systems are very flexible during training. By using these systems, ammunition and time are saved. In addition, the absence of ammunition increases the amount of shooting and allows the detection and analysis of the shooter's errors [5]. Simulations have evolved into a structure that is safer, faster and accessible to more people [6].

Simulation systems allow users to find more shooting opportunities, increase their aiming abilities, and be trained through realistic scenarios. It also ensures that security risks that may arise during real shooting are eliminated [7-9].

Shooting training through simulation attracts a lot of attention not only in military and law enforcement schools but also in the civilian field. As a result of this interest, many defense industry companies offer different software and systems to users to meet their needs. The developed systems are generally targeting military or law enforcement institution users. These systems aim to increase the success rate of users as well as increase their decision-making and scenario-based skills. For this reason, their costs are quite high. These types of systems, which are costly, are not preferred by individual users [8]. It is seen that studies on Shooting in the academic literature focus on virtual reality (VR) and augmented reality (AR) technologies. VR and AR technologies make shooting training more effective. [8,10]. In addition to the many benefits of virtual reality-based shooting simulations, their hardware requirements also require high costs.

The developed individual shooting simulation system software is designed to create an effective alternative simulation suitable for individual use apart from existing solutions and as a portable and cost-effective solution that will appeal to individual users. The developed software also allows effective personalization of shooting training. This article explains in detail the possibilities, capabilities and advantages of the developed individual shooting simulation system software.

2. MATERIALS AND METHODS

In this section, the components of the developed Individual Simulation System software and the working principles of the software are explained. In this context, the working logic of the developed software and the necessary hardware are specified step by step.

The system consists of the following basic components. The general view of the system is shown in Fig. 1.

Web Camera: Used to monitor the target and record images during shooting. Resolution and frame rate have been optimized to increase the accuracy of the system.

Computer: It is the basic hardware on which image processing algorithms are run and simulation results are analyzed.

Target Paper: Standard A4 size target papers were used to physically evaluate shooting hits and measure the performance of the system.

Laser: Two different lasers that can be mounted on the weapon or placed inside the barrel of the weapon are used. The

trigger mounted on the gun flashes momentarily due to the shock that occurs during shooting.

The laser bullet placed in the gun barrel flashes momentarily as a result of the completion of the electronic circuit after the gun needle touches the laser bullet during the trigger.

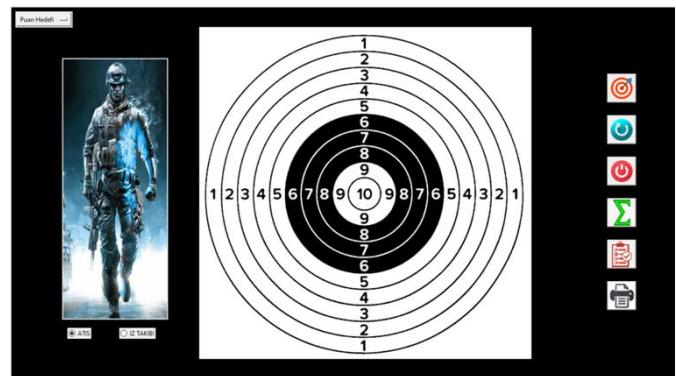


Figure 1. General view of the software

Simulation software: The software was written in Python software language using image processing algorithms and visualization interface. Python libraries used in the developed software are presented in Fig. 2.

```

1 from doctest import master
2 from multiprocessing import Process, Queue, Value
3 from datetime import datetime
4 from PIL import Image
5 import numpy as np
6 import cv2
7 import time
8 from pygame import mixer
9 from gui import GUI, DialogRecalib
10 from utils import *
11 import os
12 import sys
13 import tkinter as tk

```

Figure 2. Python Libraries Used in the Software

Individual shooting simulation system usage includes the following steps.

System Setup: The web camera is fixed facing the target paper and positioned at a certain distance. The camera is positioned to completely frame the target paper with a linear alignment. The computer is integrated with the system to process images from the webcam in real time. The developed software automatically takes action to ensure that the right camera takes the right image during startup, as shown in Fig. 3. The reason for this is that the image of the externally attached webcam is transferred to the system, not the existing camera of the computer.

```

pygame 1.9.6
Hello from the pygame community. https://www.pygame.org/contribute.html
Authorized system.
# Açılır menüyü oluştur {'name': 'Puan_Hedefi', 'img_path': 'target/data/Puan_Hedefi.jpg', 'contours_npy': 'target/data/
Puan_Hedefi.npy', 'center_coords': [575, 575], 'real_size': [200, 200]}
pygame 1.9.6
Hello from the pygame community. https://www.pygame.org/contribute.html
pygame 1.9.6
Hello from the pygame community. https://www.pygame.org/contribute.html
{'name': 'Puan_Hedefi', 'img_path': 'target/data/Puan_Hedefi.jpg', 'contours_npy': 'target/data/Puan_Hedefi.npy', 'cente
r_coords': [575, 575], 'real_size': [200, 200]}
Kamera 0 deniyor...
Resim kaydedildi.
4 / 13 inlier eşleşme bulundu
Kamera 0 için inlier sayısı: 4
Kamera 1 deniyor...
0 eşleşme bulundu, homografi tahmini için yeterli değil. Birim matris kullanılıyor.
Kamera 1 için inlier sayısı: 0.0
En iyi eşleşme için seçilen webcam: Kamera 0
affine sampling: 43 / 43

```

Figure 3. Camera selection and Sample Calculation

Image Processing: Image Acquisition, the webcam recorded high-resolution images of the target sheet after each shot. Pre-processing, the captured images were subjected to noise reduction and contrast enhancement processes. The image taken from the webcam is corrected by the software by following the correction steps. By correcting angular errors in the image taken on the webcam, the image is corrected to its actual size. In this way, it is sufficient for him to just see the target, without having to see the target directly in front of him. An image of scaling the image to its actual size is shown in Fig. 4.

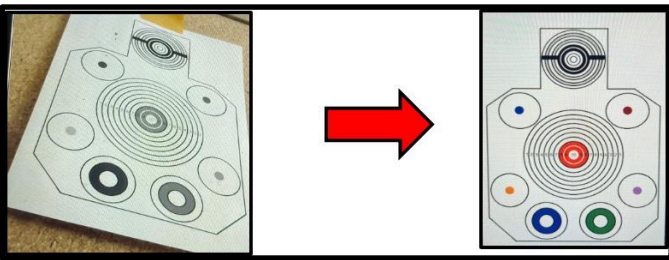


Figure 4. Scaling the image to actual size

Target Analysis: With the image processing algorithm, the position of the laser light on the target is calculated in pixels and its actual position on the aimed target is marked. Morphological operations and edge detection techniques have been used effectively in this process. Software Flow Diagram is presented in Fig. 5.

3. RESULTS

This chapter presents the findings from the implementation and testing of the Individual Shooting Simulation System software. The system was evaluated for its performance in image processing detection and analysis of shooting hits, as well as its general usability in simulating individual shooting applications.

Adding a system target; the desired target can be added to the system in A4 size. Before defining the target in the system, counter zones in the relevant areas of the target were selected and an npy. file was created for these regions.

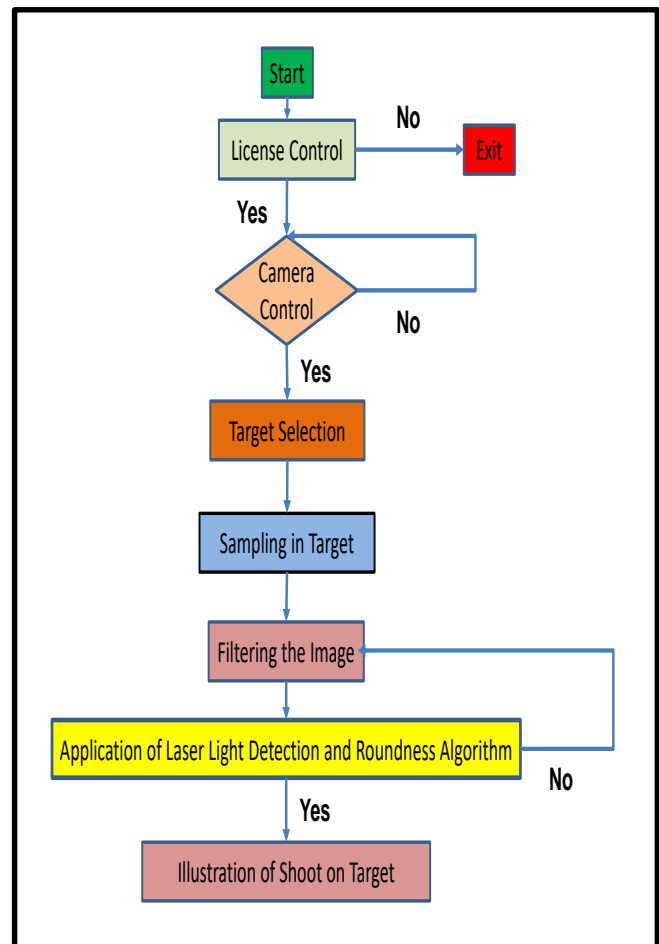


Figure 5. Software Flow Diagram

This created npy file is read from the target.json file, thus enabling the reading of descriptive information about the target after target selection from the software. The npy file created separately for each target has created target diversity and different evaluation opportunities. The codes of the target.json file, where attribute data and definitions for target selection are made, and the Target selection screen in the software interface are shown in Fig. 6.

The system was evaluated in terms of ease of use, installation and operating processes:

Positioning the camera and integrating it with the software was very simple. The automatic camera selection mechanism shown in Fig. 3 facilitated the installation process by ensuring that the correct external camera was used. The installation of the system (including turning on the computer and connecting the camera, attaching the target to the board and running the software) takes under 5 minutes.

The software enabled laser positions to be marked on the target image in real time. This feature allowed users to instantly evaluate their performance after each shot. Additionally, the system allows shooting as many times as desired without any limit. Additionally, the last shot is instantly shown in red and the other shots are shown in blue. Consecutive or serial shots are detected by the software in less than 1 second and displayed on the interface. In this way, the last shot fired can be quickly detected by the user.

```

1 {
2   "Puan_Hedefi" : {
3     "name" : "Puan_Hedefi",
4     "img_path" : "target/data/Puan_Hedefi.jpg",
5     "contours_npy" : "target/data/Puan_Hedefi.npy",
6     "center_coords" : [575, 575],
7     "real_size" : [200, 200]
8   },
9
10  },
11  "Atis_Taktik_Egitimi" : {
12    "name" : "Atis_Taktik_Egitimi",
13    "img_path" : "target/data/atis.png",
14    "contours_npy" : "target/data/atis.npy",
15    "center_coords" : [200, 282],
16    "real_size" : [210, 297]
17  },
18  "Rehine_Hedefi" : {
19    "name" : "rehine",
20    "img_path" : "target/data/rehine.jpg",
21    "contours_npy" : "target/data/rehine.npy",
22    "center_coords" : [308, 435],
23    "real_size" : [210, 297]
24  },
25  "Gogus_Hedefi" : {
26    "name" : "gogus_hedefi",
27    "img_path" : "target/data/gogus_hedefi.jpg",
28    "contours_npy" : "target/data/gogus_hedefi.npy",
29    "center_coords" : [400, 580],
30    "real_size" : [210, 297]
31  },
32  "Araba_Hedefi" : {
33    "name" : "araba_hedefi",
34    "img_path" : "target/data/ARABA1.jpg",
35    "contours_npy" : "target/data/ARABA1.npy",
36    "center_coords" : [462, 259],
37    "real_size" : [210, 297]
38  },
39  "Hata_Tespit_Hedefi" : {
40    "name" : "HATA_TESPIT_HEDEFI",
41    "img_path" : "target/data/hata_tespit.jpg",
42    "contours_npy" : "target/data/hata_tespit.npy",
43    "center_coords" : [640, 800],
44    "real_size" : [210, 297]
45  }
46 }
47

```

Figure 6. Software Flow Diagram

The Capabilities and Interface of the Developed Software are shown in Fig. 7.

- Portable and Quick Installation,
- Target Selection,
- Shooting or shooting path display option (Fig. 8),
- Software calibration according to shooting (Fig. 9),
- Display of shooting score, hit success and total score by the system (Fig. 10),
- Serial and rapid shot detection,
- Unlimited shooting opportunities,
- Hit detection from different angles up to 30 degrees,
- Reporting and shooting recording (Fig. 11),



Figure 7. The Capabilities and Interface of the Developed Software

The Individual Shooting Simulation System has been comprehensively evaluated based on different criteria. System performance was examined under the headings of accuracy, speed, flexibility and user satisfaction.

The Individual Shooting Simulation System has been comprehensively evaluated based on different criteria. System performance was examined under the headings of accuracy, speed, flexibility and user satisfaction.

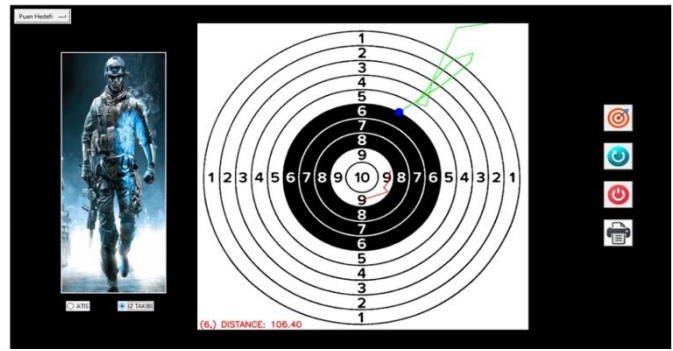


Figure 8. Shooting path display

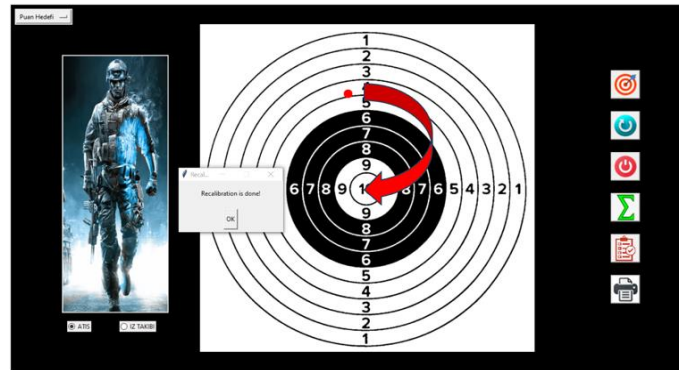


Figure 9. Software calibration according to shooting



Figure 10. Display of shooting score

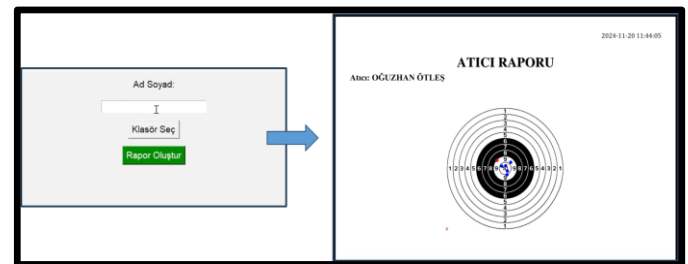


Figure 11. Reporting and shooting recording

The software showed high accuracy in detecting laser dots on the target paper. The main findings are:

The image processing algorithm detected laser points on the target consistently and with minimal error. Morphological operations and edge detection techniques enabled the laser hit points to be determined exactly and the error rate did not exceed the ± 1 pixel limit. Preprocessing steps effectively corrected angular distortions in the acquired images and ensured accurate mapping of laser points to coordinates on the

physical target. Scaling and alignment operations allowed accurate analysis regardless of camera angle differences, as shown in Fig. 4.

By optimizing the time from laser detection to result visualization, the system was able to process each shot in under 1 second. This speed has made training processes more efficient by allowing users to receive real-time feedback. The system was able to analyze consecutive shots with high processing speed and present the results to the user without any delay or data loss. The laser detection algorithm of the software worked successfully in trials conducted under different lighting conditions (low light, artificial lighting). Tests carried out especially in low light conditions have demonstrated the effectiveness of the software's image processing capabilities.

The system can detect the laser falling on the target paper. The software has been tested at distances ranging from 1 to 50 meters. At these distances, the accuracy of detection of laser points and their location on the target was preserved. It has been observed that the software will not be suitable for use in shots over 50 meters, as the appearance of the laser light on the target increases proportionally depending on the distance. If desired, the hit point can be marked by editing in the software, based on the pixel value of the center point, taking into account the size of the laser light. This means that the distance can be increased further. However, since the developed software in question was planned to be used in the classroom environment, such a need did not arise.

Instant visualization of firing points allowed users to quickly evaluate their performance. Users were able to effectively use this feedback in training improvement decisions. Users and Shooting Instructors stated that they were satisfied with the ease of installation of the system and the smoothness of the usage process. They also stated that real-time analysis and visualization features provide a significant advantage in shooting training. In the tests performed, the rate of cases in which the system could not recognize the laser points remained below 2%. These errors are generally seen in extremely bright environments or when the laser beam is directed to a point other than the target. Preprocessing steps successfully filtered out noise in the image, allowing laser points to be detected more clearly.

Individual Shooting Simulation System software has a structure that can meet the training and performance analysis needs of both amateur and professional users. The practical application potential of the system was examined under the headings of skill assessment and training flexibility. The software analyzed the position of the laser points on the target during shooting with millimetric precision. This analysis revealed the shooter's aiming accuracy and consistency. Users were able to use this data as a feedback tool to improve their shooting techniques.

The system provided the user with an overall performance evaluation after multiple shots. In the software, the total shooting score can be automatically displayed along with the shot-by-shot visual.

The system has an easily portable hardware structure. Essential components like the webcam, computer, and target paper can each be carried anywhere with a bag. The system becomes ready for use by running an exe file without requiring any special technical knowledge. The software automatically selects the camera and corrects the image of the target in the camera image, making it easier for the user to use it without any action. The system instantly displays users' shooting results

on the screen. This feature makes the education process more efficient and interactive. The software's reporting and recording feature allows the shooter's development and shooting success to be tracked over time. The results of the shooting studies conducted on different dates enable the analysis of the development of the users and the success of the training. The software is a suitable educational tool for students in military and law enforcement schools as well as professionals. While students use the system to learn basic shooting techniques, professionals use the software to maintain their performance and renew their training.

4. DISCUSSION

The developed Individual Shooting Simulation System software offers an innovative approach with its portable and cost-effective structure in both individual training. In this section, evaluations were made on the developed simulation software and its usage concept, its advantages, limitations, and the development potential of the software in the future.

The system offers its users various advantages during training:

- The system marks the position of the exact middle point of the laser circle on the target with high accuracy of ± 1 pixel. Additionally, the software detected laser light under different lighting conditions and distances, providing consistent results.
- The system has a user-friendly structure with its simple interface and portable structure. Automatic correction of the target image obtained from the camera by the software and detection of the correct camera provide convenience to the users.
- Displaying the result of the shot on the screen at the time of shooting provides a dynamic structure to the training. This feature allows shooters to make instant improvements with repeated shots.
- The system, which offers users long-term performance monitoring, has enabled them to plan their training processes more consciously. Visualization and reporting of data made it possible to use the system as a guide for individual development.

Although the system works successfully, certain limitations have been observed:

- While the system showed high performance in low light conditions, it had difficulty detecting laser light in extremely bright environments. This may require taking additional precautions to reduce the effect of intense light sources such as sunlight in outdoor use.
- Although small errors in camera alignment were tolerated thanks to image correction algorithms, alignment errors above a certain limit negatively affected system performance.
- The system requires mid-level computer hardware and a mid-level webcam to run the image processing algorithms. Also, there is laser addiction.

This system provides advantages compared to other shooting training tools, especially in terms of portability, cost effectiveness and ease of use:

- Some commercially available shooting simulation systems often require expensive and complex hardware. This developed system offers a competitive alternative by providing similar accuracy and performance levels at lower cost.
- While existing commercial systems generally target professional users, this system is designed to appeal to both

amateur and professional users. This enables the system to reach a wider user base. Additionally, any target at any level can be added to the software. The only restriction is that this target must be scaled to A4 size.

The findings obtained in this study provide several opportunities for the development of the system and its dissemination to a wider application area:

- With the development of artificial intelligence-based image processing algorithms and advanced image filters and their integration into the software, the effect of light sensitivity in detecting the shooting point can be reduced.

- Integrating the system with the mobile application can reduce users' hardware needs. In this way, users can train even at home using the cameras of their personal phones.

- A module can be added to the software in which artificial intelligence-supported shooting errors can be automatically evaluated by the system according to the point of impact.

- In line with the developments to be made in the software, visuality can be increased with a barcovision device and a more advanced camera, and scripted shooting training can be given.

5. CONCLUSION

The evaluation results of the hit points on the target showed that the Individual Shooting Simulation System software marked the laser position on the target with high accuracy.

The user-friendly structure of the software and It shows that it can be used as an effective method in shooting training with its possibilities and capabilities. In addition, it was concluded that the real-time feedback feature of the software, together with its fast installation and portable structure and components, increased the effectiveness of shooting training. The fact that the desired target can be added to the software and the target image is on A4 paper shows that the system is an ideal option for individual shooting training with all its components and software. Users have the opportunity to report their performance after shooting, allowing them to track their progress.

The developed Individual Shooting Simulation System software increases the effectiveness of individual shooting training with its innovative structure and user-friendly interface. With future studies, it is expected that the system will reach a wider user base and become an important tool in education, research and commercial fields.

The results obtained confirm that the Individual Shooting Simulation System is a reliable and effective tool for simulating shooting scenarios, allowing users to improve their performance by providing accurate feedback.

REFERENCES

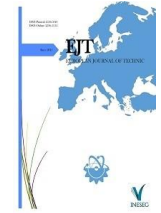
- [1] Mil, H.İ. (2014). Türkiye’de İç Güvenlik Teşkilatları ve Özellikleri. Süleyman Demirel Üniversitesi Vizyoner Dergisi, 5(11), 40-61.
- [2] Rowhani-Rahbar, A., Lyons, V.H., Simonetti, J. A., Azrael, D., & Miller, M. (2018). Formal firearm training among adults in the USA: results of a national survey. *Injury prevention*, 24(2), 161-165.
- [3] Liang, H. & Kong, B. (2006). A shooting training and instructing system based on image analysis. 2006 IEEE International Conference on Information Acquisition,
- [4] Guven, S., & Durukan, A.H. (2020). Empty Bullet-Related Ocular Injuries During Military Shooting Training: A 20-Year Review. *Military Medicine*, 185(5-6), E799-E803.

<https://doi.org/10.1093/milmed/usz400>

- [5] Fedaravičius, A., Pilkauskas, K., Slizys, E., & Survila, A. (2020). Research and development of training pistols for laser shooting simulation system. *Defence Technology*, 16(3), 530-534.
- [6] Aga, A. (2022). Sanal Gerçeklik ve Artırılmış Gerçeklik. *Eğitimde Dijitalleşme Ve Yeni Yaklaşımlar*, 7.
- [7] Davies, A. (2015). The hidden advantage in shoot/don't shoot simulation exercises for police recruit training. *Salus journal*, 3(1), 16-30.
- [8] Potts, J., Hawken, A., Hillhouse, M., & Farabee, D. (2022). Virtual reality for law enforcement training: a demonstration and implication for dispatch priming. *Police Practice and Research*, 23(5), 623-632.
- [9] Harris, D.J., Arthur, T., Kears, J., Olonilua, M., Hassan, E.K., De Burgh, T.C. & Vine, S.J. (2023). Exploring the role of virtual reality in military decision training. *Frontiers in Virtual Reality*, 4, 1165030.
- [10] Oliver, R.A., Cancio, J.M., Rábago, C.A., & Yancosek, K.E. (2019). Impact of firearms training in a virtual reality environment on occupational performance (Marksmanship) in a polytrauma population. *Military medicine*, 184(11-12), 832-838.

BIOGRAPHIES

Vedat YILMAZ obtained his BSc degree in system engineering from military Academy in 2004. I completed Digital Communication Electronics Training at Hacettepe University in 2006. My master's degree in Management and Organization at Selçuk University in 2007, and PhD degrees in Biomechanics at Hacettepe University in 2022. Additionally, I received training on Principles of Communication from Cranfield University, Cyber Security from METU, and Training on Terrorists' Use of Cyberspace from the Center of Excellence in Combating Terrorism. I managed many technology projects within the Gendarmerie General Command. Currently, I continue my studies in the fields of cyber security, artificial intelligence applications in cyber crimes, security technologies and cyber security.



Research Article

A Perspective View on Data Visualization Libraries Used in Data Analytics

Faruk Aksoy^{1*} , Mehmet Ozdem² , Resul Das³ 

^{1*}Dicle University, Ergani Vocational School, Department of Computer Technologies, Diyarbakir, Türkiye. (e-mail: faruk.aksoy@dicle.edu.tr).

²Türk Telekom, Ankara, Türkiye. (e-mail:mehmet.ozdem@turktelekom.com.tr)

³Firat University, Faculty of Technology, Department of Software Engineering, 23119 Elazig, Türkiye. (e-mail: rdas@firat.edu.tr).

ARTICLE INFO

Received: Jan., 9, 2025

Revised: Jan., 25, 2025

Accepted: Feb., 16, 2025

Keywords:

Data Visualization

Visualization Libraries

Data Visualization Libraries

Data Analytics

Corresponding author: Faruk Aksoy

ISSN: 2536-5010 / e-ISSN: 2536-5134

DOI: <https://doi.org/10.36222/ejt.1616824>

ABSTRACT

In today's data-driven world, one of the cornerstones of data science is data visualization. Data visualization makes information more understandable by presenting complex data sets through graphs, tables, and other visual tools. Thus, trends, relationships, and anomalies in the data can be easily detected. In this way, more intuitive and meaningful results are obtained from the data. In addition, decision makers are able to make the right decisions faster thanks to these visualization tools. Graphics libraries created and used in programming languages are used intensively to perform these operations. This article explores programming language-based data visualization libraries, which are widely utilized in the field of data science, and examines the key features and functionalities of these libraries. In this context, 76 visualization libraries were examined and evaluated in terms of customization level, interactive features, and the data types they support, and presented separately in tables according to programming languages. The study areas of the articles in which these libraries were used in the literature and the results obtained from the studies were also presented. In addition, the directions of future studies in this field were added to the conclusion.

1. INTRODUCTION

Data visualization is constantly changing as a developing field of data science. The amount of data loaded into data stores and flow rates contribute greatly to this rapid change [1]. In the contemporary data-driven business landscape, visualization tools are integral to facilitating decision-making processes that directly influence the considerable revenues of various industrial enterprises, thereby underscoring their critical importance in both academic research and industry applications. Because the transformation of abstract data into physical images (length, location, shape, color, etc.) is achieved through visualization [2]. Data-driven solutions that will be carried out in analytical processes related to data received from smart cities, smart systems, web-based systems and wireless sensors in today's technology world, which operates with the production and consumption [3] of such abstract data, are seen as an important field of study in the future [4], [5]. Since the data produced on these platforms is within the scope of big data [6], it is necessary to work with a structure where the data is constantly updated. For this reason, the data is structured and analyzed first. Artificial intelligence-supported intelligent systems can be used to collect data and

provide meaningful inferences. In addition, appropriate mechanisms are applied to detect anomalies in the visualized information [7].

When we look at the studies in the field of data visualization, it is seen that various visualization libraries are used. However, there is no specific standard for which libraries to be used in which situations. This article seeks to address the gap in existing literature by examining visualization libraries across various programming languages, emphasizing their advantages and limitations in the context of specific use cases. For this purpose, it is aimed to guide the library and purpose matching in future visualization studies by classifying the visualization libraries according to their years and usage purposes. As far as we are aware, no such study has been conducted previously. The process from obtaining the data to producing the image outputs is shown in Figure 1 below. The first step is carried out by analyzing the raw data from different sources. The data that needs to be worked on is filtered and sorted out from the prepared data. After matching the data to be focused on with each other with meaningful relationships, the image data is produced by processing the

geometric data obtained on the graph. These processes can also be used as a common workflow that can be used in all data visualization steps [8], [9], [10].

This study consists of four main parts. In Section 2, data visualization tools/libraries that are used extensively in programming languages are presented. Comparisons of the advantages and disadvantages of these tools are also presented in tables. In Section 3, the findings from the literature review with application examples of visualization tools are presented. In Section 4, the analysis of visualization tools and possible future directions are presented and discussed.

2. DATA VISUALIZATION TOOLS

This section discusses libraries used for visualization based on programming languages. Visualization libraries are used in industrial/academic fields and continue to be developed depending on the changing data structure. It is seen in the literature that visualization libraries are applied in very different disciplines such as health, economy, finance, cyber security [11], social media, and construction [12]. It can be used to analyze social networks [13] within the scope of big data, as well as for real-time modeling [14]. Visualization libraries in programming languages used in visualization

processes are shown in Figure 1. On the other hand, studies are also being carried out to realize solutions related to all these steps with generative artificial intelligence [15]. Interactive visualization with generative artificial intelligence is one of these areas [16].

2.1. Javascript Based Tools

When we look at the studies conducted in the field of data visualization, there are many tools based on programming languages. These languages include JavaScript, R, Python, Java, Scala, Perl, Julia. The overwhelming majority of programming language-based visualization tools, particularly those that are most commonly used, are built on JavaScript. For this reason, tools based on JavaScript will be presented first in this section. JavaScript allows users to design their charts and graphs flexibly by processing raw data with their own style of code, but these design steps can be time-consuming for those new to programming languages. Some visualization tools are integrated with JavaScript, whereas others rely on programming languages like Python, Java, PHP and R. Visualization libraries in JavaScript are explained below.

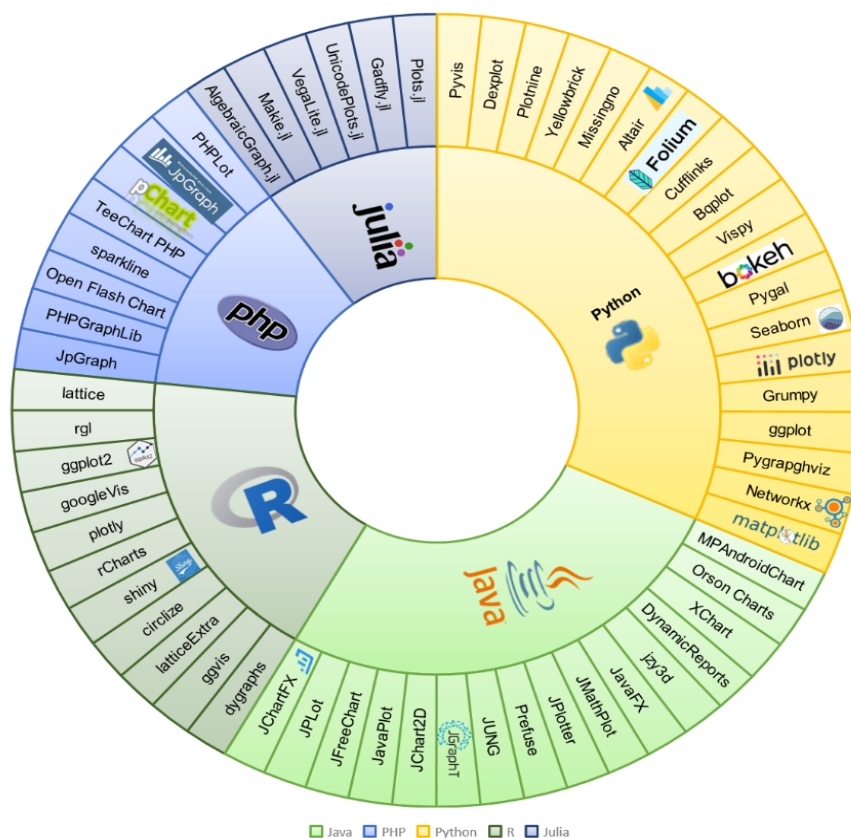


Figure 1. Distribution of graphics libraries by programming languages

TABLE 1 Javascript graphics libraries

References	Year	Tool	Features	Advantages	Disadvantages
[17]	2002	FusionCharts	Basic chart types, indicators, maps, custom visualization features	Rich chart options, easy integration	Paid license, some features limited
[18]	2004	Dojo	Charts, form elements, animations, data management	Versatile library, wide range of features	Performance issues with large data sets
[19], [20]	2005	Prototype.js	DOM manipulation, AJAX, form elements	Simple DOM manipulation, good performance	Limited chart and visualization support
[21]	2006	MooTools	Charts, animations, form elements, data management	Flexible and extendable, modern API	More complex configuration
[22]	2009	Protovis	Line charts, stacked bar charts, pie charts	Powerful data visualization, open source	Limited modern features, less up-to-date
[23]	2009	ZingChart	Various chart types, maps, network graphs, custom visualization features	Wide chart types, strong customization	Paid license, some features limited
[24]	2010	Flot	Basic chart types (line, bar, area, etc.)	Simple to use, good performance	Limited chart types and customization
[25]	2011	D3.js	Data visualization, animations, interactive charts, maps, network graphs	High customization, large community support	Learning curve, complex configuration
[26]	2013	Chart.js	Basic chart types (line, bar, pie, radar, etc.)	Easy to use, lightweight	Fewer customization options
[26]	2013	EChart.js	Various chart types, maps, network graphs, custom visualization features	Strong chart features, extensible	Performance limitations with large data sets
[27]	2014	C3.js	Built on D3.js, provides a simple API interface, line charts, bar charts, pie charts	Simple API, D3.js support	Does not support all D3.js features
[28]	2015	Vega	Data visualization, declarative charts, interactive charts, customization	Modern API, strong interaction	Learning curve, some performance issues
[29]	2010	Highcharts	Interactive charts (line, bar, pie, scatter, etc.), 3D charts, maps	Easy to integrate, rich features, good documentation	Paid license for commercial use

2.1.1. Protovis

Protovis enables the creation of custom data visualizations using basic markers such as bars and dots. It defines these markers through dynamic properties that represent the data, and incorporates inheritance, scales, and layouts to streamline the structure. Protovis is free and open-source, licensed under the BSD License. It utilizes JavaScript and SVG for web-based visualizations, requiring no plugins, though a modern web browser is necessary. Protovis is no longer in active development. The last version of Protovis was v3.3.1. The Protovis team has been developing the visualization library D3.js since June 28, 2011. D3 is based on many concepts from Protovis [22], [30], [31].

2.1.2. D3.js

D3.js is an open-source JavaScript library that combines HTML and CSS techniques to create dynamic, interactive data visualizations [32]. It leverages HTML, CSS, and SVG to generate visual representations of data, accessible in any browser. Moreover, the study [30] detailing the development of D3 demonstrates that it outperforms Protovis, achieving at least twice the speed in performance benchmarks. The D3.js website provides numerous examples, which can either inspire users to create their own visualizations or be used directly as templates [33].

2.1.3. Chart.js

Chart.js, launched in 2013, is an open-source library licensed under the MIT license and is actively maintained by a dynamic community. It includes built-in TypeScript support and is compatible with major JavaScript frameworks, such as React, Vue, Svelte, and Angular. The library is well-suited for handling large datasets, which can be efficiently retrieved in

its native format, eliminating the need for data parsing and normalization. Alternatively, users can configure data sampling to reduce the size of the dataset before rendering [34]. In one paper, the JSTrace application designed to identify error sources in web applications evaluated Chart.js as the JavaScript library with the fewest errors [35].

2.1.4. Dojo

It is an open source, modular JavaScript library, launched in 2004, designed for developing cross-platform Ajax-based applications and websites [36]. Dojo's components, known as widgets, combine HTML, JavaScript, and CSS. They provide a wide range of interactive features, including menus, tabs, tooltips, tables, dynamic charts, 2D and 3D vector graphics, and tree-like widgets with drag-and-drop functionality.

A key feature of Dojo is its support for asynchronous communication between the browser and the server, a critical aspect of Ajax applications. Dojo provides an abstracted wrapper (dojo.xhr) for different web browser implementations, enabling seamless data communication between the client and server. This facilitates the storage of user input from forms on the server, with the server returning JavaScript code that dynamically updates the content of the page [37]. Additional capabilities of Dojo include both client- and server-side data storage, along with support for the Adobe Integrated Runtime (AIR) environment. The toolkit is officially supported by major companies such as IBM, Sun Microsystems (now Oracle), and Zend Technologies, the creators of PHP.

2.1.5. Prototype.js

The Prototype JavaScript framework was developed by Sam Stephenson in February 2005 to provide Ajax support for

Ruby on Rails. Typically implemented as a single JavaScript file, `prototype.js`, it is designed to simplify the development of dynamic web applications. Prototype, as an object-oriented framework, offers extensive support for Ajax, sophisticated programming components, and efficient DOM manipulation, thereby simplifying the process for developers to build interactive and responsive web interfaces [38], [39], [40].

2.1.6. Echart.js

Echart.js is a JavaScript library for charting and data visualization, designed to create intuitive, interactive, and highly customizable charts. It can run on PC and mobile devices. It depends on ZRender, a charting engine. It is compatible with web browsers such as Safari, IE8-11, Firefox, Chrome, etc. It supports charting in ECharts, Canvas, SVG (v4.0+) and VML formats [41].

2.1.7. FusionCharts

FusionCharts is a proprietary JavaScript library that integrates multiple technologies, including JavaScript and ActionScript 3.0. The library is compatible with a diverse array of devices, browsers, and platforms. It provides over 90 unique chart types and more than 1,000 maps, covering regions from every continent. FusionCharts supports the processing of data in .xml and .json formats and allows users to export the generated charts in .jpg, .png, and .pdf file formats. Furthermore, its functionality can be extended through various official plugins and wrappers, enabling the integration of interactive charts into applications built with technologies such as JSP, PHP, jQuery, and Django [42].

2.1.8. C3.js

C3 is a reusable D3-based charting library that enables the integration of charts into web applications [43]. C3 makes it easy to create D3-based charts by packaging the code required to create the entire chart. C3.js is a JavaScript library that enables the creation of visualizations through the use of HTML, SVG, and CSS. It proposes a vast range of APIs and callbacks, allowing users to interact with and access the state of the chart [44].

2.1.9. Flot

Flot is a JavaScript library for jQuery that emphasizes ease of use, customizable styling, and interactive chart features. It supports HTML5-based charts, leveraging Canvas and VML technologies. The library distinguishes the functional logic from the HTML structure, leveraging DOM elements to generate the charts. Flot includes pre-built components for four fundamental chart types: bar charts, line charts, point charts, and segment charts. Additionally, users can easily customize and extend these charts by modifying a wide array of configuration options [45].

2.1.10. ZingChart

ZingChart integrates seamlessly with various frameworks such as Angular, React, jQuery, PHP, Ember, and Backbone

within its JavaScript library, allowing for a declarative approach to chart creation and management. ZingChart supports over 35 chart and model types. It allows users to export visualization graphs in .png, .jpg, and .pdf formats. It offers integrated graph editing capabilities. It has a drill-down function where users can select a data element within the graph [23].

2.1.11. Vega

Vega is a declarative language used to define, store, and share interactive visualization designs. With Vega, data visualizations are defined using a JSON style, allowing for the creation of interactive views through HTML5 Canvas or SVG. Vega-Lite, a higher-level language built upon Vega, enables the rapid creation of statistical graphs. [28]. If the working environment is Python instead of JavaScript, the Altair Python API is used for Vega-Lite [46].

2.1.12. Highcharts.js

Highcharts.js is a powerful and flexible data visualization library for modern web applications. It can process large datasets efficiently, thanks to its robust feature set and high performance. Its ability to generate interactive graphs makes it widely applicable in the fields of data science and software development.

The library offers a wide range of graph types. It offers a wide range of data visualization opportunities, from basic line and bar charts to complex financial and geographic maps. The dynamic and interactive charts it offers, especially Highcharts' Highstock and Highmaps add-ons, offer special solutions in the fields of financial data analysis and geographic data visualization. Thanks to these features, it is ideal for large data analysis and global data sets. Its extensible API and customizable building blocks allow users to control every aspect of the charts in detail. In addition, thanks to its mobile-friendly design and high-performance processing capabilities, it offers data visualizations seamlessly on every platform. Highcharts' commercial license model offers a suitable option for projects that require advanced features and support. These advantages make the library attractive for large-scale and commercial data visualization solutions [47].

2.2. Tools Based on Other Programming Languages

Besides JavaScript, there are a wide variety of data visualization tools and libraries available in other programming languages. There are widely used libraries in Java (Table 2), PHP (Table 3), R (Table 4), Julia (Table 5) and Python (Table 6), Scala, and Actionscript. These libraries are listed according to their production dates and the languages they belong to. Some of the most widely used libraries in different languages are described below.

TABLE 2 Java graphics libraries

Ref	Year	Tool	Features	Advantages	Disadvantages
[48]	1996	TeeChart for Java	Rich chart types, interactive visualization	Wide variety of chart types, high performance	Paid license, complex configuration
[49]	2005	JChartFX	Customizable charts, user-friendly interface	Easy to use, good performance	Limited customization options
[50]	2008	JPlot	Basic chart types, fast performance	Lightweight and fast	Few chart types and features
[51]	2000	JFreeChart	Wide range of chart types, good documentation	Widely used, open-source, large community support	Performance limitations with large data sets
[52]	2003	JavaPlot	Simple charts, mathematical functions	Simple and lightweight	Limited chart types and features
[53]	2004	JChart2D	2D charts, fast performance	Easy to use, fast rendering	Limited chart types and customization
[54]	2003	JGraphT	Focused on graph theory, supports weighted graphs	Strong graph theory processing, open-source	Limited visualization support
[55]	2004	JUNG	Network analysis, various graph algorithms	Comprehensive network analysis features	Complex usage, limited visualization
[56]	2005	Prefuse	Data visualization, dynamic interactions	Good visualization and interaction	Inadequate documentation, complex configuration
[57]	2007	JPlotter	Basic 2D and 3D charts, speed	Simple and fast	Limited features and chart types
[58]	2007	JMathPlot	Mathematical charts, 2D drawings	Suitable for mathematical data, easy to use	Few chart types and customization options
[59]	2008	JavaFX	Rich user interfaces, 2D and 3D charts	Modern interfaces, rich visualization	Performance issues with large data sets
[60]	2008	Jzy3d	3D charts, high performance	Impressive 3D charts, fast rendering	Complex configuration, learning curve
[61]	2011	XChart	Simple, lightweight charts	Easy to use, low memory usage	Few chart types and customization
[62]	2012	Orson Charts	2D and 3D charts, high-quality rendering	High-quality charts, flexible customization	Smaller community support
[63]	2013	MPAndroidChart	Rich chart types, interactive features	Optimized for Android applications	Only available for the Android platform

TABLE 3
Php graphics libraries

Ref	Year	Tool	Features	Advantages	Disadvantages
[64]	2004	PHPLot	Basic 2D charts, various chart types	Simple and lightweight, easy integration	Limited chart types and customization
[65]	2001	jpGraph	Rich chart types, high customization	Wide range of chart types, strong customization	Paid license, complex configuration
[66]	2005	pChart	Dynamic charts, various data formats	Strong visualization, good performance	Learning curve, some features are paid
[67]	2009	TeeChart PHP	Wide range of chart options, interactive charts	Wide variety of chart types, user-friendly	Paid license, complex configuration
[68]	2009	Sparkline	Small, minimalist charts	Lightweight, fast rendering	Limited chart types and features
[69]	2008	Open Flash Chart	Flash-based charts, interactive features	Web-based interaction, various chart types	Flash-based, limited mobile compatibility
[70]	2001	JpGraph	Rich chart types, high customization	Wide range of chart types, strong customization	Paid license, complex configuration

TABLE 4 R graphic libraries

Ref	Year	Tool	Features	Advantages	Disadvantages
[71]	2004	lattice	Multiple 2D charts, multidimensional data	Strong multidimensional data visualization	Learning curve, sometimes complex configuration
[72]	2008	rgl	3D charts, interactive visualization	Interactive 3D visualization, powerful	Performance issues with large data sets
[73]	2011	latticeExtra	Extra chart types, compatible with lattice	Additional features for lattice charts	More complex configuration
[74]	2005	ggplot2	Grammar of Graphics, rich chart types	Widely used, powerful customization	Performance limitations with large data sets
[75]	2010	googleVis	Google Charts integration, interactive charts	Web-based interaction, easy to use	Dependency on Google services
[76]	2013	plotly	Interactive charts, multi-language support	Rich interaction features, multi-language support	Paid plans and some features are limited
[77]	2014	rCharts	Various JavaScript libraries, interactive charts	JavaScript integration, interactive charts	Steeper learning curve, some features are paid
[78], [79]	2012	shiny	Web app development, interactive data visualization	Dynamic web applications, powerful interaction	Performance issues with large data sets
[80]	2014	circlize	Circular charts, complex data visualization	Advanced circular charts, customizable	Complex configuration, learning curve
[74]	2015	ggvis	Interactive charts, Grammar of Graphics	Interactive visualization, modern API	Advanced features are limited, some performance issues
[81]	2013	dygraphs	Time series charts, interactive	Strong time series visualization, interactive	Customization options are limited

TABLE 5 Julia graphic libraries

Ref	Year	Tool	Features	Advantages	Disadvantages
[82]	2015	Plots.jl	Multiple backend support (GR, PyPlot, Plotly, etc.), interactive and static charts	Easy to use, many backend supports, large user community	Performance can be limited in some cases, limited features for complex charts
[83]	2015	Gadfly.jl	Uses the Grammar of Graphics approach, offers extensive data visualization capabilities	Powerful and flexible, creates aesthetic charts	Performance can be low in some cases, setup and configuration can be complex
[84]	2018	Makie.jl	2D and 3D charts, high performance, interactive visualization	High performance, a wide variety of chart types, interactive capabilities	Learning and usage difficulty, potential library compatibility issues
[85]	2017	VegaLite.jl	Compatible with Vega-Lite, uses the Grammar of Graphics approach	High customization, ability to create interactive charts	Customization and performance limitations
[86]	2016	UnicodePlots.jl	Creates charts with ASCII and Unicode characters	Lightweight, fast, terminal-based visualization	Visually limited, lacks advanced chart features

TABLE 6 Python graphics libraries

Ref	Year	Tool	Features	Advantages	Disadvantages
[87]	2003	Matplotlib	2D charts, extensive customization options	Strong community support, wide range of chart types	Performance limitations, some features may be complex
[88]	2004	Networkx	Graph theory and network visualization	Strong network analysis tools, well documented	Not for general data visualization, network-focused
[89]	2006	PyGraphviz	Graph theory and network visualization, Graphviz interface	Graphviz integration, strong network visualization	Setup and dependencies may be complex
[90]	2010	ggplot	Grammar of Graphics approach, 2D charts	Strong and aesthetic charts, easy to use	Performance limitations, limited 3D support
[91]	2013	Glumpy	Fast 2D and 3D charts, uses OpenGL	High performance, interactive charts	Difficult to use, limited community support
[92]	2013	Plotly	Interactive charts, multiple chart types	Highly interactive, web-based visualization	Limited features in free version
[93]	2012	Seaborn	Statistical data visualization, built on Matplotlib	Aesthetic and understandable charts, easy to use	Limited customization options, dependency on Matplotlib
[94]	2012	Pygal	Web-based SVG charts, easy to use	Lightweight, aesthetic, and dynamic charts	Limited chart types and customization options
[95]	2013	Bokeh	Interactive charts, large data support	Web-based interactions, high performance	May have a learning curve, complex setup
[96]	2014	Vispy	High-performance 2D and 3D charts, uses OpenGL	Performance, large data, and interactive charts	Learning curve, limited community support
[97]	2015	Bqplot	Interactive charts for Jupyter Notebooks	Jupyter-compatible, interactive visualization	Limited chart types, low community support
[98]	2015	Cufflinks	Integrated with Pandas DataFrames, Plotly-based	Integration with Pandas, interactive charts	Limited customization, dependent on Plotly
[99], [100]	2014	Folium	Map visualization, based on Leaflet.js	Map-focused, web-based visualization	Not for general data visualization, map-focused
[101]	2016	Altair	Declarative data visualization, based on Vega-Lite	High-level API, aesthetic charts	Limited 3D and interactive chart support
[102]	2017	Missingno	Missing data visualization, simple charts	Specialized for missing data analysis and visualization	Limited chart types, only for missing data analysis
[103]	2016	Yellowbrick	Machine learning visualizations, integrated with Scikit-learn	ML model evaluation tools, easy to use	Limited data visualization, ML-focused
[104]	2018	Plotnine	Grammar of Graphics-based, similar to ggplot2	Strong and aesthetic charts, ggplot2-like in Python	Performance limitations, some features missing
[105]	2018	Pyvis	Interactive network visualization, integrated with Networkx	Easy interactive network graphs, good visualization	Limited data types, performance limitations
[106]	2014	Holoviews	Interactive and large data visualization	Easy to use, powerful interactive charts	Performance limitations, learning curve
[107]	2016	Datashader	Optimized for large data visualization	Fast large data visualization, effective rendering	Limited interactivity, integration issues with other libs
[108]	2012	Geopandas	Geographic data visualization, Pandas-based	Integration with geographic data, powerful features	Not for general data visualization, geography-focused

2.2.1. Gephi

Gephi is a free, open-source software developed for the purpose of network visualization and analysis. It is developed in Java, utilizing the NetBeans platform. Gephi can display the spatialization process in real time. The default layout algorithm employed is ForceAtlas2, a continuous force-directed layout method. Users have the option to import .csv data files or directly input their data into the Gephi spreadsheet. The data file is structured into two sections: the edge table and the node table. Consequently, users must prepare and organize their data into these two components in advance. It supports up to one million edges and nodes. Once the data is imported, the visualization is automatic. Users can choose an algorithm (ForceAtlas, ForceAtlas2, Fruchterman Reingold, Noverlap, etc.) to analyze the network. The generated network graph can be exported directly in .svg or .pdf formats [25], [109], [110].

2.2.2. jpGraph

jpGraph is an object-oriented library for creating graphs. If server-side graphs need to be generated, the library is ready to be used in any language. The library, which has free and paid (pro) versions, is based on PHP5 (versions above 5.1) and PHP7. It was written for PHP by Asbjørn Ulsberg. The commercial professional version of jpGraph supports additional chart types such as odometer, wind rose (a special diagram representing the distribution of meteorological data, wind speeds by class and direction, also known as a polar rose chart), and barcodes [111].

2.2.3. Matplotlib

Matplotlib is an extensive library in Python used for generating static, animated, and interactive visualizations. Some of the visualization libraries written in Python include Plotly [112], Seaborn [113], Altair [114], Pygal [115], Bokeh [116], Gleam [117], and Matplotlib [118]. Matplotlib allows you to visualize data interactively and prepare high-quality outputs suitable for publication. Both two-dimensional and three-dimensional charts can be produced. It is also a popular data visualization package that works well, including ipython shell, web application server, graphical UI toolkit, and Jupyter notebook [119], [120].

2.2.4. Folium

Folium is a library for interactive map drawing based on leaflet.js module in JavaScript language, but performs data manipulation in Python. Folium simplifies the process of visualizing data manipulated in Python on an interactive leaflet map. The library offers several built-in tile sets from sources like OpenStreetMap, Mapbox, and Stamen, and it also supports custom tile sets using Mapbox or Cloudmade API keys. Additionally, Folium accommodates various textures, including image, video, GeoJSON, and TopoJSON formats [121]. It is built with simplicity, performance, and utility in mind. It is highly performant, has a user-friendly API, and can be enhanced with various plugins [99], [100].

2.2.5. GraphX in Spark

Apache Spark is an open source library developed in Scala language that enables parallel processing on large data sets. Spark can run faster than Apache Hadoop in big data applications with its in-memory data processing feature.

Therefore, it is possible to say that Spark's analytics engine can perform faster operations by keeping data in memory while processing instead of reading or writing data from disk. Apache Spark has various libraries for visualization, machine learning, and streaming operations. One of these libraries, GraphX, is a built-in library for graph analytics and graph parallel computing in Apache Spark [13], [122].

2.2.6. Plotly

Developed by a company called Plotly Inc. It is a Python library designed for generating interactive visualizations. It is also a free and open source library compatible with JavaScript and R. Its source can be viewed on GitHub [123]. Plotly Inc. is a technology company specializing in the development of online data analytics and visualization tools. The company offers online tools for graphing, analytics, and statistics, along with scientific graph libraries for various programming languages including Python, R, MATLAB, Perl, Julia, Arduino, and REST [76].

2.2.7. Prefuse

Prefuse is a Java-based tool for creating interactive information visualization applications. It supports a rich feature set for data modeling, visualization, and interaction. It provides support for tables, graphs, trees, animation, dynamic queries, integrated search and database connectivity, and optimized data structures. It is written in Java 1.4 using the Java 2D graphics library. It can be easily integrated into Java Swing applications or web applications. Prefuse is a product of the UC Berkeley Visualization Lab and is licensed under the terms of the BSD license. It may be used freely for both commercial and non-commercial purposes [124].

2.2.8. Flare

Flare is an ActionScript-based visualization library, built on the Prefuse framework, designed to create a diverse range of interactive visualizations that operate within the Adobe Flash Player. Flare, developed by the UC Berkeley Visualization Lab, is an ActionScript 3-based toolkit designed to support data management, visual coding, animation, and interaction techniques [125]. It enables the creation of a wide range of visualizations, from basic tables and charts to intricate interactive graphics [126]. Created by Jeff Heer, Flare is used to produce everything from simple charts and complex animations to network diagrams, tree maps, and more.

2.2.9. Weave

The Web-based Analysis and Visualization Environment offers a range of visualization tools that enable users to rapidly and effectively expand their analysis. It is open sourced by the OIC (Open Indicators Consortium). It is maintained in partnership with the Institute for Visualization and Perception Research (IVPR) at the University of Massachusetts Lowell. Weave is designed to enable users to analyze, visualize, and disseminate data and indicators at geographically nested levels, from anywhere, at any time [127] [128]. It presents data in multiple formats as an intuitive application. This feature enables users to easily observe the relationships between datasets. When a user selects a data value in one of the visualization windows, the corresponding value is highlighted on the map, as well as in other tables and visualizations. Users can also incorporate additional data, access a range of tools,

and save Weave sessions for future use or sharing with other users [129], [130].

2.2.10. Ggplot2

Ggplot2 is an open-source R language software package for statistical data visualization and graphics. It is grounded in the concepts of the "Grammar of Graphics [131]," a framework developed by Hadley Wickham. This approach defines the building blocks of data visualization and makes the graphic creation process modular and reusable. Graphics are a combination of components such as aesthetics (aes), geoms, stats, coordinates, and facets in ggplot2 [132].

2.2.11. Seaborn

Seaborn is a highly influential data visualization library in the Python ecosystem, playing a key role in the visualization of statistical analysis. It is built on top of Matplotlib and offers a high-level API that facilitates the creation of more complex and aesthetically superior plots. It provides comprehensive tools for deep understanding of the internal structure and relationships of data sets. Functions such as pairplot, heatmap, violin plot provide advanced capabilities for multidimensional data analysis and pattern discovery. Since pairplot allows multidimensional visualization of relationships and distributions between variables, it provides a critical advantage in modeling and anomaly detection processes. The heatmap

function is used to visualize dense data structures such as correlation matrices, allowing visual analysis of relationships between data [133].

2.2.12. Ggvis

ggvis is a library that can create interactive and dynamic graphics among the data visualization tools in the R language. While ggvis is built on the Grammar of Graphics [131] principles established by ggplot2, it enhances the visualization functions by making them interactive, enabling users to engage with the data in real time. The ability to integrate with shiny [79] offered by ggvis provides a great advantage in web-based data analysis and visualization applications. In addition to creating interactive graphics in data visualization processes, it offers a powerful API that supports user interactions and dynamic data updates. ggvis's high-performance and fast graphics using WebGL and SVG technologies in the background provide a significant performance advantage when working with large data sets. The dynamic features of ggvis offer data scientists the ability to explore the internal structure of datasets and conduct more detailed analysis by receiving immediate feedback during decision-making. This makes ggvis a powerful tool, particularly for exploratory data analysis and user-focused data visualization projects [74].

TABLE 7 Types supported by visualization libraries

Library	Bar	Line	Pie	Radar	Scatter	Bubble	Heatmap	3D	Other Graphic Types	WebGL Support
FusionCharts	✓	✓	✓	✓	✓	✓	✓	✓	Fuzzy Charts, Fast Data Visualization	✓
Dojo	✓	✓	✓	✓	✓	✓	✓	✓	Conditional Labeling	✓
Prototype.js	✓	✓	✓	✓	✓	✓	✓		Data Binding	
MooTools	✓	✓	✓	✓	✓	✓	✓		Animations	
Protovis	✓	✓	✓	✓	✓	✓	✓		Clustering, Hierarchy	✓
ZingChart	✓	✓	✓	✓	✓	✓	✓	✓	Fast Data Binding	✓
Flot	✓	✓	✓		✓	✓	✓		Live Data Loading	
D3.js	✓	✓	✓	✓	✓	✓	✓	✓	Network Charts, Maps	✓
Chart.js	✓	✓	✓		✓	✓	✓		Innovative Animations	
ECharts	✓	✓	✓	✓	✓	✓	✓	✓	Map Visualization	✓
C3.js	✓	✓	✓		✓	✓	✓		Hierarchical Data	
Vega	✓	✓	✓	✓	✓	✓	✓	✓	Conditional Data Visualization	✓
Plots.jl	✓	✓	✓	✓	✓	✓	✓		Conditional Data	
Gadfly.jl	✓	✓	✓	✓	✓	✓	✓		Conditional Data	
Makie.jl	✓	✓	✓	✓	✓	✓	✓	✓	3D, Interactive Data	✓
VegaLite.jl	✓	✓	✓	✓	✓	✓	✓		Conditional Data	
AlgebraicGraph.jl					✓				Network Charts	
UnicodePlots.jl	✓	✓	✓		✓				Time Series	
Plots.jl	✓	✓	✓	✓	✓	✓	✓		Conditional Data	
Gadfly.jl	✓	✓	✓	✓	✓		✓		Conditional Data	
Makie.jl	✓	✓	✓	✓	✓	✓	✓	✓	3D, Interactive Data	✓
VegaLite.jl	✓	✓	✓	✓	✓	✓	✓		Conditional Data	
AlgebraicGraph.jl					✓				Network Charts	
UnicodePlots.jl	✓	✓	✓		✓				Time Series	
lattice	✓	✓	✓	✓	✓		✓		Conditional Data	
rgl	✓	✓	✓		✓			✓	3D, Interactive Data	✓
latticeExtra	✓	✓	✓		✓				Conditional Data	
ggplot2	✓	✓	✓	✓	✓	✓	✓		Conditional Data	
googleVis	✓	✓	✓	✓	✓	✓	✓		Map Visualization	
plotly	✓	✓	✓	✓	✓	✓	✓	✓	3D, Map Visualization	✓
rCharts	✓	✓	✓	✓	✓	✓	✓		Map Visualization	
shiny	✓	✓	✓		✓				Real Time Data	

circlize	✓	✓	✓	✓					Pie Charts	
ggvis	✓	✓	✓	✓	✓	✓	✓		Conditional Data	
dygraphs	✓	✓	✓	✓	✓	✓	✓		Time Series	
TeeChart for Java	✓	✓	✓	✓	✓	✓	✓	✓	3D, Network, Hierarchy	✓
JChartFX	✓	✓	✓	✓	✓	✓	✓		3D, Fast Data	✓
JPlot	✓	✓	✓	✓	✓	✓	✓		Conditional Data	
JFreeChart	✓	✓	✓	✓	✓	✓	✓		3D, Network, Hierarchy	
JavaPlot	✓	✓	✓	✓	✓	✓			Conditional Data	
JChart2D	✓	✓	✓	✓	✓	✓			Conditional Data	
JGraphT					✓				Network Chart Types	
JUNG					✓				Network Chart Types	
Prefuse	✓	✓	✓	✓	✓	✓	✓		Conditional Data	
JPlotter	✓	✓	✓	✓	✓	✓			3D, Animation	
JMathPlot	✓	✓	✓	✓	✓	✓			Hierarchy Visualization	
JavaFX	✓	✓	✓	✓	✓	✓	✓	✓	3D, Network, Hierarchy	✓
Jzy3d	✓	✓	✓	✓	✓	✓	✓	✓	3D, Fast Data	✓
DynamicReports	✓	✓	✓	✓	✓	✓	✓		Conditional Data	
XChart	✓	✓	✓	✓	✓	✓			Conditional Data	
Orson Charts	✓	✓	✓	✓	✓	✓		✓	3D, Fast Data	✓
MPAndroidChart	✓	✓	✓	✓	✓	✓	✓		Fast Data, Real Time	
Matplotlib	✓	✓	✓	✓	✓	✓	✓		Conditional Data	
Networkx					✓				Network Charts	
PyGraphviz					✓				Network Charts	
ggplot	✓	✓	✓	✓	✓	✓	✓		Conditional Data	
Glumpy	✓	✓	✓	✓	✓	✓		✓	3D, Fast Data	✓
Plotly	✓	✓	✓	✓	✓	✓	✓	✓	3D, Map Visualization	✓
Seaborn	✓	✓	✓	✓	✓	✓	✓		Time Series	
Pygal	✓	✓	✓	✓	✓	✓			Conditional Data	
Bokeh	✓	✓	✓	✓	✓	✓	✓		Map Visualization	
Vispy	✓	✓	✓	✓	✓	✓		✓	3D, Interactive Data	✓
Bqplot	✓	✓	✓	✓	✓	✓			Time Series	
Cufflinks	✓	✓	✓	✓	✓	✓	✓		Conditional Data	
Folium			✓	✓	✓	✓			Map Visualization	
Altair	✓	✓	✓	✓	✓	✓	✓		Conditional Data	
Missingno	✓	✓	✓	✓	✓	✓	✓		Data Cleaning	
Yellowbrick	✓	✓	✓	✓	✓	✓			Machine Learning	
Plotnine	✓	✓	✓	✓	✓	✓			Conditional Data	
Dexplot	✓	✓	✓	✓	✓	✓			Time Series	
Pyvis					✓				Network Charts	
Holoviews	✓	✓	✓	✓	✓	✓	✓		Conditional Data	
Datashader	✓	✓	✓	✓	✓	✓			Big Data Visualization	
Geopandas			✓	✓	✓	✓			Map Visualization	

3. DATA ANALYTIC APPLICATION EXAMPLES

In this section, studies using visualization libraries are examined. As seen below, these results are presented in Table 8. When these studies are examined, it is seen that these visualization libraries are used in many different disciplines and for various purposes. Application articles have been produced in areas such as computer systems, web page design, web security, chemistry, astronomy, data science, smart

systems, smart cities, biology, agriculture, microbiology, psychology, big data, network security, health, and mobile applications. It can be said that Python, R, and Julia tools have been used more intensively in these studies in recent years. It can also be seen that Java libraries are used for mobile applications.

TABLE 8. Application examples of visualization tools

Ref.	Date	Library	Application Field	Conclusion
[1]	2012	FusionCharts	Mainframe performance analysis system	The degree of regression has been improved to more than 97% correlation
[2]	2011	Dojo	Dynamic tree menus and categorical classification	Tree nodes can have dynamic effects such as adding, deleting, and dragging.
[19]	2015	Prototype.js	Open online courses (MOOCs) and semantic web technologies	A MOOC management system prototype powered by semantic technologies has been developed
[20]	2011	MooTools	Web security and digital rights management	Development of anti-hotlinking framework
[22]	2009	Protovis	Data visualization	Production of the Protovis tool

[23]	2022	ZingChart	Astronomy and astrophysics	A system for finding the recorded flux at a particular sky position for X-ray observations.
[24]	2014	Flot	Fusion science and remote control systems	Remote access to a web-based user interface, solving the problem of high network latency
[26]	2018	EChart.js	Web-based interactive visualization tools and visualization development frameworks	Development of ECharts framework
[27]	2019	C3.js, D3.js	Developing web-based applications for honeybee colony monitoring and data visualization	Development of the Beemon system
[28]	2017	Vega-Lite	Interactive data visualization	Evaluation of the visualization grammar Vega-Lite
[29]	2017	Highcharts	Visualization of micro video big data	Visualizing micro video data with Highcharts
[64]	2016	PHPLot	Forecasting water levels, currents and waves for web-based information systems and coastal management	Development of Jeddah CIS system
[65]	2006	jpGraph	Electronic logbook and experimental data management	The web based logbook and run information interface
[66]	2012	pChart	Analysis and visualization of multivariate health data with geographic information systems	Development of the web application Community Health Map
[67]	2015	TeeChart PHP	Water pollution control and environmental decision support systems (EDSS)	Integration of EDSS environmental simulation models into the Beiyun River
[68]	2015	Sparkline	Smart grid data visualization and analysis of electrical grid data	Effective visualization of large data sets with Sparklines
[69]	2021	Open Flash Chart	Genomic analysis	Analyses on the Sorghum genome and transcriptome
[70]	2012	JpGraph	Graphical web presentation of thermochemical properties	Two auxiliary functions have been developed for solving graphics courses with Jpgraph support.
[48]	2018	TeeChart for Java	Sentiment analysis and comparison of Lexicon-based approach and Supervised Machine Learning approaches in analysis	The accuracy of Urdu Sentiment Analyzer is 89.03% with 0.86 precision, 0.90 recall and 0.88 F-measure
[49]	2019	JChartFX	Smart cities	Drafting a suitable Enterprise Architecture (EA) for Mauritius Fire Rescue Services (MFRS)
[50]	2019	JPlot	Internet of Things (IoT)	Images taken with Raspberry Pi Zero and Raspberry Pi Camera were processed with artificial neural networks (ANN) to estimate blood glucose levels with mean absolute error (10.37%) and Clarke Grid error (90.32% Region A).
[62]	2016	JFreeChart	Relational databases and tabular data	Introduces a new software called Thoth that facilitates the visualization and analysis of data in various ways
[52]	2012	JavaPlot	Medical electronics and ECG analysis	Non-linear transformations and artificial neural networks are used for ECG signal recognition and classification
[53]	2014	JChart2D	Examining the accuracy of SLOC (source lines of code) prediction models	The prediction model provides the highest accuracy (average MMRE = 0.19 and average Pred(25) = 0.74)
[54]	2022	JGraphT	Protection against phishing threats	Proposes a fake site detection method that checks domain similarity using the Levenshtein metric
[55]	2009	JUNG	Analysis of semantic networks	Semantic network analysis with graphOnt library and JUNG framework
[56]	2012	Prefuse	Interactive visualization of academic research	It offers an information visualization system developed using XML and Java.
[57]	2019	JPlotter	Analyze nonlinear constraint optimization problems	Provides a visual representation of the evolution of the optimization process
[58]	2015	JMathPlot	Toxicity of nanomaterials	Development of nano-QSAR modeling software
[59]	2019	JavaFX	Framework for forensic investigation of drone-related crimes	Framework for forensic investigation of drone-related crimes
[60]	2017	Jzy3d	Modelling flow dynamics in lowlands	Development of Two-Scale Cellular Automation
[61]	2023	XChart	Operation and maintenance (O&M) processes of urban underground pipe networks	It presents a mobile augmented reality (MAR) based visualization framework.
[62]	2016	Orson Charts	To query, display, visualize and analyze tablesal data stored in relational databases and data files	It offers an easy-to-use data visualization and statistics software called Thoth
[63]	2023	MPAndroidChart	Collection of patient -induced health data (PGHD) and integration of these data into the hospital information system	It provided easy integration of patient data by establishing a two-way connection between the mobile application and the hospital information system via QR code.
[71]	2009	lattice	Represent biological data	Generalized lattice -like graph approach
[72]	2020	rgl	Investigation of the structural features of open source software package ecosystems using complex network analysis (CNA) methods	Complex network analysis tools provide an effective method for evaluating software package ecosystems.
[73]	2024	latticeExtra	Mapping of the water status of citrus gardens to determine field -based management zones in precision agriculture.	By reliably estimating the spatial variability of water potential in orchards, scientifically based classification has been shown to be important for precise irrigation strategies and decision support processes.
[74]	2024	ggplot2, ggvis	Data visualization	The developed VisAhoi library supports the creation of placement elements for different visualization types and datasets.
[75]	2017	googleVis	Modeling and analyzing the interactions between intestinal microbiota and its surroundings	The developed compuGUT simulation tool offered an effective calculating approach to examine the intestinal microbiota dynamics
[76]	2023	plotly	Developing web -based interfaces in order to facilitate data visualization processes of users with limited programming knowledge.	The developed web-based application allowed users to easily visualize data sets and analyze correlations between variables, providing an accessible and effective solution, especially for users with limited programming knowledge.

[77]	2022	rCharts	Performing daily global solar radiation estimates for different cities in Europe and creating future projections according to climate change scenarios.	Six different machine-learning algorithms were generally able to estimate global solar radiation with high accuracy.
[78]	2024	shiny	Developing an indicator panel that associates academic programs with career and income data	Detailed explanation of how to program and publish a dashboard that correlates academic programs with career and income data using R and Shiny
[80]	2022	circlize	Analysis of the molecular structure of consumed carbohydrates	An open-access database called the "Davis Food Glycopedia (DFG)" was created by determining the monosaccharide compositions of more than 800 foods commonly consumed in complementary foods and adult diets.
[81]	2022	dygraphs	Measurement and verification of building energy efficiency and energy savings	A web application has been developed that continuously monitors and documents energy savings.
[82]	2023	Plots.jl	Modeling the growth dynamics of Bio-Film communities, biotechnology, environmental engineering, and microbial ecology	A Julia-based software called Biofilm.jl was developed for simulation and analysis
[84]	2024	Makie.jl	Lithium-ion Battery (LIB) Research, Machine Learning (ML) Applications	Evaluating the applicability of the Variational Autoencoder (VAE) model helps identify dataset features for data preprocessing planning and discusses the interpretability of the ML model
[86]	2024	UnicodePlots.jl	Programming languages, scientific calculation, software engineering, performance analysis.	Compares the potential of Julia and Rust languages in scientific computing
[87]	2024	Matplotlib	Artificial intelligence, health informatics, eye movement tracking, autism spectrum disorder (ASD) diagnosis, neurological disorders	It offers an efficient, low-cost solution for ASD diagnosis using the Convolutional Neural Network (CNN) model.
[88]	2023	Networkx	Electricity transmission networks planning, network analysis	It presents a methodology with the NetworkX library to reduce the number of connection options of electrical transmission networks.[17]
[89]	2025	PyGraphviz	Cybersecurity, malware analysis	A new analysis technique is proposed for malware analysis using graph embedding networks.
[90]	2018	ggplot	Cyber security, malware detection (malware), graphic neural networks	The detection model developed by combining deep neural network and graph embedding methods gives 97.7% accuracy, 96.6% sensitivity, 96.8% recall and 96.4% F1-score.
[91]	2014	Glumpy	Parallel Calculation, High Performance Calculation	With the use of local memory, it aimed to improve performance by eliminating global memory access delay and analyzed the performance differences between local memory and global memory on eight different calculation devices.
[92]	2024	Plotly	The spread of sound waves, material science	Provides information such as phase and group velocities, power flow angle, enhancement factors, and polarization vectors based on elastic moduli and density of the material with the Python code SEISMIC
[93]	2024	Seaborn	Psychology, Machine Learning (ML) Techniques	Decision trees, random forests, gradient boosting, stochastic gradient boosting and XGBoost algorithms and their applications in psychology are explained and visualized in the Python environment.
[94]	2020	Pygal	Materials science, thermochemistry	Converting data into thermochemical properties and performing thermodynamic analyses with the Python-based pMuTT (multiscale thermochemistry toolbox) software library
[95]	2023	Bokeh	Decision support systems, fuzzy cognitive mapping	An open source web-based application called In-Cognitive has been developed using Bokeh, which guarantees solution convergence and is capable of performing Monte Carlo uncertainty analysis.
[96]	2022	Vispy	Structural analysis, modeling of historical structures	The software, Cloud2FEM, has been developed as an open source Python-based tool that automatically generates finite element meshes (FEM) from point cloud data of historical and existing structures.
[97]	2021	Bqplot	Hydrology, water resources management, reservoir modeling and optimization	Python-based tool called iRONS (Interactive Reservoir Operations Notebooks and Software) was developed for reservoir modeling and optimization.
[98]	2022	Cufflinks	Road safety, winter road maintenance management (WRM), data envelopment analysis	A method to estimate road surface temperature using data envelopment analysis (DEA) and machine learning techniques is proposed to improve the effectiveness of winter road maintenance management (WRM). [18]
[120]	2022	Folium	Big data analytics, data visualization, exploratory data analysis (EDA)	Data visualization and analysis techniques were examined with Python, and exploratory data analysis (EDA) methods were applied. [19,20]
[100]	2021	Folium	Human mobility analysis, social media data mining, big data analytics	The spread of Covid-19 from China and neighboring East Asian countries to the world has been studied using real-time travel data from social media platforms.
[101]	2022	Altair	Hydrology and climate change, water resources management	It shows that the Autocorrelation Function (ACF) method has the highest accuracy rate and especially the Boosted Decision Tree Regression (BDTR) model provides high R ² values in all scenarios.
[102]	2023	Missingno	Network Security and intrusion detection, detection of DDoS attacks	Random Forest algorithm showed the best performance with 97.6% accuracy rate, K-Nearest Neighbors (KNN) and Logistic Regression with 97% and 91.1% accuracy rate respectively.

[103]	2024	Yellowbrick	Waste plastic management and energy production	It shows that the Random Forest model exhibited the best performance on the test data, obtaining an R2 value of 0.941, an RMSE value of 14.69 and an MAE value of 8.66
[104]	2021	Plotnine	Heart rate (HR) detection and bioengineering	The CWT (derivative Gaussian) method achieved superior results compared to MODWT-MRA, CWT (frequency B-spline) and CWT (Shannon) methods.
[105]	2024	Pyvis	Health data analysis, interactive visualization and data analytics	Proposes a disease monitoring and impact analysis methodology based on 71,849 patients
[106]	2024	Holoviews	Genomic research and neuroscience	Presented transcriptomic analysis of 5-HT receptors, revealing differential distribution and prevalence of each Htr subtype across cell classes
[107]	2024	Datashader	Proteomic data analysis and visualization	An open source software package called AlphaRms has been developed to process high-resolution MS data.
[108]	2023	Geopandas	Human mobility analysis and data modeling	Provides the open source Trackintel Python library for human mobility analysis that adapts to different tracking data types

The integration capabilities of data visualization libraries are essential, particularly in the context of big data processing and interdisciplinary projects, as they facilitate seamless data analysis, enhance collaboration across diverse platforms, and support the synthesis of complex information from multiple domains. Future research should focus on developing solutions that enable libraries in languages like Python, Julia, and R to achieve greater integration with other data processing and analytical platforms, such as Apache Spark and TensorFlow. Such integrations can make ETL processes, data processing and visualization processes more fluid. Therefore, in this study, data visualization libraries that are widely used in the literature were examined. Thus, it is anticipated that more efficient data analysis can be achieved. Python libraries such as Matplotlib, Seaborn and Plotly are quite effective in data visualization thanks to their user-friendly interfaces and wide community support. Matplotlib's customization flexibility, Seaborn's powerful analysis capabilities on statistical data and Plotly's interactive graphics make Python a versatile tool. However, there are some limitations in terms of performance on large data sets. The ggplot2 library in the R language draws attention with the aesthetic and flexible design options it offers in data visualization. ggplot2's "Grammar of Graphics" approach allows users to easily create complex visualizations. However, R's adaptation process may take longer than Python. JavaScript libraries such as D3.js, Chart.js, and Three.js offer very convenient options for web-based interactive visualizations. The powerful data binding and dynamic visualization capabilities of D3.js, the simplicity of Chart.js, and the 3D visualization features of Three.js allow JavaScript to find a wide range of use, especially in web applications. However, JavaScript libraries usually require more technical knowledge and coding. Julia's Plots.jl and Makie.jl libraries are recommended for high-performance computing and working with large data sets. Plots.jl's wide format support and Makie.jl's advanced visualization capabilities make Julia a powerful tool in data science and scientific computing. However, Julia's ecosystem is not as mature as other languages, and community support is considered more limited.

Improving the user experience of visualization tools and increasing accessibility will support their adoption by a wide range of users. This requires libraries to be equipped with more user-friendly interfaces and to make visualizations accessible to individuals at different levels. In particular, studies should be conducted on the integration of visualization and interactive graphic design that comply with accessibility standards.

Integrating visualization libraries with artificial intelligence and machine learning can enhance the presentation of data analysis and model outcomes, making it easier to interpret and communicate complex insights. For example, libraries can be enriched with visualization tools that can automatically identify trends and anomalies within the data set. Such integrations can enable users to obtain data insights more quickly and accurately. Data security and privacy are important issues in visualization processes.

4. CONCLUSION

Studies on ergonomic improvements for the user-side use of visualization tools, providing interactive data analysis opportunities, and integrating different data sources are important. More work needs to be done on the performance and scalability of visualization libraries to cope with large data sets and real-time data streams. In particular, future research could focus on optimizing the implementation of interactive and dynamic visualizations for large datasets. Developing algorithms and techniques that enable faster rendering and minimize latency will be essential to improving the efficiency and responsiveness of these visualizations.

This paper provides critical comparisons of visualization libraries based on programming languages to researchers, data analysts, and data scientists working on data visualization libraries, and it is also anticipated that it will contribute to future studies.

REFERENCES

- [1] I. H. Sarker, 'Data Science and Analytics: An Overview from Data-Driven Smart Computing, Decision-Making and Applications Perspective', *SN Computer Science*, vol. 2, no. 5, p. 377, Sep. 2021, doi: 10.1007/s42979-021-00765-8.
- [2] X. Qin, Y. Luo, N. Tang, and G. Li, 'Making Data Visualization More Efficient and Effective: A Survey', *The VLDB Journal*, vol. 29, no. 1, pp. 93–117, Jan. 2020, doi: 10.1007/s00778-019-00588-3.
- [3] J. Nayak *et al.*, 'Intelligent Computing in IoT-Enabled Smart Cities: A Systematic Review', in *Green Technology for Smart City and Society*, R. Sharma, M. Mishra, J. Nayak, B. Naik, and D. Pelusi, Eds., in Lecture Notes in Networks and Systems. Singapore: Springer, 2021, pp. 1–21. doi: 10.1007/978-981-15-8218-9_1.
- [4] I. H. Sarker, 'Deep Learning: A Comprehensive Overview on Techniques, Taxonomy, Applications and Research Directions', *SN computer science*, vol. 2, no. 6, p. 420, 2021, doi: 10.1007/s42979-021-00815-1.
- [5] V. Mathur, Y. Saini, V. Giri, V. Choudhary, U. Bharadwaj, and V. Kumar, 'Weather Station Using Raspberry Pi', in *2021 Sixth International Conference on Image Information Processing (ICIIP)*, Shimla, India: IEEE, Nov. 2021, pp. 279–283. doi: 10.1109/ICIIP53038.2021.9702687.

- [6] D. Demiroglu, R. Das, and D. Hanbay, 'A Key Review on Security and Privacy of Big Data: Issues, Challenges, and Future Research Directions', *Signal, Image and Video Processing*, pp. 1–9, Sep. 2022, doi: 10.1007/s11760-022-02341-w.
- [7] Z. Il-Agure and J. Dempere, 'Review of Data Visualization Techniques in IoT Data', in *2022 8th International Conference on Information Technology Trends (ITT)*, May 2022, pp. 167–171. doi: 10.1109/ITT56123.2022.9863948.
- [8] R. B. Haber and D. A. McNabb, 'Visualization Idioms: A Conceptual Model for Scientific Visualization Systems', *Visualization in Scientific Computing*, vol. 74, p. 93, 1990.
- [9] N. Boukhelifa, J. C. Roberts, and P. J. Rodgers, 'A coordination model for exploratory multiview visualization', in *Proceedings International Conference on Coordinated and Multiple Views in Exploratory Visualization - CMV 2003*, Jul. 2003, pp. 76–85. doi: 10.1109/CMV.2003.1215005.
- [10] S. dos Santos and K. Brodlic, 'Gaining Understanding of Multivariate and Multidimensional Data Through Visualization', *Computers & Graphics*, vol. 28, no. 3, pp. 311–325, Jun. 2004, doi: 10.1016/j.cag.2004.03.013.
- [11] M. Sütlü and R. Daş, 'Graph Visualization of Cyber Threat Intelligence Data for Analysis of Cyber Attacks', *Balkan Journal of Electrical and Computer Engineering*, vol. 10, no. 3, pp. 300–306, Jul. 2022, doi: 10.17694/bajece.1090145.
- [12] 'A Survey of Scholarly Data Visualization | IEEE Journals & Magazine | IEEE Xplore'. Accessed: Nov. 26, 2024. [Online]. Available: <https://ieeexplore.ieee.org/document/8314667/similar#similar>
- [13] I. Soric, D. Dinjar, M. Stajcer, and D. Orescanin, 'Efficient social network analysis in big data architectures', in *2017 40th International Convention on Information and Communication Technology, Electronics and Microelectronics (MIPRO)*, May 2017, pp. 1397–1400. doi: 10.23919/MIPRO.2017.7973640.
- [14] Z. Wang, N. Ferreira, Y. Wei, A. S. Bhaskar, and C. Scheidegger, 'Gaussian Cubes: Real-Time Modeling for Visual Exploration of Large Multidimensional Datasets', *IEEE Transactions on Visualization and Computer Graphics*, vol. 23, no. 1, pp. 681–690, Jan. 2017, doi: 10.1109/TVCG.2016.2598694.
- [15] Y. Ye *et al.*, 'Generative AI for visualization: State of the art and future directions', *Visual Informatics*, vol. 8, no. 2, pp. 43–66, Jun. 2024, doi: 10.1016/j.visinf.2024.04.003.
- [16] Y. Hou, M. Yang, H. Cui, L. Wang, J. Xu, and W. Zeng, 'C2Ideas: Supporting Creative Interior Color Design Ideation with Large Language Model', in *Proceedings of the CHI Conference on Human Factors in Computing Systems*, May 2024, pp. 1–18. doi: 10.1145/3613904.3642224.
- [17] L. Shi, Z. Gao, M. Wang, and A. Liu, 'A mainframe CPU capacity prediction system based on the mathematical modeling', in *ICSSSM12*, Jul. 2012, pp. 537–540. doi: 10.1109/ICSSSM.2012.6252295.
- [18] X. Zhang, Y. Cao, and X. Mu, 'The Dynamic Retrieval Tree Menu Based on Dojo', in *2011 International Conference of Information Technology, Computer Engineering and Management Sciences*, Sep. 2011, pp. 202–205. doi: 10.1109/ICM.2011.116.
- [19] L. Zhuhadar, S. R. Kruk, and J. Daday, 'Semantically enriched Massive Open Online Courses (MOOCs) platform', *Computers in Human Behavior*, vol. 51, pp. 578–593, Oct. 2015, doi: 10.1016/j.chb.2015.02.067.
- [20] Z. Chu and H. Wang, 'An investigation of hotlinking and its countermeasures', *Computer Communications*, vol. 34, no. 4, pp. 577–590, Apr. 2011, doi: 10.1016/j.comcom.2010.05.007.
- [21] M. del P. Salas-Zárate, G. Alor-Hernández, R. Valencia-García, L. Rodríguez-Mazahua, A. Rodríguez-González, and J. L. López Cuadrado, 'Analyzing best practices on Web development frameworks: The lift approach', *Science of Computer Programming*, vol. 102, pp. 1–19, May 2015, doi: 10.1016/j.scico.2014.12.004.
- [22] M. Bostock and J. Heer, 'Protovis: A Graphical Toolkit for Visualization', *IEEE Transactions on Visualization and Computer Graphics*, vol. 15, no. 6, pp. 1121–1128, Nov. 2009, doi: 10.1109/TVCG.2009.174.
- [23] R. D. Saxton *et al.*, 'HILIGT, upper limit servers I-Overview', *Astronomy and Computing*, vol. 38, p. 100531, 2022, doi: <https://doi.org/10.1016/j.ascom.2021.100531>.
- [24] R. R. Zhang *et al.*, 'The web-based user interface for EAST plasma control system', *Fusion Engineering and Design*, vol. 89, no. 5, pp. 558–562, May 2014, doi: 10.1016/j.fusengdes.2014.02.070.
- [25] D. Han, J. Pan, X. Zhao, and W. Chen, 'NetV.js: A web-based library for high-efficiency visualization of large-scale graphs and networks', *Visual Informatics*, vol. 5, no. 1, pp. 61–66, Mar. 2021, doi: 10.1016/j.visinf.2021.01.002.
- [26] D. Li *et al.*, 'ECharts: A declarative framework for rapid construction of web-based visualization', *Visual Informatics*, vol. 2, no. 2, pp. 136–146, Jun. 2018, doi: 10.1016/j.visinf.2018.04.011.
- [27] G. Buchanan and R. Tashakkori, 'A Web-App for Analysis of Honey Bee Hive Data', in *2019 SoutheastCon*, Apr. 2019, pp. 1–6. doi: 10.1109/SoutheastCon42311.2019.9020286.
- [28] A. Satyanarayan, D. Moritz, K. Wongsuphasawat, and J. Heer, 'Vega-Lite: A Grammar of Interactive Graphics', *IEEE Transactions on Visualization and Computer Graphics*, vol. 23, no. 1, pp. 341–350, Jan. 2017, doi: 10.1109/TVCG.2016.2599030.
- [29] R. Lu and S. Cao, 'Highcharts-based implementation of the micro video big data visualization system', in *2017 2nd IEEE International Conference on Computational Intelligence and Applications (ICCI)*, Sep. 2017, pp. 1–5. doi: 10.1109/CIAPP.2017.8167049.
- [30] M. Bostock, V. Ogievetsky, and J. Heer, 'D3 Data-Driven Documents', *IEEE Transactions on Visualization and Computer Graphics*, vol. 17, no. 12, pp. 2301–2309, Dec. 2011, doi: 10.1109/TVCG.2011.185.
- [31] T. B. Chandra and A. K. Dwivedi, 'Chapter 10 - Data visualization: existing tools and techniques', in *Advanced Data Mining Tools and Methods for Social Computing*, S. De, S. Dey, S. Bhattacharyya, and S. Bhatia, Eds., in Hybrid Computational Intelligence for Pattern Analysis, Academic Press, 2022, pp. 177–217. doi: 10.1016/B978-0-32-385708-6.00017-5.
- [32] M. Bostock, 'D3.js - Data-Driven Documents'. Accessed: Nov. 25, 2022. [Online]. Available: <https://d3js.org/>
- [33] <https://www.ibm.com/cloud/learn/data-visualization>, 'What is Data Visualization?' Accessed: Dec. 08, 2022. [Online]. Available: <https://www.ibm.com/cloud/learn/data-visualization>
- [34] <https://www.chartjs.org/>, 'Chart.js \textbar Open source HTML5 Charts for your website'. Accessed: Nov. 25, 2022. [Online]. Available: <https://www.chartjs.org/>
- [35] J. Wang, W. Dou, C. Gao, and J. Wei, 'JSTrace: Fast reproducing web application errors', *Journal of Systems and Software*, vol. 137, pp. 448–462, Mar. 2018, doi: 10.1016/j.jss.2017.06.038.
- [36] <https://dojotoolkit.org/>, 'Dojo Toolkit'. Accessed: Dec. 15, 2022. [Online]. Available: <https://dojotoolkit.org/>
- [37] A. Papantoniou, V. Loumos, M. Poulizos, and G. Rigas, 'A Framework for Visualizing the Web of Data: Combining DBpedia and Open APIs', in *2011 15th Panhellenic Conference on Informatics*, 2011, pp. 240–244. doi: 10.1109/PCI.2011.32.
- [38] prototypejs, 'Prototype JavaScript framework: a foundation for ambitious web applications'. Accessed: Dec. 09, 2022. [Online]. Available: <http://prototypejs.org/>
- [39] Prototype, 'Prototype'. Accessed: Dec. 15, 2022. [Online]. Available: <https://github.com/prototypejs/prototype>
- [40] 'Frameworks for RIAs Development', in <https://services.igi-global.com/resolvedoi/resolve.aspx?doi=10.4018/978-1-4666-6437-1.ch002>, IGI Global, IAD. Accessed: Nov. 27, 2024. [Online]. Available: <https://www.igi-global.com/chapter/frameworks-for-rias-development/www.igi-global.com/chapter/frameworks-for-rias-development/117376>
- [41] EChartsJS, 'EChartsJS \textbar Home Page'. Accessed: Dec. 29, 2022. [Online]. Available: <https://www.echartsjs.com/index.html>
- [42] Idera Inc Company, 'Fusioncharts'. Accessed: Nov. 25, 2022. [Online]. Available: <https://www.fusioncharts.com>
- [43] <https://c3js.org/>, 'C3.js \textbar D3-based reusable chart library'. Accessed: Nov. 30, 2022. [Online]. Available: <https://c3js.org/>
- [44] X. Li, A. Kuroda, H. Matsuzaki, and N. Nakajima, 'Advanced Aggregate Computation for Large Data Visualization', in *2015 IEEE 5th Symposium on Large Data Analysis and Visualization (LDAV)*, Oct. 2015, pp. 137–138. doi: 10.1109/LDAV.2015.7348086.
- [45] O. Laursen, 'Flot: Attractive JavaScript plotting for jQuery'. Accessed: Mar. 20, 2023. [Online]. Available: <https://www.flotcharts.org/>
- [46] vega.github.io/, 'Vega: A Visualization Grammar', Vega. Accessed: Jan. 29, 2023. [Online]. Available: <https://vega.github.io/>
- [47] Z. Fang *et al.*, 'A Java web application based MDSplus data analysis and real-time monitoring system for EAST', *Fusion Engineering and Design*, vol. 147, pp. 11215, 2019, doi: <https://doi.org/10.1016/j.fusengdes.2019.05.034>.
- [48] N. Mukhtar, M. A. Khan, and N. Chiragh, 'Lexicon-based approach outperforms Supervised Machine Learning approach for Urdu Sentiment Analysis in multiple domains', *Telematics and Informatics*, vol. 35, no. 8, pp. 2173–2183, Dec. 2018, doi: 10.1016/j.tele.2018.08.003.
- [49] N. Manick, A. Appigadoo, and B. Z. Cadarsaib, 'Enterprise Architecture for the Fire Rescue Services', in *2019 7th International Conference on Information and Communication Technology (ICOICT)*, Jul. 2019, pp. 1–6. doi: 10.1109/ICOICT.2019.8835254.

- [50] A. Alarcón-Paredes, V. Francisco-García, I. P. Guzmán-Guzmán, J. Cantillo-Negrete, R. E. Cuevas-Valencia, and G. A. Alonso-Silverio, 'An IoT-Based Non-Invasive Glucose Level Monitoring System Using Raspberry Pi', *Applied Sciences*, vol. 9, no. 15, Art. no. 15, Jan. 2019, doi: 10.3390/app9153046.
- [51] R. R. Laher, 'Thoth: Software for data visualization & statistics', *Astronomy and Computing*, vol. 17, pp. 177–185, Oct. 2016, doi: 10.1016/j.ascom.2016.09.003.
- [52] L. N. SHORNA, 'Printing and signing ECG leads in PDF files', Jul. 2012, Accessed: Feb. 09, 2025. [Online]. Available: <https://www.politesi.polimi.it/handle/10589/56923>
- [53] Y. Zhou, Y. Yang, B. Xu, H. Leung, and X. Zhou, 'Source code size estimation approaches for object-oriented systems from UML class diagrams: A comparative study', *Information and Software Technology*, vol. 56, no. 2, pp. 220–237, Feb. 2014, doi: 10.1016/j.infsof.2013.09.003.
- [54] A. N. Privalov and V. A. Smirnov, 'Detection of Fake Educational Sites Using Fuzzy String Match', in *2022 2nd International Conference on Technology Enhanced Learning in Higher Education (TELHE)*, May 2022, pp. 31–36. doi: 10.1109/TELHE55498.2022.9800955.
- [55] S. Kelley, M. Goldberg, M. Magdon-Ismail, K. Mertsalov, W. Wallace, and M. Zaki, 'graphOnt: An ontology based library for conversion from semantic graphs to JUNG', in *2009 IEEE International Conference on Intelligence and Security Informatics*, Jun. 2009, pp. 170–172. doi: 10.1109/ISI.2009.5137292.
- [56] J. Chen, Y. Li, and J. Song, 'Research on Interactive Information Visualization System in Special Academic Discussion', in *2012 Fourth International Symposium on Information Science and Engineering*, Dec. 2012, pp. 59–63. doi: 10.1109/ISISE.2012.22.
- [57] D. Hägele, 'Visualizing Optimization Trajectories', masterThesis, 2019. Accessed: Feb. 09, 2025. [Online]. Available: <https://elib.uni-stuttgart.de/handle/11682/10841>
- [58] P. Ambure, R. B. Aher, A. Gajewicz, T. Puzyn, and K. Roy, "'NanoBRIDGES" software: Open access tools to perform QSAR and nano-QSAR modeling', *Chemometrics and Intelligent Laboratory Systems*, vol. 147, pp. 1–13, Oct. 2015, doi: 10.1016/j.chemolab.2015.07.007.
- [59] A. Renduchintala, F. Jahan, R. Khanna, and A. Y. Javaid, 'A comprehensive micro unmanned aerial vehicle (UAV/Drone) forensic framework', *Digital Investigation*, vol. 30, pp. 52–72, Sep. 2019, doi: 10.1016/j.diin.2019.07.002.
- [60] H. Kassogué, A. Bernoussi, M. Maâtouk, and M. Amharref, 'A two scale cellular automaton for flow dynamics modeling (2CAFDYM)', *Applied Mathematical Modelling*, vol. 43, pp. 61–77, Mar. 2017, doi: 10.1016/j.apm.2016.10.034.
- [61] M. Li, X. Feng, Y. Han, and X. Liu, 'Mobile augmented reality-based visualization framework for lifecycle O&M support of urban underground pipe networks', *Tunnelling and Underground Space Technology*, vol. 136, p. 105069, Jun. 2023, doi: 10.1016/j.tust.2023.105069.
- [62] R. R. Laher, 'Thoth: Software for data visualization & statistics', *Astronomy and Computing*, vol. 17, pp. 177–185, Oct. 2016, doi: 10.1016/j.ascom.2016.09.003.
- [63] C. Song *et al.*, 'Collection of patient-generated health data with a mobile application and transfer to hospital information system via QR codes', *Computer Methods and Programs in Biomedicine Update*, vol. 3, p. 100099, Jan. 2023, doi: 10.1016/j.cmpbup.2023.100099.
- [64] R. Mayerle *et al.*, 'Development of a coastal information system for the management of Jeddah coastal waters in Saudi Arabia', *Computers & Geosciences*, vol. 89, pp. 71–78, Apr. 2016, doi: 10.1016/j.cageo.2015.12.006.
- [65] T. W. Fredian and J. A. Stillerman, 'Web based electronic logbook and experiment run database viewer for Alcator C-Mod', *Fusion Engineering and Design*, vol. 81, no. 15, pp. 1963–1967, Jul. 2006, doi: 10.1016/j.fusengdes.2006.04.009.
- [66] A. Sapan, A. S.-I. Noh, S. Karol, P. Rosenfeld, G. Lee, and B. Shneiderman, 'Community Health Map: A geospatial and multivariate data visualization tool for public health datasets', *Government Information Quarterly*, vol. 29, no. 2, pp. 223–234, Apr. 2012, doi: 10.1016/j.giq.2011.10.002.
- [67] S. Zhang, Y. Li, T. Zhang, and Y. Peng, 'An integrated environmental decision support system for water pollution control based on TMDL – A case study in the Beiyun River watershed', *Journal of Environmental Management*, vol. 156, pp. 31–40, Jun. 2015, doi: 10.1016/j.jenvman.2015.03.021.
- [68] T. J. Overbye and J. Weber, 'Smart Grid Wide-Area Transmission System Visualization', *Engineering*, vol. 1, no. 4, pp. 466–474, Dec. 2015, doi: 10.15302/J-ENG-2015098.
- [69] P. Rajendrakumar, 'The Sorghum Genome: Current Status and Future Prospects', 2021. doi: 10.1007/978-981-15-8249-3_20.
- [70] P. Horovčák, J. Terpák, and B. Stehlíková, 'Selected thermochemical properties of substances and their graphic web presentation', in *Proceedings of the 13th International Carpathian Control Conference (ICCC)*, May 2012, pp. 221–226. doi: 10.1109/CarpathianCC.2012.6228643.
- [71] H. González-Díaz *et al.*, 'Generalized lattice graphs for 2D-visualization of biological information', *Journal of Theoretical Biology*, vol. 261, no. 1, pp. 136–147, Nov. 2009, doi: 10.1016/j.jtbi.2009.07.029.
- [72] M. Mora-Cantalops, S. Sánchez-Alonso, and E. García-Barriocanal, 'A complex network analysis of the Comprehensive R Archive Network (CRAN) package ecosystem', *Journal of Systems and Software*, vol. 170, p. 110744, Dec. 2020, doi: 10.1016/j.jss.2020.110744.
- [73] G. Longo-Minnolo *et al.*, 'Delineating citrus management zones using spatial interpolation and UAV-based multispectral approaches', *Computers and Electronics in Agriculture*, vol. 222, p. 109098, Jul. 2024, doi: 10.1016/j.compag.2024.109098.
- [74] C. Stoiber *et al.*, 'VisAhoi: Towards a library to generate and integrate visualization onboarding using high-level visualization grammars', *Visual Informatics*, vol. 8, no. 3, pp. 1–17, 2024, doi: <https://doi.org/10.1016/j.visinf.2024.06.001>.
- [75] A. S. Moorthy and H. J. Eberl, 'compuGUT: An *in silico* platform for simulating intestinal fermentation', *SoftwareX*, vol. 6, pp. 237–242, Jan. 2017, doi: 10.1016/j.softx.2017.06.004.
- [76] Z. K. Mundargi, K. Patel, A. Patel, R. More, S. Pathrabe, and S. Patil, 'Plotplay: An Automated Data Visualization Website using Python and Plotly', in *2023 International Conference for Advancement in Technology (ICONAT)*, 2023, pp. 1–4. doi: 10.1109/ICONAT57137.2023.10079977.
- [77] M. K. Nematchoua, J. A. Orosa, and M. Afafia, 'Prediction of daily global solar radiation and air temperature using six machine learning algorithms: a case of 27 European countries', *Ecological Informatics*, vol. 69, p. 101643, Jul. 2022, doi: 10.1016/j.ecoinf.2022.101643.
- [78] M. A. Perkins and J. W. Carrier, 'Protocol for programing a degree-to-careers dashboard in R using Posit and Shiny', *STAR Protocols*, vol. 5, no. 1, p. 102902, Mar. 2024, doi: 10.1016/j.xpro.2024.102902.
- [79] M. Figueira, D. Conesa, and A. López-Quílez, 'A shiny R app for spatial analysis of species distribution models', *Ecological Informatics*, vol. 80, p. 102542, May 2024, doi: 10.1016/j.ecoinf.2024.102542.
- [80] J. J. Castillo *et al.*, 'The Development of the Davis Food Glycopedia—A Glycan Encyclopedia of Food', *Nutrients*, vol. 14, no. 8, p. 1639, Apr. 2022, doi: 10.3390/nu14081639.
- [81] A. Severinsen and Ø. Myrland, 'ShinyRBase: Near real-time energy saving models using reactive programming', *Applied Energy*, vol. 325, p. 119798, Nov. 2022, doi: 10.1016/j.apenergy.2022.119798.
- [82] M. Owkes, K. Coblenz, A. Eriksson, T. Kammerzell, and P. S. Stewart, 'Biofilm.jl: A fast solver for one-dimensional biofilm chemistry and ecology', *Computer Physics Communications*, vol. 293, p. 108890, Dec. 2023, doi: 10.1016/j.cpc.2023.108890.
- [83] X. Pu and M. Kay, 'How Data Analysts Use a Visualization Grammar in Practice', in *Proceedings of the 2023 CHI Conference on Human Factors in Computing Systems*, in CHI '23. New York, NY, USA: Association for Computing Machinery, Apr. 2023, pp. 1–22. doi: 10.1145/3544548.3580837.
- [84] A. Yamashita, S. Berg, and E. Figgemeier, 'Unsupervised learning of charge-discharge cycles from various lithium-ion battery cells to visualize dataset characteristics and to interpret model performance', *Energy and AI*, vol. 17, p. 100409, Sep. 2024, doi: 10.1016/j.egyai.2024.100409.
- [85] I. Morales Becerra, E. Anguiano Mondragón, I. Morales Becerra, and E. Anguiano Mondragón, 'Matías Romero Avendaño ve 19. yüzyılın sonlarında Meksika'nın Oaxaca kentindeki kahve üretimi', Accessed: Feb. 09, 2025. [Online]. Available: https://www.scielo.sa.cr/scielo.php?pid=S1409-469X2022000100117&script=sci_arttext&tlng=en
- [86] M. Bitar, 'Rust and Julia for Scientific Computing', *Computing in Science & Engineering*, vol. 26, no. 1, pp. 72–76, Jan. 2024, doi: 10.1109/MCSE.2024.3369988.
- [87] H. N. P. P. Teggi, M. S. Bharadwaj, and R. K., 'Detection of Brain Disorders Using Ocular Responses', in *2024 IEEE International Conference on Distributed Computing, VLSI, Electrical Circuits and Robotics (DISCOVER)*, Oct. 2024, pp. 304–308. doi: 10.1109/DISCOVER62353.2024.10750701.
- [88] M. T. Zonin and M. Sperandio, 'Methodology for Reducing the Connection Possibilities in Transmission Network Expansion

- Planning', in *2023 15th Seminar on Power Electronics and Control (SEPOC)*, Oct. 2023, pp. 1–5. doi: 10.1109/SEPOC58810.2023.10322600.
- [89] H. J. Hadi, Y. Cao, S. Li, N. Ahmad, and M. A. Alshara, 'FCG-MFD: Benchmark function call graph-based dataset for malware family detection', *Journal of Network and Computer Applications*, vol. 233, p. 104050, Jan. 2025, doi: 10.1016/j.jnca.2024.104050.
- [90] S. K. A. Fahad and A. E. Yahya, 'Big Data Visualization: Allotting by R and Python with GUI Tools', in *2018 International Conference on Smart Computing and Electronic Enterprise (ICSCEE)*, Jul. 2018, pp. 1–8. doi: 10.1109/ICSCEE.2018.8538413.
- [91] M. Molero-Armenta, U. Iturrarán-Viveros, S. Aparicio, and M. G. Hernández, 'Optimized OpenCL implementation of the Elastodynamic Finite Integration Technique for viscoelastic media', *Computer Physics Communications*, vol. 185, no. 10, pp. 2683–2696, Oct. 2014, doi: 10.1016/j.cpc.2014.05.016.
- [92] G. Ulian and G. Valdrè, 'SEISMIC, a Python-based code of the quantas package to calculate the phase and group acoustic velocities in crystals', *Computers & Geosciences*, vol. 188, p. 105615, Jun. 2024, doi: 10.1016/j.cageo.2024.105615.
- [93] N. Kováč, K. Ratković, H. Farahani, and P. Watson, 'A practical applications guide to machine learning regression models in psychology with Python', *Methods in Psychology*, vol. 11, p. 100156, Dec. 2024, doi: 10.1016/j.metip.2024.100156.
- [94] J. Lym, G. R. Wittreich, and D. G. Vlachos, 'A Python Multiscale Thermochemistry Toolbox (pMuTT) for thermochemical and kinetic parameter estimation', *Computer Physics Communications*, vol. 247, p. 106864, Feb. 2020, doi: 10.1016/j.cpc.2019.106864.
- [95] T. Koutsellis *et al.*, 'In-Cognitive: A web-based Python application for fuzzy cognitive map design, simulation, and uncertainty analysis based on the Monte Carlo method', *SoftwareX*, vol. 23, p. 101513, Jul. 2023, doi: 10.1016/j.softx.2023.101513.
- [96] G. Castellazzi, N. Lo Presti, A. M. D'Altri, and S. de Miranda, 'Cloud2FEM: A finite element mesh generator based on point clouds of existing/historical structures', *SoftwareX*, vol. 18, p. 101099, Jun. 2022, doi: 10.1016/j.softx.2022.101099.
- [97] A. Peñuela, C. Hutton, and F. Pianosi, 'An open-source package with interactive Jupyter Notebooks to enhance the accessibility of reservoir operations simulation and optimisation', *Environmental Modelling & Software*, vol. 145, p. 105188, Nov. 2021, doi: 10.1016/j.envsoft.2021.105188.
- [98] M. Hatamzad, G. C. P. Pinerez, and J. Casselgren, 'Intelligent cost-effective winter road maintenance by predicting road surface temperature using machine learning techniques', *Knowledge-Based Systems*, vol. 247, p. 108682, Jul. 2022, doi: 10.1016/j.knsys.2022.108682.
- [99] G. Singh, D. K. Misra, C. Tanwar, and P. Narang, 'Visualization and Analysis of Populations', in *2022 International Conference on Machine Learning, Big Data, Cloud and Parallel Computing (COM-IT-CON)*, May 2022, pp. 364–368. doi: 10.1109/COM-IT-CON54601.2022.9850886.
- [100] A. Lavanya, P. Darsha, P. Akhil, J. Lloret, and N. Yogeshwar, 'A Real-Time Human Mobility Visualization of Covid-19 Spread from East Asian Countries', in *2021 Eighth International Conference on Social Network Analysis, Management and Security (SNAMS)*, Gandia, Spain: IEEE, Dec. 2021, pp. 1–8. doi: 10.1109/SNAMS53716.2021.9732103.
- [101] 'Rainfall Forecasting Using Machine Learning Algorithms for Localized Events', *Computers, Materials and Continua*, vol. 71, no. 3, pp. 6333–6350, Jan. 2022, doi: 10.32604/cmc.2022.023254.
- [102] A. Fathima, G. S. Devi, and M. Faizaanuddin, 'Improving distributed denial of service attack detection using supervised machine learning', *Measurement: Sensors*, vol. 30, p. 100911, Dec. 2023, doi: 10.1016/j.measen.2023.100911.
- [103] S. Hooda and P. Mondal, 'Predictive modeling of plastic pyrolysis process for the evaluation of activation energy: Explainable artificial intelligence based comprehensive insights', *Journal of Environmental Management*, vol. 360, p. 121189, Jun. 2024, doi: 10.1016/j.jenvman.2024.121189.
- [104] I. Sadek and B. Abdulrazak, 'A comparison of three heart rate detection algorithms over ballistocardiogram signals', *Biomedical Signal Processing and Control*, vol. 70, p. 103017, Sep. 2021, doi: 10.1016/j.bspc.2021.103017.
- [105] J. Kerexeta-Sarriegi *et al.*, 'Analysing disease trajectories in a cohort of 71,849 Patients: A visual analytics and statistical approach', *International Journal of Medical Informatics*, vol. 188, p. 105466, Aug. 2024, doi: 10.1016/j.ijmedinf.2024.105466.
- [106] R. De Filippo and D. Schmitz, 'Transcriptomic mapping of the 5-HT receptor landscape', *Patterns*, vol. 5, no. 10, p. 101048, Oct. 2024, doi: 10.1016/j.patter.2024.101048.
- [107] S. Willems, E. Voytik, P. Skowronek, M. T. Strauss, and M. Mann, 'AlphaTims: Indexing Trapped Ion Mobility Spectrometry–TOF Data for Fast and Easy Accession and Visualization', *Molecular & Cellular Proteomics*, vol. 20, p. 100149, Jan. 2021, doi: 10.1016/j.mcpro.2021.100149.
- [108] H. Martin, Y. Hong, N. Wiedemann, D. Bucher, and M. Raubal, 'Trackintel: An open-source Python library for human mobility analysis', *Computers, Environment and Urban Systems*, vol. 101, p. 101938, Apr. 2023, doi: 10.1016/j.compenvurbsys.2023.101938.
- [109] X. Chen *et al.*, 'Simulation study on water yield service flow based on the InVEST-Geoda-Gephi network: A case study on Wuyi Mountains, China', *Ecological Indicators*, vol. 159, p. 111694, 2024, doi: <https://doi.org/10.1016/j.ecolind.2024.111694>.
- [110] J. Liu, T. Tang, W. Wang, B. Xu, X. Kong, and F. Xia, 'A Survey of Scholarly Data Visualization', *IEEE Access*, vol. 6, pp. 19205–19221, 2018, doi: 10.1109/ACCESS.2018.2815030.
- [111] P. Paschalis *et al.*, 'Online application for the barometric coefficient calculation of the NMDB stations', *New Astronomy*, vol. 19, pp. 10–18, 2013, doi: <https://doi.org/10.1016/j.newast.2012.08.003>.
- [112] <https://plotly.com/>, 'Plotly: Low-Code Data App Development'. Accessed: Nov. 29, 2022. [Online]. Available: <https://plotly.com/>
- [113] M. L. Waskom, 'seaborn: statistical data visualization'. Accessed: Feb. 02, 2023. [Online]. Available: <https://joss.theoj.org/papers/10.21105/joss.03021>
- [114] J. VanderPlas *et al.*, 'Altair: Interactive Statistical Visualizations for Python', *Journal of Open Source Software*, vol. 3, no. 32, p. 1057, Dec. 2018, doi: 10.21105/joss.01057.
- [115] F. M. / Kozea, 'Pygal: A Python Svg Graph Plotting Library'. Accessed: Nov. 29, 2022. [Online]. Available: <https://www.pygal.org/>
- [116] Bokeh, 'Bokeh Documentation'. Accessed: Nov. 29, 2022. [Online]. Available: <https://docs.bokeh.org/en/latest/index.html>
- [117] M. J. MacLeod *et al.*, 'Invited Review: A Position on the Global Livestock Environmental Assessment Model (gleam)', *Animal*, vol. 12, no. 2, pp. 383–397, Jan. 2018, doi: 10.1017/S1751731117001847.
- [118] <https://matplotlib.org/>, 'Matplotlib 3.6.3 documentation'. Accessed: Feb. 04, 2023. [Online]. Available: <https://matplotlib.org/stable/index.html>
- [119] J. D. Hunter, 'Matplotlib: A 2D Graphics Environment', *Computing in Science & Engineering*, vol. 9, no. 3, pp. 90–95, 2007, doi: 10.1109/MCSE.2007.55.
- [120] G. Singh, D. K. Misra, C. Tanwar, and P. Narang, 'Visualization and Analysis of Populations', in *2022 International Conference on Machine Learning, Big Data, Cloud and Parallel Computing (COM-IT-CON)*, May 2022, pp. 364–368. doi: 10.1109/COM-IT-CON54601.2022.9850886.
- [121] Folium, 'Folium 0.14.0 documentation'. Accessed: Feb. 05, 2023. [Online]. Available: <https://python-visualization.github.io/folium/>
- [122] M. S. Kahil, A. Bouramoul, and M. Derdour, 'Multi Criteria-Based Community Detection and Visualization in Large-Scale Networks Using Label Propagation Algorithm', in *2021 International Conference on Recent Advances in Mathematics and Informatics (ICRAMI)*, Sep. 2021, pp. 1–6. doi: 10.1109/ICRAMI52622.2021.9585964.
- [123] MIT, '<https://github.com/plotly/plotly.py>'. Accessed: Feb. 05, 2023. [Online]. Available: <https://github.com/plotly/plotly.py>
- [124] J. Heer, S. K. Card, and J. A. Landay, 'prefuse: a toolkit for interactive information visualization', in *Proceedings of the SIGCHI Conference on Human Factors in Computing Systems*, in CHI '05. New York, NY, USA: Association for Computing Machinery, Apr. 2005, pp. 421–430. doi: 10.1145/1054972.1055031.
- [125] Blokt, 'Flare \textbar Data Visualization for the Web', Blokt - Privacy, Tech, Bitcoin, Blockchain & Cryptocurrency. Accessed: Dec. 02, 2022. [Online]. Available: <https://blokt.com/tool/prefuse-flare>
- [126] X. Zhang, C. Zhao, and X. Wang, 'A Survey on Knowledge Representation in Materials Science and Engineering: An Ontological Perspective', *Computers in Industry*, vol. 73, pp. 8–22, Oct. 2015, doi: 10.1016/j.compind.2015.07.005.
- [127] S. Purushe, S. K. Anbalagan, and G. Grinstein, 'Development of an Interactive Ramchandran Plot in Weave', in *2011 15th International Conference on Information Visualisation*, Jul. 2011, pp. 232–236. doi: 10.1109/IV.2011.109.
- [128] C. Dempsey, 'Weave - Open Source Data Visualization', GIS Lounge. Accessed: Dec. 23, 2022. [Online]. Available: <https://www.gislounge.com/weave-open-source-data-visualization/>

- [129] A. Baumann, S. Shams, M. Ross, W. Mass, and G. Grinstein, 'Enhancing STEM classes using weave: A collaborative web-based visualization environment', in *2011 Integrated STEM Education Conference (ISEC)*, Apr. 2011, pp. 2A-1-2A – 4. doi: 10.1109/ISECon.2011.6229637.
- [130] R. Agrawal, A. Kadadi, X. Dai, and F. Andres, 'Challenges and Opportunities with Big Data Visualization', in *Proceedings of the 7th International Conference on Management of computational and collective intelligence in Digital EcoSystems*, Caraguatutuba Brazil: ACM, Oct. 2015, pp. 169–173. doi: 10.1145/2857218.2857256.
- [131] L. Wilkinson, *The Grammar of Graphics*. Springer Science & Business Media, 2013.
- [132] N. Kruchten, A. M. McNutt, and M. J. McGuffin, 'Metrics-Based Evaluation and Comparison of Visualization Notations', *IEEE Transactions on Visualization and Computer Graphics*, vol. 30, no. 1, pp. 425–435, 2024, doi: 10.1109/TVCG.2023.3326907.
- [133] S. G. A. Swaminathan, J. B. J. S. R., and L. Nelson, 'IPL Data Analysis and Visualization for Team Selection and Profit Strategy', in *2023 7th International Conference on Computing Methodologies and Communication (ICCMC)*, 2023, pp. 592–598. doi: 10.1109/ICCMC56507.2023.10083736.

BIOGRAPHIES

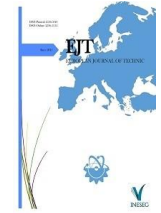
Faruk Aksoy works as a lecturer at Dicle University Ergani Vocational School Computer Technologies Department. He graduated from Selçuk University Computer Systems Teaching Department and Batman University Computer Engineering Department. He has a master's degree in Electronics-Computer Education from Firat University. He continues his doctoral studies at Firat University Software Engineering Department. His current research interests include data science, data visualization, and big data analysis.

Mehmet Özdem received the B.S. degree in Electrical and Electronics Engineering from Başkent University, Ankara, Turkey, and received the M.S degree in Information Systems from the Middle East Technical University Informatics Institute Ankara, Turkey. Currently, he is a Ph.D. student at Gazi University Faculty of Technology, and his research interests are applying open-source SDN/NFV Technologies to the services used in network infrastructure and observing effects on system performance. "Performance of distribution Networks under VBR video traffic" paper was presented at IEEE SoutheastCon 2007, Richmond, VA, USA. Since 2003, he has been with the Turk Telekom, Ankara, Turkey where he is currently network architecture and design group manager. During this time, he is involved in huge projects like NFV/SDN, IP/MPLS network design, IPTV, NGN Transformation, ATM optimization, DPI, L2/L3 VPN service developments, managing end to end architectural design for both mobile/fixed networks. He is closely working with international organizations (ITU, ETSI, ONF) about network architecture, evolution and convergence of future networks. He works as a Vice Chair of ITU-T SG12 (Performance, QoS and QoE) group. He also has CCIE R&S, PMP and ITIL certifications

Resul Das is a full professor in the Department of Software Engineering at the Faculty of Technology, Firat University. He received his B.Sc. and M.Sc. degrees in Computer Science from Firat University in 1999 and 2002, respectively, and completed his Ph.D. in Electrical and Electronics Engineering in 2008. Between 2000 and 2011, he served as a lecturer in the Department of Informatics and concurrently worked as a network and system administrator at the University's IT Center. Since 2002, he has been an instructor in the Cisco Networking Academy Program, delivering CCNA and CCNP courses. From September 2017 to June 2018, he conducted research as a visiting professor at the University of Alberta, Edmonton, Canada, under the TUBITAK-BIDEB 2219 Postdoctoral Research Fellowship program. He also held the position of Head of the Department of Software Engineering from March 2020 to April 2023.

Professor Das has served in editorial roles for several prestigious academic journals. He was an Associate Editor for IEEE Access and the Turkish Journal of Electrical Engineering and Computer Science. Currently, he is an Associate Editor for several Elsevier journals, including Internet of Things, Alexandria Engineering Journal, and Telematics and Informatics Reports, as well as the IEEE Open Journal of the Communications Society (OJ-COMS) and the International Journal of Grid and Utility Computing (Inderscience).

Globally recognized for his academic contributions, Prof. Das has been consistently listed among the top 2% of the "World's Most Influential Scientists," compiled by Stanford University researchers, for five consecutive years (2019-2024). His research interests include computer networks, cybersecurity, IoT and systems engineering, data science and visualization, and software quality assurance and testing.



Research Article

Energy Geopolitics and Policies: The Case of Türkiye

İdris Demir^{1*}, Sevda Korhan Baris²¹Social Sciences University of Ankara, Department of International Relations, Ankara, Türkiye. (e-mail: idris.demir@asbu.edu.tr).²Batman University, International Relations Office, Batman, Türkiye. (e-mail: sevdakorhan.baris@batman.edu.tr).

ARTICLE INFO

Received: Apr., 20. 2025

Revised: May., 30. 2025

Accepted: Jun., 30. 2025

Keywords:

Energy Geopolitics

Energy Policies

Energy Security

Global Energy Policies

Türkiye's Energy Policies

Corresponding author: İdris Demir

ISSN: 2536-5010 / e-ISSN: 2536-5134

DOI: <https://doi.org/10.36222/ejt.1680126>

ABSTRACT

This article aims to analyze energy geopolitics and policies in a historical, global, and national context through the case of Türkiye and to highlight the impact of energy on economic growth, security, and foreign policy. In this context, how access to energy resources shapes geopolitical balances is specifically analyzed. The relationship between energy resources and political power from the Industrial Revolution to the present day is analyzed, with a particular focus on the strategic role of oil and natural gas. In addition, concepts such as energy security, resource diversity, and geographical distribution are analyzed within the framework of international relations. The actors of global energy policies, the factors affecting the decision-making processes of these actors, and the systematic effects of energy crises are presented with examples. In the context of Türkiye, some of the advantages of the country's geographical location are analyzed within the framework of its role in energy transit routes and its dependence on imports. In addition, Türkiye's strategic and policy objectives, such as increasing domestic production, ensuring resource diversification, and shifting towards renewable energy, are included. This study offers a unique assessment of Türkiye's energy policy, examining it not only in terms of its geographical location but also at the intersection of energy transition, sustainability, and foreign policy. Through a thematic analysis method based on policy documents, a holistic relationship between energy investments, diplomatic initiatives, and security strategies has been revealed. The findings obtained in this context demonstrate that Türkiye's energy projects carry not only technical but also geopolitical implications.

1. INTRODUCTION

Energy plays a critical role in shaping modern societies as a key driver of economic growth and technological development. In particular, access to fossil resources such as oil and natural gas is of strategic importance for energy-dependent countries. In this context, energy has become not only an economic but also a geopolitical issue, triggering political and economic competition over energy resources. In this context, energy geopolitics, as a sub-branch of the discipline of energy geography, has emerged as a field that examines the balance of power and interest relations arising from the geographical distribution of energy resources and states' access to these resources [1].

With the rise of renewable energy sources and the decline in dependence on traditional sources, the global energy structure is undergoing a transformation. However, this transition also brings conflict risks due to energy supply security and geographical inequalities [2]. Most recently, the Russia-Ukraine War has destabilized energy supply, fluctuated energy prices, and caused countries to reshape their energy policies [3]. The crisis caused disruptions in the import and export of oil and natural gas and weakened the security of the energy supply. Consequently, this situation has led to

difficulties in meeting global energy demand, increased energy prices, increased costs, and hampered economic growth [4].

These developments have also disrupted the process of achieving the goals of the Paris Climate Agreement; carbon emissions have continued to increase outside the pandemic period [5]. In this context, energy policies are now being managed through political and strategic processes that include not only environmental but also geopolitical and economic dynamics. At this point, Türkiye is considered a key actor in energy transit due to its geostrategic position and shapes its policies, such as energy security and resource diversity, accordingly.

The transformation process of energy systems is also shaped by international agreements and climate commitments in the context of both supply security and economic development. In this context, the United Nations Sustainable Development Goals (particularly SDG 7 and 13), the Paris Agreement, and the Net Zero targets announced after COP26 have become decisive in determining the direction, pace, and technological preferences of energy investments. In this context, scenarios developed by the IEA, IRENA, and the European Commission propose transformations on the energy supply and demand sides with the aim of limiting global temperature increase to 1.5°C by 2050, emphasizing the need

to integrate energy efficiency, electrification, carbon removal technologies, and green financing tools [6]. In this context, it is evident that energy policies are beginning to take shape within a framework that transcends national borders, and that Türkiye must critically consider this multi-layered context in its energy transition process.

With the adoption of the Paris Agreement at COP21, the relationship between energy policies and climate diplomacy has become more visible [7]. In this context, countries are committing to both emission reductions and energy production transformation through their Nationally Determined Contributions (NDCs), which they update every five years. At the COP26, 27, and 28 summits, the goal of limiting global temperature increase to 1.5°C was clearly stated scientifically, but data as of 2023 showing that this limit has been exceeded demonstrates how fragile these goals are [8]. The scenarios developed to overcome this fragility divide the energy transition into different strategic paths; some focus on electrification and efficiency, while others propose solutions based on carbon removal technologies. This diversity highlights that energy policies encompass technical, normative, and geopolitical dimensions.

This study aims to contribute to the literature by examining Türkiye's energy policies not only in terms of transit routes and access to resources but also in a comprehensive manner within the context of the energy transition process, sustainability goals, and foreign policy. In this regard, the overlapping objectives between Türkiye's energy projects and foreign policy strategies have been analyzed using thematic content analysis, and the interaction between energy security, environmental sustainability, and regional diplomacy has been evaluated in a multidimensional manner.

In this study, the historical process of energy geopolitics, energy policies, Türkiye's place in this field, and the policies it pursues will be discussed in general terms. The historical development of energy geopolitics will be examined comprehensively, starting from the Industrial Revolution, through the Cold War period, to the present day, especially in the 21st century, when renewable energy resources have come to the fore. Energy geopolitics will be evaluated within the framework of basic topics such as energy security, resource diversity, and geographical distribution of energy resources. In the case of Türkiye, energy geopolitics and policies will be discussed in detail; the country's geopolitical position, its role in energy corridors, its existing and potential energy resources, and its relations and cooperation in the field of energy will be analyzed. In addition, this study will provide a broad view from the Turkish perspective and include policy evaluations in the context of ensuring energy security, increasing renewable energy investments, and regional and international cooperation.

2. HISTORICAL DEVELOPMENT OF ENERGY GEOPOLITICS

The indirect relationship between energy and national power has been an important element of state policies since the Industrial Revolution. The success of England and Germany in the industrialization process, thanks to their coal resources, constitutes one of the important examples of the link between energy resources and economic and military power [9, 10]. By the 20th century, oil had replaced coal and assumed a key role in energy production thanks to its advantages, such as high

energy density and easy portability [11]. During this period, the United States considered access to overseas oil resources as one of its main geopolitical priorities [12].

After the Second World War, the US increased its regional influence through energy by making oil deals with countries such as Saudi Arabia and Iran. The US also strengthened its military presence in the region to ensure the security of oil resources [13]. In fact, it can be said that the post-World War II period was characterized by relatively abundant and cheap oil. This stimulated global economic growth and enabled the development of new industries and markets. Highway construction, suburban housing, and air travel are some of the important trends that helped increase oil consumption during this period. In addition, the petrochemical industry - plastics, synthetic fibers, and other petroleum-based products - expanded greatly during this period. Continued oil discoveries and relatively low extraction costs made it possible for oil to be widely used and for new industries and markets to emerge [14].

However, the OAPEC (now OPEC) embargo in response to the Yom Kippur War in 1973 triggered the global oil crisis and brought energy security to the forefront of the agenda in Western countries [15]. In terms of major industrial powers such as the US, Japan, and Western Europe, the fact that these countries meet a significant portion of their energy needs from the Persian Gulf has increased their dependence on the region. The US, in particular, has adopted establishing close relations with the oil-rich states in the Middle East as a strategic priority to sustain its economic growth and ensure energy supply security [16]. In this context, strategic gateways such as the Strait of Hormuz began to play a critical role in global energy security [17].

During the Cold War, access to oil resources became one of the determining factors in the balance of power that ideological blocs tried to establish. The importance of the oil reserves of the Middle East and the Gulf countries increased even more during this period. The decline in domestic production in the US and nationalist movements in the Middle East led to supply disruptions and price hikes [18].

The crises of the 1970s reshaped US energy strategies; energy policies against the Soviet Union became a priority. Even if the oil crises were not directly caused by the conflict between the US and the Soviet Union, they had a significant impact on the Cold War. The US withdrawal from Vietnam, the Watergate crisis, the wave of revolutions in the Third World, the Soviet Union's nuclear parity with the US, and the decline in US oil production due to increased competition from Western Europe and Japan coincided with the period of oil crises [18].

The post-1990s period, after the end of the Cold War, established a clearer and more visible link between access to energy resources and security, and energy became one of the main elements of the new security paradigm [11]. In this process, the possession of energy resources began to be perceived as a direct reflection of economic and military power. Indeed, when we look at the energy geopolitics of the 20th century, it can be seen that the struggles over the control and distribution of oil resources were the main factors determining the strategic and economic dynamics of this period. In the post-Cold War era, Russia consolidated its geopolitical power by controlling energy resources in Central Asia and the Caucasus, while China's Belt and Road Initiative reshaped the economic and energy balances in the region [19, 20]. This competition has increased the geopolitical value of

energy transmission lines and made energy diplomacy a key strategic tool in foreign policy [21].

By the 21st century, the importance of renewable energy sources had increased, and energy policies had begun to take shape in line with goals of environmental sustainability and carbon neutrality. Geopolitical crises such as the Ukraine War brought the question of the reliability of fossil fuels to the agenda and accelerated the shift towards technologies such as zero emission [22, 23]. On the other hand, OPEC's influence on the market continues to shape global energy balances with volatility in energy prices and supply-demand imbalances [24].

3. GLOBAL ENERGY GEOPOLITICS

The concept of geopolitics was first used by Rudolf Kjellén in 1905 and is characterized as an approach to explain the position of nation-states in the international balance of power through geographical, historical, and social factors [25]. Kjellén's views were later developed by theorists such as Ratzel, Mackinder, and Mahan, creating new areas of analysis through the political effects of energy resources [26]. In this context, geopolitics evaluates the effects of geography on both domestic and foreign policy through elements such as borders, resources, and population [25, 27].

The increasing competition over energy resources during the Cold War and decolonization periods reinforced the importance of energy geopolitics [28]. The crises in the Middle East brought energy-based political strategies to the forefront; factors such as geographical location, administrative structure, and natural resources have been decisive in energy geopolitics [29]. The oil-rich Persian Gulf and Caspian Basin have become one of the main lines of regional instability and military tensions [27].

Today, the ownership of energy resources is considered a major indicator of geopolitical power. While the US, Saudi Arabia, and Russia are the largest producers, the US, China, and India are among the largest consumers [30, 31]. This situation creates the need for two opposite concepts, such as "competition" and "cooperation" over energy resources at the same time. In this context, the impact of energy geopolitics on the balance of power in the international system becomes inevitable. However, since the positioning of the great powers in the global system varies according to the geographical distribution of energy resources, it can sometimes encourage cooperation and sometimes bring about polarization and conflict. In this process, states are observed to act according to their geostrategic goals.

The fact that control over energy resources and transportation routes plays such an important role in global power struggles is embodied in the intense interest in the Middle East. Similarly, geopolitical and geostrategic struggles over the Caspian Basin and Central Asia constitute one of the main lines of energy competition in the 21st century [14].

While the weakening of US hegemony has led to fundamental changes in the international oil system, the decline in America's production capacity has also limited its "capacity to provide energy to allies" that it maintained throughout the post-Cold War period [32]. Keohane sees this development as "a widening of the space for international cooperation" and characterizes crises as incentives for cooperation. Indeed, the economic summits of 1975 were born in response to events such as the oil crisis and the collapse of Bretton Woods, and ultimately aimed to increase coordination among major economies [32]. Similarly, the transition from coal to synthetic

oil from the oil crises of the 1970s to the current "golden age of gas" has been shaped by cooperation between states and energy companies [33]. In this context, the \$100 billion oil deal between Russia and China in 2009 and the \$400 billion natural gas deal in 2014 deepened the strategic partnership in the energy field. The ultimate outcome of this cooperation was to increase China's energy security while providing economic and political advantages to Russia [34].

In conclusion, from a realist perspective, it can be said that the struggle for access to energy resources and energy security is often accompanied by competition and power struggle. In particular, the fact that most of the hydrocarbon reserves are concentrated in regions such as the Middle East, Russia, and Venezuela increases the competition for access to resources among energy-importing countries (See Table I). Developing countries such as Brazil, Indonesia, Malaysia, South Korea, and Türkiye are also participating in this competition, both to meet their energy needs and to have a greater say on a global scale [14].

TABLE I
TOP 10 COUNTRIES WITH THE LARGEST OIL RESERVES IN 2024

Rank	Country	Oil Reserves (billion barrels)	Share of Global Reserves
1	Venezuela	303.8	%17.6
2	Saudi Arabia	297.5	%17.3
3	Canada	168.1	%9.8
4	Iran	157.8	%9.2
5	Iraq	145.0	%8.4
6	Russia	107.8	%6.3
7	Kuwait	101.5	%5.9
8	United Arab Emirates	97.8	%5.7
9	United States	68.8	%4.0
10	Libya	48.4	%2.8

However, some views question the classical understanding of energy geopolitics. According to them, traditional factors such as energy resources have become less influential, while relatively new factors such as technology, ideology, and economics have become more decisive [35]. Indeed, several paradigmatic shifts such as nuclear deterrence, the end of colonialism, and environmental concerns, support this view. However, fossil fuels continue to meet the bulk of energy demand. Although the share of renewable energy in electricity generation is increasing, it is still far from meeting the total energy supply. After all, even in the most affluent countries of the world, the proportion of electricity provided by wind and solar energy combined in their electricity sectors has not reached more than one-third of the total [23].

In addition, the other side of energy geopolitics puts pressure on fossil fuel industries with demands for environmental sustainability. In this context, governments and NGOs are focused on developing solutions to reduce carbon emissions [2]. Technologies such as LNG, shale gas, and integrated refineries increase energy efficiency, while strategies supported by technologies such as artificial intelligence, blockchain, and the Internet of Things provide a significant competitive advantage in the sector [22, 36].

3.1. Diversity of Energy Resources

Diversifying energy sources is of strategic importance for energy supply security, cost reduction, and mitigation of geopolitical risks. This diversification includes renewable energy (solar, wind, hydro), nuclear, and fossil fuels (oil,

natural gas, coal). Renewable resources are critical for sustainable development in the long term as they can be continuously replenished. However, costs, technical barriers, and lack of infrastructure can make their utilization difficult. Technological advances and government support can mitigate these problems [37].

Nuclear energy offers an environmentally friendly alternative with low carbon emissions, but poses challenges such as the risk of radioactive waste and plant safety [38]. Fossil fuels still meet most of the world's energy needs. In 2020, oil and natural gas met 31.2% and 24.7% of energy demand, respectively. By 2040, oil and natural gas demand are expected to increase by 34% and 70%, respectively. On the other hand, while the share of coal is decreasing, the importance of renewable energy sources is increasing [39].

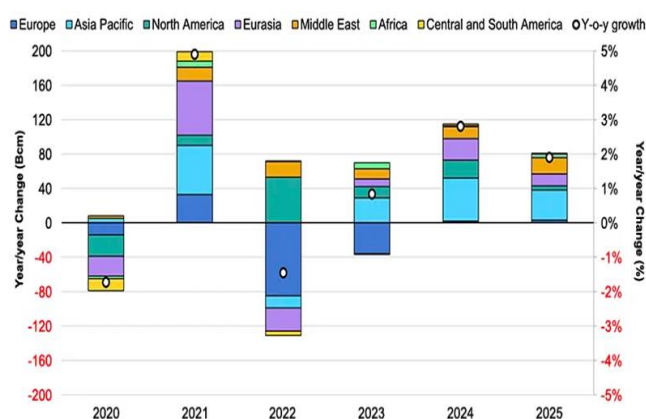


Figure 1. Global Natural Gas Demand Growth in the 2020-2025 [40].

According to BP projections, energy demand is expected to increase by up to 25% by 2050, and energy resource diversity will play an important role in managing this demand. In the Rapid scenario, the share of fossil fuels falls to 18%, natural gas rises to 21%, and the share of renewable and non-fossil sources rises to 60% [41]. According to the Net-Zero Emissions scenario, global energy expenditures will shift towards electricity and renewables, while spending on oil products is projected to decline dramatically (See Figure 2).

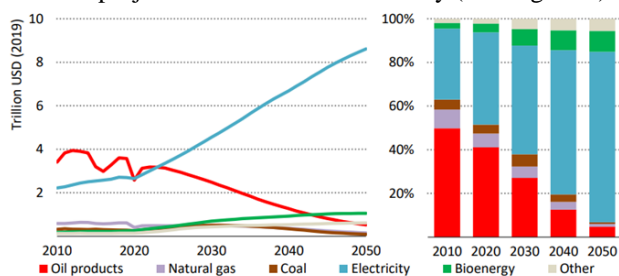


Figure 2. Global Energy Spending by Fuel in the Net-Zero Emissions [42].

The concentration of energy resources in certain countries forces energy importers to establish strategic alliances, which increases geopolitical risks based on energy imports [33]. In particular, Russia's invasion of Ukraine has reshaped Europe's energy policies, forcing them to increase investments in renewable resources and energy efficiency [3]. This could lead to an increase in energy costs, disruption of industrial activities, and public discontent. Such a crisis may encourage governments to use more coal and nuclear energy as a short-term solution [43].

3.2. Geographical Distribution of Energy Resources

Geography and natural resources have historically been the main determinants of states' foreign policies and international strategic orientations. A country's strategic location - for example, its proximity to important sea routes, energy reserves, or transmission lines - directly affects its capacity for economic growth, security, and geopolitical influence. In this context, access to and control over energy resources have become a decisive factor shaping international power relations. Countries form alliances or engage in conflicts to maintain or increase access to these resources.

Russia-Iran relations are a concrete example that can be considered within this framework. Russia, which has distanced itself from Western actors since the 2000s, has deepened its strategic cooperation with non-Western countries such as Iran. While the geo-economic interests of both countries in the Caspian Sea reinforce this relationship, this partnership, which has developed in a geographical and historical context, coincides with Russia's "near abroad" strategy [44, 45]. This dynamic shows that geopolitical relations are shaped by the balance of power as well as regional history and spatial configurations.

This approach, integrated with Kjellén's definition of geopolitics, redefines the power and influence of states in the international arena with access to energy resources. In particular, strategic infrastructures such as pipelines, ports, and energy corridors, coupled with the economic and political value of this access, provide states with a significant advantage.

In this context, it can be said that classical geopolitical theories still retain their explanatory power. Halford Mackinder's Heartland Theory defined the natural resource-rich interior regions of Eurasia as the axis of the global power struggle [46, 47]. This idea was reinterpreted in Brzezinski's "Grand Chessboard" metaphor, emphasizing the decisive influence of whoever dominates Eurasia on Western Europe, East Asia, and the Middle East [48]. While traditional geopolitical approaches are still valid, new layers such as technology, energy infrastructure, and economic integration have been added to this framework.

The geographical remoteness of energy resources increases both logistical costs and national security risks. Most oil and natural gas reserves are concentrated in the Middle East, North Africa, and Russia, while Europe, the US, and Asia, which are major consumers, are geographically distant from these resources [33] (See Figure 3).

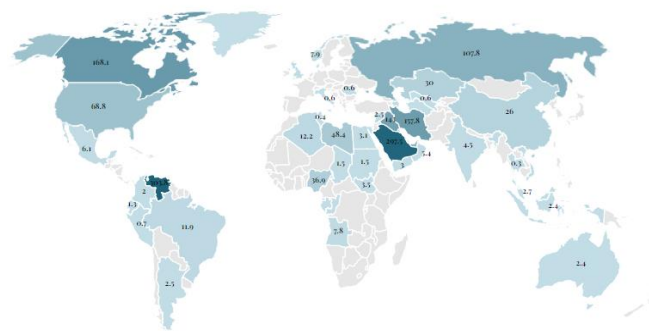


Figure 3. Oil Reserves by Country [49].

This situation is known to lead to cost increases and political tensions in energy trade. In addition, many of the

regions where energy reserves are concentrated face political and social instability. Civil wars in the Middle East, infrastructure deficiencies in Africa, and harsh natural conditions in Central Asia directly and indirectly affect energy production and transportation [33]. Such geographical and political barriers create uncertainty in energy supply and complicate energy-based foreign policies.

3.3. Global Energy Policies

Today's global energy policies are driven by a number of actors with different interests and priorities. Their decisions are decisive on key issues such as energy security, resource management, prices, infrastructure investments and combating climate change [12]. As such, energy policies can often become a negotiation process characterized by bargaining, interdependence and conflicts of interest.

The advantage of holding energy resources can elevate states to an important position in energy policies. Especially the oil and natural gas-rich countries in the Middle East owe their strong position in the energy markets to these resources. According to BP data, 93.5% of the world's proven oil reserves are under the control of only 14 countries [50]. However, political instability in these countries brings with it more complex factors that shape their energy policies. International relations theories often consider this situation within the framework of multifactorial cause-and-effect relationships and argue that political stability is as decisive as the availability of energy resources [51].

Energy geopolitics lies in the so-called “gray area” between power politics and markets. This space is highly sensitive to conjunctural shifts. For instance, Russia, which was a reliable energy partner for Europe before the Ukraine Crisis, started to use energy as a tool of pressure after the crisis. This has contributed to the positioning of energy not only as a market but also as a power. Russia used the power of its energy to influence the European economy and politics. This development has created the necessity to embrace energy as an instrument of economic and geopolitical power. In the face of this situation, European countries have resorted to diversifying their imports by developing alternative policies to reduce their energy dependence on Russia [52].

In this context, energy security has become a multidimensional phenomenon. Factors such as resource diversity, reducing external dependence, strengthening infrastructure, and environmental sustainability are among the main components of energy security. In recent years, the main drivers of the energy transition that countries have been trying to realize, such as reducing the use of fossil fuels and achieving net-zero carbon targets, have also become priorities in energy policies. This transformation in energy policies can be said to be related to the concept of the “energy trilemma”, which combines three factors: security, accessibility, and sustainability [53].

Energy transition is a structural and long-term transformation process that refers to the shift from fossil fuel-based systems to low-carbon, sustainable, and digitized energy infrastructures. This transformation is not merely a technical change; it also involves economic, administrative, and social restructuring. While only a limited number of countries had set renewable energy targets at the beginning of the 2000s, these targets have nearly reached a universal level in the post-2020 period, with global public support for clean energy investments

exceeding USD 2 trillion. However, the majority of these resources are concentrated in developed economies such as China, the EU, and the US, while developing countries still face structural and financial barriers [54, 55].

Despite some progress, it can be said that this transition process faces many structural challenges. In particular, factors such as infrastructure dependence on fossil fuels, the high costs of renewable technologies, and insufficient energy storage capacity are slowing down and hindering this process. On the other hand, the fact that the transformation of the energy system requires changes at the technical, political, economic, and social levels further complicates this process [16].

The International Energy Agency (IEA) predicts that the world's population will increase by around 2 billion by 2040, leading to a 50% increase in electricity consumption as living standards rise. Currently, 66% of energy demand is met by fossil fuels, a proportion that is projected to remain largely unchanged until 2050. In the same period, a 28% increase in natural gas demand and a 17% increase in oil demand are expected [56].

As of 2021, daily oil production is around 93 million barrels, while consumption is over 100 million barrels. The pressure on the global energy market caused by increasing energy demand in large countries such as China is a harbinger that this ratio will increase day by day [3]. The Energy Information Administration (EIA) estimates that if current policies continue, global energy consumption will increase by 50% by 2050 [57].

Some experts argue that these risks can be mitigated by developing accessible energy sources, even if they are more expensive. Some, such as Daniel Yergin, argue that this approach will both increase political cooperation and encourage R&D for more sustainable energy solutions [33].

In this case, sustainability has become a key element not only of environmental policies but also of development strategies. At this point, it is essential that the energy transition of countries takes place without completely disconnecting from fossil fuels. Ultimately, while the demand for oil and natural gas will continue to persist in this process, the countries that control resources will also maintain their influence on global policies. Moreover, the rise of actors such as Russia, China, and India is redefining the position of actors such as the US and the European Union (EU) in the international system, while regional powers such as Türkiye continue to increase their geopolitical importance [12].

This global energy geopolitical framework provides a meaningful backdrop for assessing Türkiye's energy strategies and foreign policy preferences. Türkiye is one of the few countries where global dynamics directly influence local policy-making processes, due to both its geographical location and its dependence on energy imports. In the following section, we will analyze how global trends are reflected in Türkiye's energy security, energy supply diversity, and green transformation strategies. With this transition, we will explain how the transnational effects of the geopolitical energy conjuncture play a transformative role in Türkiye's domestic policy-making.

4. TÜRKİYE'S ENERGY POLICIES

Daniel Yergin traces the root causes behind the conflicts over the Middle East's oil reserves throughout the 20th century to the birth of the oil industry. According to Yergin, the complex

and complicated relations between the Ottoman Empire, Britain, and Germany outlined the framework of energy competition in the region. The “Treaty of Foreign Affairs” signed in 1914 on the initiative of one of the prominent figures in this context, the Armenian-born businessman Calouste Gulbenkian (known as “Mr. Five Percent” due to his 5% share in international oil deals), distributed important oil concessions among the Anglo-Persian Group, Deutsche Bank and Shell, limiting the influence of external actors in energy production in the Ottoman territories (except for Egypt, Kuwait and some areas on the Turkish-Iranian border). Yergin argues that this agreement shaped the development and control of the Middle East's energy resources and set the stage for conflicts that would last throughout the 20th century [2].

Although this agreement is considered one of the turning points in the regional energy struggle, it should not be forgotten that the new political structures that emerged after the First World War and the dissolution of the Ottoman Empire also affected this process. In this process, the reshaping of the Middle East and the sharing of energy resources became one of the most important issues in international politics. Today, dynamics such as the shift towards renewable energy, the discovery of new reserves, and the changing balance of power continue to influence the course of energy policies in the region. Nevertheless, it can be said that oil continues to be the main determinant of strategic struggles in the Middle East.

Although Türkiye is not directly related to the energy wealth of the Middle East in historical and geographical terms, it has a critical position in regional energy equations. Although Türkiye does not have rich hydrocarbon reserves within its borders, its geographical location has made it an important energy transit country. The fact that the logistical transit routes of oil and natural gas transported from the Middle East to Europe and other markets pass through Türkiye increases the country's geostrategic importance. Türkiye's energy policies are built on ensuring the security of these transit routes and directing energy diplomacy.

At the turn of the 20th and 21st centuries, Türkiye started to shape its energy geopolitics more actively in line with the transformations taking place at the international level. With the end of the Cold War, the replacement of military-oriented policies with economic-based strategies in the global system has led to some transformations in the energy policies of states. In particular, the rise in importance of neoliberal economic policies has brought along the process of evaluating strategic areas such as energy outside the security axis. In this context, states have started to evaluate energy not only within the framework of security, but also on the axis of economic development. Within the framework of these developments, developing countries such as Türkiye have also sought to utilize their existing natural and geographical resources more effectively for development purposes by keeping pace with the conjunctural change [29].

As a country that is aware of this economic and geopolitical transformation, Türkiye aims to play an active role in regional and international energy agreements and thus both maintain and strengthen its geopolitical position (See Table II). Türkiye's energy strategies are shaped in parallel with organizations such as the IEA and the International Atomic Energy Agency (IAEA), prioritizing issues such as energy security, resource diversity, and sustainability [58].

In addition, Türkiye has pioneered important pipeline projects, aiming to become a central country in energy trade.

Projects such as the Baku-Tbilisi-Ceyhan (BTC) oil pipeline and the Trans-Anatolian Natural Gas Pipeline (TANAP) have strengthened Türkiye's role in energy transportation and have been a driving force in increasing the country's domestic energy supply security and influence in foreign markets. In this context, Türkiye transports oil from Azerbaijan and Northern Iraq to the Mediterranean Sea through the port of Ceyhan, and Russian and Azerbaijani oil to Europe through the Straits. As for natural gas, Türkiye imports most of its needs from Russia, Iran, and Azerbaijan [46] (See Figure 4).

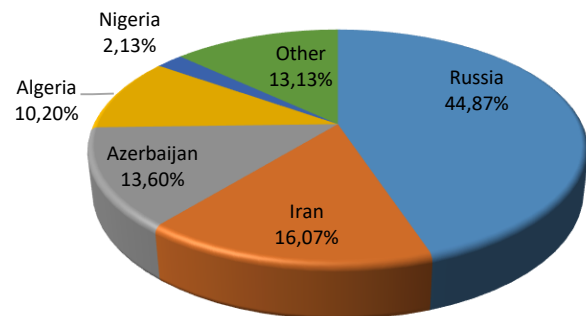


Figure 4. Türkiye's Natural Gas Imports by Source Countries in 2021 (%) [59].

Türkiye's natural gas outlook shows that Russia is the largest supplier of natural gas to Türkiye, followed by Iran and Azerbaijan. Although there are periodic variations in this distribution, the general trend is largely constant [60] (See Figure 5). Türkiye supplies about half of its natural gas consumption from Russia, one of the largest natural gas producers in the world energy market. At this point, it can be said that Russia is a vital supplier for Türkiye [3]. Although political relations between the two countries are strained from time to time, the interdependence established through the energy sector stabilizes this relationship. Economic integration, especially in the energy sector, is one of the main reasons why the two countries continue to cooperate despite their foreign policy differences. However, all these factors aside, it can be said that Türkiye's energy dependence on Russia forms the basis of the strategic energy partnership between the two countries [61].

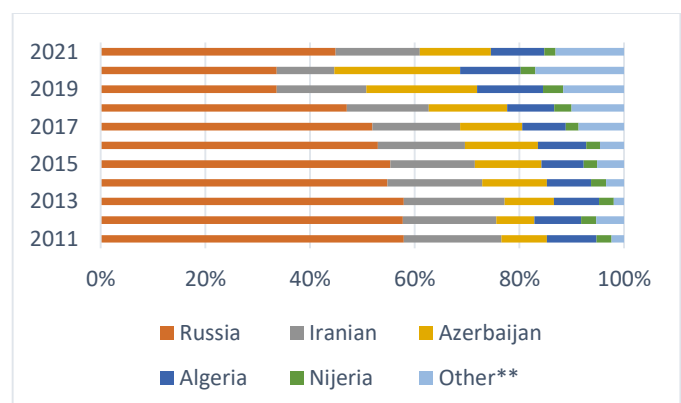


Figure 5. Changes in the Shares of Türkiye's Import Sources Between 2011-2021 [59].

Türkiye also aims to strengthen its energy relations with Europe and to integrate with Europe in the energy sector [58]. At this point, Türkiye needs to diversify its natural gas

resources and create alternative supply lines to Russia in the process of EU membership. In this framework, the Nabucco Project, which was planned in 2009, was considered a strategic initiative for the EU's energy security. Although this project was cancelled in 2013, the subsequent realization of TANAP within the scope of the Southern Gas Corridor is promising [46]. This project aims to reduce dependence on Russia by transporting gas resources from Central Asia and the Middle East to Europe.

In response to these developments, Russia brought the South Stream Project to the agenda to have a greater say in energy exports, but when this project failed, it launched the TurkStream Project, which aims to transport natural gas to Türkiye via the Black Sea. However, the crisis in Turkish-Russian relations following an airspace violation in 2015 disrupted cooperation in this area, but relations were normalized again in 2016, and the TurkStream process was continued [62].

Intending to diversify its natural gas sources and increase its influence in the energy market, Türkiye has been developing strategic cooperation with both major producing countries, such as Russia, and neighboring actors such as Iran. While ongoing energy relations with Iran create economic interdependence, the potential threats stemming from Iran's nuclear activities can be a concern for Türkiye. Despite this, Türkiye has preferred to develop its economic and energy relations with Iran and has adopted a cautious policy on sanctions. However, the trade balance with Iran is unfavorable to Türkiye, which weakens the economic dimension of this relationship. To overcome this imbalance based on energy imports, it is important to diversify export items [63].

Finally, Türkiye's energy partnership with Azerbaijan is of great importance not only for both countries but also for regional energy security. Thanks to the TANAP Project, Türkiye has concretized its ambition to become an energy hub rather than an energy terminal. While increasing Europe's gas supply security, this project has also further strengthened the energy relations between Türkiye and Azerbaijan [64].

Countries with energy resources are in an advantageous position in terms of economic and political power, while countries that are energy importers are more vulnerable [3]. Although Middle Eastern countries have the potential to be energy hubs, they have to undertake the challenging task of ensuring regional stability to maintain this role. Otherwise, it can be said that security vulnerabilities could become defenseless against foreign interference. Türkiye, too, needs to utilize its geopolitical advantage in line with its strategic interests by maintaining stability in its domestic and foreign policies. Although Türkiye today serves as a bridge between energy-rich regions such as the Middle East, the Caucasus, and the Caspian Sea basin and regions with high energy consumption such as Europe, external dependence is a serious risk factor for Türkiye.

Energy self-sufficiency refers to the capacity of a country to meet its energy demand with its resources. This ratio is calculated based on production over total primary energy supply (TPES), and any ratio below 100% indicates import dependency [65]. According to the International Energy Agency, Türkiye imports 93% of its oil and 99% of its natural gas (See Figure 6). This dependency is one of the main factors increasing the foreign trade deficit and debt [66]. As a matter of fact, it is known that the increase in demand and exchange

rate fluctuations after the COVID-19 pandemic have also negatively affected prices. In particular, the significant depreciation of the Turkish lira in 2022 increased imported energy costs, while wholesale natural gas prices reached record highs in 2023 [67]. This problem is exacerbated by the fact that households, industry, and power plants, which are the main users of natural gas, cannot be brought under control [68].

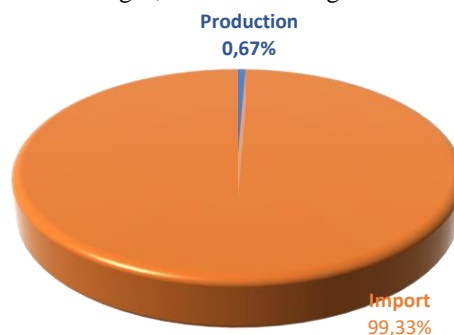


Figure 6. Shares of Sources of Total Natural Gas Supply in 2021 (%) [59].

According to data from the IEA, Türkiye's energy trade balance was consistently negative between 2000 and 2023 [69]. As can be seen from the graph above, during this period, the volume of imports (blue columns) remained well above exports (dark blue), and the energy trade deficit (orange line) continued to deepen (see Figure 7). It is observed that imports increased significantly until 2015, and although there has been a partial balance since then, Türkiye remains a net importer as of 2023. This situation makes it necessary to address Türkiye's energy policies not only through new investments but also in terms of structural external dependence. Supply security, economic vulnerabilities, and foreign policy risks are directly affected by the energy trade deficit and limit the pace of the energy transition process. Therefore, when evaluating the sustainability and impact of energy investments, the balance of trade and import structure must be considered.



Source: International Energy Agency. Licence: CC BY 4.0

Figure 7. Türkiye's Energy Trade Balance (2000–2023) [69].

Despite significant investments in Türkiye's energy policies over the past 20 years, domestic production capacity remains limited in terms of meeting total energy demand. According to IEA data (see Figure 8, 9), the most notable increase in domestic energy production between 2000 and 2023 has been in coal-based production [69]. While this situation provides short-term relief in terms of energy supply security, it has led to serious debates regarding environmental sustainability. This is because production from other sources such as hydroelectric, natural gas, and biomass has been inconsistent, while production levels in innovative areas such as biofuels and

waste-based production have remained low. This production structure indicates the instability of renewable energy investments and the slow pace of transition away from fossil fuel infrastructure. Therefore, the impact of the investment-policy relationship on reducing energy import dependency should be evaluated not only based on the existence of investments but also in conjunction with structural transformations in production capacity.

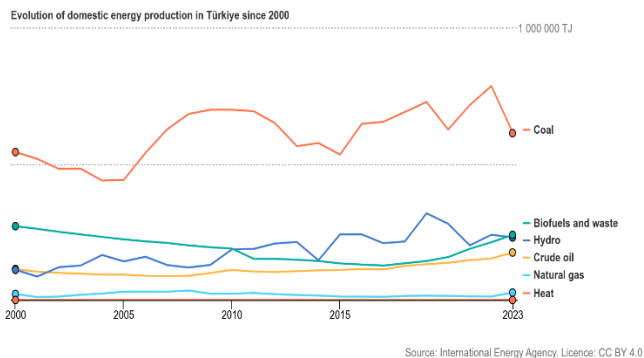


Figure 8. Development of Domestic Energy Production in Türkiye (2000–2023) [69].

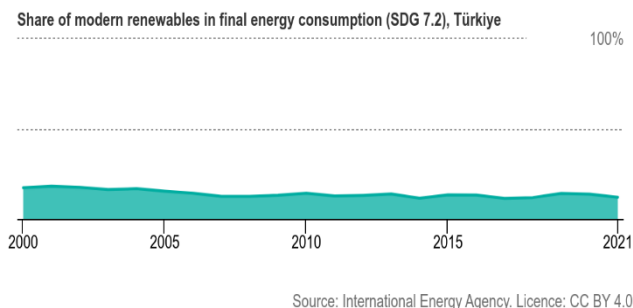


Figure 9. Share of Modern Renewable Energy in Final Energy Consumption in Türkiye (2000–2021) [69].

When evaluated in the context of energy supply security, it is clear that simply increasing supply is not enough. In addition, the source structure must be diversified, and environmental risks must be reduced. In 2020, 42.85% of global CO₂ emissions originated from electricity and heat production; this data highlights the need to consider energy investments in conjunction with climate and security policies. In this context, renewable energy investments have become elements that contribute not only to low-carbon targets but also directly to supply security. As of 2021, the global capacity of wind and solar energy has exceeded 1,700 GW, while microgrid systems have enabled the integration of these investments into the distributed production infrastructure [70]. In this context, it can be said that Türkiye continues to face supply security risks and a structure that supports external dependency.

Such structural problems are a call for Türkiye to accelerate its search for alternative energy policies. Increasing investments in renewable resources and nuclear energy will have a positive impact on energy dependence in the long run. Considering Türkiye's potential in wind, geothermal, and hydroelectric resources, it can be said that investments in these areas will further increase their strategic importance in terms of energy security and sustainable development [71].

In this transformation process, Türkiye is focusing its strategic priorities on three main areas in line with its Net Zero 2053 target: ensuring energy supply security, increasing energy independence, and managing the decarbonization process in line with the net-zero target. These three main objectives, clearly outlined in the Ministry of Energy and Natural Resources' 2024 Launch Report, are supported by multi-dimensional sub-priorities ranging from digitalization to hydrogen technologies, and from institutional restructuring to market reforms [72].

The process, which began with the adoption of the Renewable Energy Law in 2005, gained momentum in the post-2010 period with policy tools such as the YEKDEM application, YEKA tenders, and unlicensed production systems. Türkiye's renewable installed capacity was 33% in 2005, and this ratio has reached 59% as of 2024. Investments in wind and solar energy, which stood at 250 MW in 2013, have exceeded 31 GW in 2024; the overall target is to reach 120 GW of installed capacity by 2035. This growth demonstrates Türkiye's commitment to institutionalizing its energy transition, but it also highlights that the country is still in the “infrastructure alignment” and “grid transformation” phases. For example, an investment of \$28 billion is projected for transmission infrastructure, a key component of the green energy transition, by 2035, including plans for a 14,700 km HVDC network [72].

Türkiye's Green Deal Action Plan, published in 2021, strengthens the institutional foundation of energy transformation with 81 actions covering carbon border adjustment, sectoral roadmaps for green transformation, environmental labeling, circular economy, clean energy, and green finance. The plan envisages critical steps such as a green bond/sukuk guide, green OSB certification, emission reduction roadmaps, and a national carbon pricing mechanism [73]. These structural targets show that Türkiye is striving to rapidly increase its technical capacity in the energy transition; however, when compared to European countries, the transition process has not yet reached a “fully synchronized” point.

On the other hand, the success of the energy transition depends not only on technological developments but also on long-term financing and international policy alignment. In the post-2021 period, the European Green Deal, CBAM, REPowerEU, and the global climate agenda have created increasing pressure for transformation on Türkiye's foreign trade and investment structure. In this context, the World Bank CCDR and Türkiye's Updated National Contribution Statement (NDC) set a target of reducing greenhouse gas emissions by 41% by 2030, while also highlighting the need for at least an additional USD 165 billion in investments for green transformation between 2022 and 2040. However, while half of these investments are expected to be covered by the private sector, the current green finance capacity falls significantly short of this need [74].

Green financing in Türkiye still relies heavily on short-term loans; the share of institutional investors, such as long-term capital market instruments, insurance, and pension funds, is well below the OECD average. Green bond issuance is limited, and private sector capital investments are risky due to exchange rate fluctuations. This situation both increases the burden on the banking system and hinders companies' long-term green

transition investments [74]. Therefore, a national green taxonomy, transparency standards, and the strengthening of secondary capital markets are priority reform areas for ensuring the financial sustainability of Türkiye's energy and climate policies.

5. THE CENTER OF ENERGY: TÜRKİYE

Türkiye's energy policies are determined by factors such as increasing energy demand, dependence on imports, and geopolitical proximity to reserves. These strategies are shaped under basic headings such as ensuring diversity of sources and routes, aiming to become a hub in regional energy trade, promoting sustainable development, reducing environmental impacts, and shifting towards renewable and nuclear energy. In this context, Türkiye is pursuing comprehensive policies to reduce import dependency, expand the use of domestic and renewable resources, and diversify its energy portfolio. In terms of renewable energy capacity, Türkiye ranks 5th in Europe and 12th in the world [58]. Since most of the energy resources are located in the east and consumer countries in the west, Türkiye's position as a natural energy bridge between these two axes gives it a strategic advantage [29].

Türkiye's current oil reserves are approximately 1.2 billion tons. Of this, 239 million tons are suitable for production. So far, 170 million tons of production have been realized, and about 71 million tons of producible reserves remain [75]. As of 2021, onshore reserves are set at 412 million barrels of oil and 3.1 billion cubic meters of natural gas. In the same year, an average of 69 thousand barrels of crude oil was produced daily, while 631 thousand barrels of crude oil and 260 thousand barrels of processed products were imported [39, 76].

The Thrace region is home to Türkiye's largest domestic natural gas reserves. Tekirdağ stands out in this area, while the Southeastern Anatolia region (Adıyaman, Batman, Diyarbakır) stands out in oil production [77, 78]. However, current production is far from meeting Türkiye's total demand. This is because access to the deep geographical layers where the reserves are located requires advanced technology and high costs [75].

Oil production has gained momentum in recent years, especially with the discovery of 150 million barrels of reserves in Gabar Mountain. Starting with a daily production of 5 thousand barrels, the number of wells in this field is planned to be increased, and its annual economic contribution is expected to be 2.9 billion dollars. This discovery is expected to increase Türkiye's total oil reserves to 1.2 billion barrels [57, 79].

Lignite coal has a significant share among domestic resources. Although there has been a general increase in energy production since the 1990s, lignite and hard coal production have declined. Coal, hydroelectricity, and other renewable resources are important in Türkiye's energy production. These include wood, plant and animal waste, geothermal, and solar energy [80].

According to the International Energy Agency, 54% of Türkiye's electricity generation in 2021 was from renewable sources [81]. In 2022, coal accounted for 34.6%, natural gas 22.2%, hydroelectric 20.6%, wind 10.8%, solar 4.7%, geothermal 3.3%, and other sources 3.7% of electricity generation. By the beginning of 2023, the installed electricity generation capacity reached 104,038 MW [82].

TABLE II
PRIMARY ENERGY: CONSUMPTION BY FUEL [5].

Fuel Type	2020	2021
Oil	1.84	1.89
Natural Gas	1.66	2.06
Coal	1.70	1.74
Nuclear Energy	–	–
Hydroelectric	0.74	0.52
Renewable	0.50	0.61
Total	6.44	6.83

In 2020, Türkiye's primary energy supply reached 147.2 million tons of oil equivalent. Of this supply, 24.6% was used in industry, 22.7% in the conversion sector, 18.3% in transportation, 17.5% in housing, and 7.8% in the service sector. In terms of sources, 28.7% of the supply came from oil, 27.7% from coal, and 27% from natural gas. In the period 2009-2019, primary energy supply increased, but the total share of oil and natural gas decreased to 55.7% in 2020 [39]. This distribution reveals the resource diversity of Türkiye's energy system and the balance between imports and domestic production.

Türkiye's National Energy Efficiency Action Plan (NEEAP), prepared to increase energy efficiency, covers the period 2017-2023 and includes 55 actions in six different areas [83]. In the 2017-2021 period, energy efficiency investments reached USD 6.4 billion, resulting in energy savings of 4,473 ktoe and economic benefits of USD 1.56 billion. It was observed that the targets of NEEAP for this period were realized with a 109% success rate [84].

6. CONCLUSION

In the simplest terms, energy constitutes one of the cornerstones of modern life and economic activities. Even the smallest price fluctuations in this cornerstone can have global effects. These fluctuations make energy security one of the important agenda items of international politics. In this context, countries are turning to strategies such as promoting domestic production, ensuring diversity in energy production, and increasing investments in advanced technologies. On the other hand, countries with large energy reserves use these resources as a strategic power tool in international relations and have an impact on the global balance of power [85].

Energy geopolitics, on the other hand, is a multidimensional field that calls for greater cooperation and dialogue in the international system. Stabilizing or effectively managing competition and conflicts of interest in this field seems essential for lasting and final solutions. In this context, policies that encourage cooperation are vital for both sustainability and the development of environmentally friendly and innovative energy technologies. However, chronic competition over energy resources makes tensions inevitable. Therefore, while energy competition may be inevitable, managing it through sustainable and peaceful mechanisms would constitute a more stable and long-term approach [14].

Likely, the struggle for power and dominance over energy and raw material resources will remain among the main issues occupying the international agenda for the rest of the 21st century. Therefore, it is important to keep international cooperation and approaches based on common norm-building

efforts on the agenda. While the current crises increase the pressure on energy geopolitics, this may also act as a parallel pressure tool on international organizations and agreements. Consequently, this may lead to a process of updating these organizations and agreements.

From a historical perspective, energy crises seem to have “recurrent” effects. For example, some parallels can be drawn between the oil crises of the 1970s and some of today's energy crises. The obvious difference is that the causes behind the crises at the time were clearly identifiable, and the search for solutions was mostly focused on reducing dependence on imported oil. Today's crises, on the other hand, are much more complicated. This is because this process is now a comprehensive phenomenon that involves not only traditional energy sources, but also natural gas, coal, electricity, and climate change. Therefore, the solution strategies to be determined are expected to address this wide range of areas and factors.

In the case of Türkiye, the country's energy policies are mostly geared towards meeting its growing energy needs and ensuring security of supply. The increase in energy demand, which is a natural consequence of Türkiye's rapidly growing economy and growing population, makes policies to reduce dependence on imports more urgent.

In this context, the most fundamental finding of this study is that Türkiye's energy investments are positioned to increase both supply security and foreign policy effectiveness. In particular, the projects developed are considered to be tools for strengthening Türkiye's position as a regional power, beyond energy security and economic benefits. The acceleration of renewable energy investments and the trend toward alignment with EU energy policies reveal that the energy transition is progressing in sync with foreign policy. In this regard, the study examines the energy transition not merely as a technical process but as a strategic whole in which geopolitical, economic, and environmental factors are intertwined.

In the energy transition process, Türkiye has adopted the 2053 Net Zero target as a strategic orientation; in this direction, it has defined its policy priorities in three main axes: ensuring energy supply security, increasing energy independence, and accelerating decarbonization. These pillars focus on sub-headings such as digitalization, energy efficiency, hydrogen and new technologies, market reforms, institutional restructuring, and the carbon market. In the current structure, where 59% of installed capacity is provided by renewable sources, project and distributed production investments are particularly noteworthy. However, the low share of modern renewable energy in final energy consumption indicates that transformation is still limited in areas such as grid integration, energy storage, and financial sustainability. Therefore, Türkiye's energy transition process is still in the “technical capacity development and regulatory compliance” phase and requires stronger structural steps to be taken in practice.

The relationship between the targets set out in policy documents and investment behavior has been evaluated based on concrete outputs during the implementation process. Energy projects carried out in Türkiye and the incentives provided directly affect the investment environment, leading to an increase in investment intensity and expansion of renewable energy capacity. Incentive policies are reflected in the field in terms of the number of new investments and increases in installed capacity. Within the scope of energy efficiency strategies, certain levels of energy savings are achieved as a

result of the applications, greenhouse gas emissions decrease, and application models based on public-private sector cooperation are becoming widespread. Despite Türkiye's continued high levels of energy import dependency, gradual improvements in energy supply security are being observed thanks to increasing renewable energy investments; this development is creating a relative balancing effect on the energy trade balance.

Accordingly, Türkiye's energy policies should be evaluated along three main axes: (i) increasing the exploration and production of domestic resources, (ii) ensuring diversity in energy imports (iii) increasing renewable energy investments. To accelerate energy transition and contribute to sustainable development goals, a series of policy steps can be proposed in the short, medium, and long term. In the short term, simplifying legislation and incentive mechanisms, establishing regular feedback channels to make the developed systems investor-friendly, and introducing microfinance applications that support entrepreneurship are priorities. In the medium term, it is necessary to gradually implement a national carbon pricing mechanism (carbon tax or emissions trading system), integrate the green finance taxonomy and sustainable investment guidelines into the legal framework, and implement green infrastructure projects such as smart grids and energy storage through public-private partnerships. In the long term, the establishment of technology R&D centers based on domestic production to reduce energy dependence, the implementation of mandatory emission standards across all sectors, and educational curriculum reforms centered on energy and climate literacy are among the key strategic priorities.

In conclusion, it can be said that Türkiye's energy transformation process involves a comprehensive policy that cannot be addressed from a single perspective. It is clear that this transformation process requires long-term strategies, strong investments, and infrastructure efforts. However, the gains to be achieved in the end will be able to meet both today's needs and the stability of the future.

ACKNOWLEDGEMENT

This study has been compiled and prepared based on the chapter "Energy Geopolitics and Policies: The Case of Türkiye," previously published in the book *Energy Systems Analysis* by Batman University Press.

REFERENCES

- [1] Yang, Y., Xia S. and Qian X., Geopolitics of the Energy Transition, *Journal of Geographical Sciences*, 33 (2023), 4, pp. 683–704.
- [2] Yergin, D., *The Prize: The Epic Quest for Oil, Money, and Power*, New York: Simon & Schuster Building Rockefeller Center, 1991.
- [3] Kissane, C., Academic Webinar: The Geopolitics of Oil, 2023.
- [4] International Energy Agency, World Energy Outlook 2021, 2022.
- [5] British Petrol, Statistical Review of World Energy 2022 | 71st edition, 2021.
- [6] Dagnachew, A. G, Hoff, A. F.; Lucas, P. L.; van Vuuren, D. P., Insight into Energy Scenarios A comparison of key transition indicators of 2 °C scenarios, PBL Netherlands Environmental Assessment Agency, September 2019.
- [7] United Nations Framework Convention on Climate Change, “Key aspects of the Paris Agreement,” UNFCCC. [Online]. Available: <https://unfccc.int/most-requested/key-aspects-of-the-paris-agreement>. [Accessed: Jun. 9, 2025].
- [8] United Nations, “Degrees of global warming matter,” *United Nations*, <https://www.un.org/en/climatechange/science/climate-issues/degrees-matter>. [Accessed: Jun. 9, 2025].

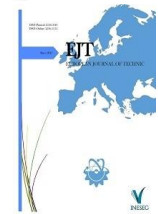
- [9] Haradhan, M., The First Industrial Revolution: Creation of a New Global Human Era, *Journal of Social Sciences and Humanities*, 5 (May 2019), 4, pp. 377-387.
- [10] Ateş, D., Industrial Revolution: Impetus Behind the Globalization Process, *Yönetim ve Ekonomi*, 15 (2008), 2, pp. 31-48.
- [11] Balamir Coşkun, B., Carlson, R., New Energy Geopolitics: Why does Turkey Matter? *Insight Turkey*, 12 (2010), 3, pp. 205-220.
- [12] Ülke Arıboğan, D., Bilgin, M., New Energy Order Politics Neopolitics: From Geopolitics to Energieopolitics, *International Relations*, 5 (Winter 2009), 20, pp. 109-132.
- [13] Glaser, C. L., How Oil Influences U.S. National Security, *International Security*, 38 (Fall 2013), 2, pp. 112-146.
- [14] Klare, M., *Rising Powers, Shrinking Planet: The New Geopolitics of Energy*, Glasgow: Oneworld Publications, 2008.
- [15] Yılmaz, S., Kalkan, D. D., Enerji Güvenliği Kavramı: 1973 Petrol Krizi Işığında Bir Tartışma, *Uluslararası Kriz ve Siyaset Araştırmaları Dergisi*, (December 2017), pp. 169-199.
- [16] Yergin, D., Ensuring Energy Security, *Foreign Affairs*, 85 (March-April 2006), 2, pp. 69-82.
- [17] Schlesinger, J. R., The Geopolitics of Energy, *The Washington Quarterly*, 3 (July 1979), 2, pp. 3-7.
- [18] Painter, D. S., Oil and geopolitics: the oil crises of the 1970s and the Cold War, *Historical Social Research*, 39 (2014), 4, pp. 186-208.
- [19] Eletek, Ö., Russia's New Central Asia Strategy, *ANKASAM*, 14 May 2021.
- [20] Zreik, M., Contemporary Geopolitics of Eurasia and the Belt and Road Initiative, *Eurasian Research Journal*, 4 (January 2022), 1, pp. 7-26.
- [21] Cohen, S. B. Presidential Address: Global Geopolitical Change in the Post-Cold War Era, *Annals of the Association of American Geographers*, 81 (December 1991), 4, pp. 551-580.
- [22] Cavcic, M., Energy transition and geopolitics to 'weigh heavily' on oil & gas industry in 2023, *Offshore Energy*, 2 May 2023.
- [23] Finance & Development, The Scramble for Energy, A Quarterly Publication of the International Monetary Fund, 2022.
- [24] Statista, OPEC net oil export revenue from 2005 to 2021, with a forecast for 2022 and 2023, Statista, 2023.
- [25] Tunander, O., Swedish-German geopolitics for a new century Rudolf Kjellén's 'The State as a Living Organism', *Review of International Studies*, (2001), 27, pp. 451-463.
- [26] İşcan, İ. H., Uluslararası İlişkilerde Klasik Jeopolitik Teoriler ve Çağdaş Yansımaları, *Uluslararası İlişkiler*, 1 (Summer 2004), 2, pp. 47-79.
- [27] Blondeel, M., Bradshaw, M. J., Bridge G. and Kuzemko, C., *The Geopolitics of Energy System Transformation: A Review*, Geography Compass, 2021.
- [28] Sevim, C., Küresel Enerji Jeopolitiği ve Enerji Güvenliği, *Journal of Yasar University*, 26 (2012), 7, pp. 4378 - 4391.
- [29] Semrari, M. C., Enerji Güvenliği Bağlamında Orta Asya Enerji Politikaları, Master Thesis, Erzurum: Atatürk University, 2015.
- [30] Aydoğmuş, H., Dünyanın En Büyük Petrol Üreticileri, TRT Haber, 2019.
- [31] Kutlu, Ö., ABD Petrol Üretimi ve Tüketiminde Yine Lider, Anadolu Ajansı, 2020.
- [32] Keohane, R. O., *After Hegemony: Cooperation and Discord in the World Political Economy*, New Jersey: Princeton University Press, 1984.
- [33] Lehmann, T. C., The Geopolitics of Global Energy, in *The Geopolitics of Global Energy: The New Cost of Plenty*, Colorado, Lynne Rienner Publishers, 2017, pp. 1-23.
- [34] Ünalldılar Kocamaz, S., The Rise of New Powers in World Politics: Russia, China and the Shanghai Cooperation Organization, *Uluslararası İlişkiler*, 16, (March 2019), 61, pp. 127-141.
- [35] Overland, I., The Geopolitics of Energy: out with the Old, in with the New? Oxford Energy Forum, 2021.
- [36] Demir, İ. Assessing the Correlation Between the Sustainable Energy for All with Doing a Business by Artificial Neural Network, *Neural Computing and Applications*, 34 (August 2022), 1, p. 22087-22097.
- [37] Öymen, G., Ömeroğlu, M., Yenilenebilir Enerjinin Sürdürülebilirlik Üzerindeki Rolü, *İstanbul Ticaret Üniversitesi Sosyal Bilimler Dergisi*, (2020), 39, pp. 1069-1087.
- [38] Ergün, S., Atay Polat, M., Nükleer Enerji ve Türkiye'ye Yansımaları, *İnönü Üniversitesi Uluslararası Sosyal Bilimler Dergisi*, 1 (2012), 2, pp. 34-58.
- [39] Türkiye Petrolleri A.O., 2021 Petrol ve Doğalgaz Sektör Raporu, 2021.
- [40] Cocklin, J., Global Natural Gas Supplies Forecast to Remain Tight in 2025 as Demand Growth Continues, IEA Says, Natural Gas Intelligence, 2025.
- [41] TÜBA Doğal Gaz Raporu, Türkiye Bilimler Akademisi Yayınları, Ankara, 2021.
- [42] IEA, Net Zero by 2050: A Roadmap for the Global Energy Sector, IEA, 2021.
- [43] Yu, K., Outlook 2023: The Return of Geopolitical Risk in the Energy Market, *Petroleum Economist*, 22 December 2022.
- [44] Miguel, M. B., *Russia's Relationship with Iran in the Context of the 21st Century Geopolitics*, Opinion Paper IEEE, 2022.
- [45] Ozawa, M., Russia's Energy Relations with Turkey and Iran: Between Commercial Interests and Regional Competition, *NATO Defense College*, (2021), pp. 39-49.
- [46] Austvik, O. G., Rzaeva, G., Turkey in the Geopolitics of Energy, *Energy Policy*, (2017), 107, pp. 539-547.
- [47] Özey, R., Mackinder'in Heartland Teorisi'nin Düşündürdükleri, *Marmara Coğrafya Dergisi*, (January 2017), 35, pp. 95-100.
- [48] Knutsen, T. L., Halford J., Mackinder, Geopolitics, and the Heartland Thesis, *The International History Review*, 36 (2014), 5, pp. 835-857.
- [49] "Oil Reserves by Country," *Wisevoter*. [Online]. Available: <https://wisevoter.com/country-rankings/oil-reserves-by-country/>. [Accessed: Apr. 19, 2025].
- [50] Deshmukh, A., Which Countries Have the World's Largest Proven Oil Reserves? *Visual Capitalist*, 7 June 2021.
- [51] Wohlforth, W. C., Realism and the End of the Cold War, *International Security*, 19 (Winter 1994-1995), 3, pp. 91-129.
- [52] The Global Energy Center, The 2023 Global Energy Agenda, Atlantic Council, Abu Dhabi, 2023.
- [53] British Petrol, Energy Outlook 2023 Edition, 2023.
- [54] Hafner, M., Tagliapietra, S. (eds.), *The Geopolitics of the Global Energy Transition*, Lecture Notes in Energy, vol. 73, Cham: Springer International Publishing, 1st ed., 2020.
- [55] International Energy Agency, *State of Energy Policy 2024*, Sept. 2024.
- [56] "Canada's Oil & Natural Gas Producers", [Online]. Available: <https://www.capp.ca/energy/world-energy-needs/>. [Accessed: 10 April 2023].
- [57] Morrow, S., World Energy Demand Will Increase 50% by 2050: EIA, *Anadolu Agency*, October 2021.
- [58] Republic of Türkiye, Ministry of Energy and Natural Resources, *Renewable Energy 2035 - Energy Transition*, Ankara, 2024.
- [59] T.C. Dışişleri Bakanlığı, Türkiye'nin Uluslararası Enerji Stratejisi, 2023.
- [60] T.C. Enerji Piyasası Düzenleme Kurumu, 2021 Yılı Doğal Gaz Piyasası Sektör Raporu, 2021.
- [61] Tokyay, M., Azerbaycan'ın Türkiye'ye Doğal Gaz Sevkiyatında Liderliği Ne Anlam Taşıyor? *Euronews*, 2 June 2020.
- [62] Koutroumpis, J., Russia and Turkey: An Ambiguous Energy Partnership, *E-International Relations*, 11 September 2019.
- [63] Sıvış, E., Enerji Politikalarında Denge Arayışı, ABD - Rusya ve Avrupa Birliği Üçgeni: TürkAkım Projesinin Belirleyici Faktörleri, *Atatürk Üniversitesi Sosyal Bilimler Enstitüsü Dergisi*, 23 (2019), 3, pp. 1373-1388.
- [64] Özbey, H., İran'a Yönelik Yaptırımlar: Türkiye - İran Enerji İlişkilerine Etkisi, *Mecmua Uluslararası Sosyal Bilimler Dergisi*, 4 (Fall 2019), 8, pp. 98-124.
- [65] Erdoğan, N., TANAP Projesinin Türkiye ve Azerbaycan Enerji Politikalarındaki Yeri ve Önemi, *Ömer Halisdemir Üniversitesi İktisadi ve İdari Bilimler Fakültesi Dergisi*, 10 (July 2017), 3, pp. 10-26.
- [66] Anugrah, P., How Self-sufficient is ASEAN in Energy? *ASEAN Centre for Energy*, 2017.

- [67] Cohen, P., Turkey Is Strengthening Its Energy Ties with Russia, *The New York Times*, 12 September 2022.
- [68] "Turkey hikes electricity, gas prices by 50% for industry, 20% for homes," *Reuters*, Sep. 1, 2022. [Online]. Available: <https://www.reuters.com/business/energy/turkey-hikes-electricity-gas-prices-by-50-industry-20-homes-2022-09-01/>. [Accessed: Apr. 19, 2025].
- [69] Yıldırım, A. B., A Cold Winter: Turkey and the Global Natural Gas Shortage, *EDAM*, 6 October 2021.
- [70] International Energy Agency, "Türkiye: Energy mix," *IEA*, <https://www.iea.org/countries/turkiye/energy-mix>. [Accessed: Jun.7, 2025].
- [71] Long, Y., Liu, X., Optimal green investment strategy for grid-connected microgrid considering the impact of renewable energy source endowment and incentive policy, *Energy*, 295 (2024), 131073.
- [72] Demir, İ., Turkey's Energy Security: Balancing Between 'Dependence' and 'Independence', in: *Turkey's Foreign Policy and Security Perspectives in the 21st Century: Prospects and Challenges*, Brown Walker Press, 2016, pp. 195-218.
- [73] Republic of Turkey Ministry of Treasury and Finance, *Sustainable Finance Framework*, Ankara, Nov. 2021.
- [74] International Bank for Reconstruction and Development, *Project Appraisal Document on a Proposed Loan to Türkiye Sınai Kalkınma Bankası A.Ş. for a Green Finance Project*, Report No: PAD5380, Washington, D.C., Oct. 2023.
- [75] Becerikli, U., Türkiye'nin 1 Milyar Tondan Fazla Petrolü Var, *TRT Haber*, 2 May 2023.
- [76] Willrich, M., International Energy Issues and Options, *Annu. Rev. Energy*, 1976, pp. 743-772.
- [77] Trakya Kalkınma Ajansı, TR21 Trakya Bölgesi Enerji Raporu, 2012.
- [78] "Energy Resource Guide – Turkey - Oil and Gas," *International Trade Administration*, U.S. Department of Commerce. [Online]. Available: <https://www.trade.gov/energy-resource-guide-turkey-oil-and-gas>. [Accessed: Mar. 12, 2023].
- [79] Yüksel, F., Morrow, S., Gabar'daki Petrol Keşfi Türkiye'nin Enerjide Bağımsızlık Politikasını Güçlendirecek, *Anadolu Ajansı*, 13 December 2012.
- [80] Kumbur, H., Özer, Z., Özsoy, H. D. and Avcı, E. D., Türkiye'de Geleneksel ve Yenilenebilir Enerji Kaynaklarının Potansiyeli ve Çevresel Etkilerinin Karşılaştırılması, Mersin University, 2005.
- [81] International Trade Administration, Turkey - Country Commercial Guide, 2022.
- [82] "Electricity," *Republic of Türkiye Ministry of Energy and Natural Resources*. [Online]. Available: <https://enerji.gov.tr/infobank-energy-electricity>. [Accessed: Mar. 1, 2023].
- [83] Republic of Turkey Ministry of Energy and Natural Resources, *National Energy Efficiency Action Plan (NEEAP) 2017–2023*, 2017.
- [84] "Ulusal Enerji Verimliliği Eylem Planı," *T.C. Enerji ve Tabii Kaynaklar Bakanlığı*. [Online]. Available: <https://enerji.gov.tr/bilgi-merkezi-enerji-verimliliği-ulusal-enerji-verimliliği-eylem-planı>. [Accessed: Feb. 19, 2023].
- [85] International Energy Agency, *The Contribution of Social Dialogue to the Decarbonisation of the Economy*, Oct. 2022.

Sevda Korhan Barış completed her undergraduate education in International Relations at Selçuk University in 2016 with a third degree. In the same year, she started her master's degree in International Relations at Selçuk University and completed her master's degree in 2018 with her thesis titled "The Changing Parameters of International Relations in Cyberspace". Subsequently, she started her PhD program in the same department at Istanbul Medeniyet University in 2018. While her doctoral education continued, she was in Italy for the Erasmus program at the University of Naples Federico II in the fall semester of 2021-2022. In 2024, she completed her PhD program titled "The Problem of Global Digital Governance: The Case of the Internet Governance Forum (IGF) in the Context of Cyberlaw" and received the title of doctor by completing her doctoral education. As of 2023, Korhan Barış, who has been working as a lecturer at Batman University International Relations Office, conducts her studies in the context of cyber policies, cyber law, cyber power dynamics, cyber deterrence strategies, cyber governance, and digital diplomacy.

BIOGRAPHIES

İdris Demir graduated from Gazi University, Department of English Language Teaching, in 1999. After completing his master's degree in the Department of International Relations at Middle East Technical University, he completed his second master's degree at the University of Dundee Energy, Petroleum, Mining Law and Policy Center. In 2007, he completed his PhD at Gazi University, Department of International Relations. In 2014, he became an associate professor, and in 2019, he became a professor. Demir worked at Kırşehir Ahi Evran University between 2009-2013 and at Istanbul Medeniyet University between 2013-2019. He was a visiting professor at the University of Oxford in the 2016-2017 academic year. İdris Demir's academic interests include energy, diplomacy, and strategy studies, and he has numerous articles and works published in national and international publishing houses and refereed journals.



Research Article

Slope Stability Analysis in Road Cuts

Sema Nasiroglu^{1*} , Mehmet Hayrullah Akyildiz² 

¹Dicle University, Engineering Faculty, Civil Engineering Department, Diyarbakır, Turkey. (semanasiroglu@gmail.com).

²Dicle University, Engineering Faculty, Civil Engineering Department, Diyarbakır, Turkey. (hayrullah.akyildiz@dicle.edu.tr).

ARTICLE INFO

Received: May., 16. 2025

Revised: Jun., 16. 2025

Accepted: Jul., 01. 2025

Keywords:

Landslide

Slope stability

Finite element method

Limit equilibrium method

Corresponding author: Sema Nasiroglu

ISSN: 2536-5010 / e-ISSN: 2536-5134

DOI: <https://doi.org/10.36222/ejt.1700831>

ABSTRACT

The stability problems observed in the cut section during the highway construction works in Aktaş Village of Siirt Province (eastern Turkey) were analysed by the limit equilibrium and finite element methods, and factor of safety and collapse surfaces were determined. This section is of critical importance since similar high cut sections are frequently encountered in the study area. In the light of field investigations, laboratory and literature shear strength parameters for analyses were obtained. In stability problems, it is difficult to determine the location and shape of the sliding surface. On the model reflecting the current situation, collapse surfaces were detected and calculations for safety analysis were made by using Plaxis V24 2D, which is based on the finite element method, and Slide2, which is based on the limit equilibrium method. Although the two methods seem compatible in terms of factor of safety, factor of safety obtained with the finite element method are lower. In addition, it has been determined that the finite element method gives more positive and reliable results in terms of determining the locations of failure zones in the soil and obtaining stress deformation curves.

1. INTRODUCTION

Slopes become unstable when the shear stresses required to establish equilibrium on a given potential sliding surface reach or exceed the available shear resistance [1]. Although slope stability is an interdisciplinary subject, it has become one of the main problems of geotechnical engineering, differing from others in terms of the causes, effects and numerical explanation of the phenomenon. In the event that adequate drainage is not provided, *i*) the increase in pore water pressures caused by surface and rainwater, *ii*) disruption of natural drainage as a result of heavy rainfall, *iii*) careless excavations during road widening, *iv*) accumulation of load-forming material on sloping land, and *v*) earthquakes and volcanic events are the most important factors that cause stability problems that disrupt the structure of sloping lands. In Turkey and elsewhere in the world, landslides have occurred in the past and continue to in the present time both because they are natural events that shape the world and because appropriate measures have not been taken, and they subsequently have caused serious loss of life and property and agricultural damages. The first reliable record of a historical landslide is on the one that occurred in the Romance river valley in 1219, during which a landslide mass formed a dam on the river, which subsequently collapsed, killing thousands of people [2]. In 1960, 116 students at a school in Wales, England, were killed when piles of slag slid into residential

areas following a mining excavation [3]. According to 2018 Natural Disaster Statistics Report of Disaster Management in Turkey, landslides ranked second to earthquakes among natural disasters between 1980-2017[4].

When we look at the causes of landslides occurring along the highways in our country, the main reasons can be listed as morphological structure including mountainous areas and crossing points, being located in active earthquake zones, having high slope gradients and unfavorable geological conditions. When landslides are considered as a soil mechanics problem, attention should be paid to surface and groundwater as well as the shear strength parameters of the soil. Knowledge on these parameters plays an important role in determining the collapse mechanism. Analyses performed in regard to shear strength parameters of the soil are defined as the slope stability analyses [5]. Slope stability analyses first appeared in 1773 when Coulomb focused on parameters such as shear strength angle and cohesion. At the same time, Coulomb's development of the equilibrium state of the forces in the shear wedge in the soil mass was examined in detail [6]. When the stability of a slope failed, the factor of safety of the slope is considered to be one (1.0). Among many methods used by researchers, the two most widely used ones are the finite element and the limit equilibrium methods. In limit equilibrium method, a potential shear surface is defined as an inclined surface and the soil shear strength is calculated by considering the equilibrium state of the forces and moments

acting on the soil mass on the shear surface according to the "Coulomb" collapse criterion [1]. The finite element method, on the other hand, is a method in which the stress and strain behavior of the soil is taken into account. This method, considering the soil geometry and boundary conditions, provides the closest results to the reality. A review of the literature also shows that the finite element and the limit equilibrium are the most widely used analysis methods in slope stability problems.

Keskin and Laman (2007) determined that displacement and stress states can be obtained by using the finite element method in slope stability problems and pointed out the advantages of this method over the limit equilibrium method [7]. Moudabel (2013) analyzed a slope case using the finite element and limit equilibrium methods and concluded that the factor of safety obtained was higher in the finite element method than the limit equilibrium method [8]. Bol et al. (2017) used the limit equilibrium and finite element methods to ensure the safety of a highway slope that lost its stability due to excessive rainfall and developed appropriate solutions [9]. Huvaj and Oğuz (2018) compared the safety and collapse surface factors with deterministic and probabilistic approaches using the limit equilibrium and finite element methods for a landslide in Norway [10]. Büyükağınacı and Işık (2019) studied stability analysis in three slope cases and compared the success of TS 8853, Eurocode 7 and BS 8006 standards. In another study, the finite element and limit equilibrium methods were used in the analyses and it was determined as a result of the study that the TS 8853 and limit equilibrium methods were more reliable than the Eurocode 7 for stability analysis [11]. Gör (2021) addressed a slope stability problem observed on a highway in Van province with the limit equilibrium method and developed appropriate solution proposals with static and earthquake analysis [12]. Mburu et al. (2022) studied two cases of landslides due to rainfall infiltration and obtained different results in terms of margins of error by using the slip surface search method utilizing a software that included the finite element and limit equilibrium methods for the stability of unsaturated slopes [13]. Ullah et al. (2020) investigated slope stability analysis using five methods: finite element method, limit equilibrium method, artificial neural network method, limit analysis and vector method. The study showed that the finite element method gave the most realistic result [14].

In this study, during the highway construction works carried out by the 9th Regional Directorate of Highways in Aktaş Village of Siirt Province, the stability problems observed in the cut section were analyzed by the finite element and limit equilibrium method in static and earthquake conditions and were compared in terms of collapse surfaces and factor of safety.

2. MATERIAL AND METHOD

2.1 Study Area and Its Geological Framework

In 2019 during the highway construction work in Aktaş Village, Kurtalan District, Siirt Province a movement was observed on the cut and fill slope and the work was stopped. It was anticipated that weakness of the geological units, weather conditions and precipitation triggered the landslide and in 2021 the movement repeated itself at Km:13+600-14+600 of the Siirt-Kurtalan Road. The study area falls within the borders of Siirt province and is included in the span of authority of the 9th Regional Directorate of Highways as shown in Fig. 1.

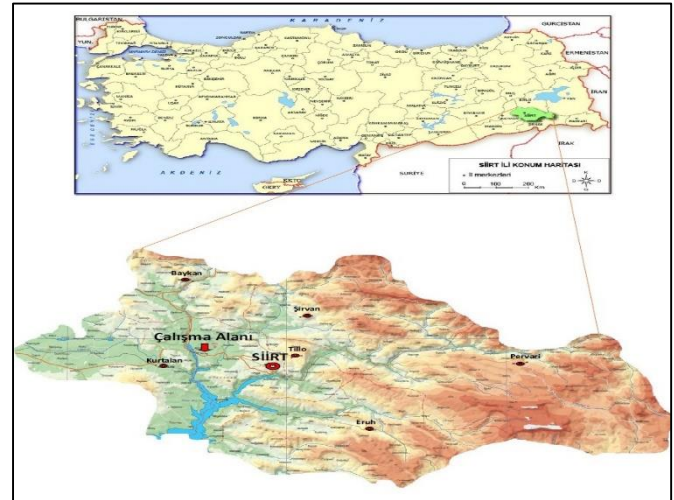


Figure 1 Location map of the study area [15]

As seen on a 1/500.000 scale geological map (Fig. 2) the study area and its immediate vicinity is covered by Late Eocene-Oligocene Germik Formation. The residual soil observed at the higher elevations of the area where the slope instability is observed consists of a clayey gravel - silty clay unit which can be defined as light brown - brown, grayish - grayish green, beige in color and very firm to hard, solid to very solid, with medium to high plasticity, and moist. The rock units in the area are consisted of shale, anhydrite and gypsum. These rocks are mostly light brown - brown, grayish green, grayish white colored, and are generally moderately to very but sometimes completely weathered. They are weak, very weak, but sometimes extremely weak in strength. In some places these rocks are strong to moderately strong, generally very fractured - fractured, and fragmented. Fractures are filled by clay, joint surfaces are generally slippery, sometimes rough, sometimes friable to dispersible. Cracks along the joint planes are filled by clay and gypsum.

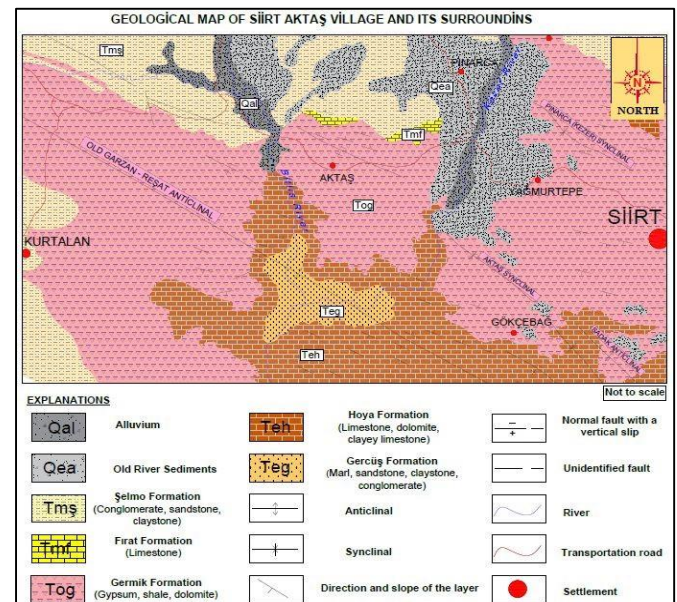


Figure 2 General geology map of the study area [16]

2.2 Field and Laboratory Studies

In order to detail the geological-geotechnical aspects of the geological units in the study area, to determine the groundwater level, to determine the engineering properties of the units observed in the study area and to examine the

existing and potential geotechnical problems, exploratory boreholes (267.00 m in total) were drilled in ten locations, and in four of the boreholes inclinometers were used (Fig. 3), and observations were made at different locations in the study area (Fig. 4). During the drilling of the boreholes, parallel to the progress, SPT in-situ tests were carried out, and core samples (RC) and undisturbed samples (UD) were collected. During the drilling works groundwater was encountered at different levels in different locations (Table 1) because groundwater changes the shear strength of the soil and therefore may adversely affect the slope stability. Soil and rock samples were collected according to the methods recommended in the relevant standards, namely TS 1900-2/T1 [17], ISRM [18], TS EN ISO 17892-1 [19], TS EN ISO 17892-2 [20], TS EN ISO 17892- 8 [21], ASTM D2487 [22], AASHTO T88 [23], AASHTO T89 [24], AASHTO T90 [25].

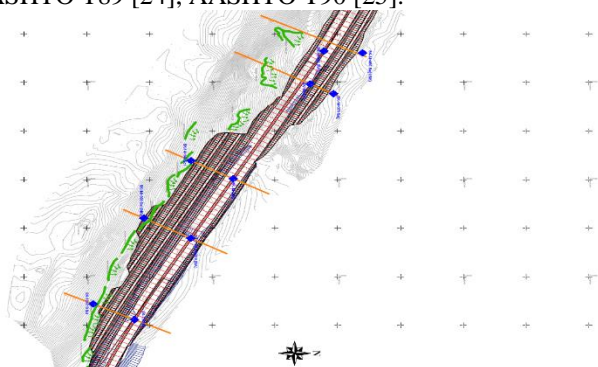


Figure 3 Drilling plan



Figure 4 Bird's-eye view of the landslide area

Drilling Number	Location of Drilling	Depth (m)	Groundwater Level (m)	Coordinates (Ed50 3°)		Elevation (m)
				North	East	
1	SK-13+810	21,00	2,00	420287,639	483688,34	631,17
2	SK-13+810 Sol	35,00	-	420281,05	483656,16	659,57
3	SK-14+000 (INK)	21,00	1,90	420296,605	483520,85	626,79
4	SK-14+000 Sol (INK)	39,00	-	420289,128	483479,49	659,90
5	SK-14+140	18,00	1,70	420303,363	483398,25	620,26

6	SK-14+140 Sol	35,00	2,00	420296,634	483361,17	649,00
---	---------------	-------	------	------------	-----------	--------

Groundwater status of the ground and the existing soil layers in the study area were evaluated as a result of the studies. Critical embankment section was determined to solve the stability problem in the cut section along the road. According to Technical Specifications of K.G.M Research Engineering, slope stability analyses should be performed to determine the slope ratios safely when the cut height is $h \geq 15$ m [26]. In this case, the cut section with a height of 39 m was determined as the critical section. For the Km:14+000 cut section, drilling data from SK-14+000 (INK) and SK-14+000 Sol (INK) were utilized as indicated in Figs. 5 and 6.

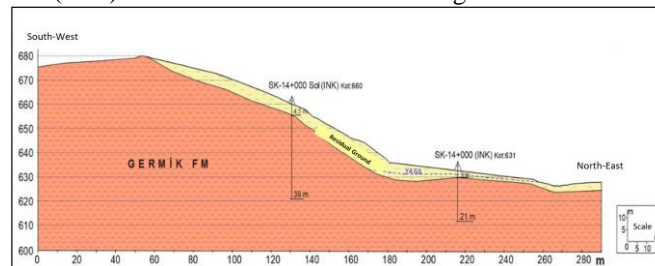


Figure 5 Critical geological cut section Km:14+000



Figure 6 Core samples collected during the study

Parameters were calculated for the soil and rock mass to be used in the analysis by using literature, field and laboratory data. These parameters are summarized in Table 2.

TABLE 2
ENGINEERING PARAMETERS OF SOIL AND ROCK MATERIALS TO BE USED IN THE ANALYSIS

Material	Material Model	Material Behavior	c' kPa	ϕ °	E kN/m ²	ν	Ψ °	γ dry kN/m ³	γ sat kN/m ³
Clay-Silt	Mohr Coulomb	Drained	7	3	49600	0,35	-	17	20
Gypsum-Shale-Anhydrite			187	3	207010	0,25	7	20	22

2.3 Numerical Modeling

In this part of the study, slope stability analyses were investigated by deterministic methods, finite element and limit equilibrium methods, in order to provide the closest solution to the stability problem. The purpose of the limit equilibrium method is to determine the static or seismic equilibrium conditions at the assumed critical sliding surface with a factor of safety. The limit equilibrium method is a frequently used method in slope stability analyses because it is applicable to soils and weathered rocks that acquired soil

properties, and shear stresses can be determined along the sliding surfaces assuming that a slope is collapsing. In the analyses carried out with the limit equilibrium method, the Simplified Bishop Method, which deals with the equilibrium of a circular sliding surface, where a sliding mass can be divided into slices and equilibrium equations can be written for each of slice is used. This method, first developed in its general form by Bishop [27], which is based on the assumption that the shear stresses between the circular shear slices are assumed to be zero and the normal stress and weight exerted on the center of the slice. When the forces in the vertical direction of a slice in Fig. 7 are split into their components, they contribute to determination of a factor of safety and the relation (1) in Fig. 7 is obtained in terms of total stresses. The factor of safety provides information about whether or not a slope is stable, or to what extent it is stable.

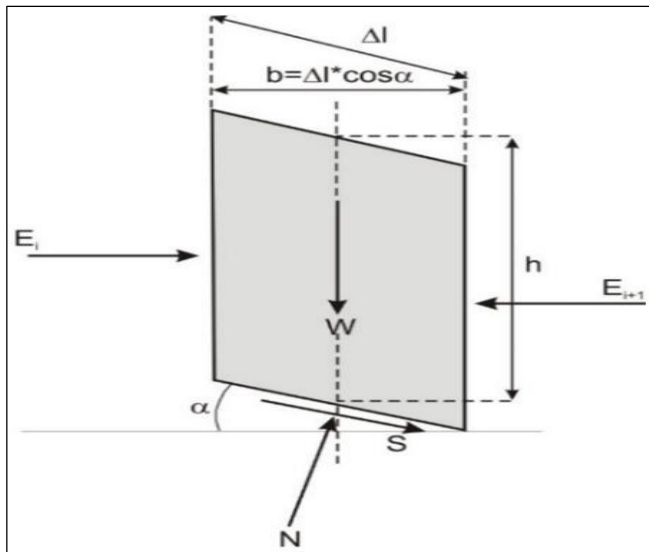


Figure 7 Forces acting on the slice according to the Simplified Bishop Method

$$F = \frac{\sum \left[\frac{c + \Delta l \cdot \cos \alpha + W \cdot \tan \Phi}{\cos \alpha + (\sin \alpha \cdot \tan \Phi) / F} \right]}{\sum W \cdot \sin \alpha} \quad (1)$$

One of the methods developed to investigate the behavior of soils is the finite element method. In addition to the factor of safety, information such as displacement, change in pore water pressure and determination of the location of failure zones in the soil are also needed. In such cases, stress-deformation analysis of the soil is also required. In the slope and slope environment, these calculations can be performed numerically by the finite element method under the assumption of a continuous medium in two or three dimensions. The most important feature of the finite element method is that the stress-strain properties of the soil can be represented by models such as linear-elastic, hyperbolic-elastic and elasto-plastic models based on the results of laboratory tests [2]. This method was described by Zeinkiewicz (1977) as a method to mathematically model and analyse a continuous system [28]. Since the total stress is divided into pore water pressure and effective stress in soil mechanics problems, the material behavior is expressed as effective stress. By finite element analysis, vertical and lateral movements, stresses, pore water pressure and water flow status can be determined. Although many software programs have been developed for the limit equilibrium method and finite element methods, in this study, Slide2 software was used for the limit equilibrium method and Plaxis V24 2D

software was used for the finite element method and stability analyses were performed for both static and seismic conditions. Stability analysis in case of earthquakes can be performed as pseudo-static analysis. This approach was first applied to seismic slope stability by Terzaghi (1950). Pseudo-static accelerations produce inertial forces and the magnitude of acceleration is related to the magnitude of ground motion. Terzaghi (1950) suggested that these coefficients can be taken as in Table 3 [29].

TABLE 3
SEISMIC COEFFICIENTS OF EARTHQUAKES (TERZAGHI,1950).

Explanation	Seismic coefficient
In severe earthquakes (Rossi-Forrel IX)	$k_h = 0.10$
In destructive earthquakes (Rossi-Forrel IX)	$k_h = 0.20$
In catastrophic earthquakes	$k_h = 0.50$

The ground acceleration coefficient for Siirt - Kurtalan Divided Road (Aktaş Variant) Km: 13+700 - 14+600 was determined as 0.237 g by using the "Earthquake Hazard Map of Turkey" which was prepared by AFAD (2018) to indicate the earthquake zones in the country (Fig. 8). However, the value for ground acceleration is taken as 0.1185 g, half of the maximum ground acceleration value (0.237 g) to include the increasing or decreasing effects of the quasi-static coefficient [30].

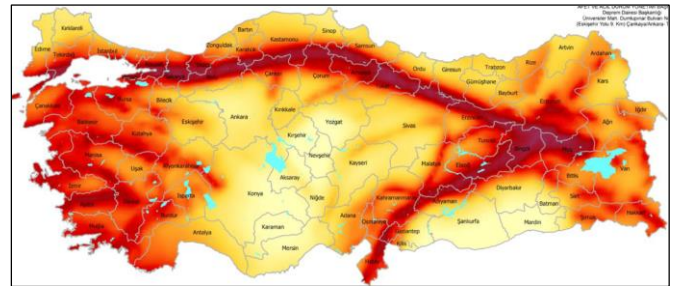


Figure 8 Earthquake hazard map of the study area [31]

Local Soil Class and Earthquake Ground Motion Level were determined as ZD and DD-2, respectively. The model of the slope for the Km:14+000 section, which was determined as the critical section, is shown in Figs. 9 and 10.

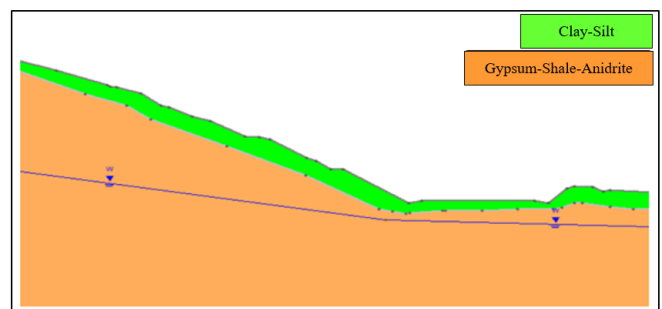


Figure 9 Slope model of Km:14+000 cut section used in the analysis (Slide2) [32]

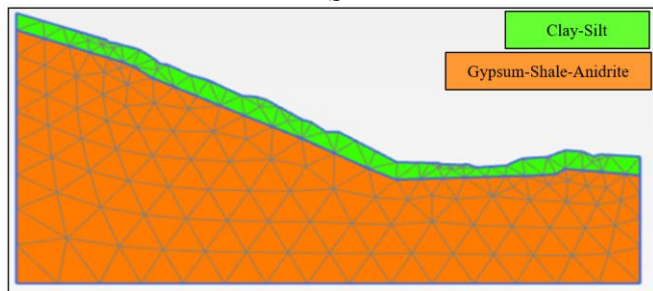


Figure 10 Geometric model and finite element mesh of Km:14+000 cut section (Plaxis V24 2D) [33]

In the design calculations, the Mohr-Coulomb Model was used for the silty-clay unit specified as residual soil whereas the Generalized Hoek Brown soil behavior model was used for the gypsum-shale-anhydrite unit. Standard boundary conditions were assumed in both Plaxis and Slide programs. Default boundary conditions, all displacements are limited at the bottom of the soil section. Lateral displacements are limited on the left and right boundaries. The most suitable mesh structure was investigated in the finite element network and analyzed by selecting the medium (mesh).

3. RESEARCH FINDINGS

Since the slope height is 39 m, Km:14+000 cut section is of critical importance and for this cut section the analysis was carried out in two stages. Accordingly, slope stability analysis was performed according to the limit equilibrium and finite element methods, and the factor of safety obtained is given in Table 3. In the factor of safety analyzes made with Plaxis, calculations were made using the strength reduction method. In this method, the shear strength parameters, cohesion and friction angle are gradually reduced until the slope collapses and factor of safety at the moment of collapse is determined. Since the model geometry is not horizontal, the “weight loading” calculation was made in Plaxis at the first stage before starting the analysis.

TABLE 4

RESULTS OF FACTOR OF SAFETY ANALYSIS FOR KM:14+000 CUT SECTION

Method	Conditions	Initial Status	Design Status	Specification Criteria
Finite Element Method (Plaxis V24)	Static	1,444	2,01	1,5
	Earthquake	1,068	1,921	1,1
Limit Equilibrium Method (Slide2)	Static	1,431	1,706	1,5
	Earthquake	1,126	1,436	1,1

As shown in Fig. 11, first of all, it is seen that the slope is stable but does not meet the specification criteria in the analyses performed using the finite element and limit equilibrium methods under static loads in sloping terrain conditions. When earthquake loads are applied, it is seen that the slope is in equilibrium but again does not meet the specification criteria.

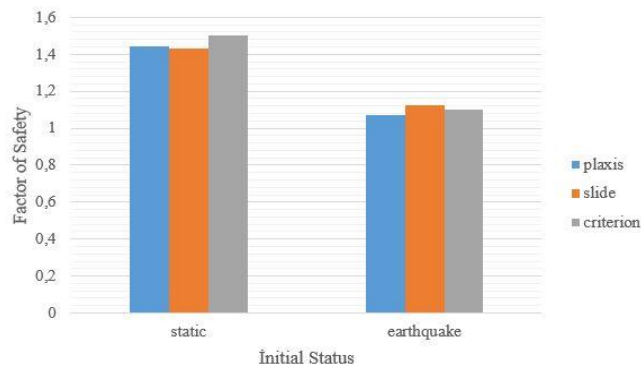


Figure 11 Km: 14+000 section in the initial state factor of safety analysis

When the safety coefficient was evaluated in terms of the method used, the calculation results of the two methods are observed to be similar. However, the finite element method (Plaxis) concludes the slip circle at a single point giving the smallest safety coefficient. Although this may seem useful to stay on the safe side, it should be taken into account that slip circles may occur in other parts of the section. In the limit equilibrium method (Slide2), the slip circle can be determined anywhere in the ground. The slip plane determined by the finite element and limit equilibrium methods in the slope stability analysis under static and earthquake loading for Km: 14+000 section is shown in Figs.12 and 13.

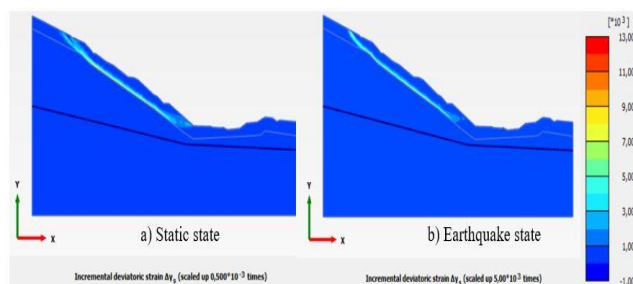


Figure 12 The slip plane determined by the finite element method in the initial state of Km:14+000 section (Plaxis V24 2D)

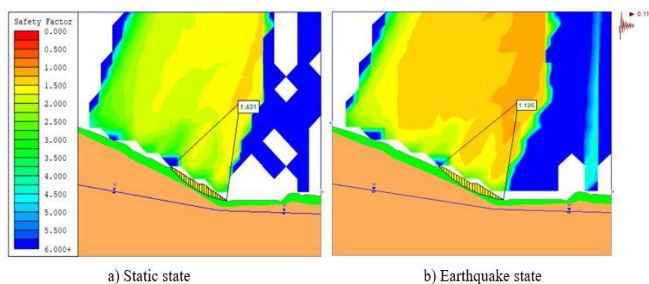


Figure 13 Slip plane determined by the limit equilibrium method in the initial state at Km:14+000 section (Slide2)

In the initial condition, the slope was found to be unsafe according to the specifications, so the cut slope was tilted at a slope ratio of 3/2 (horizontal/vertical) and supported with a shoring wall. As shown in Fig. 14, the safety coefficient of the slope supported by the shoring wall shows values above the specification criteria. Thus, the slope has been made safe.

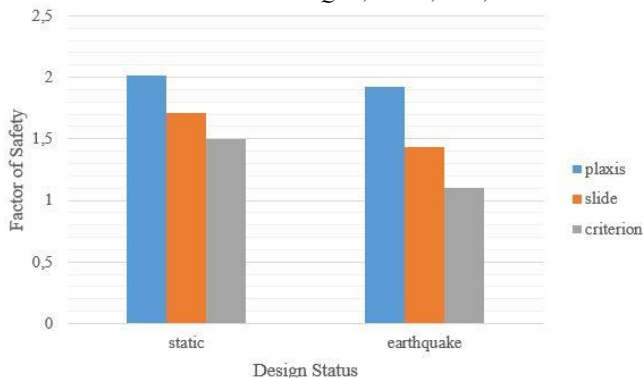


Figure 14 Km: 14+000 section factor of safety analysis in design condition

With the shoring wall design, the problem on the left slope has been eliminated and the new slip circle is seen on the right cut slope but it is safe. Figs. 15 and 16 show the slip plane in the design case.

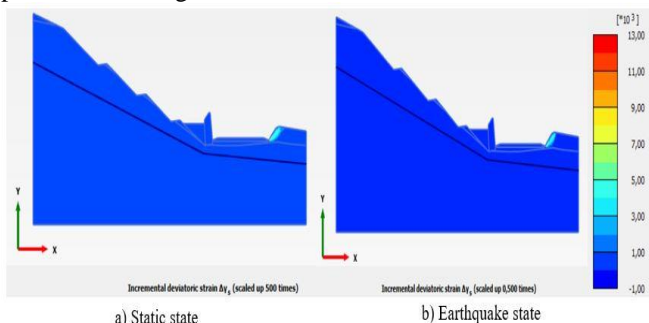


Figure 15 Slip plane determined by the finite element method in the design condition of Km:14+000 section (Plaxis V24 2D)

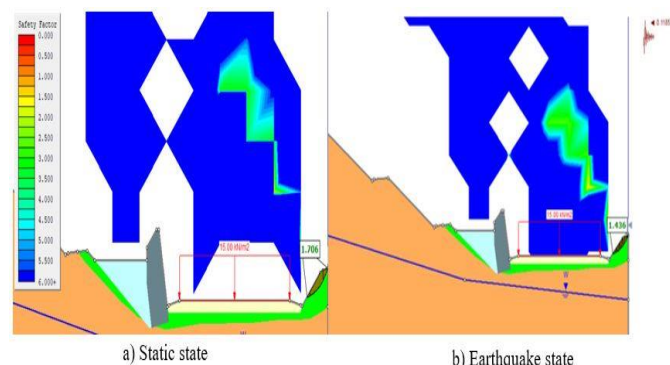


Figure 16 Km: 14+000 section design case slip plane determined by the limit equilibrium method (Slide2)

Vertical and horizontal displacements may occur in the ground during a mass movement. In order to determine the displacement of the slope section at Km:14+000, deformation analysis was performed by the finite element method. These analyses were performed using Plaxis V24 2D software. Fig. 17 show the total displacement values at initial and design state for static and seismic conditions.

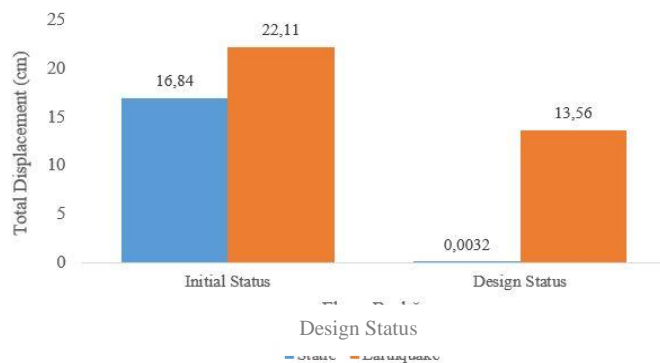


Figure 17 Total displacements at Km:14+000 slope section

In Fig.17, it is observed that the displacement value in the ground decreases with the wall design when both static and earthquake loads are applied. The deformations in the shear plane in the initial state are shown in Fig.18.

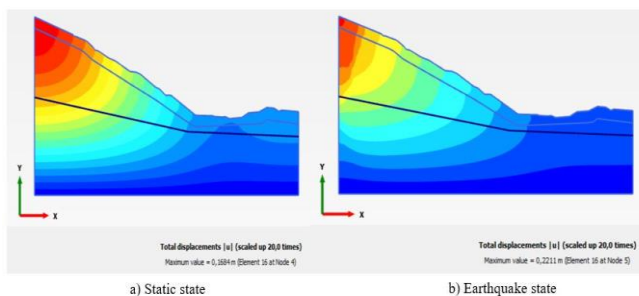


Figure 18 View of total displacements in the initial state by the finite element method (PLAXIS V24 2D)

The deformations in the shear plane after wall design are shown in Fig.19.

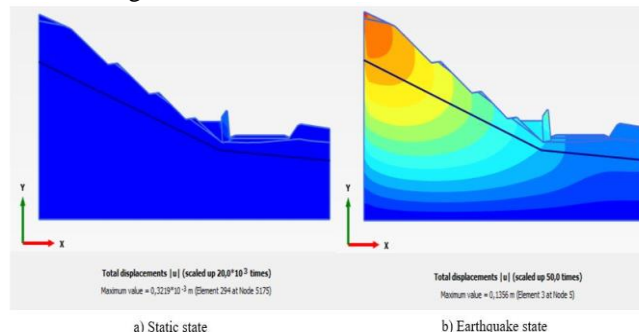


Figure 19 View of the total displacements in the design state by the finite element method (PLAXIS V24 2D).

In Fig. 19, no slippage or deformation of the slope is observed with the wall design in the static case. In the case of earthquake, the deformations decreased significantly. It can be said that the stability problem on the slope has been solved significantly with the wall design.

4. CONCLUSION AND RECOMMENDATIONS

In this study, by applying the limit equilibrium analysis and the finite element methods, static and earthquake analysis of a mass movement occurred during excavation works on the highway were performed and were compared in terms of factor of safety and collapse surfaces. In the initial condition, it is observed that the Km:14+000 cut section is stable under static and earthquake load but does not meet the limit of the Specification for Highways Research Engineering Works. For this reason, the cut slope was tilted at a slope ratio of 3/2

horizontal/vertical) and supported with a shoring wall. Stability analysis of the design condition shows that the slope is safe and meets the specification criteria. When the coefficient of safety was evaluated in terms of the method used, the calculation results of the two methods were similar. However, the finite element method (Plaxis) concluded that the slip circle at a single point giving the smallest coefficient of safety. Although this seems useful to stay on the safe side, it should be taken into consideration that the slip circles may occur in other parts of the section. In the limit equilibrium method (Slide2), the slip circle can be determined anywhere in the soil. Plaxis stays on the safer side in terms of the safety factor and helps to take precautions in advance to avoid any problems in the future. It can be said that the slip plane in the slope passes through the same region in the analyses performed by both methods. In addition, it is possible to determine the lateral and vertical displacements in the slope and to obtain the stress-deformation graph with the finite element method. It helps to understand the slope stability problem in a better way. It can be said that the finite element method, which depends on the unit deformation affecting the safety coefficient of the slope, is superior to the limit equilibrium method.

ACKNOWLEDGEMENT

This study, with the Project Number MÜHENDİSLİK.23.010, is supported by the Coordination Unit of Dicle University Scientific Research Projects. This article is derived from a doctoral dissertation conducted at Dicle University, Institute of Natural and Applied Sciences, Department of Civil Engineering and contains no conflict of interest

REFERENCES

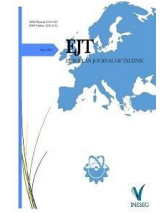
- [1] S.L. Kramer, Geotechnical Earthquake Engineering, (1996), pp.466.
- [2] A. Önalp, E. Arel, Geoteknik Bilgisi 2 Yamaç ve Şevlerin Mühendisliği, Birsen Yayınevi, (2004).
- [3] R.L. Schuster, L.M. Highland, "The Third Hans Cloos Lecture. Urban Landslides: Socioeconomic Impacts and Overview of Mitigative Strategies", Bulletin of Engineering Geology and The Environment, 66 pp.1-27, (2007).
- [4] Türkiye'de Afet Yönetimi ve Doğal Kaynaklı Afet İstatistikleri, (2017). Access Date: 20.12.2023. [Online]. www.afad.gov.tr
- [5] B.M. Das, Principles of Geotechnical Engineering, Boston: Cengage Learning, (1994)
- [6] A.Tekin, "Sonlu Elemanlar ve Limit Denge Yöntemleri ile Şev Stabilité Analizi", (Yüksek Lisans Tezi), İstanbul Üniversitesi, (2011).
- [7] M.S.Keskin, M. Laman, "Sonlu Elemanlar Yönteminin Şev Stabilité Problemlerinin Analizinde Kullanılması", Çukurova Üniversitesi Mühendislik ve Mimarlık Fakültesi Dergisi, Cilt:22 Sayı:1, (2007).
- [8] O.A. Moudabel, "Slope Stability Case By Limit Equilibrium And Numerical Methods", Doctoral Dissertation, Oklahoma State University, Libya, (2013).
- [9] E. Bol, S. Sert, A. Özocak, "Kazıklı İksa Sistemi ile Şev Duraylılığının Sağlanması" Sakarya Üniversitesi Fen Bilimleri Enstitüsü Dergisi, 21(5), 860-870,(2017).
- [10] N. Huvaj, and E.A. Oğuz, "Probabilistic Slope Stability Analysis: A Case Study", Sakarya Üniversitesi Fen Bilimleri Enstitüsü Dergisi, 22(5),n1458-1465, (2018).
- [11] C.Z. Büyükağın, ve N.S. Işık, "Şev Duraylılığı Analizlerinde Limit Denge Yöntemleri, Eurocode 7 ve BS 8006 Standartlarıyla Hesaplanan Başarı Oranlarının Karşılaştırılması" TÜBAV Bilim Dergisi, 12(2), 18-29, (2019).
- [12] M. Gör, "Limit Denge Analizi (Bishop Metodu) İle Kütle Hareketinin Mekanizması ve Önlem Yapısının Analizi: Van İli Örneği", GÜFBED, 11(2): 597-608, 2021
- [13] W. Mburu, A.J. Li, H.D. Lin, C.W. Lu, "Investigations of Unsaturated Slopes Subjected to Rainfall Infiltration Using Numerical Approaches— A Parametric Study and Comparative Review", Sustainability, 14, 14465,2022 <https://doi.org/10.3390/su142114465>

- [14] S. Ullah, M. U. Khan, G. Rehman, "A Brief Review Of The Slope Stability Analysis Methods". Geological Behavior, 4, 73-77, 2020
- [15] Harita Genel Müdürlüğü, <https://www.harita.gov.tr/urun/siirt-fiziki-il-haritasi/336>, Erişim tarihi: 17.03.2024
- [16] <https://www.mta.gov.tr/v3.0/hizmetler/500bas> Access Date: 17.01.2024. [Online].
- [17] TS 1900-2, İnşaat mühendisliğinde zemin laboratuvar deneyleri - Bölüm 2: Mekanik özelliklerin tayini, Türk Standartları Enstitüsü, Ankara, 15-5, 2006
- [18] ISRM (International Society for Rock Mechanics), In: Brown E.T., editor. ISRM suggested method: rock characterization, testing and monitoring, London: Pergamon Pres, 21 Ipp, 1981.
- [19] TS EN ISO 17892-1, Geoteknik Etüt Ve Deneyler - Zemin Laboratuvar Deneyleri - Bölüm 1: Su İçeriğinin Belirlenmesi, Türk Standartları Enstitüsü, Ankara, 2014.
- [20] TS EN ISO 17892-2, Geoteknik Etüt Ve Deneyler - Zemin Laboratuvar Deneyleri - Bölüm 2: Birim Hacim Kütleinin Belirlenmesi, Türk Standartları Enstitüsü, Ankara, 2014
- [21] TS EN ISO 17892- 8, Geoteknik Etüt Ve Deneyler - Zemin Laboratuvar Deneyleri - Bölüm 8: Konsolidasyonsuz ve Drenajsız Üç Eksenli Deney, 2018
- [22] ASTM D2487, Standard Practice for Classification of Soils for Engineering Purposes (Unified Soil Classification System), 2020
- [23] AASHTO T88, Standard Method of Test for Particle Size Analysis of Soils, (2020).
- [24] AASHTO T89, Standard Method of Test for Determining the Liquid Limit of Soils, 2022
- [25] AASHTO T90, Standard Method of Test for Determining the Plastic Limit and Plasticity Index of Soils, 2020.
- [26] Karayolları Genel Müdürlüğü. Araştırma Mühendislik Hizmetleri Teknik Şartnamesi, 2005
- [27] A. W. Bishop, The use of the slip circle in the stability analysis of slopes, Geotechnique, 5(1), 7-17, (1955). <https://doi.org/10.1680/geot.1955.5.1.7>
- [28] O.C. Zienkiewicz, The Finite-Element Method. 3rd Ed., New York, McGraw-Hill Book Co., 787p, (1977).
- [29] Terzaghi, K., Mechanism of Landslides, New York: The Geological Society of America, Berkeley, Volume:83, (1950).
- [30] Marcuson, W.F., Moderator's report for session on earth dams and stability of slopes under dynamic loads, Proceedings, International Conference on Recent Advances in Geotechnical Earthquake Engineering and Soil Dynamics, St. Louis, Missouri, Vol.3 p.1175, (1981)
- [31] Earthquake Engineering and Soil Dynamics, St. Louis, Missouri, Vol.3 p.1175, (1981). <https://tdth.afad.gov.tr/TDTH/main.xhtml> 14.02.2024. [Online].
- [32] Rocscience Inc., Slide v. 06 Software, 31 Balsam Ave., Toronto, Canada, (2024). <https://www.rocscience.com>
- [33] PLAXIS, User Manual. 2D V.20.02, Delft University of Technology&PLAXIS b.v., The Netherlands, 2020.

BIOGRAPHIES

Sema NASIROĞLU Sema Nasıroğlu graduated from Fırat University, Department of Civil Engineering in 2014 and received her bachelor's degree. After receiving her master's degree in 2018 from the same university's Institute of Science/Civil Engineering Construction Technologies department, she started her public service at the 9th Regional Directorate of Highways. She started her doctorate education at Dicle University, Institute of Science, Department of Civil Engineering in 2019. She has conducted academic studies on soil mechanics and geotechnical engineering.

Mehmet Hayrullah Akyıldız University of Near East, Civil Engineering Department Undergraduate degree, University of Sakarya institute of science/civil engineering department master's degree, master's thesis titled "Examination of the effects of sewage and garbage leachate on concrete strength" University of Sakarya institute of science and civil engineering department PhD graduate, Floor in solid waste sanitary landfills Parameters affecting impermeability He completed his research with the thesis titled. He currently works as an academician in the Department of Civil Engineering at Dicle University.



Research Article

Instagram Use in Education: Trends, Themes and Bibliometric Findings

Merve Gulmus Yelmen¹ , Muzeyyen Bulut Ozek² , Fatih Kalemkus³ 

¹ Cukurova University, Adana, Turkey. (e-mail: mgulmus@cu.edu.tr).

² Firat University, Elazig, Turkey. (e-mail: mbozek@firat.edu.tr).

³ Kafkas University, Kars, Turkey. (e-mail: kalemkus@kafkas.edu.tr).

ARTICLE INFO

Received: May, 07, 2025

Revised: May, 25, 2025

Accepted: Jun., 02, 2025

Keywords:

education, instagram, social media application, social media, bibliometric analysis

Corresponding author: *Muzeyyen Bulut Özek*

ISSN: 2536-5010 / e-ISSN: 2536-5134

DOI: <https://doi.org/10.36222/ejt.1693364>

ABSTRACT

Today, social media tools are increasingly playing a role in learning processes. Instagram, which is a visual and interactive tool in particular, stands out as one of the tools that support learning. Thus, assessing the state of Instagram studies in educational research today helps to imagine the future. Therefore, in this study, studies published on the use of Instagram in education were examined using the bibliometric analysis method. In the study, 836 academic studies published between 2015-2024 in the Web of Science (WoS) database were analyzed. The findings obtained show that research in this field has increased rapidly, especially since 2020. It has been determined that studies are focused on the use of Instagram in higher education as well as in education such as medical education and language learning. In addition, the USA stands out as the country with the most publications in articles published on the use of Instagram in education, followed by Spain and the UK. In addition to these findings, the "Cureus Journal of Medical Science" stands out as a journal in terms of the frequency of published articles, while the "University of Barcelona" stands out in terms of institutions. On the other hand, although "Li JW" stands out as the most published author among the authors who published articles on the use of Instagram in education, "Elizabeth R. Lyden" stands out as the most cited author and the author who is in a central position with extensive collaboration. The research findings were evaluated in the context of the literature and some suggestions were made.

1. INTRODUCTION

Today, educational technologies have become one of the elements that reshape learning processes [85]. This digitalization process in education transforms traditional teaching methods and makes learning processes more interactive [1]. Therefore, social media platforms are at the center of this process and provide students with access to information, sharing and interaction [2-4]. In this way, these platforms can allow students to actively and creatively participate in learning processes [86]. Because, according to the Constructivist approach, the development of virtual learning can be facilitated by developing materials on educational devices or organizing media with the use of social networks in education [5]. In addition, [6] have drawn attention to the role of social media as a learning environment that provides potential contributions to entertainment, satisfaction, professional and personal gains and success. In this context, Instagram, one of the widely used social media platforms, provides an interactive and dynamic learning environment for students and educators and allows the enrichment of the learning process [7].

Instagram can be defined as an application that allows several users to come together in a community to interact with each other or allows a user to take, edit and share photos with other users [8, 9]. Instagram is a social network that has evolved significantly since its establishment only ten years ago [10] and stands out as the third most important social network platform growing with 2 billion monthly active users in 2024 [11]. In addition, according to the report published by We Are Social in early 2024, the number of social media users in our country constitutes 66.8% of the country's population [12], while DATAREPORTAL revealed in its report published in 2025 that 85.5% of these users are Instagram users [13]. Due to this situation, it can be said that the number of Instagram users in our country is a considerable number. Instagram [14], one of the most used networks worldwide, where users share photos or short videos that can be accompanied by up to 2,200 characters, includes analysis of audiences, profiles and users, brands, companies and marketing, political communication and education [10]. In addition, Instagram introduced "reels", short-form videos that can be uploaded or created within the application, in August 2020 [15] and announced that all

uploaded videos will be converted to reels as of July 2022 [16]. This means that users will be able to create their own videos to a limited extent using videos uploaded to reels [17]. These videos are categorized differently from images and multimedia posts by the Instagram algorithm [18]. It can be said that these opportunities provided by Instagram in the context of video content can provide important opportunities for users in educational environments [19, 87]. In addition, Instagram offers easily accessible and engaging platforms for educational content [19]. The visually appealing and interactive nature of these platforms can attract students' attention and motivate them to learn educational materials [20]. In addition, Instagram's image and video editing tools can also be used to make educational posts [21]. Therefore, it can be said that Instagram is an important tool that can be used to facilitate educational processes [88].

Numerous studies have examined how Instagram use affects learning and how to address related issues. For example, [22] describes Instagram as a valuable teaching tool that can increase academic productivity, engagement, motivation, and performance. Therefore, the literature indicates that Instagram plays an important role both for social interaction and in developing and improving the quality of learning in the digital age. Instagram is seen to support language learning [23-28] and communication skills [29, 30]. In the study conducted by Maierová, Instagram was used to support English language teaching and it was seen that Instagram supported language learning, especially positively affecting student motivation and writing skills [28]. In the study conducted by González-Mohino et al., it was concluded that the use of Instagram in the learning process increased students' motivation, communication, and engagement [30]. Al-Ali investigated the integration of Instagram as a mobile learning tool in foreign language classes, finding that it provided unique opportunities to create personalized learning experiences for language learners and was highly effective in creating a strong sense of community among students [31]. [32] stated that Instagram can be used as a teaching tool in language education with creative classroom activities, [33] while Instagram can be used to enhance English language learning in addition to formal teaching. [34] emphasized that Instagram offers unique opportunities for immersive language learning and can transform educational practices, especially in areas with limited resources.

Instagram is also frequently used in the learning process of health professionals [5, 35-37]. In their study, Gutiérrez-Marín and colleagues used Instagram as a teaching tool in Orthodontics and Pedodontics courses [5]. Different Instagram accounts were created for each course and supportive information was shared on these accounts. As a result of this study, it was determined that using Instagram made the learning process more dynamic and increased student motivation. In the study of Hussain and colleagues, how the posts made using the #anatomynotes tag on Instagram were used in anatomy education and how they changed over time [36]. The study revealed that Instagram is a powerful tool especially for visual learning and that students actively participate in this area. [38] It was stated that Instagram can provide benefits to medical and dental anatomy education, but that limitations such as passive learning should be taken into consideration.

The use of Instagram as a supportive tool in higher education can increase student learning outcomes and participation [39]. The use of Instagram in education is also noteworthy in terms

of increasing students' digital literacy [89-90]. It is of great importance for individuals growing up in the digital age to gain critical thinking skills and to produce information rather than just consuming it [91-92]. In this context, Instagram helps students gain critical thinking skills and produce original content by supporting their digital literacy [40, 41]. The use of social media platforms such as Instagram in education enables students to develop their digital identities, create educational content, share their own projects, and gain different perspectives by examining their peers' work [40]. Comparative analysis of the literature review is presented in Table 1.

TABLE 1 COMPARATIVE ANALYSIS OF LITERATURE REVIEW

Study	Purpose	Method	Type of Analysis	Main Findings
[5]	Dentistry education	Applied qualitative method	Descriptive statistics + Chi-square	Students who interacted heavily with the Story feature found Instagram useful.
[22]	Opinions on social media	Survey-based quantitative research	Descriptive analysis	Students found social media useful for communication and motivation.
[28]	Use of Instagram in English classes	Mixed method	Survey + observation + interview	Writing and creativity improved.
[29]	Measuring Instagram's effect on speaking skills	Quantitative case study	Interactional model analysis	66% improvement observed, participation and motivation increased.
[30]	Analyzing Instagram's effect on student satisfaction	Quantitative study	Structural equation modeling	Instagram had a positive effect in all dimensions.
[31]	Testing Instagram's suitability as a mobile learning tool	Action research	Reflective diary + SAMR model	Although initial reluctance was observed, creative production increased over time.
[33]	Investigating Instagram's effect on EFL students' language development	Mixed method	Survey + experimental t-test + interview	Instagram improved writing skills, vocabulary, and self-confidence. Positively contributed to academic achievement.
[36]	Analyzing the use of the #anatomynotes tag in medical education	Content analysis	Time-based content analysis	It was found to be a powerful tool supporting visual learning.
[37]	Evaluating the effect of Instagram in hematology-oncology education	Cross-sectional quantitative study	Descriptive statistics + t-test	Humorous and clinical content was effective, interaction increased.
[38]	Evaluating the role of Instagram in medical and dental anatomy education	Literature review + Instagram account analysis	Interpretive content analysis + table-based user and content comparison	Visuality and the use of hashtags provided an advantage.

It can be said that Instagram has gone beyond being a socialization tool like other technologies and has become widespread in every area of life [93]. Therefore, studies on the use of Instagram in education show the role of this platform in supporting learning processes and its increasing acceptance [19, 39, 42, 43]. Due to this situation, it can be thought that the use of Instagram in education has become an interesting field of study and has increased the tendency to evaluate its impact in educational sciences [94]. However, studies conducted in this field should be examined from a broad perspective and it should be determined in which areas more research is needed [30, 95]. Because studies conducted have stated that bibliometric analysis studies are needed to develop a more comprehensive understanding of the effects of social media use in education [44-46]. In addition, in future studies, database searches should be expanded with newly determined keywords and existing technologies in education should be investigated [47]. Therefore, when previous studies are examined; although the trends in educational research on social media are examined with the bibliometric analysis method [46, 48, 49], it can be said that bibliometric research is needed specifically for Instagram. Because trend studies are considered useful in terms of revealing the current situation in the field, directing new research and determining changes in certain time intervals [50]. Therefore, it can be stated that this study has the potential to provide valuable contributions to the development of technology-based education using Instagram in the future, which has not yet been discovered. Therefore, this study aimed to determine the trends of the studies conducted on the use of Instagram in education by examining them through bibliometric analysis and to reveal which topics and researchers are prominent. It is expected that the findings obtained within the scope of the research will contribute to a better understanding of the potential use of Instagram in education by both educators and researchers and to the development of effective usage strategies. In line with the purpose of the research, the following questions were sought:

1. What is the distribution of articles published on Instagram use in education by year?
2. What is the distribution of articles published on Instagram use in education by country?
3. What is the distribution of articles published on Instagram use in education by journals?
4. What is the distribution of articles published on Instagram use in education by authors?
5. What is the distribution of articles published on Instagram use in education by co-authorship status?
6. What is the distribution of authors who published articles on Instagram use in education by citation networks?
7. What is the distribution of countries by citation in articles published on Instagram use in education?
8. What is the distribution of institutions by citation in articles published on Instagram use in education?
9. What is the distribution of articles published on Instagram use in education by keywords used?

2. METHODS

Within the scope of the research, the articles selected by following the PRISMA (Preferred Reporting Items for

Systematic Reviews and Meta Analyses) flow diagram [51] were performed using the bibliometric analysis method. Bibliometric analysis is a widely used approach to update the progress of published publications in the field [52]. In other words, the bibliometric analysis method can be expressed as the use of statistical and quantitative analysis methods to determine the general characteristics of studies published in a specific field or subject [54]. It can be said that this method allows visualization by looking at the studies in the literature from a broad perspective. On the other hand, thanks to the bibliometric mapping analysis, the scientific flow of institutions, researchers and studies on the determined subject can be followed [54].

In performing bibliometric analyses, some researchers use various software such as Bibliometrix [96], CitNetExplorer [97], CiteSpace [99], VisualBib [98], and VOSviewer [100]. However, in this study, we chose VOSviewer because it is user-friendly, freely available, has extensive documentation and numerous online tutorials, and receives constant updates from its developers. VOSviewer can be accessed at <https://www.vosviewer.com/>. In this study, the Web of Science (WoS) database was used because it provides easy access to databases and citation data [55] and is one of the most widely used databases [56]. WoS was chosen because it is considered a complete and comprehensive data source and contains reliable and high-quality publications [57]. In addition, WoS offers an independent and comprehensive editorial process, as well as the ability to provide a wide range of data from various fields and a reliable citation network thanks to its integration with Clarivate Analytics [58].

2.1. Data Collection

In line with the purpose of the research, the WoS query text in Figure 1 was used on 13.02.2025 in order to access relevant studies from the WoS database.

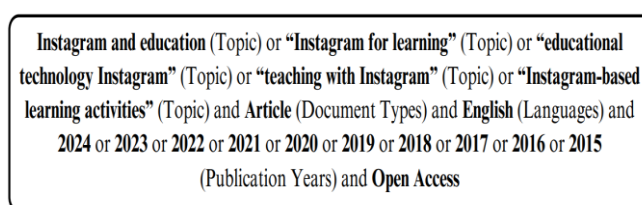


Figure 1 Search Parameters Used to Access Articles in WoS

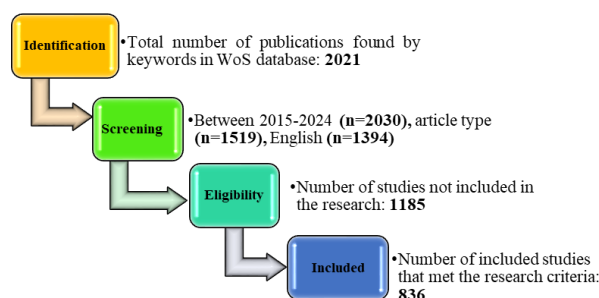


Figure 2. PRISMA Flow Diagram Followed in the Research of the Reviewed Articles

In the selection process of the articles accessed from the WoS database using the query text in Figure 1, the PRISMA (Preferred Reporting Items for Systematic Reviews and Meta Analyses) flow diagram [51] was used. Therefore, the studies accessed from the WoS database were filtered in line with the purpose of the research. Therefore, when selecting the articles

to be included in the analysis, articles with full-text access published in English between 2015 and 2024 were taken into consideration. The PRISMA flow diagram followed during the data collection process of the research is presented in Figure 2.

2.2. Analysis of Data

Bibliometric analysis is a widely used approach to update the progress of published publications in the field [52]. Initially, articles on Instagram usage in education were scanned from the WoS database for bibliometric analysis and the obtained data were examined with descriptive analysis. Then, the obtained articles were filtered according to the purpose of the research and a suitable data set was obtained for bibliometric analysis. The data set was reviewed separately by the researchers in the Microsoft Excel 2016 program and it was decided that all data were valid and usable. Bibliometric data of 836 publications examined in the research were analyzed using VOSviewer software. This program, developed by [59], is a free software that allows creating numerical and visual maps. The reason for choosing this software is that VOSviewer is quite functional for bibliometric analysis, both in functional visualization [60] and in directly viewing and interpreting images quantitatively [59]. On the other hand, the elements defined as objects in the VOSviewer program can represent journals, institutions, authors, countries and keywords and form clusters or networks with connections [61]. In the bibliometric analysis process, co-occurrence analysis [61] was performed, which includes counting the data that appear together within a unit. When two elements occur together at the same time, there is a relationship between these elements [62] and the frequency of these two elements appearing together indicates that the relationship between them is strong [63]. A threshold value must be determined for bibliometric association and combination analyses. The threshold value indicates the minimum number of elements to be included in the analysis [61]. The threshold value, which determines the minimum number of publications per journal by bibliometric matching of journals by researchers, was determined as 2. In the study, citation (institution, country, author, publication and journal), co-citation (author), co-author (institution) and co-word analyses were performed with the VOSViewer software.

3. FINDINGS

In this part of the research, bibliometric data of articles on the use of Instagram in education were examined and findings regarding the distribution of articles according to the years they were published, the countries they were published in, the journals they were published in, their authors, their co-authorships, the citations of the authors, the citations of the countries they were published in, the citations of the institutions and the keywords used were included. The distribution of articles published on the use of Instagram in education by year is given in Figure 3.

When Figure 3 is examined; it is determined that the years with the largest areas in articles published are 2022, 2023 and 2024. It can be said that articles on the use of Instagram in education have increased in intensity in these years. In previous years, especially between 2015-2019, the number of publications remained at lower levels, but a significant increase has started as of 2020. In addition, it is seen that articles published on the use of Instagram in education have increased rapidly, especially since 2020. While the highest number of

publications was reached in 2022, a significant increase was also observed in 2023 and 2024. It can be said that this situation reveals that there is an increasing interest in the academic field on the subject and that the research focus has intensified in recent years. The distribution of published articles by country is given in Tables 1-2 as the number of articles (N) and percentage (%).

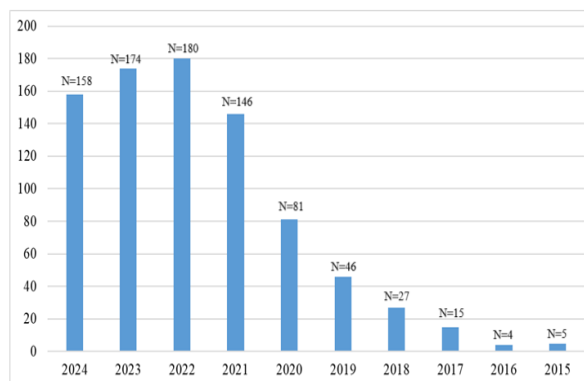


Figure 3 Distribution of Articles By Year

TABLEII DISTRIBUTION OF ARTICLES BY COUNTRY

Country	N	%
USA	237	28,34
Spain	98	11,72
England	58	6,93
India	53	6,34
Saudi Arabia	49	5,86
Brazil	44	5,26
Germany	39	4,66
Italy	31	3,70
Australia	30	3,58
Canada	29	3,46
Turkey	29	3,46
Indonesia	28	3,34
China	28	3,34
Netherlands	18	2,15
Pakistan	18	2,15
Switzerland	17	2,03
Iran	16	1,91
South Korea	16	1,91
Malaysia	15	1,79
Russia	15	1,79
United Arab Emirates	14	1,67
Poland	13	1,55
Egypt	12	1,31
Czech Republic	10	1,19

When the findings in Table 1 are examined, it is seen that the articles published are mostly published in the USA (28.34%). It can be said that this country is followed by Spain (11.72%), England (6.93%) and India (6.34%). It was also determined that a significant number of articles were published in countries such as Saudi Arabia (5.86%), Brazil (5.26%) and Germany (4.66%). Turkey's share in the total publications is 3.34%, which is at a similar level to Indonesia. The countries with the least publications are Poland (1.55%), Egypt (1.31%) and the Czech Republic (1.19%). When the geographical distribution of the articles is examined in general, it can be said that the use of Instagram in education attracts global attention, but more research has been done in some countries. The distribution of articles according to the journals in which they were published is given in Table 3 as the number of articles (N) and percentage (%).

TABLE III DISTRIBUTION OF ARTICLES BY JOURNALS

Journal	N	%
Cureus Journal of Medical Science	27	3,23
Journal of Medical Internet Research	23	2,75
International Journal of Environmental Research and Public Health	15	1,79
IEEE Access	14	1,67
Sustainability	13	1,55
Plos One	11	1,31
Social Media Society	11	1,31
Applied Sciences Basel	10	1,19
JMIR Formative Research	9	1,07
Frontiers in Communication	8	0,95
Heliyon	8	0,95
JMIR Public Health and Surveillance	8	0,95
Media and Communication	7	0,83
Frontiers in Psychology	6	0,71
Nutrients	6	0,71
Frontiers in Education	5	0,59
Healthcare	5	0,59
Aesthetic Surgery Journal	4	0,47
Arab World English Journal	4	0,47
BMC Medical Education	4	0,47
BMC Public Health	4	0,47
Computational Intelligence and Neuroscience	4	0,47
Education and Information Technologies	4	0,47
JBJS Open Access	4	0,47
Journal of Assisted Reproduction and Genetics	4	0,47

TABLE IV DISTRIBUTION OF ARTICLES BY AUTHORS

Yazar	N	%
Li JW	6	0,718
Mackey TK	6	0,718
Unger JB	5	0,598
Barroso-Moreno C	4	0,478
Marsch LA	4	0,478
Shah N	4	0,478
Akdagli A	3	0,359
Allem JP	3	0,359
Carpenter JP	3	0,359
Felix M	3	0,359
Gabarron E	3	0,359
Gil-fernandez R	3	0,359
Hassanpour S	3	0,359
Karayigit H	3	0,359
Kim Y	3	0,359
Mulcahey MK	3	0,359
Panagopoulos M	3	0,359
Rais-bahrami S	3	0,359
Ranker LR	3	0,359
Rayon-rumayor L	3	0,359
Singh NP	3	0,359
Vlachou S	3	0,359
Wijaya D	3	0,359
Wu JX	3	0,359
Wynn R	3	0,359

When the findings in Table 2 are examined, it is determined that the articles published are mostly published in the “Cureus Journal of Medical Science (%3.23)” journal. It is seen that this journal is followed by the “Journal of Medical Internet Research (%2.75)” and “International Journal of Environmental Research and Public Health (%1.79)” journals, respectively. In addition, it can be said that the journals in which the fewest articles on the use of Instagram in education are published include “Education and Information Technologies (%0.47)”, “JBJS Open Access (%0.47)” and “Journal of Assisted Reproduction and Genetics (%0.47)”. According to Table 2, it can be said that the articles published on the use of Instagram in education generally vary in terms of the journals in which they are published. The distribution of

articles according to authors is expressed in Table 3 as the number of articles (N) and percentage (%). When Table 3 is examined, it is seen that among the authors of articles published, authors such as “Li JW” and “Mackey TK” stand out with 6 publications (0.71%) each. These authors are followed by “Unger JB” with 5 publications (0.59%) and “Barroso-Moreno C”, “Marsch LA”, “Shah N” and “Akdagli A” with 4 publications (0.47%). In addition, when the distribution in Table 3 is considered, it can be said that the authors who discuss the use of Instagram in education are diverse. The findings regarding the co-authorship analysis of the authors who published articles are presented in Figure 4.

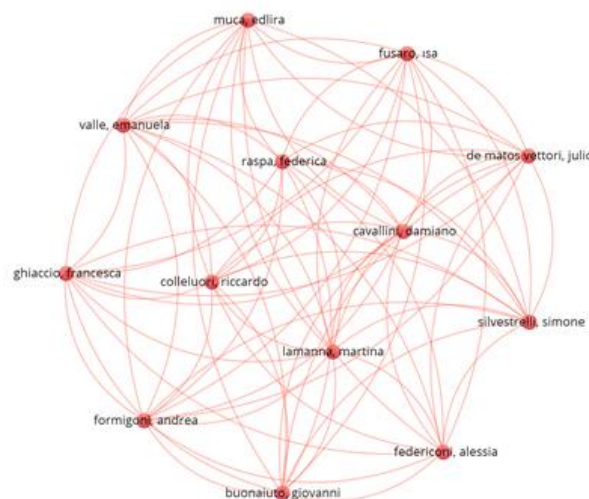


Figure 4. Co-Authorship Analysis of Authors

When Figure 4 is examined, it is seen that among the researchers who published, only the “light brown” cluster occurred and in this case, there are connections between all the authors. While the nodes on the map represent individual authors, the lines between the nodes reveal the articles these authors wrote together. The network structure reveals that some authors collaborate with each other intensively, with researchers such as “Federica Raspa”, “Edlira Muca”, “Isa Fusaro” and “Damiano Cavallini” being at the center. According to Figure 4, it can be said that the authors who published articles on the use of Instagram in education collaborate to a large extent. The findings regarding the citation analysis of the authors of the articles are presented in Figure 5.

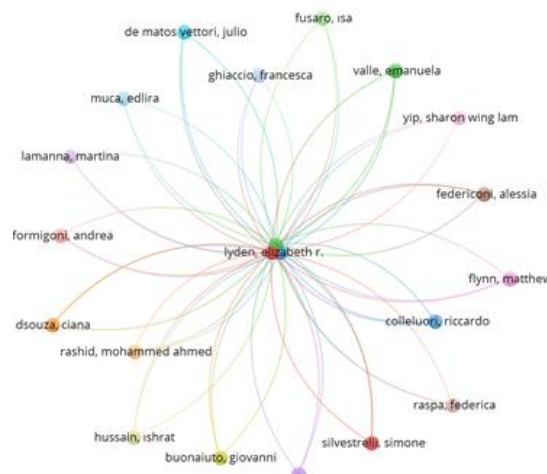


Figure 5. Authors' Citation Analysis

The author citation analysis map in Figure 5 visualizes the extent to which authors' work has had an impact on articles published and how they cite each other. The colors on the map represent author groups or clusters in research themes. "Elizabeth R. Lyden" stands out as the author with the most citations and the widest collaboration network, being at the center of the network. On the other hand, authors such as "Julio De Matos Vettori", "Isa Fusaro", "Emanuela Valle" and "Giovanni Buonaiuto" also have important connection points and can be said to have high academic interactions. The distribution of authors who published articles in terms of the number of publications (NP), number of citations (NC) and link strength (LS) is given in the Table 5.

TABLE V DISTRIBUTION OF AUTHORS PUBLISHING ARTICLES ACCORDING TO NUMBER OF PUBLICATIONS, NUMBER OF CITATIONS AND LINK STRENGTH

Author	Number of Publications (NP)	Number of Citations (NC)	Link Strength (LS)
Calderon-Garrido, Diego	2	10	4
Gil-Fernandez, Raquel	2	10	4
Carpenter, Jeffery P.	2	31	0
Otto, Thorsten	2	2	0
Thies, Barbara	2	2	0
Lyden, Elizabeth R.	1	17	18
Nguyen, Vuvi H.	1	17	18
Yoachim, Shayla D.	1	17	18
Giroux, Catherine M.	1	6	7
Moreau, Katherine A.	1	6	7
Barsukova, Mariya	1	6	4
Buonaiuto, Giovanni	1	40	3
Cavallini, Damiano	1	40	3
Colleluori, Riccardo	1	40	3
De Matos Vettori, Julio	1	40	3

When the findings in Table 4 are examined, "Giovanni Buonaiuto", "Julio De Matos Vettori", "Damiano Cavallini" and "Riccardo Colleluori" stand out as the most cited authors with high academic impact (NC=40). However, it can be said that authors such as "Elizabeth R. Lyden", "Vuvi H. Nguyen" and "Shayla D. Yoachim" stand out in terms of both the strength of connections and the number of citations, despite being among the authors with the fewest number of articles published (NP=1; NC=17; LS=18). On the other hand, "Jeffrey P. Carpenter" draws attention in terms of the number of publications and the number of citations (NP=2; NC=31). Based on these findings, it can be said that the authors with the highest values in terms of strength of connections increase academic interaction by participating in extensive collaborations. The findings regarding the citation analysis according to the countries where the articles were published are presented in Figure 6, and the distributions in terms of the number of publications (NP), number of citations (NC) and link strength (LS) are presented in Table 6.

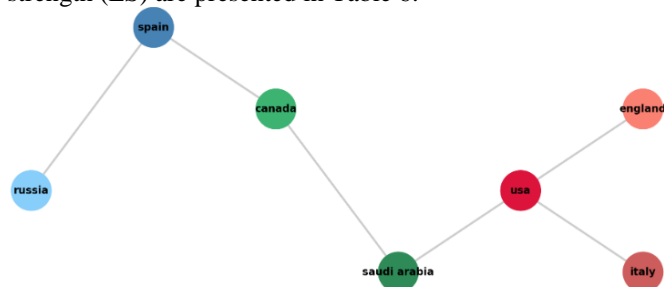


Figure 6. Citation Analysis of Countries

TABLE VI DISTRIBUTION OF ARTICLES BY COUNTRY IN TERMS OF NUMBER OF PUBLICATIONS, NUMBER OF CITATIONS AND LINK STRENGTH

Country	Number of Publications (NP)	Number of Citations (NC)	Link Strength (LS)
Spain	14	70	2
USA	8	81	3
Saudi Arabia	4	18	2
Germany	4	29	0
Canada	2	6	2
England	2	15	1
Italy	2	43	1
Afghanistan	2	10	0
Egypt	2	10	0
Russia	1	6	1
Austria	1	1	0
Bangladesh	1	10	0
Kazakhstan	1	8	0
Malaysia	1	2	0
Pakistan	1	2	0

According to Figure 6, while the USA, Spain and Saudi Arabia are in the central position in academic collaborations, countries such as the England, Italy, Canada and Russia also support the network with various connections. Spain is seen to be one of the strongest nodes. Saudi Arabia and Canada are bridge countries representing different research collaborations. This distribution shows that some countries are more involved in scientific production.

When Table 5 is examined, it is seen that Spain (NP=14; NC=70) and the USA (NP =8; NC=81) are the countries with the highest academic impact. It can also be said that the USA plays an important role in international collaborations (LS=3). Italy, despite receiving particularly high citations, has more limited international collaborations (NP=2; NC=43). In addition, other countries have relatively lower citation and connection power and seem to have less impact in terms of academic collaboration. The findings regarding the citation analysis of the article authors according to their institutions are given in Figure 7, and their distribution in terms of the number of publications (NP), number of citations (NC) and link strength (LS) are given in Table 7.

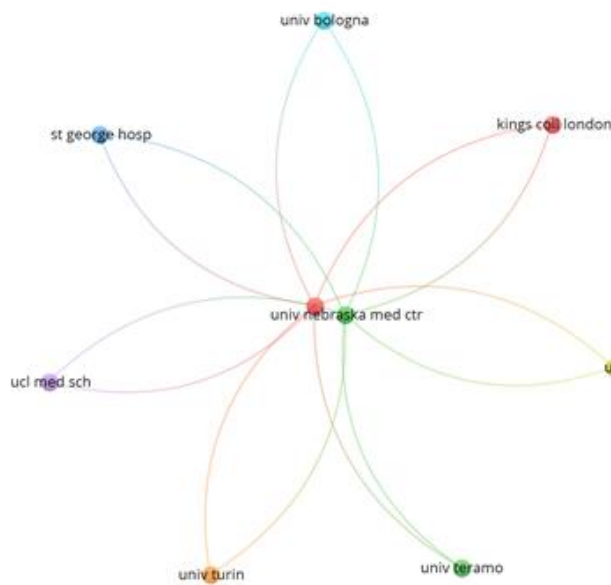


Figure 7. Citation Analysis of Institutions

TABLE VII DISTRIBUTION OF ARTICLES BY INSTITUTIONS IN TERMS OF NUMBER OF PUBLICATIONS, NUMBER OF CITATIONS AND LINK STRENGTH

Institution	Number of Publications (NP)	Number of Citations (NC)	Link Strength (LS)
University of Barcelona	3	20	3
Prince Sattam bin Abdulaziz University	3	11	0
European University of Madrid	2	5	1
Elon University	2	31	0
Technische Universität Braunschweig	2	2	0
University of Nebraska Medical Center	1	17	7
University of Texas School of Dentistry	1	17	7
International University of La Rioja	1	2	3
King's College London	1	1	2
Orenburg State University	1	6	2
Russian State Agrarian University	1	6	2
Russian State Social University	1	6	2
University of Bologna	1	40	2
University of Ottawa	1	6	2
University of Teramo	1	40	2

According to Figure 7, which shows the citation links of the institutions in the examined articles, the “University of Nebraska Medical Center” is at the center of the network and has strong connections with other institutions. It can be said that institutions such as “University of Bologna”, “King's College London”, “University of Turin” and “University of Teramo” are directly related to this center. When Figure 7 is taken into consideration, it can be thought that certain universities and research centers have more academic interaction with each other and carry out joint studies at the international level.

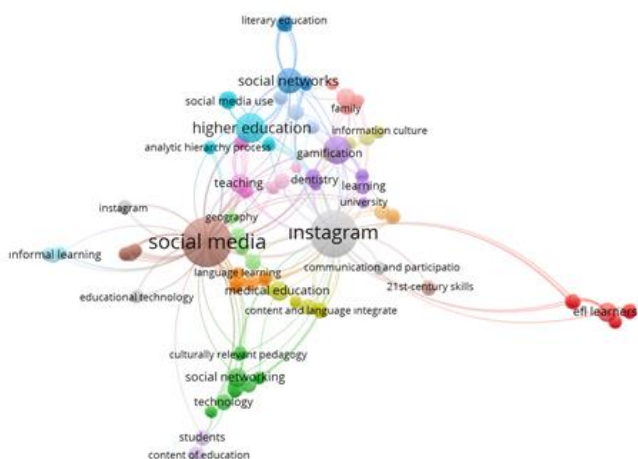


Figure 8. Co-occurrence of all keywords

According to the findings in Table 6, “University of Barcelona (NP=3)” and “Prince Sattam bin Abdulaziz University (NP=3)” stand out as the institutions that stand out in terms of the number of publications. In addition, “University of Teramo (NC =4)” and “University of Ottawa (NC =40)” stand out as the institutions with the highest international academic impact in terms of the number of citations, while “University of

Nebraska Medical Center (BG=7)” and “King’s College London (LS=7)” stand out as the institutions with the highest academic collaboration in terms of connection strength. Considering Table 6, it can be said that some institutions have high academic impact, while others are integrated into wider research networks. The findings regarding the keyword analysis of the articles are presented in Figure 8, and their distributions in terms of frequency (f) and link strength (LS) are presented in Table 8.

TABLE VIII DISTRIBUTION OF KEYWORDS USED IN ARTICLES IN TERMS OF FREQUENCY AND LINK STRENGTH

Keywords	Frequency (f)	Link Strength (LS)
Social media	19	77
Instagram	17	81
Higher education	7	32
Education	6	25
Social networks	5	27
Teaching	3	16
EFL learners	3	15
Medical education	3	11
Pandemic	3	11
Social networking	3	11
Distance learning	2	11
Undergraduate medical education	2	11
Youtube	2	11
Students	2	10
Ict	2	10
E-learning	2	9
Gamification	2	9
Nursing students	2	9
Social networking sites	2	9
Teaching english	2	9

When Figure 8 is examined, it is seen that “Social media” and “Instagramın” are the most central words and have strong connections with the keywords “EFL Learner”, “Medical education”, “Higher education” and “Social media”. Concepts such as “Higher education”, “social networks”, “medical education” and “language learning” highlight how Instagram is used in the context of education. Terms such as “Gamification”, “technology” and “students” indicate areas related to educational technologies, while “EFL learners” form a distinct cluster, revealing the strong connection with language learning. This analysis shows that Instagram and social media are increasingly present in educational processes and are used as effective tools in different learning areas.

When Table 7 is examined, it is seen that the keywords “social media (f=19; LS=77)” and “Instagram (f=17; LS =81)” are the most frequently used words and have the highest connection strength. In addition, considering the frequency of use and connection strength of the keyword “Higher education (f=7; LS=32)”, it can be said that the research mostly focuses on the use of Instagram in the education of higher education students. In addition, words such as “Education (f=6; LS=25)” and “Social networks (f=5; LS=25)” emphasize the importance of social media in the context of education. In addition, words such as “Teaching (f=3; LS=16)”, “EFL learners (f=3; LS=15)” and “Medical education (f=3; LS=11)” may suggest that the research focuses on the use of Instagram in foreign language teaching and medical education.

4. RESULTS, DISCUSSION AND RECOMMENDATIONS

Today, the digitalization process in learning-teaching environments is rapidly progressing and social media platforms

are increasingly taking place in this process. In this research, studies on the use of Instagram in learning-teaching environments were examined using the bibliometric analysis method.

As a result of the analysis, it was seen that studies on the use of Instagram in education have increased significantly especially since 2020. This increase indicates that digital technologies and social media platforms are increasingly taking place in learning processes [64]. The reason for this can be shown as the transfer of learning-teaching environments to online environments due to the COVID-19 pandemic experienced in our country and the world in 2019 and later [65, 66]. In addition, Instagram's central role as social media in collaboration and professional development among teachers [101] may have led to an increase in these posts during the pandemic period. Despite this, in future studies, the reasons for the steady increase in research on the use of Instagram in educational environments after 2020 can be examined in detail and educators and researchers can be guided.

The research findings reveal that the USA plays an important role and is in a central position in articles on the use of Instagram in education, both in terms of the number of publications and the number of citations to publications. Because as technology develops, there has been a significant expansion in online course programs in the USA, allowing students to follow programs that provide completely online courses in various disciplines [67]. This situation has caused the research field of digital technology-based educational applications in the USA to enter a rapid development phase, especially with the impact of the Covid-19 pandemic, and the publications in this field have peaked [68]. Therefore, due to the efforts to integrate current technologies into learning environments in the USA, researchers may have focused on researching the use of current technologies such as Instagram in education. According to the research findings, it is considered noteworthy that Spain is one of the countries that comes to the fore after the USA, and that the "University of Barcelona", which continues its educational activities in Spain, stands out in the examination made on the basis of institutions. It can be said that this situation is due to the effectiveness of the education policies implemented in line with the 2030 Sustainable Development Goals in Spain [102]. Despite this, it can be said that the USA is quite prominent, as it is more than twice as many as Spain, which comes after it, in terms of the number of publications and citations (Table 1; Table 5). The concentration of academic output in the USA generally leads to increased investment in research and development, technological infrastructure, and the involvement of higher education institutions in cutting-edge research, as well as intensive links and collaborations with that country [103]. It can be said that many countries, including the USA and Spain, as well as our country, have turned to research in this area in recent years. However, considering that better education can be provided by using the best technologies in the process of adapting Education 5.0 in underdeveloped or developing countries [69], it can be said that more research is needed on the use of Instagram in education, especially in our country and other countries.

Another prominent finding within the scope of the research is that the articles examined were mostly published in the journals "Cureus Journal of Medical Science", "Journal of Medical Internet Research" and "International Journal of Environmental Research and Public Health". It is noteworthy that the common feature of these journals is that they are

journals that publish in the fields of medicine and health. Instagram, one of the social media applications, offers unique ways to disseminate medical promotion and educational information [70], which may have directed journals publishing in the field of medicine to such research. In addition, according to the findings obtained within the scope of the research, it was determined that the keyword Instagram has strong connections with the keywords "EFL Learner", "Medical education" and "Higher education". Based on this finding, it can be said that the use of Instagram in medical education in higher education institutions is widely researched. Because social media tools play an important role in facilitating education in different medical fields [71-73]. The strong connection of Instagram with foreign language teaching as well as medical education is also striking. Because Instagram has become one of the most researched social media tools due to its potential to make foreign language learning easy and interesting [74-76]. Because studies on the use of Instagram in education show that Instagram is used in different areas such as language learning [75], medical education [77, 78], learning motivation [79,80] and digital literacy [81]. It can be said that this situation is due to the interactive and visual-oriented structure of Instagram. In the study [28], it was concluded that Instagram supports writing skills in language learning and increases student motivation. Similarly, in the study conducted by [36], it was emphasized that Instagram used in medical education is a powerful tool that supports visual learning. In addition, Instagram is also seen as a tool that supports students to collaborate with their peers and create academic content [82]. However, considering that Instagram can be used as an effective teaching tool in different disciplines and education levels [83, 84], it can be suggested that future studies focus on research on the use of Instagram in different disciplines and education levels.

As a result of the analysis conducted in the research, "Li JW (<https://www.webofscience.com/wos/author/record/68323594>)", "Mackey TK (<https://www.webofscience.com/wos/author/record/504935>)" and "Unger JB (<https://www.webofscience.com/wos/author/record/29206102>)" stand out in terms of the number of publications, while "Elizabeth R. Lyden (<https://www.webofscience.com/wos/author/record/25126897>)" stands out as the most cited author and the author in a central position with extensive collaboration. In addition, research on the use of technology in medical education draws attention as a common feature of these authors. While "Li JW" continues his research at a university in China, it is noteworthy that the other authors conduct research at universities in the USA. It can be said that these authors have made significant contributions to the use of Instagram in education with different researchers and have focused on this area. In conclusion, this research reveals the increasing academic interest in the use of Instagram in education and the main areas where research in this field focuses. It reveals that research on the use of Instagram in education has increased over the years and that it makes significant contributions especially in supporting language learning, medical education and higher education. In addition, it has been determined that countries such as the USA, Spain, England and India are the leaders in academic production in this field, that certain authors publish more on the subject and that certain journals publish these studies more. These findings show that the role of Instagram in education is increasingly accepted in academic circles and that it is used in different disciplines. In line with the findings obtained, in order to use Instagram more effectively in education, educators can

combine Instagram with interactive teaching strategies to provide students with easier access to course content. Student participation and interaction can be supported by using interactive features such as question-answer, live broadcast and survey.

LIMITATIONS

The data obtained on 13.02.2025 within the scope of this study is limited to the WoS database. Therefore, studies in other databases could not be examined within the scope of this analysis. In addition, Instagram, one of the social media platforms, was examined in the study. Another limitation is that the study only covers studies conducted between 2015-2024.

REFERENCES

- [1] D. Çapar, Eğitimde Dijital Dönüşüm. Eğitim Bilimleri Alanında Uluslararası Araştırmalar XXIII, vol. 35, 2024.
- [2] S. Manca, and M. Ranieri. "Is Facebook Still a Suitable Technology-Enhanced Learning Environment? An Updated Critical Review of the Literature from 2012 to 2015." *Journal of Computer Assisted Learning*, vol. 32, no. 6, 2016, pp. 503-528. <https://doi.org/10.1111/jcal.12154>.
- [3] V. Raut, and P. Patil. "Use of Social Media in Education-Positive and Negative Impact on the Students." *International Journal on Recent and Innovation Trends in Computing and Communication*, vol. 4, no. 1, 2016, pp. 281-285.
- [4] M. A. Özer, and A. M. Kırık. "Eğitimde Sosyal Medyanın Kullanımı." *The Journal of Academic Social Science Studies*, vol. 14, no. 87, 2024, pp. 393-408.
- [5] N. Gutiérrez-Marín, I. Miranda-Garro, and A. López-Soto. "Instagram as a Pedagogical Tool in Pediatric Dentistry and Orthodontic Courses." *Odovtos-International Journal of Dental Sciences*, vol. 26, no. 2, 2024, pp. 71-81.
- [6] F. Sarsar, M. Basbay, , and A. Basbay. "Öğrenme-Öğretme Sürecinde Sosyal Medya Kullanımı." *Mersin Üniversitesi Eğitim Fakültesi Dergisi*, vol. 11, no. 2, 2015, pp. 418-431. <https://doi.org/10.17860/efd.98783>.
- [7] S. Manca, "Snapping, Pinning, Liking or Texting: Investigating Social Media in Higher Education beyond Facebook." *The Internet and Higher Education*, vol. 44, 2020, p. 100707.
- [8] J. Enterprise, Instagram untuk Fotografi Digital dan Bisnis Kreatif. Elex Media Komputindo, 2014.
- [9] S. D. Alyusi, Media Sosial: Interaksi, Identitas dan Modal Sosial. Prenada Media, 2019.
- [10] J. C. Figueroa-Benítez, F. González-Quiñones, and J. D. Machin-Mastromatteo. "Instagram Como Objeto de Estudio en Investigaciones Recientes: Una Revisión de Literatura con Enfoque en Revistas Científicas." *Ámbitos Revista Internacional de Comunicación*, vol. 53, no. 53, 2021, pp. 9-23.
- [11] Backlinko. Instagram Statistics: Key Demographic and User Numbers. Accessed 20 Apr. 2025. <https://backlinko.com/instagram-users>.
- [12] We Are Social. Digital 2024: 5 Billion Social Media Users. Accessed 29 Apr. 2025. <https://wearesocial.com/uk/blog/2024/01/digital-2024-5-billion-social-media-users/>
- [13] DATAREPORTAL. Digital 2025: Turkey. Accessed 27 Apr. 2025. <https://datareportal.com/reports/digital-2025-turkey>.
- [14] I. Roa, "Utilización de Instagram Como una Herramienta Pedagógica para la Enseñanza de Morfología en Tiempos de COVID-19." *International Journal of Morphology*, vol. 39, no. 4, 2021, pp. 1063-1067.
- [15] Instagram. Introducing Instagram Reels. Accessed 29 Apr. 2025. <https://about.instagram.com/blog/announcements/introducing-instagram-reels-announcement>.
- [16] Instagram. New Video Posts on Instagram Will Be Shared as Reels. Accessed 29 Apr. 2025. <https://business.instagram.com/blog/instagram-video-now-instagram-reels>.
- [17] HubSpot. How to Make Instagram Reels and Use Them to Your Advantage. Accessed 29 Apr. 2025. <https://blog.hubspot.com/marketing/instagram-reels>.
- [18] Meta. See How Instagram Algorithms Can Work for You. Accessed 29 Apr. 2025. https://creators.instagram.com/grow/algorithms-and-ranking?locale=en_US.
- [19] Meirbekov, A., et al. "Digitisation of English Language Education: Instagram and TikTok Online Educational Blogs and Courses vs. Traditional Academic Education. How to Increase Student Motivation?" *Education and Information Technologies*, vol. 29, 2024, pp. 13635-13662. <https://doi.org/10.1007/s10639-023-12396-y>.
- [20] Y. J. Lee, "Language Learning Affordances of Instagram and TikTok." *Innovation in Language Learning and Teaching*, vol. 17, no. 2, 2023, pp. 408-423. <https://doi.org/10.1080/17501229.2022.2051517>.
- [21] F. M. Sari, and A. Y. Wahyudin. "Undergraduate Students' Perceptions toward Blended Learning through Instagram in English for Business Class." *International Journal of Language Education*, vol. 3, no. 1, 2019, pp. 64-73.
- [22] G. Lampropoulos, P. Makkonen, and K. Siakas. "Social Media in Education: A Case Study Regarding Higher Education Students' Viewpoints." *Mobility for Smart Cities and Regional Development - Challenges for Higher Education*, edited by M. E. Auer, H. Hortsch, O. Michler, and T. Köhler, Lecture Notes in Networks and Systems, vol. 389, Springer, Cham, 2022. https://doi.org/10.1007/978-3-030-93904-5_73.
- [23] H. Abdulaziz Al Fadda, "Determining How Social Media Affects Learning English: An Investigation of Mobile Applications Instagram and Snapchat in TESOL Classroom." *Arab World English Journal*, vol. 11, 2020.
- [24] N. Aloraini, "Investigating Instagram as an EFL Learning Tool." *Arab World English Journal*, vol. 4, 2018, pp. 174-184. <https://doi.org/10.24093/awej/call4.1>.
- [25] P. Brebera, "Formal, Informal, and Non-Formal Language Learning Contexts for University Students." *Proceedings of the European Conference on E-Learning*, 2018, pp. 54-59.
- [26] T. Gonulal, "The Use of Instagram as a Mobile-Assisted Language Learning Tool." *Contemporary Educational Technology*, 2019. <https://doi.org/10.30935/CET.590108>.
- [27] V. Leier, "Using Instagram in a Tertiary German Language Course: Students' Perceptions and Approaches." *The New Zealand Language Teacher*, vol. 44, 2018, pp. 77-90. <https://search.informit.org/doi/10.3316/informit.087766999442708>.
- [28] E. Maierová, "Instagram in Teaching English for Specific Academic Purposes." *Advanced Education*, 2024, pp. 75-91.
- [29] M. R. Elvira Rosyida, and S. Seftika. "How Is Instagram Implemented in Teaching Speaking?" *Eleventh Conference on Applied Linguistics (CONAPLIN 2018)*, Atlantis Press, June 2019, pp. 386-388.
- [30] M. González-Mohino, et al. "Maximizing Student Satisfaction in Education: Instagram's Role in Motivation, Communication, and Participation." *The International Journal of Management Education*, vol. 22, no. 3, 2024, p. 101045.
- [31] S. Al-Ali, "Embracing the Selfie Craze: Exploring the Possible Use of Instagram as a Language mLearning Tool." *Issues and Trends in Educational Technology*, vol. 2, no. 2, 2014, pp. 1-16.
- [32] F. Handayani, "Instagram as a Teaching Tool? Really?" *Proceedings of ISELT FBS Universitas Negeri Padang*, vol. 4, no. 1, 2015, pp. 320-327.
- [33] A. Erarslan, "Instagram as an Education Platform for EFL Learners." *Turkish Online Journal of Educational Technology-TOJET*, vol. 18, no. 3, 2019, pp. 54-69.
- [34] N. C. Méndez, "Instagram's Impact on Rural Colombian English Education: A Fourth Industrial Revolution Perspective." *Journal of Digital Learning and Education*, vol. 4, no. 2, 2024, pp. 100-113.
- [35] G. P. D. S. Faustino, et al. "Outline of a Project for Nursing Health Education on the Instagram Social Network." *Revista Brasileira de Enfermagem*, vol. 76, 2023, p. e20220301.
- [36] I. Hussain, et al. "#Anatomynotes: A Temporal Content Analysis of Anatomy Education Posts on Instagram." *Anatomical Sciences Education*, vol. 17, no. 2, 2024, pp. 227-238.
- [37] J. F. L. Koenig, et al. "Using Instagram to Enhance a Hematology and Oncology Teaching Module during the COVID-19 Pandemic: Cross-Sectional Study." *JMIR Medical Education*, vol. 7, no. 4, 2021, p. e30607.
- [38] N. K. M. Douglas, et al. "Reviewing the Role of Instagram in Education: Can a Photo Sharing Application Deliver Benefits to Medical and Dental Anatomy Education?" *Medical Science Educator*, vol. 29, 2019, pp. 1117-1128.
- [39] M. Obeso, et al. "Enhancing Students' Learning Outcomes through Smartphones: A Case Study of Using Instagram in Higher Management Education." *The International Journal of Management Education*, vol. 21, no. 3, 2023, p. 100885.
- [40] A. Durmaz, and S. A. Taşçı. "Ortaokul Öğrencilerinin Sosyal Medya Kullanımı ve Dijital Okuryazarlıklarının Farklı Değişkenler Açısından İncelenmesi." *Kapadokya Eğitim Dergisi*, vol. 2, no. 2, 2021, pp. 26-31.
- [41] R. K. Rinda, A. Novawan, and A. H. Miqawati. "Students' Perspectives on Social Media-Based Learning of Writing through Instagram." *Journal of English in Academic and Professional Communication*, vol. 5, no. 1, 2018.
- [42] B., Darmawati, et al. "Contemporary Mathematics Learning: Instagram-Based Math Learning Medium Increased Elementary School Students' Math Literacy." *Journal of Teaching and Learning Mathematics*, vol. 1, no. 2, 2024, pp. 142-150. <https://doi.org/10.22219/jtlm.v1i2.31310>.

- [43] S. A. Minhalina, et al. "A Literature Review of Digital Marketing Strategies to Build Brand Awareness for Children's Educational Flashcards Business through Instagram: A Case Study of Flashy." *Jurnal Manajemen Bisnis dan Terapan*, vol. 3, no. 1, 2025, pp. 50-58. <https://doi.org/10.20961/meister.v3i1.1954>.
- [44] D. H. Luong, et al. "Social Media in General Education: A Bibliometric Analysis of Web of Science from 2005-2021." *Journal of Scientometric Research*, vol. 12, no. 3, 2023, pp. 680-690.
- [45] I. M. R. Mu'aggiil, and N. W. T. Pido. "Social Media as Learning Tools: A Bibliometric Study of Educational Applications." *Journal of English Teaching and Linguistic Issues (JETLI)*, vol. 2, no. 2, 2023, pp. 65-74.
- [46] A. K. P. Nasution, "Analyzing the Use of Social Media in Education: A Systematic Review of Research Publications." *Education and Information Technologies*, vol. 29, no. 8, 2024, pp. 9495-9516. <https://doi.org/10.1007/s10639-023-12179-5>.
- [47] Mukul, E., and G. Büyükközan. "Digital Transformation in Education: A Systematic Review of Education 4.0." *Technological Forecasting and Social Change*, vol. 194, 2023, p. 122664. <https://doi.org/10.1016/j.techfore.2023.122664>.
- [48] E. Yeşiltaş, and G. Şeker. "Sosyal Medya ile İlgili Yapılan Eğitim Araştırmalarının Bibliyometrik Analizi." *Journal of World of Turks/Zeitschrift für die Welt der Türken*, vol. 13, no. 2, 2021.
- [49] M. Artsin, et al. "Bibliometric Analysis of Social Media Studies within Educational Research." *Turkish Online Journal of Distance Education*, vol. 25, no. 4, 2024, pp. 162-184.
- [50] F. U. Erdoğan, and K. Çağiltay. "The General Trend in Master's and Doctoral Theses Published in the Field of Instructional Technology in Turkey." *Fundamentals of Instructional Technologies: Theories, Research, Trends*, edited by K. Çağiltay and Y. Göktaş, 2nd ed., Pegem Akademi, 2016, pp. 567-581.
- [51] Liberati, A., et al. "The PRISMA Statement for Reporting Systematic Reviews and Meta-Analyses of Studies That Evaluate Health Care Interventions: Explanation and Elaboration." *PLoS Medicine*, vol. 6, no. 7, 2009, p. e1000100. <https://doi.org/10.1371/journal.pmed.1000100>.
- [52] D. T. K. Ng, et al. "A Review of AI Teaching and Learning from 2000 to 2020." *Education and Information Technologies*, vol. 28, no. 7, 2023, pp. 8445-8501. <https://doi.org/10.1007/s10639-022-11491-w>.
- [53] A. Pritchard, "Statistical Bibliography or Bibliometrics?" *Journal of Documentation*, vol. 25, 1969, pp. 348-349.
- [54] J. Martí-Parreño, et al. "The Use of Gamification in Education: A Bibliometric and Text Mining Analysis." *Journal of Computer Assisted Learning*, vol. 32, no. 6, 2016, pp. 663-676. <https://doi.org/10.1111/jcal.12161>.
- [55] B. Karasözen, et al. "WoS ve Scopus Veri Tabanlarının Karşılaştırması." *Türk Kütüphaneciliği*, vol. 25, no. 2, 2011, pp. 238-260.
- [56] F. Albaş, "Web of Science (WoS) Veri Tabanında İşe Angaje Olma Konulu Çalışmaların Bibliyometrik Analiz Yöntemi ile İncelenmesi." *Artuklu Kaime Uluslararası İktisadi ve İdari Araştırmalar Dergisi*, vol. 6, no. 2, 2023, pp. 131-155.
- [57] A. K. Shukla, et al. "Engineering Applications of Artificial Intelligence: A Bibliometric Analysis of 30 Years (1988-2018)." *Engineering Applications of Artificial Intelligence*, vol. 85, 2019, pp. 517-532. <https://doi.org/10.1016/j.engappai.2019.06.010>.
- [58] Clarivate Analytics. "Research Areas (Categories/Classification)." *Web of Knowledge*, 2021. Accessed 30 Apr. 2025, https://images.webofknowledge.com/images/help/WOS/hp_research_areas_easca.html.
- [59] N. Van-Eck, and L. Waltman. "Software Survey: VOSviewer, a Computer Program for Bibliometric Mapping." *Scientometrics*, vol. 84, no. 2, 2010, pp. 523-538. <https://doi.org/10.1007/s11192-009-0146-3>.
- [60] I. Goksu, et al. "The Content Analysis and Bibliometric Mapping of CALL Journal." *Computer Assisted Language Learning*, 2020, pp. 1-31. <https://doi.org/10.1080/09588221.2020.1857409>.
- [61] A. Aktoprak, and C. Hursen. "A Bibliometric and Content Analysis of Critical Thinking in Primary Education." *Thinking Skills and Creativity*, vol. 44, 2022, pp. 1-22. <https://doi.org/10.1016/j.tsc.2022.101029>.
- [62] J. W. Buzdylowski, "Co-Occurrence Analysis as a Framework for Data Mining." *Journal of Technology Research*, vol. 6, 2015, pp. 1-19.
- [63] D. Hernández-Torrano, and L. Ibrayeva. "Creativity and Education: A Bibliometric Mapping of the Research Literature (1975-2019)." *Thinking Skills and Creativity*, vol. 35, 2020, pp. 1-17. <https://doi.org/10.1016/j.tsc.2019.100625>.
- [64] L. Andrade-Vargas, et al. "YouTube and Instagram in Higher Education: Media Competencies of University Teachers." *RIED-Revista Iberoamericana de Educación a Distancia*, vol. 27, no. 2, 2024.
- [65] O. B. Adedoyin, and E. Soykan. "Covid-19 Pandemic and Online Learning: The Challenges and Opportunities." *Interactive Learning Environments*, vol. 31, no. 2, 2023, pp. 863-875. <https://doi.org/10.1080/10494820.2020.1813180>.
- [66] Y. Cui, et al. "A Survey on Big Data-Enabled Innovative Online Education Systems during the COVID-19 Pandemic." *Journal of Innovation & Knowledge*, vol. 8, no. 1, 2023, pp. 1-18. <https://doi.org/10.1016/j.jik.2022.100295>.
- [67] D. Jhurry, and R. Rampersad. "From Online Learning to Digital Transformation: The New University Normal." 2022, pp. 57-76. <https://doi.org/10.36615/9781776402304-04>.
- [68] C. Wang, et al. "Education Reform and Change Driven by Digital Technology: A Bibliometric Study from a Global Perspective." *Humanities and Social Sciences Communications*, vol. 11, no. 1, 2024, pp. 1-17. <https://doi.org/10.1057/s41599-024-02717-y>.
- [69] A. M. Alharbi, "Implementation of Education 5.0 in Developed and Developing Countries: A Comparative Study." *Creative Education*, vol. 14, no. 5, 2023, pp. 914-942. <https://doi.org/10.4236/ce.2023.145059>.
- [70] K., Thawanyarat, et al. "#PRS: A Study of Plastic Surgery Trends with the Rise of Instagram." *Aesthetic Surgery Journal Open Forum*, vol. 5, 2023, p. ojad004, pp. 1-7. <https://doi.org/10.1093/asjof/ojad004>.
- [71] L., Kauffman, et al. "Social Media Usage for Radiology Education: A One-Month 2022 Global Survey." *Current Problems in Diagnostic Radiology*, vol. 52, no. 3, 2023, pp. 153-163. <https://doi.org/10.1067/j.cpradiol.2023.01.007>.
- [72] A. Pozdnyakov, et al. "The Growing Role of Social Media for Research and Education in Radiology." *Diagnostic and Interventional Imaging*, vol. 104, no. 6, 2023, pp. 265-268. <https://doi.org/10.1016/j.diii.2023.01.007>.
- [73] C. Seifen, et al. "Patient Education on Instagram? Structured Content Analysis of the Hashtag 'ObstructiveSleepApnea'." *European Archives of Oto-Rhino-Laryngology*, 2025, pp. 1-7. <https://doi.org/10.1007/s00405-025-09211-4>.
- [74] R. W. Agustin, and M. Ayu. "The Impact of Using Instagram for Increasing Vocabulary and Listening Skill." *Journal of English Language Teaching and Learning*, vol. 2, no. 1, 2021, pp. 1-7.
- [75] A. K. P. Nasution, "Instagram in English Language Learning: A Systematic Literature Review." *Journal of Linguistics, Literature, and Language Teaching (JLLLT)*, vol. 3, no. 1, 2023, pp. 33-52. <https://doi.org/10.37249/jlllt.v3i1.708>.
- [76] M. A. S. Khasawneh, "Exploring How Language Learning Platforms on Instagram and TikTok Can Facilitate Collaborative Foreign Language Learning Experiences of Undergraduates." *Research Journal in Advanced Humanities*, vol. 5, no. 3, 2024, pp. 174-187. <http://dx.doi.org/10.58256/nmfqr89>.
- [77] R. R. Gulati, et al. "Instagram for Peer Teaching: Opportunity and Challenge." *Education for Primary Care*, vol. 31, no. 6, 2020, pp. 382-384.
- [78] A., Escamilla-Sanchez, et al. "Instagram as a Tool to Improve Human Histology Learning in Medical Education: Descriptive Study." *JMIR Medical Education*, vol. 11, no. 1, 2025, p. e55861.
- [79] D. Hortigüela-Alcalá, et al. "Social Networks to Promote Motivation and Learning in Higher Education from the Students' Perspective." *Innovations in Education and Teaching International*, vol. 56, no. 4, 2019, pp. 412-422.
- [80] T. Otto, and B. Thies. "Exploring the Influence of Instagram Use on Materialism and Situational Intrinsic Learning Motivation: An Online Experimental Study." *Education and Information Technologies*, 2024, pp. 1-32.
- [81] D. Fardiah, et al. "Instagram Content Impact on Digital Literacy Capability." *Jurnal Aspikom*, vol. 8, no. 1, 2023, pp. 79-94.
- [82] R. O. D. Santos, and R. M. L. Rudnik. "Instagram and Education: Some Considerations." *Revista Brasileira de Educação*, vol. 27, 2022, p. e270099.
- [83] V. Y. K. Gusti, et al. "The Development of Instagram Filter-Based Learning Media for Mathematics in Junior High School." *Development*, vol. 4, no. 1, 2023, pp. 1-9.
- [84] S. J. Kathuria, "A Study of the Usage and Perception of Instagram as a Learning Tool." *i-Manager's Journal of Educational Technology*, vol. 21, no. 3, 2024, pp. 30-47. <https://doi.org/10.26634/jet.21.3.21279>.
- [85] A. Birhanlı, "Eğitimde Yenilikçi Özümler: Dijital Dönüşüm." *International Journal of Educational and Social Sciences*, vol. 4, no. 1, 2025, pp. 67-84. <https://doi.org/10.5281/zenodo.15448854>.
- [86] C. O'Reilly, A. Devitt, and N. Hayes, "Critical Thinking in the Preschool Classroom -A Systematic Literature Review," *Think Skills Creat*, vol. 46, 2022, p. 101110, <http://doi.org/10.1016/j.tsc.2022.101110>.
- [87] F. Seraji, R. Malmir, H. A. Kasani, & H. Abedi, "Teacher-generated content in social media: Studying the experience of Iranian teachers." *Teaching and Teacher Education*, vol. 121, 2023, pp. 103955. <https://doi.org/10.1007/s10639-023-12396-y>.
- [88] M. Aydoğmuş, E. Tut, & Y. Karadağ, "Teachers' experiences regarding the use of social media for educational purposes." *International Journal of Psychology and Educational Studies*, vol. 10, no. 1, 2023, pp. 69-82. <https://doi.org/10.52380/ijpes.2023.10.1.855>.
- [89] F. Jimola, "Undergraduate Students' Exploration of Instagram and Tiktok in Learning Language Skills Contents: A Leverage to Digital Literacy." *Interdisciplinary Journal of Education Research*, vol. 5, 2023, pp. 84-95.
- [90] R. K. Anwar, U. L. S. Khadijah, & E. Rizal, "Instagram and Digital Media Literacy among Teenagers in Bandung." *Communicatus: Jurnal Ilmu Komunikasi*, vol. 7, no. 2, 2023, pp. 123-142. <https://doi.org/10.15575/cjik.v7i2.23640>

- [91] K. Ciampa, Z. M. Wolfe, & B. Bronstein, (2023). "ChatGPT in education: Transforming digital literacy practices." *Journal of Adolescent & Adult Literacy*, vol. 67, no. 3, 2023, pp. 186-195. <https://doi.org/10.1002/jaal.1310>
- [92] Y. Walter, "Embracing the Future of Artificial Intelligence in the Classroom: The Relevance of AI Literacy, Prompt Engineering, and Critical Thinking in Modern Education." *International Journal of Educational Technology in Higher Education*, vol. 21, no. 1, 2024, pp. 15. <https://doi.org/10.1186/s41239-024-00448-3>
- [93] G. Erol, & M. Kuyucu, (Eds.), "Advancements in Socialized and Digital Media Communications.", 2024. IGI Global.
- [94] N. Al-Qaysi, A. Granić, M. Al-Emran, T. Ramayah, E. Garces, & T. U. Daim, "Social Media Adoption in Education: A Systematic Review of Disciplines, Applications, and Influential Factors." *Technology in Society*, vol 73, 2023, pp. 102249. <https://doi.org/10.1016/j.techsoc.2023.102249>
- [95] B. Graefen, & N. Fazal, "Revolutionizing Education Through Instagram in the Post-Covid Era." *European Journal of Education Studies*, vol. 10, no. 8, 2023, pp. 38-50. <http://dx.doi.org/10.46827/ejes.v10i8.4900>
- [96] M. Aria, & C. Cuccurullo, "Bibliometrix: an R-tool for Comprehensive Science Mapping Analysis." *Journal of Informetrics*, vol. 11, no. 4, 2017, pp. 959-975. <https://doi.org/10.1016/j.joi.2017.08.007>
- [97] N. J. van Eck, & L. Waltman, "CitNetExplorer: A New Software Tool for Analyzing and Visualizing Citation Networks." *Journal of Informetrics*, vol. 8, no. 4, 2014, pp. 802-823. <https://doi.org/10.1016/j.joi.2014.07.006>
- [98] A. Dattolo, & M. Corbato, "VisualBib: A Novel Web App for Supporting Researchers in the Creation, Visualization and Sharing of Bibliographies." *Knowledge-Based Systems*, vol. 182, no. 9, 2019, pp. 104860. <https://doi.org/10.1016/j.knosys.2019.07.031>
- [99] C. Chen, "CiteSpace II: detecting and visualizing emerging trends and transient patterns in scientific literature." *Journal of the American Society for Information Science and Technology*, vol. 57, no. 3, 2006, pp. 59-377. <https://doi.org/10.1002/asi.20317>
- [100] N. J. van Eck, & L. Waltman, "Software survey: VOSviewer, a computer program for bibliometric mapping." *Scientometrics*, vol. 84, no. 2, 2010, pp. 523-538.: <https://doi.org/10.1007/s11192-009-0146-3>
- [101] E. Doğan, E. Güven, B. Koyuncu, & T. Ünlü, "Öğretmenlerin sosyal medya kullanımı: Eğitimde iletişim ve öğrenmeyi destekleme potansiyeli." *Ulusal Eğitim Dergisi*, vol. 3, no. 10, 2023, pp. 1705-1721.
- [102] A. M. F. Ramadhan, F. Angeli, & R. A. Ananda, "Bibliometric Analysis of Gender Equality And Education Quality To Achieve Sustainable Development Goals (Sdgs) In 2030." *Jurnal Ilmiah Hubungan Internasional Fajar*, vol. 2, no. 2, 2024, pp. 29-40. <https://doi.org/10.47354/jihif.v2i2.784>
- [103] C. Wang, X. Chen, T. Yu, Y. Liu, & Y. Jing, "Education Reform and Change Driven by Digital Technology: A Bibliometric Study From a Global Perspective." *Humanities and Social Sciences Communications*, vol. 11, no.1, 2024, pp. 1-17. <https://doi.org/10.1057/s41599-024-02717-y>

BIOGRAPHIES

Merve Gülmüş Yelmen completed her undergraduate and graduate education at Firat University, Department of Computer Education and Instructional Technology. She is currently continuing her doctorate education in the same department. She is also working as a lecturer at Çukurova University, Department of Computer Aided Design and Animation. Her current research interests include instructional technologies, artificial intelligence applications in education, computer-aided design and animation applications.

Müzeyyen Bulut Özek graduated B.S. and M.S. degrees from the Department of Computer Science at the Firat University in 2002 and 2004 respectively. Then she received Ph.D. degree at the Department of Electrical Electronics Engineering at the same university in 2010. Her current research areas include artificial intelligence applications in education, educational technologies, intelligent teaching systems, e-learning.

Fatih Kalemkuş worked as an information technologies teacher at the secondary school level in the previous years. He works as an assistant professor at Kafkas University in Turkey. He researchs on instructional technologies.